Application of Magneto-Rheological Dampers in Tuned Mass Dampers for Floor Vibration Control

by

John Kenneth Ritchey

Thesis submitted to the Faculty of the
Virginia Polytechnic Institute and State University
in partial fulfillment of the requirements for the degree of

MASTER OF SCIENCE

in

Civil Engineering

Dr. Mehdi Setareh **Co-Chairman**	**Dr. Thomas M. Murray** **Co-Chairman**
Dr. Mehdi Ahmadian	**Dr. Alfred Wicks**

October 2003
Blacksburg, Virginia

semi-active, floor vibration, tuned mass damper

Application of Magneto-Rheological Dampers in Tuned Mass Dampers for Floor Vibration Control

by

John Ritchey
Mehdi Setareh and Thomas M. Murray, Chairman
Civil Engineering

(ABSTRACT)

The purpose of this research is to establish the effectiveness of tuned-mass-dampers (TMD) using semi-active magneto-rheological (MR) dampers to mitigate annoying floor vibrations. Annoying floor vibration is becoming more common in today's building structures since building materials have become stronger and lighter; the advent of computers has resulted in "paperless" offices; and the use of floors for rhythmic activities, such as aerobics and concerts, is more common. Analytical and experimental studies were conducted to provide an understanding of the effects of incorporating the semi-active-TMD as a remedy to annoying floor vibration.

A pendulum tuned mass damper (PTMD) in which the tuning parameters could independently be varied was used. Closed form solutions for the response of the floor using passive dampers were developed. In addition, a numerical integration technique was used to solve the equations of motion where semi-active dampers are utilized. The optimum design parameters of PTMDs using passive and semi-active dampers were found using an optimization routine. Performances of the PTMD in reducing the floor vibration level at the optimum and when subjected to off-tuning of design parameters using passive and semi-active dampers were compared.

To validate the results obtained in the analytical investigation, an experimental study was conducted using an 8 ft x 30 ft laboratory floor and a commercial PTMD. Comparative studies of the effectiveness of the PTMD in reducing floor vibrations using semi-active and passive dampers were conducted.

ACKNOWLEDGMENTS

This project is collaborative and I would like to give thanks and recognition to all those involved.

I am speechless at the dedicated time, aid, patience, mentoring, and guise of Dr. Setareh and Dr. Wicks have shown me during this ordeal we call growth. And grow, I have. It was an honor and privileged to work with the both of you. I will never forget what you have done. I am left inspired. Thank you.

I would like to thank Dr. Murray for this experience and his constant patience, support and mentoring throughout this project. Thank you.

To Dr. Ahmadian and Jeong-Hoi Koo for their patience, time, and assistance in seeing the final steps of the project to its completion. Thank you.

To my family for their love, trust, faith, prayers and support back home. Thank you.

To God above, thank you for Your light and wisdom to a man's journey on this earth.

TABLE OF CONTENTS

Page

LIST OF FIGURES

LIST OF TABLES

Application of Magneto-Rheological Dampers in Tuned Mass Dampers for Floor Vibration Control

CHAPTER 1

INTRODUCTION AND LITERATURE REVIEW

1.1 Introduction

Annoying floor vibration due to human occupancy has become a serviceability problem in building structures. This is primarily due to enhancements in computer structural analysis and optimization, methods of construction, implementation of higher-strength and light-weight materials, and the modern trend of large open-space areas. These create a floor system that is susceptible to excessive floor vibrations due to human movements.

Floor systems have several serviceability symptoms that can be associated with problematic floors – frequency, amplitude, and duration. A floor system with a low natural frequency is susceptible to resonance with a harmonic of human activities, which can cause large displacement and acceleration. This affects the visual and physical perception of humans and can be disturbing. Human perception studies have revealed thatfloor steady-state displacements "of less than 0.040 in. can be very annoying" (Shope and Murray 1995). Bachman et. al (1995) recommend composite floors be constructed with a natural frequency greater than 7 or 8 Hz to separate the natural frequency of the floor with the frequency at which human activities occur. Low levels of damping allow the magnitude of the floor's response to be large with a low dissipation in energy; the duration of response will last for a significant amount of time and it can be annoying to occupants. Lenzen (1966) states that if the damping diminishes the floor vibration in less than five cycles, occupants will only perceive the impact. If the response duration lasts longer than twelve cycles, the occupants will react to the vibration as if it were steady-state.

Floor serviceability criterion have been provided since 1828 (Murray et al. 1997) as a preventive measure against annoying floor vibrations and to provide human comfort. These have been developed with continued research, and there is extensive literature on

the topics of human perceptibility and structural performance. Currently designers are using AISC Design Guide 11 (Murray et al. 1997) which employs International Standards Organization (ISO) guidelines for determining acceptable floor acceleration levels for human occupancy. The acceleration level is presented as a percentage of gravity. The acceptable floor acceleration level in offices, residences, and churches is 0.5% g. For shopping malls, it is 1.5% g; indoor footbridges, 1.5% g and outdoor footbridges, 5% g. Minimum, perceptible, acceleration levels are 1% g and 2% g; these are typically not annoying to humans.

Structural floor systems designed without considering the vibration serviceability criteria or a change in occupancy can render a floor susceptible to annoying floor vibrations. Remedies to this situation include modification of the mass, increasing damping, increasing stiffness, relocation of the source of vibration or the sensitive occupancy, or a combination to establish an acceptable floor system. These can be expensive, architecturally incompatible, and decrease the benefits gained with the lightweight floor system.

As an alternative to the aforementioned solutions, which in most cases are not practical, a passive or active tuned mass damper (TMD) can be implemented to mitigate resonant vibrations. They can be installed above (disguised as furniture), in (within a floor cavity), or below the problematic floor (integrated into the supporting floor structure) at the point of maximum deflection. A passive TMD is a cost-effective method of targeting a single mode of vibration. It has the disadvantage of being prone to off-tuning, not good for closely spaced modes, and require one TMD per problematic mode of vibration. An active TMD produces the largest decrease in peak acceleration by putting energy into the floor system with respect to a defined control policy. It has the disadvantage of being very costly, requiring high maintenance, and a continuous energy supply to function.

In lieu of the previous remedial measures and the focus of this study, a semi-active tuned mass damper (SATMD) can be implemented. It is a compromise between the passive and active tuned mass dampers. A MR damper replaces the passive viscous dashpot and it is regulated using a displacement-based ground-hook control policy. A low-voltage power source is required to maintain the magnetic field regulated by the

semi-active control policy programmed in a computer. MR dampers are cost effective, and can decrease the peak acceleration over a larger band-width.

1.2 Literature Review

MR damper have been used in several areas of vibration control. Bridges, off-shore-oil platforms, and building structures have implemented MR technology to minimize the overall structural response to lateral excitations, such as wind and earthquakes. The device has been incorporated into the structure's lateral resisting system or base-isolation system. The automobile industry has implemented this technology in suspension systems and passenger seats to reduce vibration in the vehicle chassis and to the passengers.

Comprehensive studies of the characteristics and behavior of the magneto-rheological dampers are found in the literature. The MR damper has been implemented in single- and multi-degree-of-freedom systems. Comparative analytical and experimental studies of the passive systems have demonstrated the effectiveness of implementing this technology to control vibration.

The main focus of this study is the application of the MR dampers in a tuned mass damper arrangement to reduce the vibration of floors. These motions are at low frequencies and relatively small amplitudes. The use of the MR damper to control the overall structural response of large-scale structures is a study of the ability of the MR to regulate vibration at very low frequencies and relatively large displacements.

The following section is a historical review of tuned mass dampers as related to control of floor vibrations. It covers the past analytical and experimental studies, as well as, permanent installations and their reported success.

1.2.1 Historical Floor Vibration Mitigation

Ormondroyd and Den Hartog (1928) developed the concept of a passive tuned vibration absorber. The model consists of a mass supported by a spring. The mass and spring are chosen to isolate a specific frequency of the problematic system. The concept has been applied in both mechanical and civil engineering structures. The inclusion of a

viscous damper, in parallel with the absorber's spring, increases the amount of energy dissipated; and therefore; it results in a further reduction in system response.

The largest decrease in floor response will occur when the vibration absorber is "tuned." Den Hartog (1947) presents a "fixed-point" method to achieve a tuned state for a damped vibration absorber implemented on an un-damped main system. He defines the combined system dynamically in terms of non-dimensional parameters mass ratio, frequency ratio, and damping ratio. He develops a closed form solution for the system configuration, and two equations that provide the optimum frequency ratio and damping ratio to obtain the tuned response of the system. Den Hartog shows that when the vibration absorber is tuned, the response curve has equal peaks at the two resonant modes.

Allen and Pernica (1984) discuss the application of a simple plank absorber to reduce vibrations of long-span floor structures. Using an experimental test floor structure at the Division of Building Research, National Research Council of Canada they produced response curves with and without the plank absorber. Allen and Pernica elaborate on these curves and provide rules of thumbs and formulas to design, tune, and implement a plank absorber. No case studies or experimental details are provided.

Thornton et al. (1990) applied a set of passive TMDs in two cases. The first case is a high school where accelerations of 2.5% g at 4.5 Hz and 0.6% g at 5.5 Hz were measured in adjacent second and third floors respectively. This level of vibration was induced by the rhythmic activities that took place within the gymnasium and occurred at a frequency range of 2-2.5 Hz. This was approximately half a harmonic of the natural floor frequency. The third-floor damping ratio was measured to be less than 1% of critical damping. Modal analysis of the third-floor revealed the first four modes occurred at 4.0, 4.6, 5.3, and 6.0 Hz. The damping associated with each of the modes was reported to range from 1.7 percent for the first mode to as low as 0.9 percent for the second mode.

Eight TMDs were designed and installed to tune to each of the problematic modes. The TMDs were suspended from the concrete T-beams beneath the gym floor. No detailed information is provided about the TMD. Post analysis of the floor revealed a reduction in both the second and third floors "by more than a factor of two or more". The author notes "they still know when aerobics class in action, but the vibrations are

perceived as transient rather than continuous" (Thornton 1990). Occupants reported the gym floor felt stiffer.

The second case presented by Thornton (1990) was a seven-story college building. A two-story gym, starting at the fifth floor, and spanning 70 ft produced annoying floor vibrations from the second floor on up, especially during high-impact aerobics. The natural frequency of the structural system was double the frequency of the aerobics. TMDs were designed and presented in two solution schemes. The first scheme implemented small TMD units at specific locations throughout the structure; they would be disguised as furniture in the spaces and suspended below the gym floor. The TMD unit weights were ranged from 50,000 to 100,000 lbs. The second scheme involved treating the seventh-floor with one TMD, decoupling a 3.5 Hz mode, and treating it with two more TMDs. Each of the TMDs was tuned to the forcing function, the floor's natural frequency, or both to achieve a specific and acceptable level of acceleration.

Setareh and Hanson (1992) implemented TMDs to mitigate the vibrations of an auditorium balcony located in Detroit, Michigan. This space was designated for concerts and live performances. The balcony is constructed of longitudinal truss and girders and transverse cantilevered beams.

An experimental investigation of the balcony was performed. At the time of measurement, the balcony was bare: there was no carpeting or people. Using a shaker and transducers, and a spectral analyzer the response of the system was recorded. The first two natural frequencies of the system where measured to be 2.93 and 4.24 Hz. The respective damping was calculated to be 1.39% and 1.83%. During a live performance, the first two modal frequencies were measured to be 2.75 and 3.85 Hz.

A computer model of the entire balcony was developed incorporating the weight of the structural framing, suspended ceiling, ductwork into the model. Shear deformation was included in the model. The first two modal frequencies were 3.16 and 4.54 Hz. The respective modal damping was 1.6% and 1.1%. To predict the balcony response under full occupancy and seats, this weight was added to the model. The first two natural frequencies were 2.55 and 3.68 Hz. The first modal frequency "falls in the center of the audience participation rock music beat frequency" (Setareh and Hanson 1992).

Five passive TMDs were built. Each TMD was composed of steel plates, eight springs, two shock absorbers to provide damping, and encased in a damper box; the tuning parameters where determined by using the equivalent single-degree-of-freedom model for the optimization. Two TMDs weighing 4,000 lbs were implemented to isolate the first mode of vibration, and three TMDs weighing 2,000 lbs were used for the second mode of vibration.

A subsequent experimental evaluation of the balcony was performed. Recorded accelerations ranged from 2% g to 7% g depending on the occupancy at the time of the record. Comparing this acceleration to the ISO criteria, this was deemed an acceptable level of vibration. Compared to the balcony without TMDs, an approximate decrease of 78% in the amplitude of vibration was observed. A 80% decrease was the design goal.

Webster and Vaicaitis (1992) applied TMDs to reduce the floor accelerations of a long-span, composite, floor at the Terrace on the Park Building in New York City. It was initially an exhibition building at the 1964 World's Fair.

The ball-room levels were approximately rectangular in plan and encompassed by an elliptical promenade. Four columns support six floors and a cross-shaped system of girders and elliptical ring girder. The floor girder to ring girder span is 17.37 m. The girders support a radial set of cantilever beams that span beyond the ring 17.07 m.

During dining and dancing, annoying floor vibrations disturbed the occupants. Dining occurred in the center of the floor plan; dancing around the perimeter over the cantilevered beams. During occupancy of the floor, accelerations were measured as high at 7 m/sec^2 and displacements of 3.3 mm. A natural frequency of 2.3 Hz was measured in one quadrant of the floor which corresponds to the frequency of dancing. The modal damping for the first mode of the floor ranged from 2.8 percent to 3.6 percent of critical.

Four passive TMDs were implemented in an attempt to control the floor vibrations. They were placed near the tips of the cantilevered beams and concealed in available closets. Each TMD was constructed of a concrete-filled steel box and steel plates supported by springs and viscous dashpots. The total weight of each TMD was 18,400 lbs; this relates to a mass ratio of 0.044. Tuning of the TMD was achieved via a variable-speed mass shaker to excite the floor. The installation of the four TMDs on the dance floor alleviated the annoying floor vibration. Post-measurement of the floor

showed a 60 percent decrease in the floor accelerations. The author notes no further complaints were reported since the installation of the TMDs.

Bell (1994) introduced TMDs as a measure to alleviate annoying floor vibrations of a museum footbridge. To allow the passage of light to lower floors, a "bridge slab" was installed within the floor. A "bridge slab" is the remaining portion of the floor after openings are provided on either side. It is constructed of two girders and cross beams. The deck type was not specified. Measurements of the existing floor revealed a natural frequency at 3.7 Hz and a damping ratio of 1 percent.

The TMD introduced into the system weighed 1,925 lbs. No information is given about the spring type or assembly. A viscous damper was used. The TMD was suspended below the center of the floor. Damping was increased from 1% to 5.8%. TMDs were installed at each of the problematic bridges. The installation of the passive TMDs resulted in an acceptable floor.

Shope and Murray (1995) installed TMDs to reduce annoying floor vibration on an existing office floor. Each TMD was constructed of a multi-celled liquid damper supported on steel plate. Additional steel plates were added for mass. The TMD was investigated experimentally before its implementation and post-installation measurements were performed. An experimental single-bay floor was constructed in a lab. It consisted of a 3.5 in. concrete slab on steel deck supported by open-web steel joists spanning 25 ft and spaced at 30 in. on center. The joists were supported on hot-rolled, wide-flange steel beams. A modal analysis of the floor, prior to the installation of the TMDs, produced modal frequencies at 7.3 Hz and 17 Hz. The floor was excited by heel-drops. The authors state that the floor had a low amount of damping; a value is not specified except that it took 3 seconds for the floor's response to subside. A peak acceleration of 1% g was measured.

Four TMDs, two for each mode, were constructed, tuned, and then placed at specific locations respective to maximum displacement for each mode. Post installation and positioning of the dampers demonstrated a reduction in the floors peak response. Heel drops were performed and the decay rate increased to one second according to the author. Observation of the auto-spectrum revealed a significant decrease in the peak

acceleration for each mode. The acceleration time history for walking showed a decrease in the average acceleration from 6% g to 1% g.

A retrofit, using the multi-celled liquid dampers, was performed on the second story of a new office building. The floor system is composed of 4.5 in. normal weight concrete on metal deck. The floor is supported on open-web joists that span 52 ft, and they are spaced at 48 in. on center. The joists are supported on joist girders that span 16 ft. A series of heel drop tests were performed on the floor to establish its modal characteristics. The natural frequency of the floor ranged from 5.13 Hz to 5.25 Hz when measured: at the center of the floor or on a column line respectively. The second mode vibrated at 6.5 Hz.

Fourteen TMDs were installed to control the vibration acceleration levels. Tuning was performed in the lab, but post-installation tuning was performed to tailor the overall response, improve the overall effectiveness of the TMDs, and reduce the peak acceleration. All the TMDs used a span of 8 ft, and the added mass ranged from 160 lbs to 600 lbs. The TMDs were suspended beneath the office floor using metal rods attached to the floor joists and a metal angle to support the TMD. Measurements after the TMDs were installed and tuned showed a decrease in floor acceleration at each of the problematic modes. A reduction was observed in the time histories and frequency response spectrum for both heel drop and walking excitations (perpendicular to the joists). "The response of the occupants using the 'fixed' floor has been very positive" (Shope and Murray 1995).

Hanagan and Murray (1995) have tested an active tuned mass damper to control unwanted floor vibration in commercial structures. Analytical and experimental studies have been conducted. A control policy was developed "utilizing the measured movement of the floor to compute the input signal to an electromagnetic actuator which, by the movement of the actuator reaction mass, supplies a force that reduces the transient and resonant vibration levels."

An electromagnetic-shaker served as the active tuned mass damper to mitigate floor vibration. The TMD is diagramed as a two mass system: One mass represents the static support frame of the shaker and the other mass is the dynamic reaction mass. Stiffness is provided via the reaction mass suspension system. Damping is assumed as viscous; this

value accounts for the damping from the "internal motor properties and friction" (Hanagan and Murray 1995).

The control policy is based on a single-input/single-output methodology. The control law used by Hanagan is "collocated rate feedback with a simple command limiter" (Hanagan and Murray 1995). Experimentally, the control law parameters are measurable and sent back to the computer. "The input signal, which is a voltage proportional to the velocity of the floor motion at the collocated actuator/sensor location, is generated by a piezoelectric transducer" (Hanagan and Murray 1995). The signal is sent through an analog to digital converter and then to the computer. The computer calculates the required output signal via a control program that contains the control law. The digital signal is sent through a digital to analog converter to the amplifier that sends the control voltage to the shaker. This entire process occurs in milliseconds. Optimization of the ATMD takes place on-site.

An office floor, in a light manufacturing facility, had annoying levels of vibration due the occupancy. This floor was very sensitive to human motion, even in several bays away. A joist-supported floor with 2.5 in. light-weight concrete deck had a problematic span of 28' 4 in. The type of office could be defined as an "electronic office," with computers on almost every desk.

The experimental implementation of the control actuator and sensor were established at a specific location. Details to the particular location are not given. Walking perpendicular to the span, measurements were obtained both pre- and post-operation of the ATMD. A 300% reduction in peak acceleration was observed.

A chemistry laboratory floor at a university employed ATMD technology to control annoying floor vibrations due to occupant movement. The floor span is 28' 7 in., joist-supported, and supports a 3.5 in. deck. An ATMD actuator and sensor where applied to the floor, and a reduction of 400% in floor walking acceleration is reported by the author.

The ATMD is quick to install, fairly compact, and produces a dramatic reduction in peak floor accelerations. The ATMD is expensive; "the hardware components alone have a total cost of $21,300 for a single control circuit" (Hanagan 1995). For a typical 30

ft x 30 ft bay, the overall cost would be approximately $24 per square foot. ATMDs require a continuous source of power, maintenance, and repair.

Ohta et al. (1996) experimentally investigated the use of a semi-active TVA, utilizing an electro-rheological (ER) damper, to reduce floor vibration. The ER fluid is "a suspension containing small particles that are uniformly distributed through the dielectric oil. The apparent viscosity of the fluid is variable due to the strength of the applied electric field" (Ohta et al. 1996). The electric field causes the particles in the suspension to become electrified and chained with one another due to dielectric polarization. The fluid has a quick response to electrical variation.

A mass damper was constructed. An enclosure encases a mass, resting on a spring. A hollow void on each side of the mass is filled with ER fluid. The TMD was tested to establish its modal characteristics, using a slow sweep produced by a shaker. The damping ratio was 8% and the natural frequency 5.15 Hz. Damper hysteretic response and force versus electric field were developed by fixing the ER damper in a horizontal position under a table and exciting a shaker that is attached to the top of table with a sine wave. "The load and displacement were measured with a load cell and a non-contact sensor respectively" (Ohta et al. 1996). An empirical equation for damper force versus voltage per millimeter plot was established.

Analytical and experimental tests were conducted. Further relationships involving the control policy, optimum control force, and the control voltage are given. Experimentally, a beam was "forcibly vibrated" (Ohta et al. 1996). Numerical simulations were performed and compared favorably to the experimental testing. Both displacement and acceleration showed good correlation to experimental measurements. Figures are provided to demonstrate the effectiveness of the ERTMD, but no numbers are provided for a comparative improvement over the passive system.

Seiler et al (2002) shows the effectiveness of a magneto-rheological damper in a Den Hartog model tuned-mass damper to reduce vibration of a footbridge in Forchheim, Germany through computer simulations. A non-linear numerical model of system established by Occhiuzzi et al (2002) to simulate the response of the footbridge subjected

to wind and pedestrians loads. These results are directly compared to the system with no TMD, a passive TMD, and semi-active TMD.

The footbridge in Forchheim, Germany is a typical light frame, low stiffness, structural system. The footbridge deck is supported by eight steel cables that stretch down from a 30 m pylon. The deck is composed of wooden planks. The total span is 117.5 m.

Numerical simulation was performed to produce the dynamics of the system. The natural frequencies ranged from 1 to 3.5 Hz and justified with experimental testing. The system was optimized passively and the passive damper was simply replaced by a magneto-rheological damper. Simulation showed that at the optimal level, the semi-active system did not show any reduction beyond passive. Mass was added to the system to simulate to the maximum pedestrian occupancy. The semi-active system showed an accommodation of the magnetorheological-damper's control policy to mitigate off-tuning and keep the footbridge response around the tuned passive response, unlike the passive system that became off-tuned.

Collette (2002) implemented a passive TMD to reduce the annoying floor vibration for an assembly of suspended footbridges and meeting boxes. The system is composed of three footbridges that span 28 m between two concrete buildings. Cables connected to roof girders suspend the footbridge on each side and along its length. The footbridges are connected to the meeting boxes.

The system dynamics were determined experimentally. The natural frequency of the mode, at was 4.7 Hz, had a large measured acceleration. This corresponds to the in phase vibration of the footbridge and meeting box with a peak accelerations of 0.86 % g and 0.3 % g respectively when excited by walking at the second harmonic. The ISO recommended comfort criteria were used for the allowable acceleration response.

Two vertical passive TMDs were implemented to reduce the vibration. Using a mass of about 1000 kg, corresponding to a mass ratio of about 0.5%, the optimum parameters were determined using the method suggested by Den Hartog (1947). After installation, the TMDs were adjusted and resulted in a mass of 910 kg, 4.5 Hz natural frequency, and 14% damping ratio.

Post installation measurements were performed with an individual walking at 2.35 Hz. The peak footbridge acceleration was reduced to 0.57 % g; and the meeting box to 0.13 % g. These peak weighted accelerations were doubled to account for larger footbridge occupancy. These values of acceleration also satisfied the comfort criteria established by ISO.

Hatanaka and Kwon (2002) implemented a passive tuned mass damper to reduce excessive vibration levels of a footbridge. This footbridge spanning 47.7 m has a low distributed mass (11.2 kN/m) and stiffness. The natural frequency of the system is 1.84 Hz, and the damping ratio is 1.1%.

The response of the system was measured as a person walked across the footbridge with a metronome set at 1.84 Hz. The peak velocity was 3.97 cm/sec.

Numerical simulation with a passive TMD was performed on the two-degree of freedom system representing the footbridge and TMD. Walking was simulated with a semi-sine wave function which showed a close correspondence to the measured response of the footbridge. The mass of the TMD was determined by plotting the peak velocity response versus the mass ratio of the system. A mass ratio of 1% showed the largest reduction and was a conservative estimate. The TMD was attached to the underside of the footbridge within the space created by the railing. The mass, stiffness, and damping were placed on a linear guide so that the TMD would vibrate vertically. An air spring was used as a damper.

Post installation and fine-tuning of the TMD in field revealed a reduction in footbridge velocity. The system damping increased to 0.14, (12.7 times the original measured bare damping). The peak velocity decreased from 3.97 cm/s to 0.75 cm/s. The RMS velocity reduced from 2.81 cm/s to 0.53 cm/s. This is an 81% reduction from the uncontrolled system.

1.3 Magnetorheological damper

Originating in the 1940s magneto-rheological (MR) fluids are defined as a suspension containing micron-sized, magnetizable particles in oil. The consistency of the fluid is typically similar to motor oil. If used in a sponge, it is more like light grease.

Application of a magnetic field transforms the fluid into a semi-solid in milliseconds. Removal of the magnetic field returns the fluid to its initial state. The degree of change is proportional to the applied magnetic field. Application of magnetic field "causes the MR fluid in the matrix to develop a yield strength and resist shear motion" (Chrzan and Carlson 2001).

Magneto-rheological dampers are very robust and has several positive traits. MR dampers "enable low-cost, controllable fluid applications by eliminating the need for most of the high-cost components normally associated with a fluid filled device." They are "appropriate for less demanding, low-force applications where a high degree of control is desired." The fluid is implemented to circumvent typical problems associated with fluids. The MR fluid is "not susceptible to gravitational settling or sedimentation of MR fluid suspension" and the "base oil is chosen to have a low vapor pressure to minimize any evaporation" (Chrzan and Carlson 2001).

According to Carlson and Weiss (1994) MR dampers has several advantages over their electro-rheological counterparts. ER fluids are susceptible to inadequate performance if subjected to impurities (such as water) during the manufacturing process. They require high-voltage power supplies in order to control the ER fluids. The required power supplies have a low availability; and therefore, a high cost. Safety regulations pertaining to high-voltage sources dampen the use of ER in a commercial market demanding a large volume at low market prices. Magneto-rheological fluids are high strength, low viscosity, require a low-voltage source, and are stable over a broad temperature range.

1.4 Purpose of Research

The purpose of this research is to establish the effectiveness of tuned-mass-dampers using semi-active control magneto-rheological dampers to mitigate annoying floor vibrations. Both analytical and experimental studies are performed to understand the effects of incorporating the semi-active-TMDs to reduce vibration.

1.5 Scope of Research

For the analytical investigation a closed form solution of a passive pendulum tuned mass damper (PTMD) and a numerical integration routine for the semi-active PTMD were employed. In addition, a comparative analysis between the two systems to mitigate floor vibration is conducted. Optimization routines are used to establish the design parameters of the PTMD that minimize the reduction in floor vibration. Both, the time-history and frequency spectra are used.

Experimentally, a magneto-rheological damper is incorporated into a PTMD and the response of a 8 ft x 30 ft laboratory floor is measured. The main focus is on the ability of the semi-active PTMD to reduce the footbridge acceleration induced by walking and heel drops, as compared to its equivalent passive counterpart. In addition, the performance of the semi-active PTMD, when subjected to off-tuning, is studied.

CHAPTER 2

ANALYTICAL INVESTIGATION

2.1 Overview

To gain insight into the experimental behavior and to perform a comparative study of the performance of semi-active versus passive systems implemented on the experimental floor (presented in Chapter 3), analytical formulations of the system dynamics for each of the respective systems are developed and presented. An equation of motion for a simplified two-degree of freedom model of the PTMD and floor is developed; a closed-form, non-dimensional, acceleration response equation is given only for the passive system; and to model the piece-wise linear behavior of the semi-active tuned mass damper, Runge-Kutta integration routine is coupled with the displacement-based ground-hook control policy. These were implemented in an optimization routine to find the minimum peak response. Systematic variation of each of the system parameters from this minimum point (off-tuning) is presented. The reduction of the experimental PTMD to a simplified point-mass pendulum model is also presented.

2.2 System Representation

2.2.1 Establishment of an Appropriate Shape Function

To check the validity of the pendulum model (rigidity assumption), the changes in the mode shape based on variation of the spring and flexural stiffness are studied. This understanding is important to devise an appropriate shape function for the system.

The shape functions, given by Equation 2.1 and 2.2, are obtained from the static deflection equations of a propped, pinned-end cantilever beam. They are superimposed for an overall approximation of the mode shape due to the inertial mass, Figure 2.1.

$$f(x_1) = \frac{-w(L-l_s)^2 x_1}{12EIl_s}(l_s^2 - x_1^2) + \frac{-wx_1}{24EI}(l_s^3 - 2l_s x_1^2 + x_1^3) + \frac{-R_s x_1}{kl_s} \qquad (2.1)$$

$$h(x_2)=\frac{wx_2}{24EI}\left[4(L-l_s)^2 l_s+6(L-l_s)^2 x_2-4(L-l_s)x_2^2+x_2^3\right]+\frac{wl_s^3 x_2}{24EI}+\left[\frac{\frac{-R_s L}{kl_s}+\frac{R_s}{k}}{L-l_s}x_2-\frac{R_s}{k}\right] \quad (2.2)$$

Where

E = modulus of elasticity of the beam

I = moment of inertia of the beam

L = total length of beam

l_s = distance to spring measured from pin support

k = stiffness of the spring

R_s = force reaction at spring

w = distributed load per unit length of the beam

x_1 = variable distance measured from the pin support to the spring location

x_2 = variable distance measured from the spring location to the end of the beam

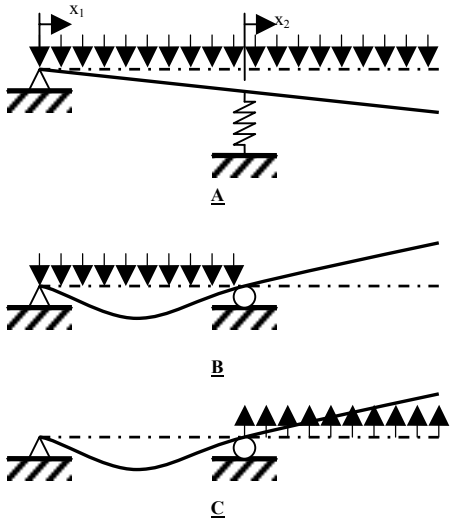

Figure 2.1 – Static Deflected Shapes

A general form of Equations 2.1 and 2.2 are given by 2.4 and 2.5 via substitution of the assumption and Equation 2.3. Figure 2.2 demonstrates the shape function of the

system for various values of, γ. By inspection, increasing the spring stiffness and beam length result in a more dominant contribution to deflection from flexural stiffness of the beam and vice versa. This is summarized by Equation 2.3. Therefore, for large ratios, greater than 5, the flexural contribution should be taken into account in the mode shape. For smaller ratios, the beam can be considered to deflect as a rigid.

$$\gamma = \frac{kL^3}{EI}; \quad \text{where, } l_s \cong 0.5L \tag{2.3}$$

$$f(a) = -\frac{a}{192} * (3\gamma - 16\gamma a^2 + 8\gamma a^3 + 384); \quad 0 \le a \le 0.5 \tag{2.4}$$

$$h(b) = -\frac{1}{192} * (16b^3 - 8b^4 - 5b - 12b^2)\gamma - (2b+1); \quad 0 \le b \le 0.5 \tag{2.5}$$

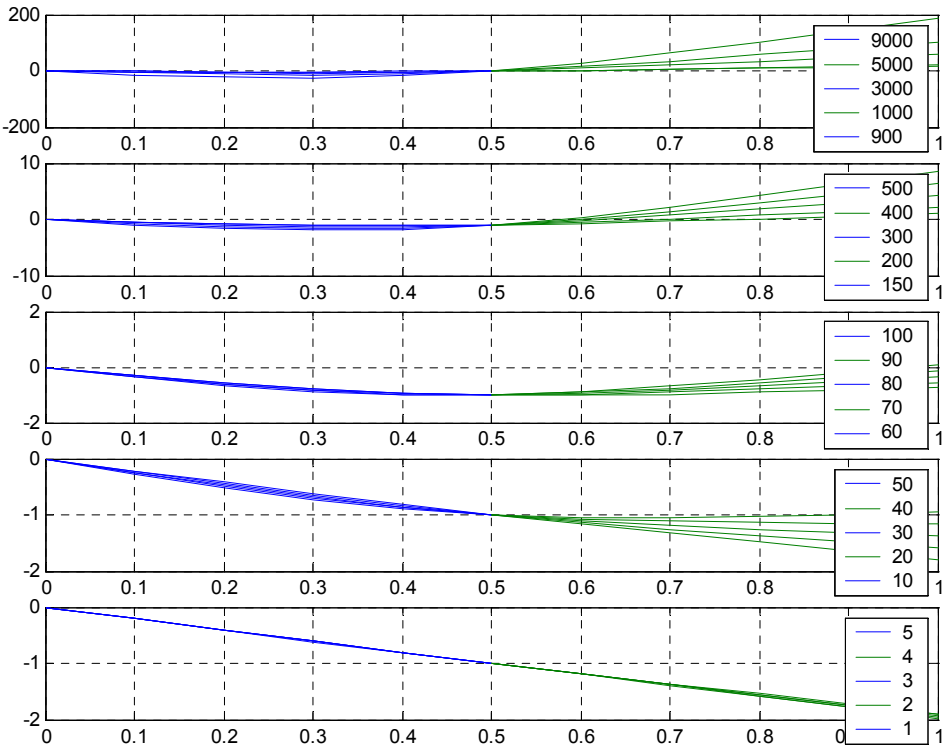

Figure 2.2 – Static Deflected Shape (Equations 2.4 and 2.5) for Various Values of γ

$$\psi(x) = \frac{x}{L} \tag{2.6}$$

Equation 2.6 is recommended for values of γ less or equal to 11. This limit is established for a mode shape that is within 10% of a linear mode shape.

2.2.2 Pendulum Model

The appropriate shape function is implemented with Rayleigh's Quotient, Equation 2.7, to obtain the fundamental frequency of the system.

$$f_n = \frac{1}{2\pi}\sqrt{\frac{\int_0^L EI(x)[\psi''(x)]^2\,dx + \sum_{i=1}^{N} k_i[\psi(x_i)]^2}{\int_0^L m(x)[\psi(x)]^2\,dx + \sum_{j=1}^{N} M_j[\psi(x_j)]^2}} \tag{2.7}$$

Where

f_n = natural frequency of the system, i.e. the rate of energy transfer between the stiffness (potential energy) and mass (kinetic energy)

$EI(x)$ = flexural rigidity in the system

$\sum_{i=1}^{N} k_i[\psi(x_i)]^2$ = summation of the produce of the discrete spring stiffness(s) and shape function evaluate at the respective location

$m(x)$ = distributed mass in the system

$\sum_{j=1}^{N} M_j[\psi(x_j)]^2$ = summation of the produce of the discrete lumped mass(s) and shape function evaluate at the respective location

The following figures provide insight into the geometry and distribution of mass and stiffness for the experimental PTMD shown in Chapter 3. Figure 2.3 shows a PTMD used to quell floor vibrations; it utilizes the pendulum configuration for operation. Figure 2.4 provides a plan and elevation of the system. Figure 2.5 is the dynamic model that reflects the distribution of mass and stiffness approximately and used in conjunction with Rayleigh's method.

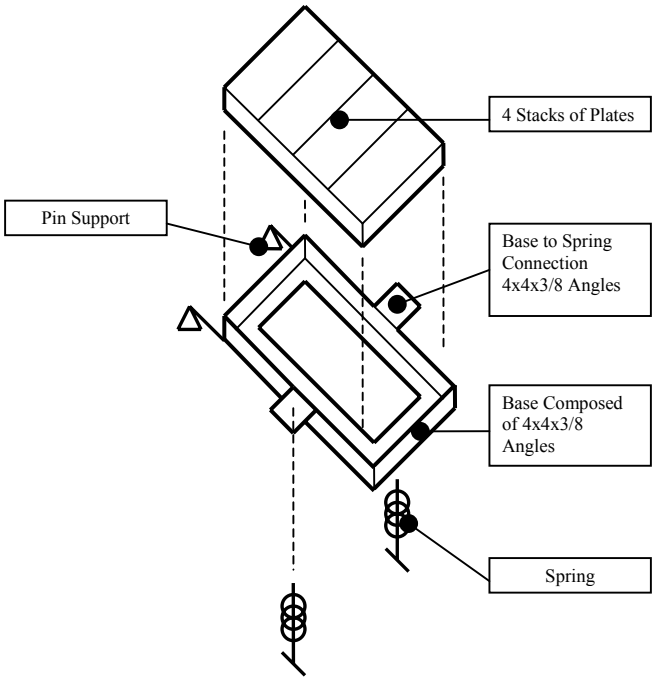

Figure 2.3- Pendulum Tuned Mass Vibration Absorber (ESI Inc. 1970)

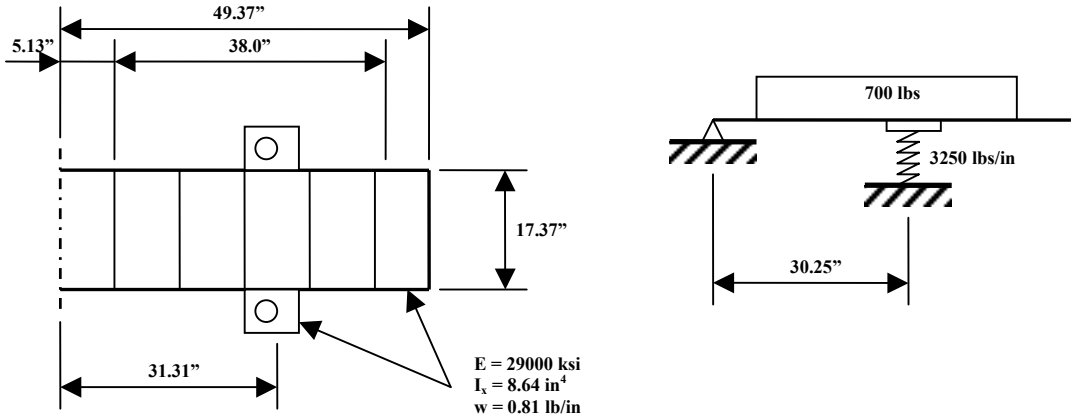

Figure 2.4 - PTMD (ESI Inc. 1970) Plan (left) and Elevation (right)

The model is assumed to be rigid since the ratio, γ, is 1.56. This is low ratio; therefore Equation 2.6 will be used for the shape function. The calculated natural frequency for this system configuration is 6.956 Hz, Equation 2.8. (This is a very good approximation of the measured frequency, approximately 6.95 Hz presented in Chapter 3.)

$$f_n = \frac{1}{2\pi}\sqrt{\frac{\int_0^L EI(x)[\psi''(x)]^2\,dx + k[\psi(l_s)]^2}{\int_0^L m_1(x)[\psi(x)]^2\,dx + \int_{l_o}^{l_o+l_p} m_2(x)[\psi(x)]^2\,dx + M_1[\psi(l_{M1})]^2 + M_2[\psi(l_{M2})]^2 + M_3[\psi(l_{M3})]^2}} = 6.956\,Hz \qquad (2.8)$$

$g = 386$ in./s^2
$l_o = 5.13$ in.
$l_p = 38$in.
$l_s = 30.25$ in.
$w_{bar} = 0.81$ lbs/in.
$W_{plates} = 700$ lbs
$m_1(x) = 2*w_{bar} / g = .004$ lbs s^2/in.
$m_2(x) = W_{plate} / (g*l_p) = 0.048$ lbs s^2/in.
$k = 3250$ lbs/in.
$E = 29000$ ksi
$I = 8.64$ in.^{4}
$M_1 = w_{bar*}17.37$ in./g $= 0.036$ lbs
$M_2 = w_{bar*}2*6$ in./g $= 0.025$ lbs
$M_3 = M_1$

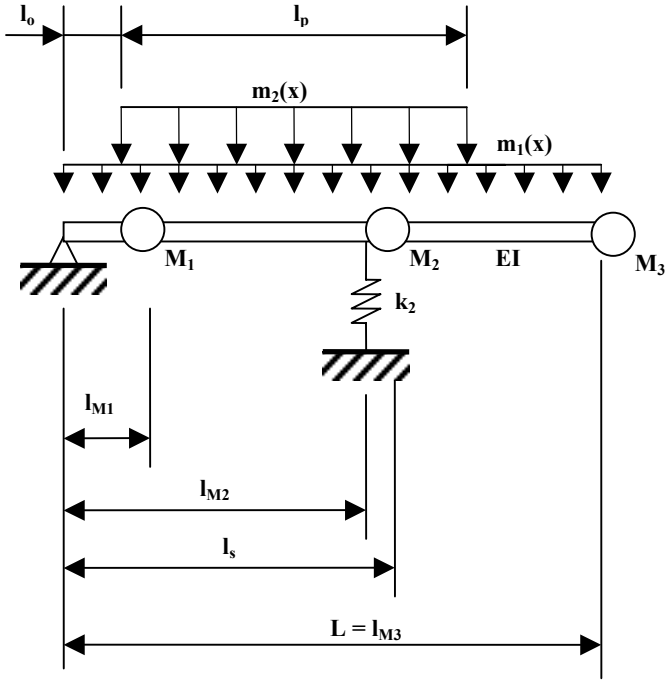

Figure 2.5 – Distributed Mass Single-Degree-of-Freedom Pendulum Model

2.2.3 Equivalent SDOF Model of the PTMD

The effective mass, Equation 2.9, of the PTMD is given from the denominator of Rayleigh's Quotient, Equation 2.8.

$$M_{eff} = \int_0^L m_1(x)[\psi(x)]^2 dx + \int_{l_o}^{l_o+l_p} m_2(x)[\psi(x)]^2 dx + M_1[\psi(l_{M1})]^2 + M_2[\psi(l_{M2})]^2 + M_3[\psi(l_{M3})]^2 \tag{2.9}$$

The shape function given by Equation 2.6 is substituted into Equation 2.9. It is simplified to obtain Equation 2.10.

$$M_{eff} = \frac{m_1 L}{3} + \frac{m_2}{3L^2}(3l_p l_o^2 + l_p^3 + 3l_p^2 l_o) + M_1 \frac{l_o^2}{L^2} + M_2 \frac{l_{sa}^2}{L^2} + M_3 \tag{2.10}$$

Figure 2.5, presents a system with a distributed mass. To simplify the model based on the understanding of its dynamic response, presented in the previous section; a relationship is developed to associate the distributed mass system to a lumped mass system, Figure 2.6. The distribution of mass between the two models is different, but using the effective mass given by Equation 2.10, the system can be represented equivocally.

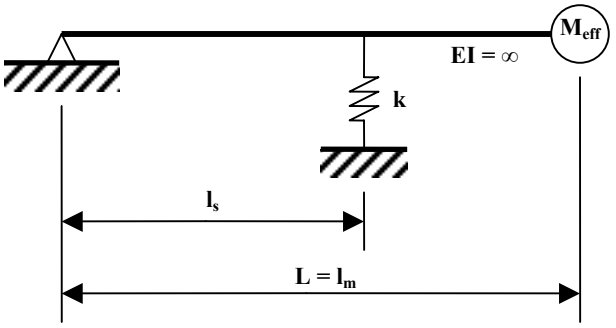

Figure 2.6 – Equivalent Single Degree of Freedom Model of PTMD

The natural frequency of this system is given by Equation 2.11

$$f_n = \frac{1}{2\pi}\sqrt{\frac{kl_s^2}{M_{eff} l_M^2}} = 6.956\ Hz \tag{2.11}$$

$g = 386$ in./s^2
$l_o = 5.13$ in.
$l_p = 38$in.
$l_s = 30.25$ in.

$L = 49.37$ in.
$l_m = L$
$w_{bar} = 0.81$ lbs/in.
$W_{plates} = 700$ lbs
$m_1(x) = 2*w_{bar} / g = .004$ lbs s^2/in.
$m_2(x) = W_{plate} / (g*l_p) = 0.048$ lbs s^2/in.
$k = 3250$ lbs/in.
$M_1 = w_{bar*}17.37$ in./g $= 0.036$ lbs s^2/in.
$M_2 = w_{bar*}2*6$ in./g $= 0.025$ lbs s^2/in.
$M_3 = M_1$
$M_{eff} = 0.639$ lbs s^2/in. (from Equation 2.49)

It is interesting to note that approximately 30% of the total PTMD mass is effective.

2.2.4 Equations of Motion

To develop an analytical representation for the experimental system, several assumptions were made for this model. The pendulum arm is rigid, and the pendulum mass is at the tip of the arm. The floor vibrations are small (0.001 in. to 0.01 in.); therefore, small angle theory can be applied. The PTMD length to the experimental floor span ratio is small; thus, the PTMD acts at the center of mass of the experimental floor. This configuration will inhibit the first bending mode of vibration.

A two-degree of freedom model of the experimental floor and passive PTMD is shown in Figure 2.7. The mass, stiffness, and damping of the floor is represented by m_1, k_1, and c_1 respectively. The mass, stiffness, and damping of the passive PTMD is represented by m_2, k_2, and c_2 respectively.

A closed-form solution is developed for the two-degree of freedom passive PTMD and floor system. This model will serve two purposes. First, it will allow insight into the passive dynamic interaction of the two systems. Secondly, it will serve as a base-line comparison to the semi-active model. A closed form solution cannot be developed for the semi-active PTMD and floor system because of the time dependency of the damper control policy. Runge-Kutta numerical routine is implemented with the equation of motion of the two-degree-of-freedom system and control policy to obtain accelerance response of the floor.

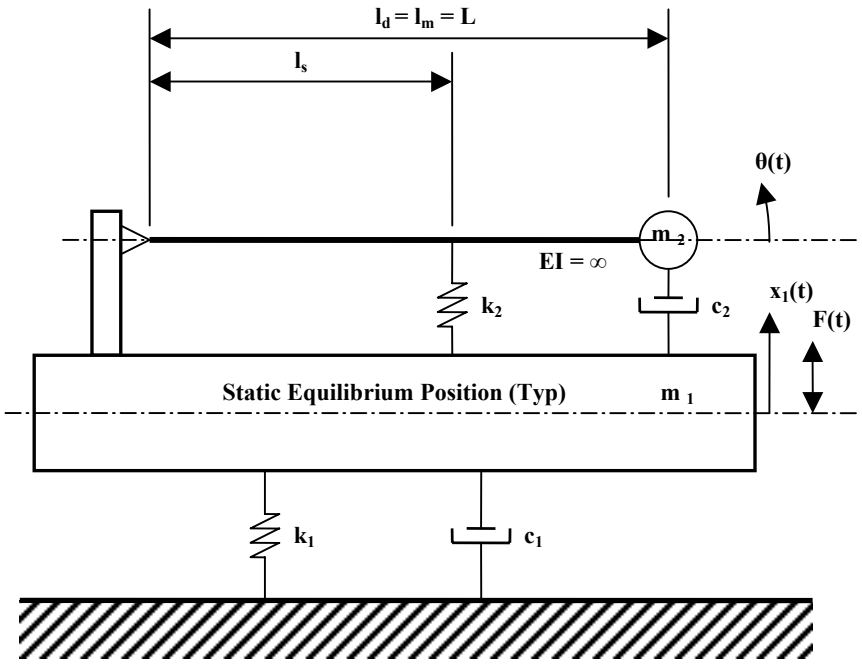

Figure 2.7 – Passive Two Degree of Freedom Model

Analytical mechanics was used to capture the dynamics of the two-degree-of-freedom system representing the floor and the PTMD. These methods are based on calculating the kinetic and potential energy of the system as a whole. Then a minimum is sought. The general coordinates x_1 and θ are assigned to the floor and PTMD respectively.

Equation 2.12 is Rayleigh's treatment of the nonconservative damping force; this comes with the assumption that the damping is proportional to the velocity (Inman 1994).

$$F = \frac{1}{2}c_1\dot{x}_1^2 + \frac{1}{2}c_2(l_d\dot{\theta})^2 \tag{2.12}$$

The partial derivative of Equation 2.12 with respect to the generalized coordinates, x_1 and θ, to obtain the generalized forces, Equation 2.13 and 2.14:

$$F_1 = F(t) - \frac{\partial F_{c1}}{\partial \dot{x}_1} = F(t) - c_1\dot{x}_1 \tag{2.13}$$

$$F_2 = 0 - \frac{\partial F_{c2}}{\partial \dot{\theta}} = -c_2 l_d^2\dot{\theta} \tag{2.14}$$

Equation 2.15 describes the velocity of the PTMD mass, m_2. The fixed-axis rotation and vertical translation of the pendulum mass are represented in this formula. A local coordinate system, at the center of mass of M_{eff}, is defined by "*i*" being the vertical component, and "*j*" the horizontal component. It should be noted, that mass moment of inertia is intrinsically included in Equation 2.16 (Hibbeler 2001):

$$\vec{v}_2 = [\dot{x}_1 + l_m\dot{\theta}\cos(\theta)]i + [-l_m\dot{\theta}\sin(\theta)]j \tag{2.15}$$

The kinetic and potential energies of the system are given by Equations 2.16 and 2.17, respectively.

$$T = \frac{1}{2}m_1\dot{x}_1^2 + \frac{1}{2}m_2\vec{v}_2 \cdot \vec{v}_2 \tag{2.16}$$

$$U = \frac{1}{2}k_1x_1^2 + \frac{1}{2}k_2(l_s\theta)^2 \tag{2.17}$$

Equations 2.16 and 2.17 are substituted into the Lagrange equations, Equation 2.18 and 2.19, and the respective derivatives are taken for each generalized coordinates:

$$\frac{\partial}{\partial t}\left(\frac{\partial T}{\partial \dot{x}_1}\right) - \frac{\partial T}{\partial x_1} + \frac{\partial U}{\partial \dot{x}_1} \tag{2.18}$$

$$\frac{\partial}{\partial t}\left(\frac{\partial T}{\partial \dot{\theta}_1}\right) - \frac{\partial T}{\partial \theta_1} + \frac{\partial U}{\partial \dot{\theta}_1} \tag{2.19}$$

The result from Equation 2.18 is equated to the result of Equation 2.13, and the result of Equation 2.19 is equated to Equation 2.14. These are shown in Equations 2.20 and 2.21, respectively.

$$k_1x_1 - m_2l_m\dot{\theta}^2\sin(\theta) + (m_1+m_2)\ddot{x}_1 + m_2l_m\ddot{\theta}\cos(\theta) = F(t) - c_1\dot{x}_1 \tag{2.20}$$

$$k_2l_s^2\theta + m_2l_m\ddot{x}_1\cos(\theta) + l_m^2m_2\ddot{\theta} = -c_2l_d^2\dot{\theta} \tag{2.21}$$

Assuming θ is small, Equations 2.20 and 2.21 simplify to Equations 2.22 and 2.23.

$$(m_1+m_2)\ddot{x}_1 + m_2l_m\ddot{\theta} + c_1\dot{x}_1 + k_1x_1 = F(t) \tag{2.22}$$

$$m_2l_m\ddot{x}_1 + l_m^2m_2\ddot{\theta} + c_2l_d^2\dot{\theta} + k_2l_s^2\theta = 0 \tag{2.23}$$

Equations 2.22 and 2.23 are the system equations of motion and their matrix form is:

$$\begin{bmatrix} m_1+m_2 & l_mm_2 \\ l_mm_2 & l_m^2m_2 \end{bmatrix}\begin{Bmatrix} \ddot{x}_1 \\ \ddot{\theta} \end{Bmatrix} + \begin{bmatrix} c_1 & 0 \\ 0 & l_d^2c_2 \end{bmatrix}\begin{Bmatrix} \dot{x}_1 \\ \dot{\theta} \end{Bmatrix} + \begin{bmatrix} k_1 & 0 \\ 0 & l_s^2k_2 \end{bmatrix}\begin{Bmatrix} x_1 \\ \theta \end{Bmatrix} = \begin{Bmatrix} F(t) \\ 0 \end{Bmatrix} \tag{2.24}$$

2.2.5 Closed-Form Solution

Neglecting the transient response, our interest is focused on the steady-state forced vibration (Den Hartog 1947). It is assumed that the harmonic motion of the system is at a frequency equal to the forcing frequency. This assumption is mathematically expressed by Equations 2.25 and 2.26.

$$x_1 = Xe^{at} \tag{2.25}$$

$$\theta = \theta e^{at} \tag{2.26}$$

where,

$a = i\omega$; (a is the s-plane variable and used to avoid confusion with the subscript "s")

(2.27)

For a sinusoidal force, the following relationship can be developed via Euler's equations.

$$F(t) = F_o \sin(\omega t) = F_o e^{at} \tag{2.28}$$

Equations 2.25 through 2.28 are substituted into Equation 2.24 and respective derivatives computed.

$$\begin{bmatrix} m_1 + m_2 & l_m m_2 \\ l_m m_2 & l_m^2 m_2 \end{bmatrix} \begin{Bmatrix} a^2 X e^{at} \\ a^2 \theta e^{at} \end{Bmatrix} + \begin{bmatrix} c_1 & 0 \\ 0 & l_d^2 c_2 \end{bmatrix} \begin{Bmatrix} aXe^{at} \\ a\theta e^{at} \end{Bmatrix} + \begin{bmatrix} k_1 & 0 \\ 0 & l_s^2 k_2 \end{bmatrix} \begin{Bmatrix} Xe^{at} \\ \theta e^{at} \end{Bmatrix} = \begin{Bmatrix} F_o e^{at} \\ 0 \end{Bmatrix} \tag{2.29}$$

After simplifications:

$$\begin{bmatrix} m_1 + m_2 & l_m m_2 \\ l_m m_2 & l_m^2 m_2 \end{bmatrix} \begin{Bmatrix} a^2 X \\ a^2 \theta \end{Bmatrix} + \begin{bmatrix} c_1 & 0 \\ 0 & l_d^2 c_2 \end{bmatrix} \begin{Bmatrix} aX \\ a\theta \end{Bmatrix} + \begin{bmatrix} k_1 & 0 \\ 0 & l_s^2 k_2 \end{bmatrix} \begin{Bmatrix} X \\ \theta \end{Bmatrix} = \begin{Bmatrix} F_o \\ 0 \end{Bmatrix} \tag{2.30}$$

The matrix multiplication result in:

$$X[(m_1 + m_2)a^2 + c_1 a + k_1] + \theta(l_m m_2 a^2) = F_o \tag{2.31}$$

$$X(l_m m_2 a^2) + \theta(l_m^2 m_2 a^2 + l_d^2 c_2 a + l_s^2 k_2) = 0 \tag{2.32}$$

Using Cramer's rule and substitution of "a", Equation 2.27, we can obtain the complex values for X, Equation 2.36, and θ, Equation 2.37.

$$D = \det \begin{vmatrix} ((m_1 + m_2)(i\omega)^2 + c_1(i\omega) + k_1) & (l_m m_2 (i\omega)^2) \\ (l_m m_2 (i\omega)^2) & (l_m^2 m_2 (i\omega)^2 + l_d^2 c_2 (i\omega) + l_s^2 k_2) \end{vmatrix} \tag{2.33}$$

$$D_X = \det \begin{vmatrix} F & (l_m m_2 (i\omega)^2) \\ 0 & (l_m^2 m_2 (i\omega)^2 + l_d^2 c_2 (i\omega) + l_s^2 k_2) \end{vmatrix} \tag{2.34}$$

$$D_\theta = \det\begin{vmatrix} ((m_1+m_2)(i\omega)^2 + c_1(i\omega) + k_1) & F \\ (l_m m_2 (i\omega)^2) & 0 \end{vmatrix} \tag{2.38}$$

$$X = \frac{D_X}{D} \tag{2.36}$$

$$\theta = \frac{D_\theta}{D} \tag{2.37}$$

To obtain the response in dimensionless form, the following relationships, Equations 2.38 through 2.45, are presented and substituted into Equation 2.36 and 2.37.

$$f = \frac{\omega_2}{\omega_1} \tag{2.38}$$

$$\omega_1 = \sqrt{\frac{k_1}{m_1}} \tag{2.39}$$

$$\omega_2 = \frac{l_s}{l_m}\sqrt{\frac{k_2}{m_2}} \tag{2.40}$$

$$g = \frac{\omega}{\omega_1} \tag{2.41}$$

$$x_{st} = \frac{F}{k_1} \tag{2.42}$$

$$\mu = \frac{m_2}{m_1} \tag{2.43}$$

$$\xi_1 = \frac{c_1}{2m_1\omega_1} \tag{2.44}$$

$$\xi_2 = \frac{c_2 l_d^2}{2m_2 l_m^2 \omega_2} = \frac{c_2}{2m_2\omega_2} \qquad (l_d = l_m, \text{ see Figure 2.8}) \tag{2.45}$$

For brevity, the final result is presented here.

$$\frac{X}{x_{st}} = \frac{(f^2 - g^2) + i(2\xi_2 gf)}{((1-g^2)(f^2-g^2) - fg^2(4\xi_1\xi_2 + f\mu)) + i(2g)(\xi_2 f(1-g^2-g^2\mu) + \xi_1(f^2-g^2))} \tag{2.46}$$

$$\left|\frac{X}{x_{st}}\right| = \sqrt{\frac{(f^2-g^2)^2+(2\xi_2 gf)^2}{[(1-g^2)(f^2-g^2)-fg^2(4\xi_1\xi_2+f\mu)]^2+[(2g)(\xi_2 f(1-g^2-g^2\mu)+\xi_1(f^2-g^2)]^2}} \tag{2.47}$$

$$\frac{l_m\theta}{x_{st}} = \frac{g^2}{((1-g^2)(f^2-g^2)-fg^2(4\xi_1\xi_2+f\mu))+i(2g)(\xi_2 f(1-g^2-g^2\mu)+\xi_1(f^2-g^2))} \tag{2.48}$$

$$\left|\frac{l_m\theta}{x_{st}}\right| = \sqrt{\frac{(g^2)^2}{[(1-g^2)(f^2-g^2)-fg^2(4\xi_1\xi_2+f\mu)]^2+[(2g)(\xi_2 f(1-g^2-g^2\mu)+\xi_1(f^2-g^2)]^2}} \tag{2.49}$$

$$\left|\frac{m_1 A}{F_o}\right| = g^2\left|\frac{X}{x_{st}}\right| \tag{2.50}$$

The displacement response factor for the floor is equivalent to a damped main system with a TMD as presented by Setareh and Hanson (1992). However, the response of the PTMD is not the same. Equation 2.48 is similar to the relative motion of the 2DOF of floor and TMD. Floor vibration control pertains to mitigation of the floor acceleration. The acceleration response factor is given by Equation 2.50.

2.3 Implementation of the MR into the PTMD

Implementation of an MR damper into the PTMD to replace the passive damper is simple. Figure 2.8 shows the substitution into Figure 2.7. Equations 2.51 and 2.52 are the resulting equations of motion implemented into the Runge-Kutta numerical routine with the control policy given in the Section 2.4.

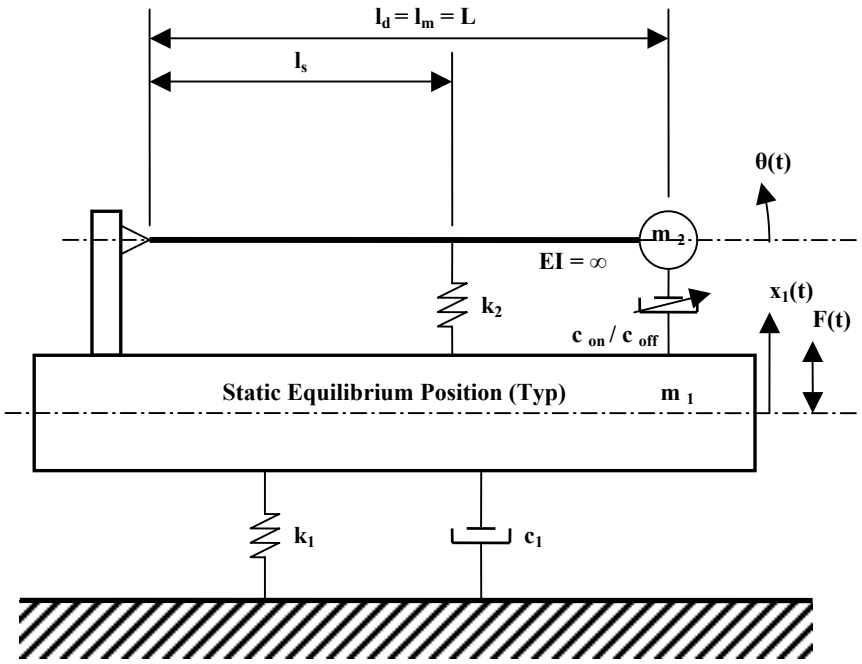

Figure 2.8 – Semi-active Two Degree of Freedom Model

$$\begin{bmatrix} m_1 + m_2 & l_m m_2 \\ l_m m_2 & l_m^2 m_2 \end{bmatrix} \begin{Bmatrix} \ddot{x}_1 \\ \ddot{\theta} \end{Bmatrix} + \begin{bmatrix} c_{on} & 0 \\ 0 & l_d^2 c_{on} \end{bmatrix} \begin{Bmatrix} \dot{x}_1 \\ \dot{\theta} \end{Bmatrix} + \begin{bmatrix} k_1 & 0 \\ 0 & l_s^2 k_2 \end{bmatrix} \begin{Bmatrix} x_1 \\ \theta \end{Bmatrix} = \begin{Bmatrix} F(t) \\ 0 \end{Bmatrix} \tag{2.51}$$

$$\begin{bmatrix} m_1 + m_2 & l_m m_2 \\ l_m m_2 & l_m^2 m_2 \end{bmatrix} \begin{Bmatrix} \ddot{x}_1 \\ \ddot{\theta} \end{Bmatrix} + \begin{bmatrix} c_{off} & 0 \\ 0 & l_d^2 c_{off} \end{bmatrix} \begin{Bmatrix} \dot{x}_1 \\ \dot{\theta} \end{Bmatrix} + \begin{bmatrix} k_1 & 0 \\ 0 & l_s^2 k_2 \end{bmatrix} \begin{Bmatrix} x_1 \\ \theta \end{Bmatrix} = \begin{Bmatrix} F(t) \\ 0 \end{Bmatrix} \tag{2.52}$$

Equation 2.51 represents the on-state of the system, and Equation 2.52, the off-state.

2.4 MR Control Policy – Displacement Based Ground-hook

To regulate the dynamics of the magneto-rheological damper, a control policy is required. Koo (2003) demonstrates that the on-off displacement-based ground hook (DBG) control policy suppressed the vibration of the main structure more than on-off velocity-based, continuous velocity-based, and continuous displacement-based ground hook control. On-off DBG will be implemented throughout this research, analytically and experimentally.

On-off DBG dictates the state of the magnetic field applied to the MR fluid via feed back from dynamics of the floor and PTMD. If the product of the floor

displacement, x_1, and the relative velocity, $\dot{x}_{12}$, between the PTMD and floor is equal to or greater than zero, the magnetic field is applied; this is referred to as the "on-state" of the MR damper. Otherwise, the magnetic field is removed; this is the "off-state" of the MR damper. This policy is given by Equation 2.53 (Koo 2003). The dynamic range of the MR damper is shown in Figure 2.9.

$$x_1\dot{x}_{12} \geq 0 \rightarrow c_{on}\text{; Equation 2.50} \quad (2.53)$$

$$x_1\dot{x}_{12} < 0 \rightarrow c_{off}\text{; Equation 2.51}$$

Where,

$$\dot{x}_{12} = \dot{x}_1 - \dot{x}_2 \quad (2.54)$$

Koo also presents the practical limits of the MR damper and those are implemented in the section on optimization of the PTMD, as well as, the provided damping force from the MR damper given in Chapter 3.

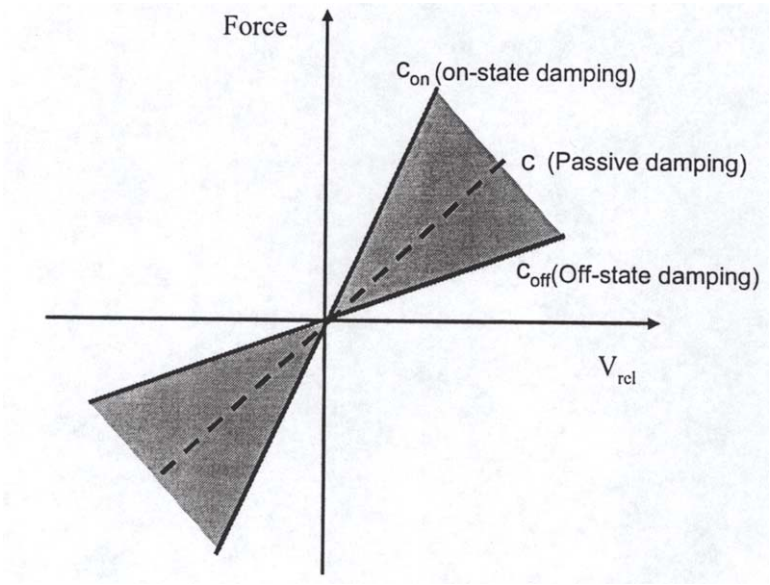

Figure 2.9 – MR Damper Damping Range (Koo 2003)

2.5 Analytical Simulation

To simulate the benefits obtained from implementing MR technology into a tuned mass damper to reduce floor vibrations, analytical routines are composed that encompass

the measured parameters of the floor and allow for simulation of the given system. The passive PTMD is compared with the semi-active PTMD.

The numerical integration of the equations of motion is carried out using the fourth-order Runge-Kutta method (Recktenwald 2000). This integration will serve to produce the accelerations, velocities, and displacements of the system under an applied excitation to the floor. The time step of the numerical simulation, dictated by the rate the MR damper can switch (100 Hz), is 0.01 seconds (Koo et al. 2003).

2.5.1 System Parameters

Table 2.1 presents the floor and PTMD parameters obtained from the experimental data as given in Chapter 3, respectively. These parameters are used to compare the performance of the PTMD using the semi-active and passive dampers and the remaining analytical investigations of the system. The experimental section gives insight into the origin of these parametric values.

Table 2.1 – Lab Floor and PTMD System Modal Parameters

Floor Parameters		
$W_{Flr,tot}$	14.339	kips
$m_{1,efff}$	0.020	k s^2 / in.
k_1	27.5	k / in.
c_1	0.015	k in./ s
ω_1	46.5	rad / s
f_{n1}	7.4	Hz
ξ_1	0.008	
TMD Parameters		
$m_{2,efff}$	0.000639	k s^2 / in.

2.6 Optimization

To establish the expected reduction in the acceleration of the lab test floor when the PTMD is introduced into system, an optimization routine is implemented in conjunction with the developed system equation of motion, Equation 2.24. The ratio of the peak response of the floor without the PTMD to the peak response with the PTMD is used for comparing the analytical and experimental results.

The optimization routine utilizes a function, *fmincon*, provided in Matlab's optimization toolbox. This function serves to find the minimum peak response of the system. For simplicity, this function performs an iterative analysis on the equation of motion via adjusting specific parameters of the system until the minimum peak accelerance response is located.

To simulate the experimental tuning of the PTMD in the lab, the optimization routine will affect the following parameters of the PTMD. The mass ratio, Equation 2.43, will be held constant. The frequency ratio, Equation 2.38, will be modified by the location of the spring along the PTMD arm. The damping location will remain constant, but the amount of damping provided will be varied via the damping ratio, Equation 2.45.

2.6.1 Optimization of the Passive PTMD Design Parameters

The optimization of the passive system is presented in this section. Equation 2.24 is the equation of motion when using passive PTMD with the closed form solution given by Equation 2.50. With the parameters in Table 2.2 (mass ratio and floor damping ratio) and the closed form solution given by Equation 2.50, the floor acceleration response without and with the optimized PTMD are shown in Figures 2.10 and 2.11 respectively.

Without the PTMD, the floor has a peak response of 62.5; with the optimized PTMD this reduces to 7.1. This represents an 88.7% decrease in the peak acceleration response of the floor via implementing a PTMD into the floor system. The optimized parameters are given in Table 2.2.

Table 2.2 - Passive PTMD Optimized Parameters

ξ_1	0.00800
μ	0.0319
f	0.9852
ξ_2	0.1106
peak value	7.1

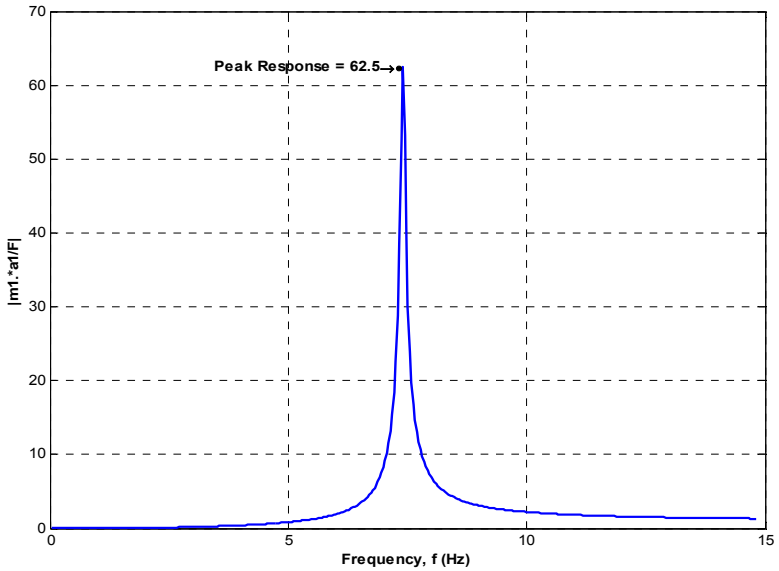

Figure 2.10 – Acceleration Response Factor of Floor without PTMD

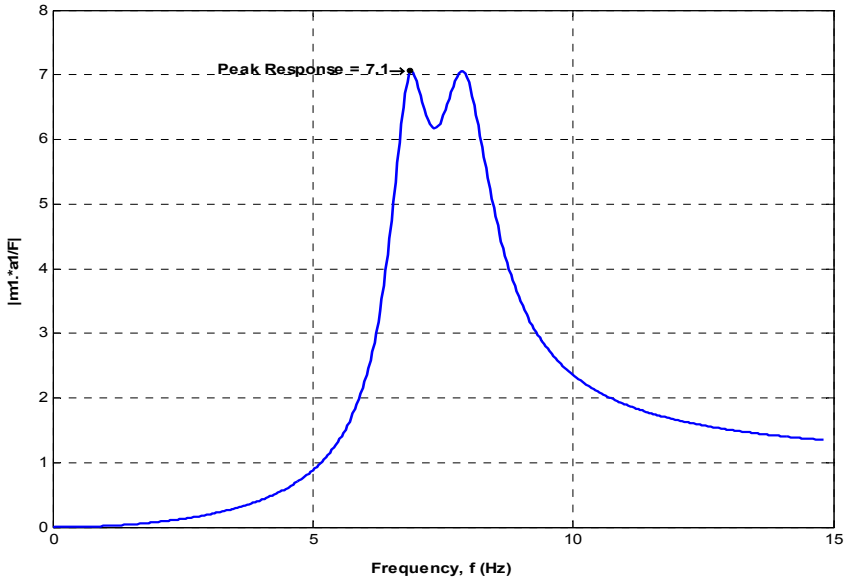

Figure 2.11 - Acceleration Response Factor of Floor with the Passive PTMD

2.6.2 Optimization of the Semi-Active PTMD Design Parameters

The optimization of the semi-active system is presented in this section, and the result is shown in Figure 2.12. The general equation of motion of the system is given by Equations 2.51 and 2.52. The control policy of Equation 2.53 was used to mitigate the state-space damping variable to the respective "on" and "off" values. The fourth-order Runge-Kutta numerical routine is implemented to determine the frequency response of the system for a given set of parameters. A time step of 0.01 seconds, or 100 hertz sampling rate, is used. The PTMD damping is kept constant within each time step of the numerical integration. The floor is excited by a sinusoidal force with constant amplitudes and varying frequencies within a band, which is referred to as a "slow sweep". The steady-state peak amplitude of the time history of the floor response is obtained and plotted with its corresponding frequency to develop the frequency spectrum of the system. The optimization routine monitors the peak response of this function and seeks the minimum (minimum/maximum problem).

Without the PTMD, the floor has a peak response factor of 62.5; it reduces to 6.40 with the optimized PTMD. This represents an 89.8% decrease in the peak acceleration response of the floor via implementing a semi-active PTMD into the floor system to quell floor vibration. The optimized parameters and optimization constraints are in Table 2.3. The boundary conditions reflect the physical limitations of the system.

Table 2.3 - Semi-active PTMD Optimized Parameters

ξ_1	0.00800	
μ	0.0319	
f	1.0137	$\mathbf{0 \le f \le 1.5}$
ξ_{on}	0.7	$\mathbf{0.1 \le \xi_{on} \le 0.7}$
ξ_{off}	0.0596	$\mathbf{0.01 \le \xi_{off} \le 0.09}$
peak value	6.4	

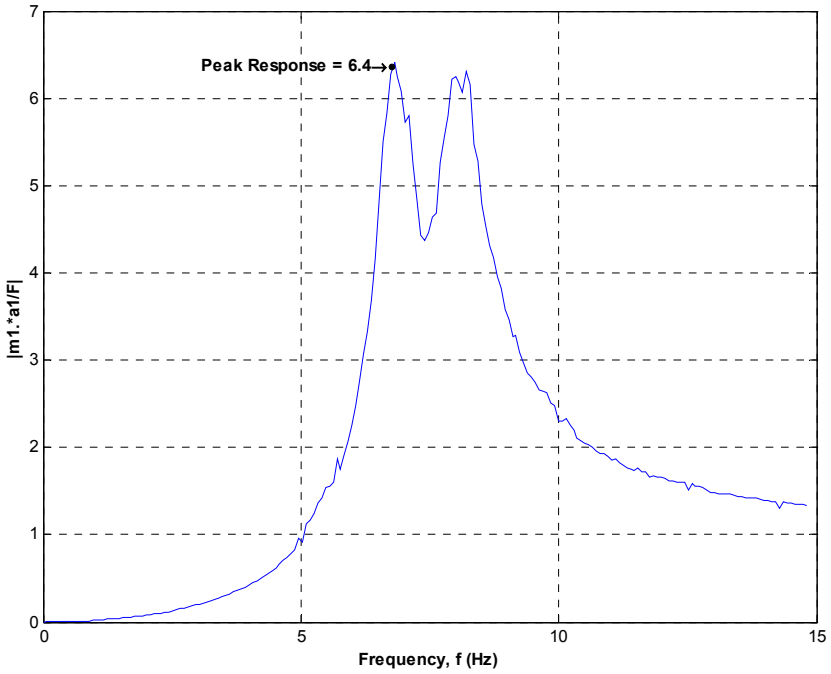

Figure 2.12 - Acceleration Response Factor of Floor with the Semi-Active PTMD

Figure 2.13 shows the extent of the obtained solution for various floors. This figure presents the percent reduction, obtained using a semi-active system in lieu of a passive system, for various mass and damping ratios. The figure demonstrates that for low damping and mass ratios the semi-active system out performs the passive equivalent counterpart. But, the amount of reduction past the passive system is small compared to that already achieved by the passive system which is about 85% typically.

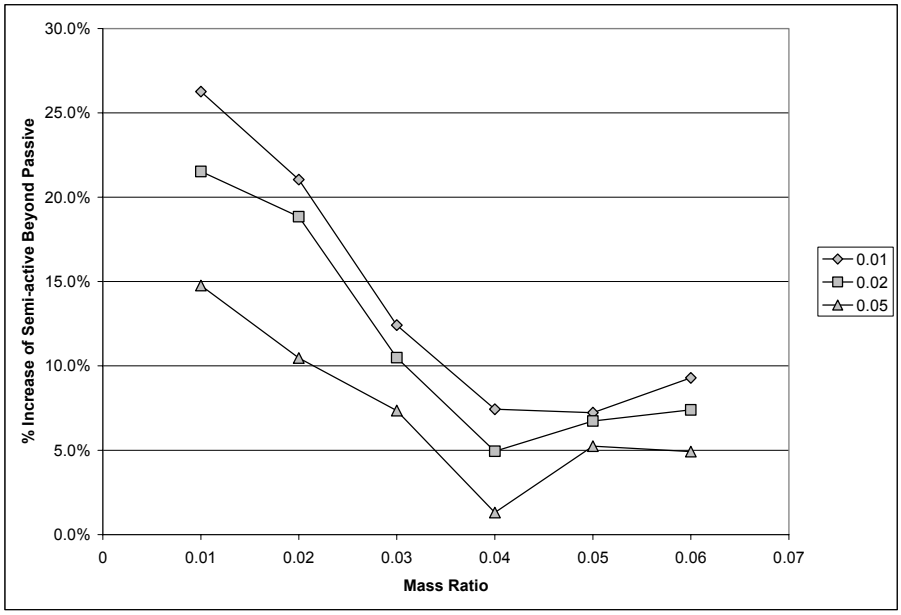

Figure 2.13 - Performance of Semi-active Over Passive for Various Mass and Damping Ratios

2.6.3 Comparison of the Performance of Optimal Passive versus Semi-Active PTMDs

To understand the benefits of using MR technology to reduce the floor acceleration levels; it is worthwhile to compare the optimization results obtained using both passive and semi-active PTMDs. The passive system saw a reduction of 88.7% and the semi-active, 89.8%. The difference is obviously very small. The MR only provides an additional 9% in reduction in the peak response of the floor system beyond passive control. The additional increase is the result using the MR damper is due to the fact that theoretically the damper provides damping when it is needed. For a smaller time step a further decrease would have been seen, because the system would be under an increased level of control. In other words, the damper can switch faster and therefore adapt more readily to the dynamics of the system. If the system was under continuous control, the response would at an ultimate minimum. The analytical system is limited to the experimental switching of the MR, which is 100 Hz.

2.7 Comparison of Off-Tuning Effects for the Passive and Semi-Active PTMDs

Presented in this section is the parametric variation of each of the system parameters - frequency, damping, and mass ratios - to determine their influence on the PTMD effectiveness. This is performed to compare the passive and semi-active systems. Each parameter was reduced to ¼ of its optimum value and increased by twice its optimum value.

For a complete insight into the system response all of the system parameters will be observed. In typical commercial facilities, the mass ratio is decreased from the tuned system due to increases in the floor mass, but it can go either way depending on occupancy, activity, and technology. Floor stiffness is rarely affected and can be a consequence of a structural retrofit or full-height partitions. Damping of a floor can be affected by either of the floor parametric changes within the system. Changing the mass and stiffness of the PTMD is unlikely within the lifespan of the device. PTMD damping can diminish over time with use and exposure to the surrounding environment; however, this is considered as defective equipment and requires replacement.

This section focuses on changes in the floor parameters using the passive and semi-active systems, and the resulting off-tuning effects. For completeness, all the floor parameters will be investigated. In reality, as mentioned previously, changes in the floor mass are the most prevalent in commercial structures.

2.7.1 Variation of the Floor Mass

From the variation of response with respect to changes in floor mass, it is apparent, from Figure 2.14 and 2.15, that when the floor mass is more than optimum the off-tuning effect is more significant than when the floor mass is less than optimum. This is due to changes in the mass ratio as for larger mass ratios the ability of the PTMD to reduce vibrations is much better than when the mass ratio is smaller when subjected to off-tuning.

The overall trend is similar between the two systems. The semi-active PTMD is able to maintain a lower peak accelerance for each parametric variation. Semi-active shows a larger reduction beyond passive for increases of the mass ratio.

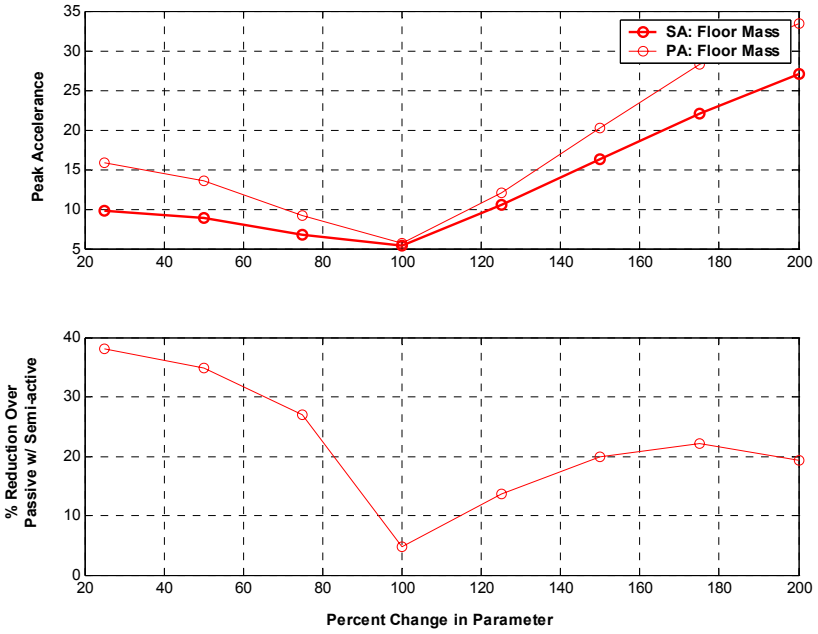

Figure 2.14 – Variation in Peak Response to Changes in Floor Mass

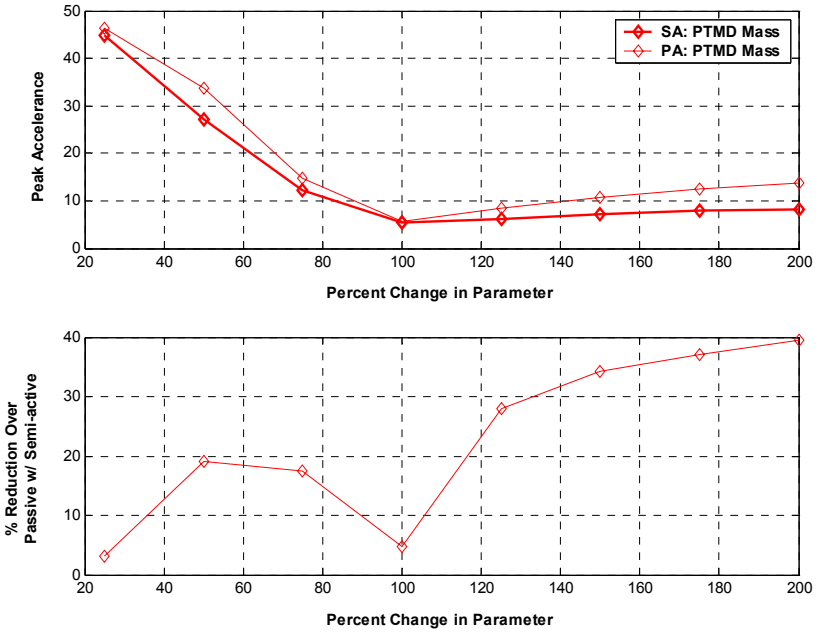

Figure 2.15 – Variation in Peak Response to Changes in PTMD Mass

2.7.2 Variation of the Floor Stiffness

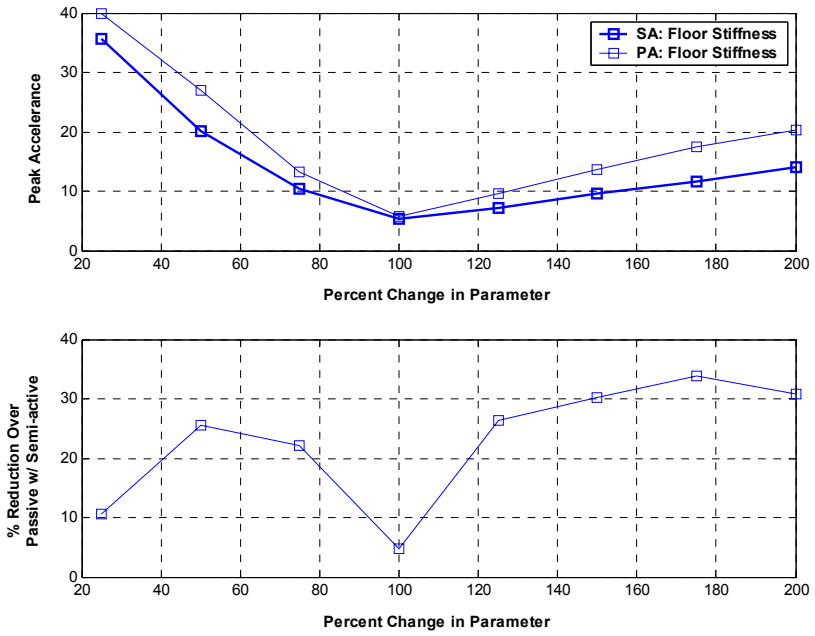

Figure 2.16 – Variation in Peak Response to Changes in Floor Stiffness

As the stiffness of the floor is varied, the frequency ratio varies; therefore, the system becomes off-tuned. Stiffening the floor system reduces the peak accelerance better than if the floor was "softened," or made less stiff. A soft system is easier to excite because less energy is required.

Variations in the PTMD stiffness off tune the system. Increasing the spring's stiffness increases the frequency ratio, but it will eventually become a rigid link and render the PTMD useless. Decreasing the stiffness of the PTMD will decrease the frequency ratio, and it will isolate the PTMD's mass from the floor. Once again, this renders the PTMD ineffective.

The overall trend is similar between the two systems. The semi-active PTMD is able to maintain a lower peak accelerance for each parametric variation. Semi-active shows a larger reduction beyond passive for decreases in the frequency ratio. See Figures 2.16 and 2.17.

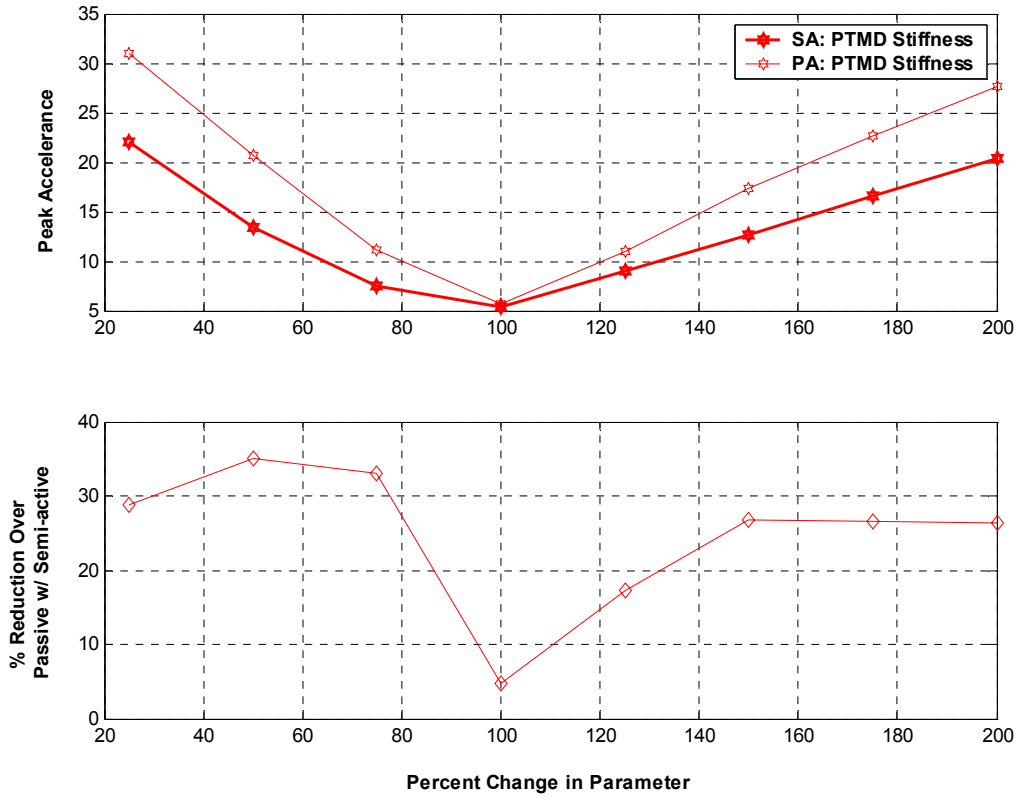

Figure 2.17 – Variation in Peak Response to Changes in PTMD Stiffness

2.7.3 Variation of the Floor Damping

Increasing the floor damping requires more energy to be dissipated; therefore reducing the damping has a larger effect in increasing the peak response from the optimum point. The semi-active and passive systems are similar in their off-tuning responses. Refer to Figure 2.18.

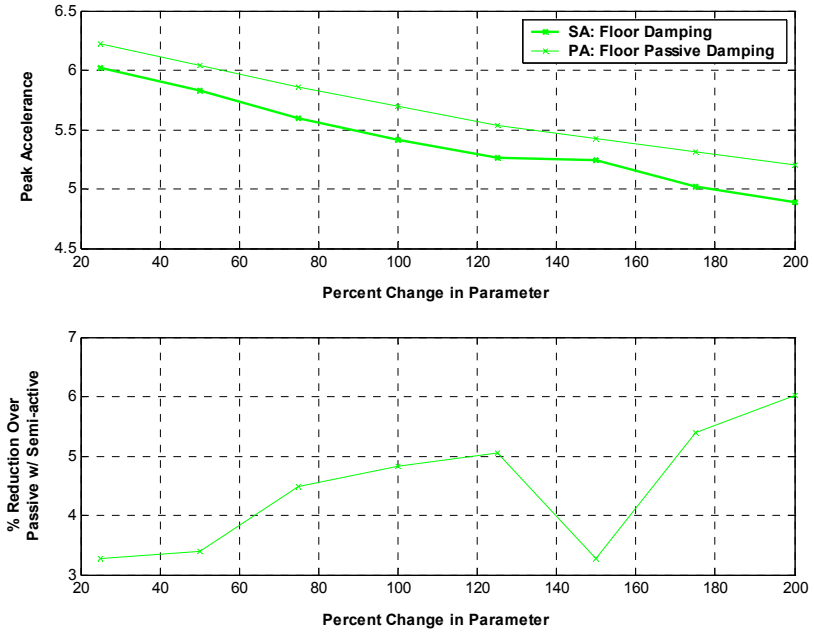

Figure 2.18 – Variation in Peak Response to Changes in PTMD Damping

2.7.4 Variation of PTMD Damping

Figure 2.19 shows the variation of the PTMD damping. The increased response, when reducing the passive damping, is a result of not enough damping. The increased response from adding damping is a result of "lock-up", the damper becomes a rigid link between the sprung mass and floor. An increase in "on" damping results in a continuous decrease in floor peak response. This is attributed to the control policy; the damping is provided only when needed. An increase in response due to a reduction in "on" damping is the result of applying not enough damping to the floor. The increase observed by increasing the "off" damping is a result of the damper approaching a passive device as the "off" damping approaches the "on" damping value. Reduction in the "off" damping results in a decreased floor response as it should. When the "off" state of the damper is implemented in the control policy, the damper is more able to "let go" from the system and not drag the floor past its equilibrium position.

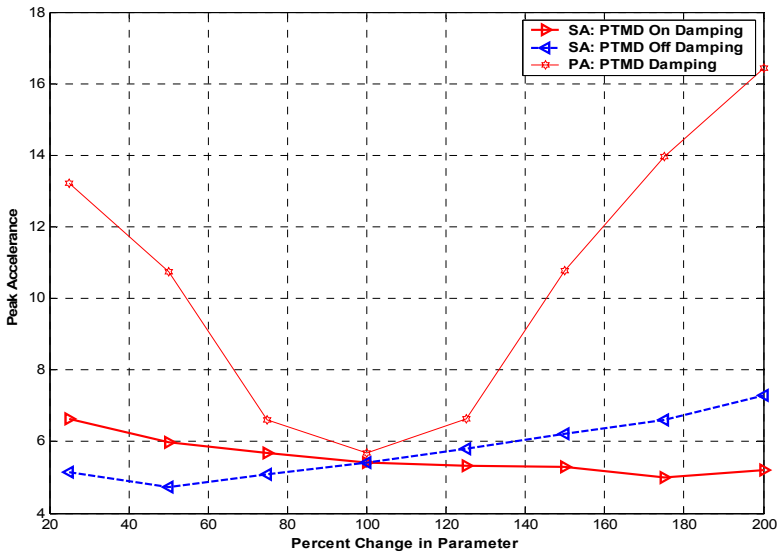

Figure 2.19 – Variation in Peak Response to Changes in PTMD Damping

2.7.5 Floor Response: Overlay of Parametric Studies

Figure 2.20 shows the general comparison of the floor peak acceleration for each parametric variation. Although the other two cases are not predominant in commercial facilities, an increase in the floor damping and stiffness would be preferred over an increase in floor mass. This opposite is true for a reduction in floor stiffness and mass.

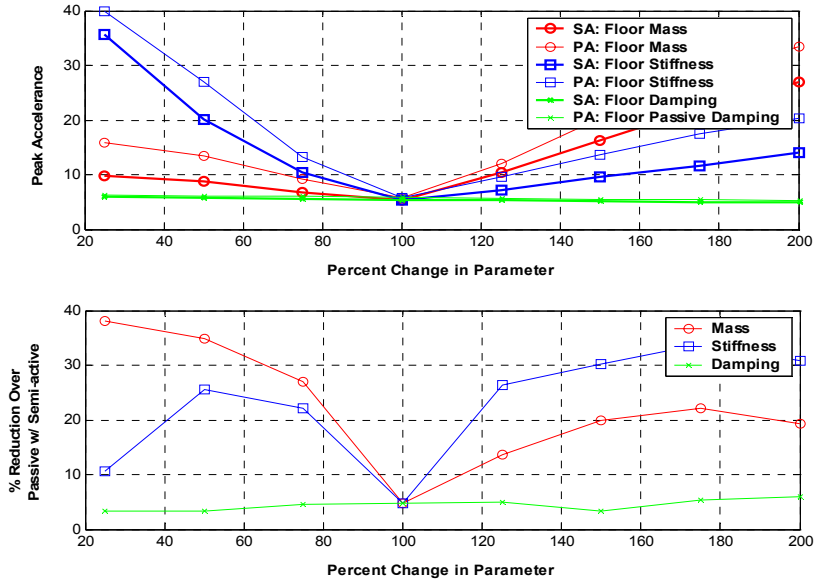

Figure 2.20 – Variation in Peak Response to Changes in Floor Parameters

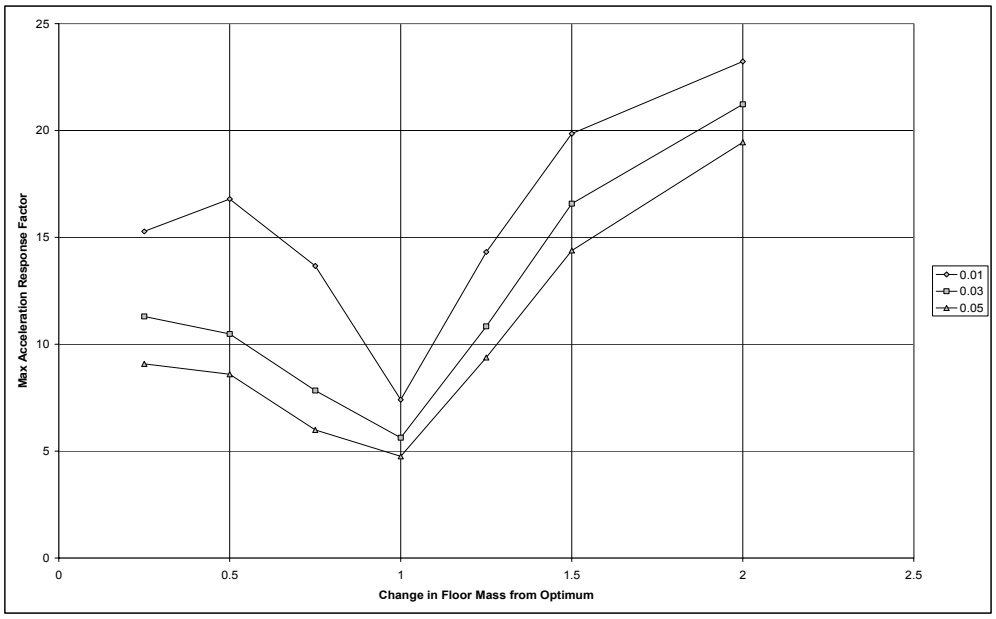

Figure 2.21 – Generalized Variation in Peak Response to Changes in Floor Mass

Figure 2.21 shows the generalized response of the floor with respect to changes in mass for a few of the optimized systems presented in Figure 2.14. Each line has a constant floor damping. The variation in floor mass is the most predominated instance of off-tuning seen in commercial facilities, and this trend is comparable to the experimental floor's response obtained from the previous analytical study.

2.8 Passive versus Semi-Active Walking Response

AISC Steel Design Guide 11 (Murray et al. 1997) provides a forcing function to simulate walking, Equation 2.55. The function is a time dependent harmonic force component which matches the fundamental frequency of the floor:

$$F_i = P\alpha_i \cos(2\pi i f_{step} t) \tag{2.55}$$

For the scope of this research, the first harmonic will be utilized and the AISC Steel Design Guide 11 recommended parameters are substituted into Equation 2.55. For the first harmonic P is equal to 157 lbs; "i" is equal to one, and "α_i" is equal to 0.5. These substitutions result in Equation 2.56 and depicted in time and frequency domains in Figure 2.22.

$$F = 78.5\cos(2\pi f_{step} t) \tag{2.56}$$

where,

F = walking force (lbs)

f_{step} = step frequency (Hz)

t = time (sec)

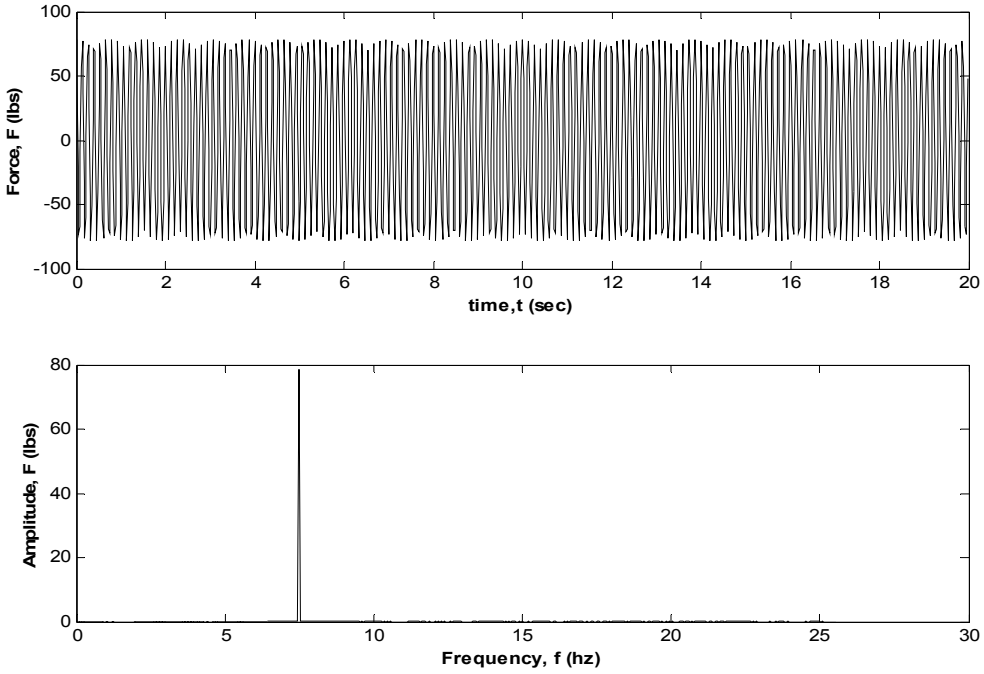

Figure 2.22 – Walking Time and Frequency Spectrums

To give insight into the ability of the MR to reduce floor accelerations, a typical time history for walking is shown in Figure 2.23. The forcing function is given by Equation 2.56. This particular time history represents a 23% reduction in acceleration of the floor's resonant frequency.

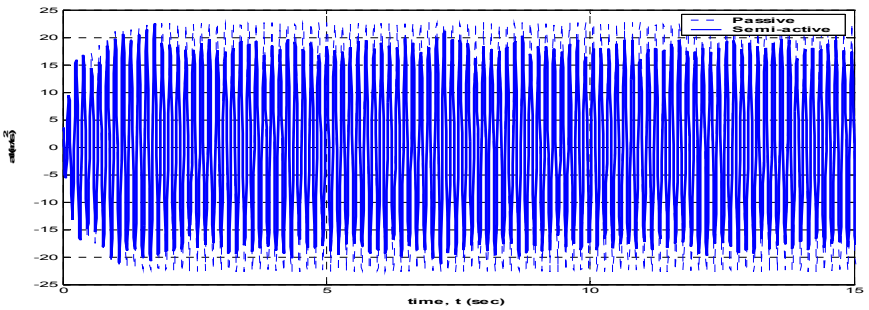

Figure 2.23 - Reduction in Walking Response at Resonance of the Floor using Semi-Active Control of Magneto-rheological Damper.

CHAPTER 3

EXPERIMENTAL INVESTIGATION

3.1 Overview

Experimental evaluation of the ability of the semi-active PTMD to reduce floor acceleration versus its passive counterpart was conducted at the Civil and Environmental Engineering Structures and Materials Lab. An existing 8 ft x 30 ft floor was utilized for the experiment. A pendulum-tuned mass damper (PTMD), provided by ESI Inc., was used for this purpose.

Testing was conducted in three separate stages. The floor accelerations were measured with the bare-floor, the passive PTMD added, and then the semi-active PTMD. The results using passive PTMD serves as the baseline for comparison of the performance of the passive and semi-active PTMDs.

The test focused on the reduction in floor acceleration for the first bending mode of the floor. The examination of the acceleration response of the floor in the frequency domain (accelerance) is the primary tool for evaluation of the system performance. The optimal responses of the floor using passive and semi-active PTMDs are compared. The acceleration time histories for walking and heel drop are also investigated.

The robustness of the semi-active PTMD to off-tuning is presented. The floor's acceleration response due to changes in the floor mass and PTMD spring location are presented. System response to changes in PTMD parameters, both passive and semi-active, is presented. An additional study of the passive and semi-active PTMDs performance when subjected to off-tuning by the addition of a group of people standing, sitting, and standing with knees bent on the test floor is also presented.

3.2 Test Specimens and System Identification

This section establishes components used during the experimental testing. Insight into the floor and PTMD geometry and dynamics are presented along with the overall

system responses. Experimental equipment will be identified, and the overall arrangement of this equipment for passive and semi-active PTMD testing is given.

3.2.1 Floor

The floor is a common slender structural system susceptible to walking vibration. Requirements for floor vibration acceptability are given for floors in the AISC Design Guide 11 (1997).

3.2.1.1 Floor Geometry

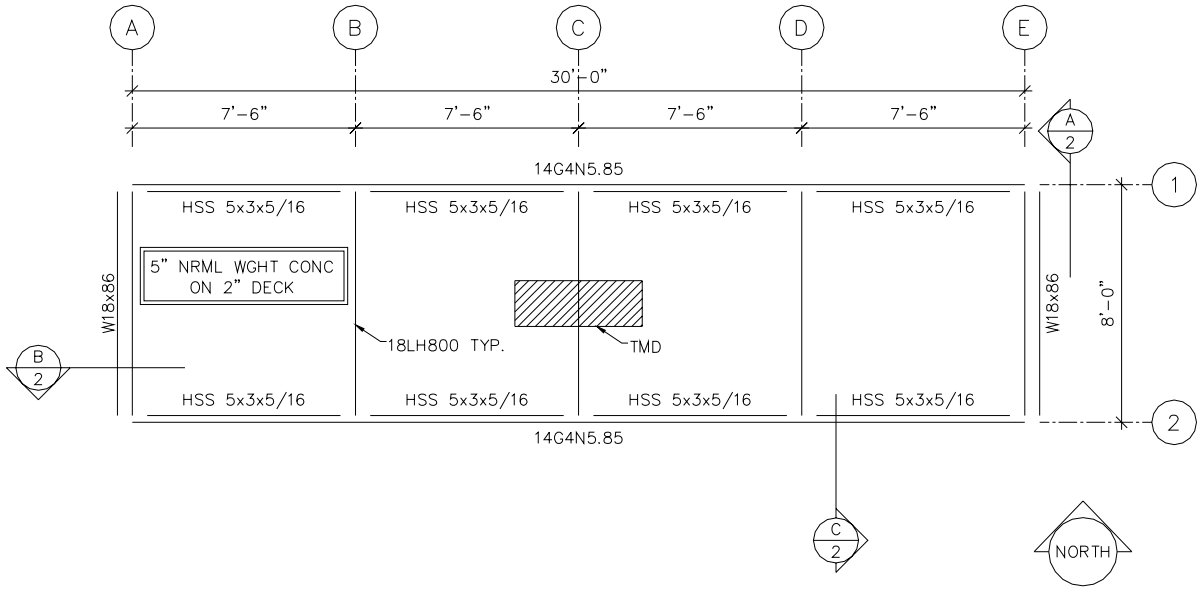

Figure 3.1 – Experimental Floor Plan

The floor, shown in Figures 3.1 through 3.3, is composed of a 2 in. deck with a 5 in. normal-weight concrete slab supported on 18LH800 Vulcraft floor joists at 90 in. on center. The joist-girders are 14G4N5.85 Vulcraft long-span joists and span 30 ft. HSS 5x3x5/16 sections were added between each pair of joists seats in "an attempt to attain full composite action" (Warmoth 2002). The joist-girders are placed on W18 hot-rolled sections without any physical connections. The W18's sit perpendicular to the 30 ft span

and span the 8 ft. width between the joist-girders. No pin connection is made at the supports, just bearing. The joist girder bears on the W18 and the wide-flange section bears on the lab floor.

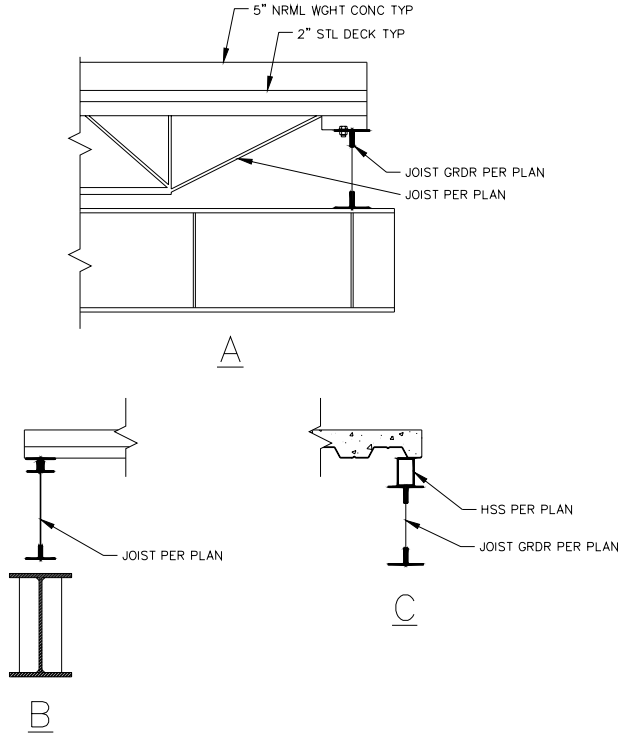

Figure 3.2 – Experimental Floor Sections

Figure 3.3 – Experimental Floor (left) and End Condition (right)

3.2.2 PTMD

The PTMD used in this study is presented in Figure 3.4 which was provided by ESI Engineering. It offers advantages over the standard sprung mass configuration (Den Hartog 1947). The spring position is adjustable, and also the configuration amplifies the inertial force, spring force, and damper force per the distance squared from the support. The shallow geometry allows it to be placed within floor cavities. A disadvantage to the PTMD is the partial effective mass; this is shown analytically in Chapter 2.

Figure 3.4 – Experimental passive PTMD (ESI 1970)

3.2.2.1 PTMD Geometry

Four stacks of steel plates provide the mass. Two springs, one on each side of the PTMD, provide an adjustable stiffness via the attached slotted plate. Each spring is composed of two springs, one inside the other. They act in series at each spring support. Three viscous dashpots are located at the end of the PTMD, opposite the pin support. The dashpots are manufactured by Airpot Inc., Figure 3.5. The specification is given in the appendix.

Figure 3.5 – PTMD Passive Dampers (Airpot Inc.)

A special pin was implemented into this PTMD. It is referred to as a "rigid cross-bar" pin and offers very little friction at the joint. This is significant for two reasons. First, the PTMD can begin to approach the idealization assumed in analytical models. Secondly, this significantly reduced friction found in typical connections and allows the PTMD to respond readily to the floor response and quell vibration more effectively. Any "slop", or friction, will reduce the effectiveness of PTMD and it is a critical point in a PTMD designed to be effective for small displacements.

The "MR sponge damper" was provided by the Lord Corporation. The damper characteristics are discussed in Chapter 2 from page 49. This damper "provides the necessary on-state damping force when energized and has a reasonably low off-state damping" (Koo 2002). An estimate of the required damping force was made and it was decided that it was within the range of operation of the MR damper. Figure 3.6 shows the allowable range that the sponge damper can provide, and by inspection of the figure, it is sufficient.

The MR damper used is shown in Figure 3.7. The electrical leads supply the necessary current across the damper to energize, the grey, absorbent matrix to obtain a desired level of damping. It is an absorbent matrix to contain the MR fluid by capillary action: open-celled foam, felt, or fabric. The sponge, typically polyurethane foam, keeps the MR fluid in the region of the applied magnetic field. The sponge surrounds a steel bobbin and coil, and it is attached to a shaft that moves axially within a hollow shaft. There are no seals or bearings.

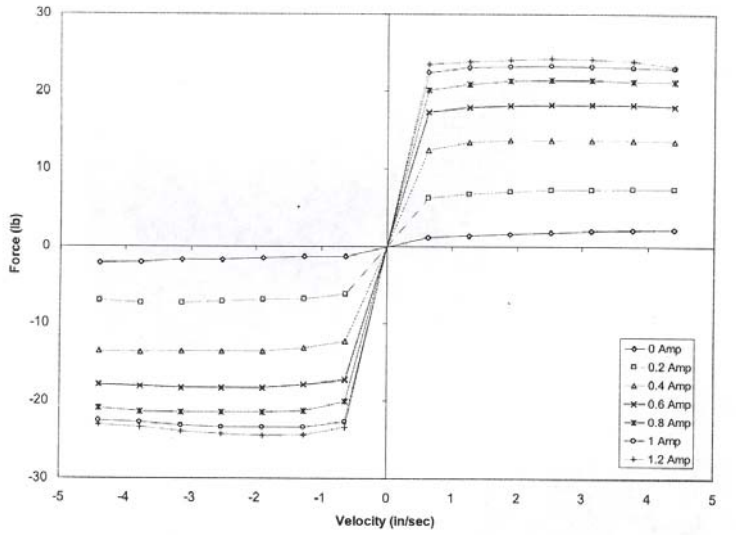

Figure 3.6 – Magneto-rheological Damper Damping Force (Koo et al. 2003)

Figure 3.7 – Magneto-rheological Damper (Courtesy of Lord Corporation)

To accommodate the MR damper, an end plate with clevis was designed. This is presented in Figure 3.8. A second clevis was attached to the floor. The damper is connected via pins at the top and bottom. Washers were placed on either side as infill to prevent any lateral motion of the PTMD as the system vibrated.

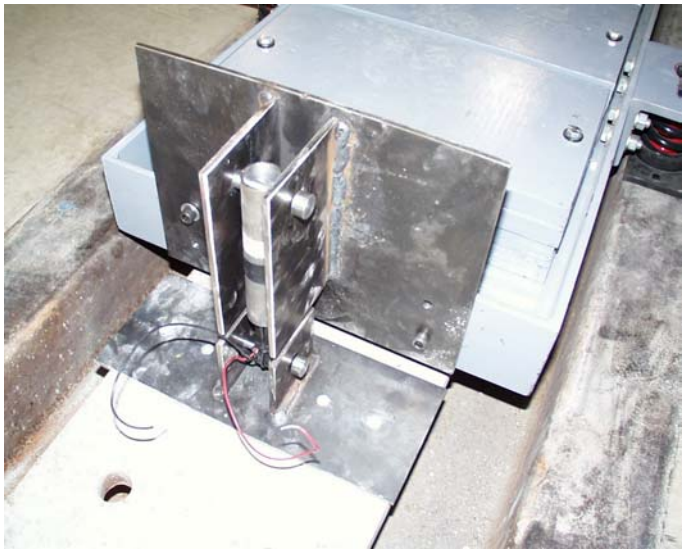

Figure 3.8 – MR Damper Retrofit to PTMD

3.3 Data Acquisition

An impulse force hammer and shaker were used to impart a force on the system. Two accelerometers and a force plate are used to measure the response of the system and the force on the floor respectively. A data acquisition was used for signal processing and monitoring of the system.

A PCB Impulse Force Hammer, Figure 3.9, was used to generate an impulse force. This force excited a desired band of frequency to obtain the frequency response of the system. The force hammer utilizes a piezo-based transducer to capture the imparted force. The sensitivity of the hammer is 0.85 mV/lb.

Figure 3.9 – PCB Impulse Force Hammer

The primary force generator used on the floor was an APS Electro-Seis, Model 400 Shaker, see Figure 3.10. The dynamic mass of the shaker is provided by four blocks weighing 67.4 lbs suspended by rubber bands. The core of the shaker weighs 170.6 lbs for a total shaker weight of 238 lbs. It has a frequency range from 0 to 200 Hz. From 0.10 to 20 Hz the shaker has a force rating of 100 lbs. The floor was typically excited using a chirp swept from 4 to 15 Hz.

Figure 3.10 – APS Electro-Seis, Model 400 Shaker

A chirp is a sinusoidal function with linearly increasing frequency as a function of time. Equation 3.2 is the mathematical model used throughout this research. Typically, the chirp is swept from zero to twice the natural frequency of the floor. It is shown in both and time and frequency in Figure 3.11.

$$F = A\sin(2\pi(\frac{(f_{\max} - f_{\min})\cdot t}{T} + f_{\min})t) \tag{3.2}$$

where,

F = Chirp (lbs)

A = Amplitude of chirp signal (lbs)

f_{min} = frequency of chirp signal at time zero (Hz)

f_{max} = frequency of the chirp signal at time, T; typically twice the frequency of interest (Hz)

t = time (sec)

T = number of periods or time interval (sec)

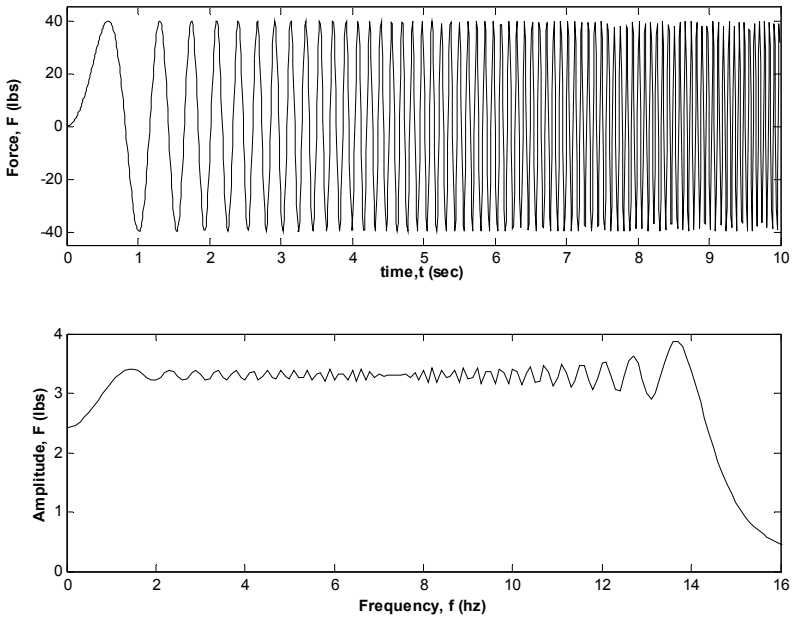

Figure 3.11 – Chirp Time and Frequency Spectrums

An APS, Dual-Mode, Model 144 Amplifier, Figure 3.12, was used to send a voltage signal to the shaker. The desired voltage signal, in the form a desired force excitation, was provided by the data acquisition system. The desired voltage signal is sent to the amplifier that converts this signal to current to drive the shaker.

Figure 3.12 – APS Dual-Mode, Model 144 Amplifier (APS Inc.)

To measure the response of the floor, two PCB 393C accelerometers were used. A typical accelerometer is shown in Figure 3.13. The accelerometers are piezo-based, have a sensitivity of 1 V/g and can cover a frequency range from 0.025 to 800 Hz.

Figure 3.13 – PCB 393C Accelerometer (PCB Inc.)

The force plate was used to measure the input force of the shaker and heel-drops. See Figure 3.14. The force plate is supported by 3 cantilevered load cells radiating outward to the 3 corners of the triangular, aluminum plate. It uses a summing amplifier +shown in Figure 3.15. The switch controls the amount of gain on the signal used. Appendix K gives the various sensitivities and gains attainable from this device.

Figure 3.14 – Force Plate

Figure 3.15– Summing Amplifier

Data analysis was accomplished with Matlab's SigLab hardware and software. The SigLab analyzer has four channels. It provided the means to record and analyzes the response of the system via its capability for real-time signal processing. See Figure 3.16.

When the MR damper was implemented into the system and semi-active control used, additional equipment was required. A 12 and 15 V power supplies were used. A multi-meter was used to monitor the output current to the MR damper. A current circuit driver (Koo et al., 2003) was installed in the circuit. It amplified "the current in the output signal of the control policy." Two additional accelerometers were used for the control policy. They are PCB capacitive accelerometers and each had its own power supply. These two accelerometers brought the floor and PTMD responses for feedback information to the control policy in dSPACE.

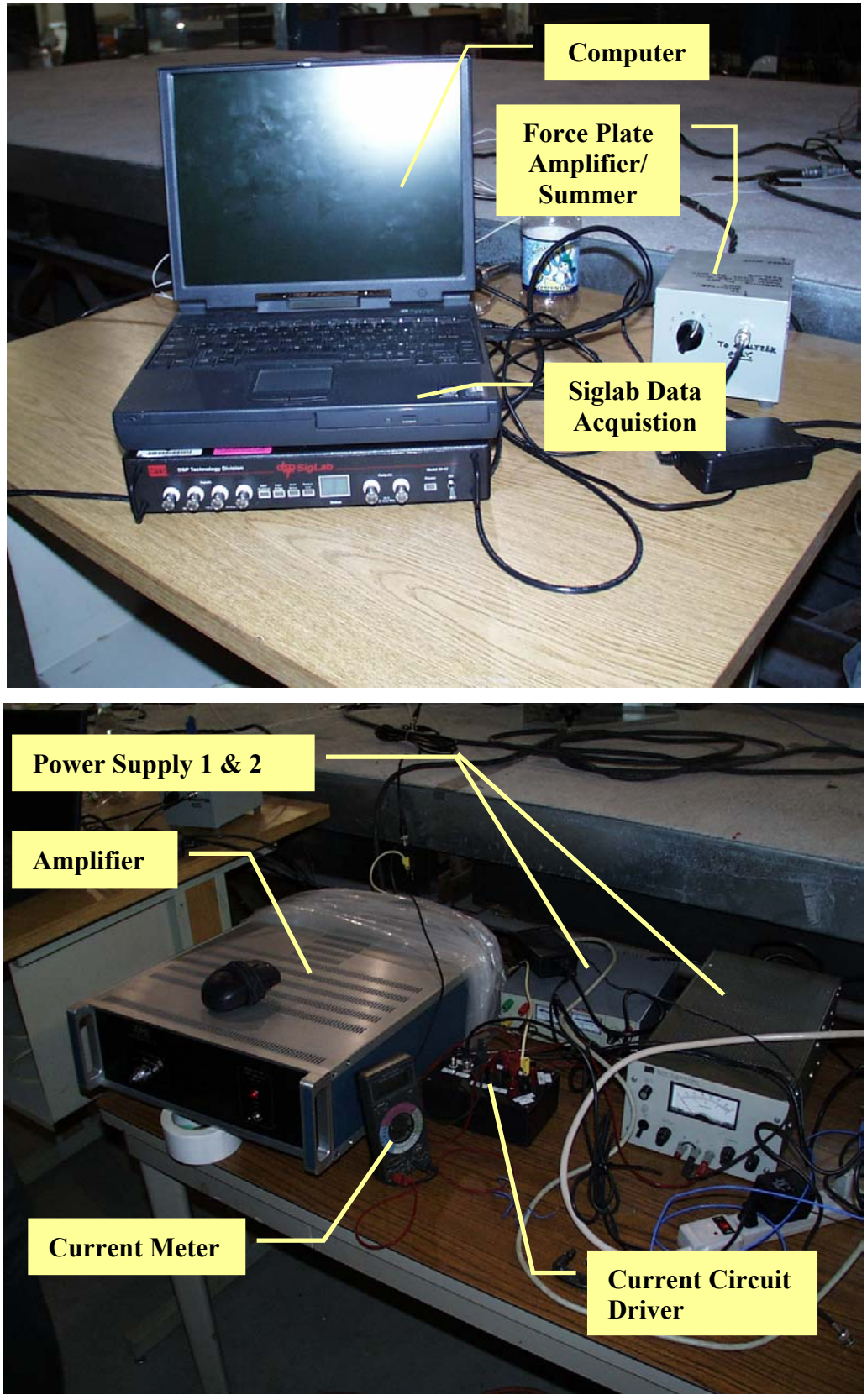

Figure 3.16 – Semi-Active Experimental Test Equipment

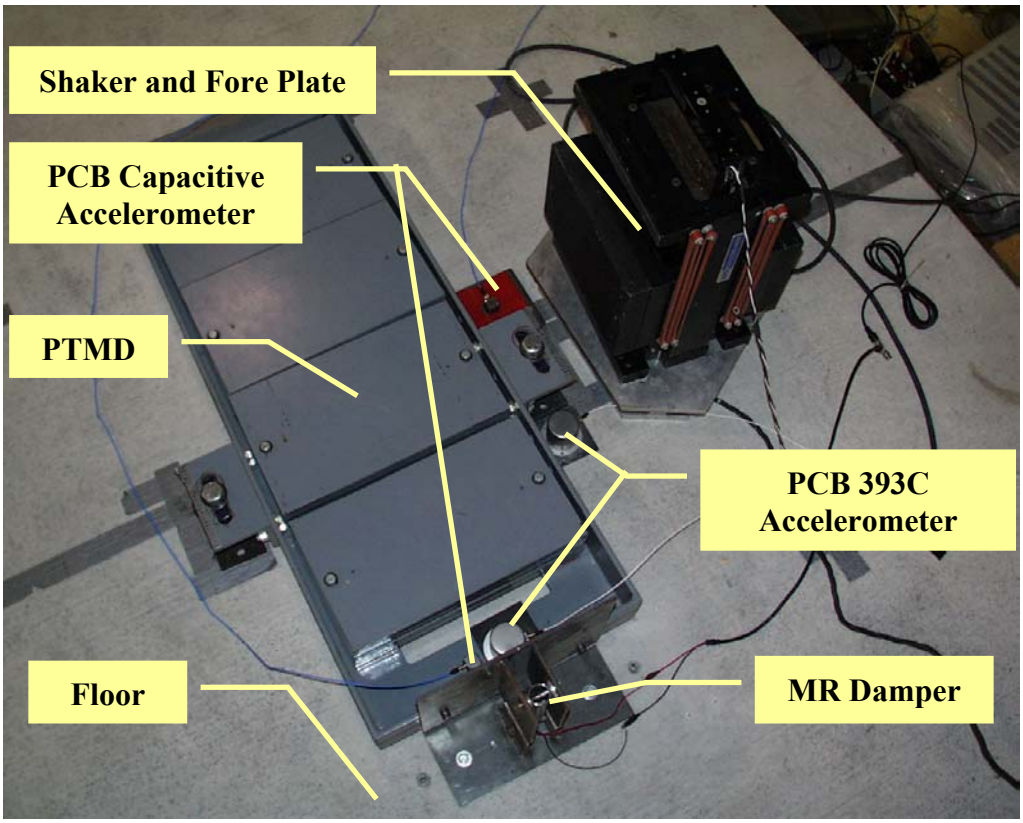

Figure 3.16 – Semi-Active Experimental Test Equipment

3.4 System Configuration

Figure 3.17 is a schematic diagram of the passive system. The shaker sits atop the force plate. A desired force input signal originates from the SigLab. This signal is sent to the amplifier. The amplifier sends the signal to the shaker to generate the force physically upon the floor. The force generated by the shaker is measured by the force plate, sent to the gain and summer box, and it is recorded as the floor excitation by SigLab. The floor and PTMD responses are measured with the accelerometers at their respective locations. One accelerometer is placed at the centerline of the floor, to one side of the PTMD. The other is placed at the tip of the PTMD. Each of these responses is digitally processed by the SigLab.

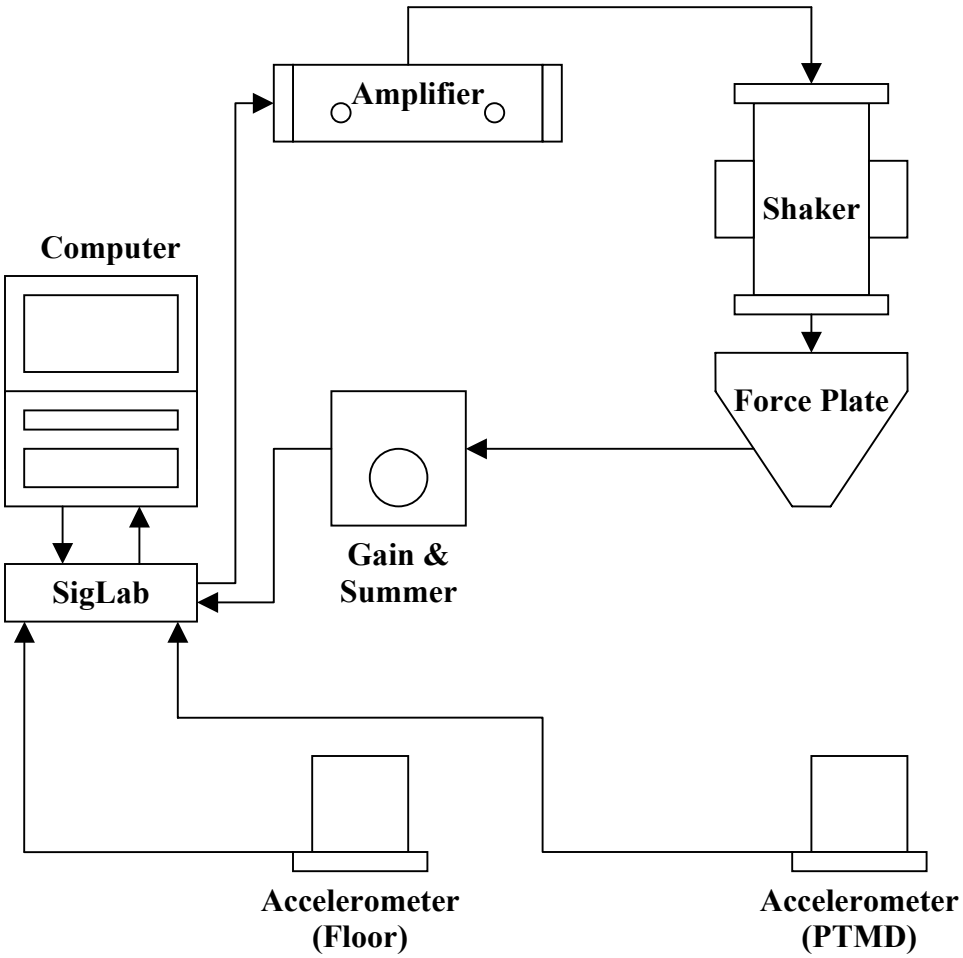

Figure 3.17 – Diagram of Experimental Passive System

Figure 3.18 is a schematic diagram of the semi-active system. This system is similar to the passive system, with the addition of the dSPACE controller card, current driver circuit box, amp-meter, and MR damper to replace the passive damper in the PTMD. The accelerometers signals are used as control feedback for the controller card. From these signals, the control policy is established per instant in time. This control policy determines the state of the MR damper, "on" or "off", and sends the respective current through an analog to digital converter. This signal is sent to the current driver circuit box and onward to the MR damper.

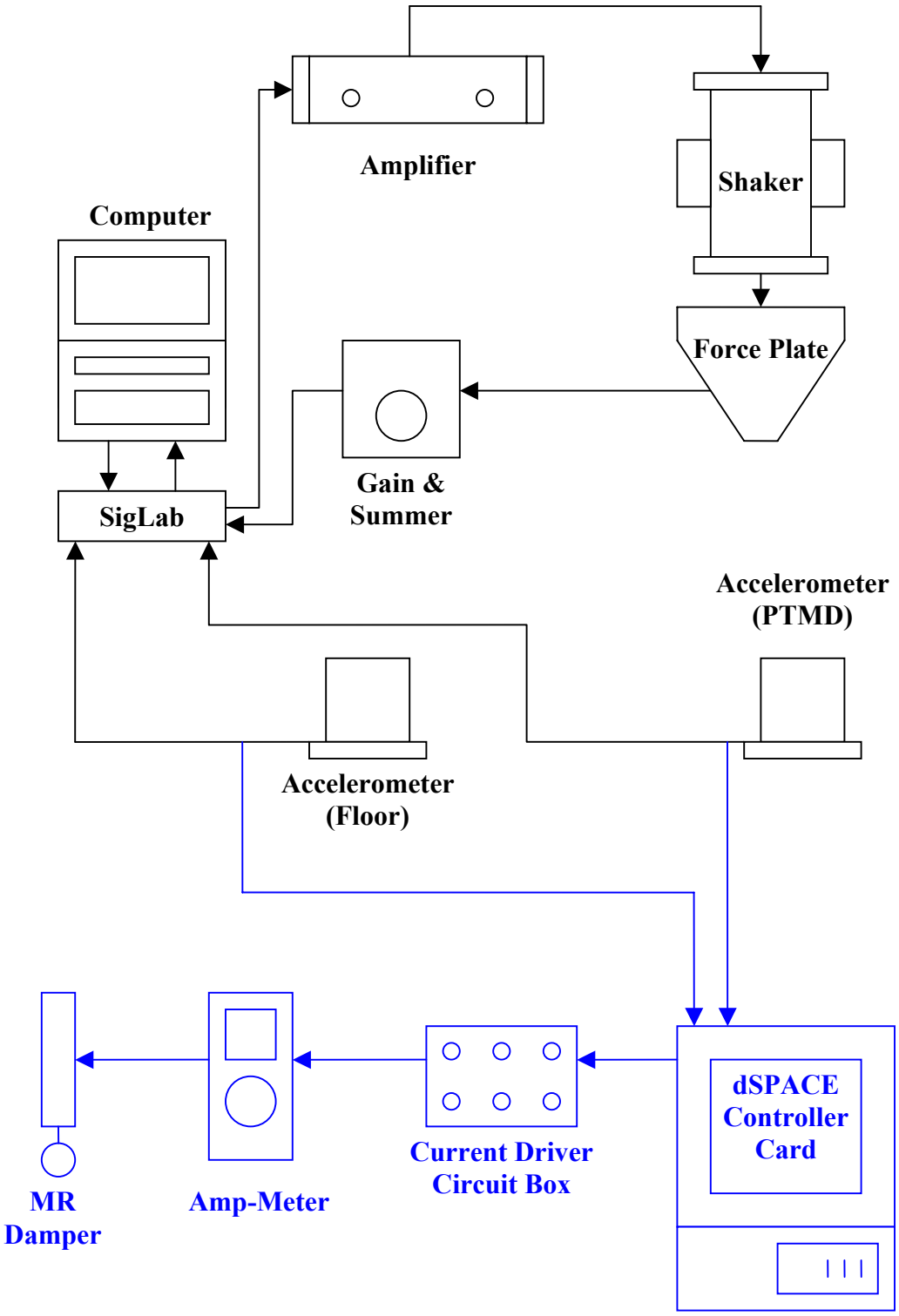

Figure 3.18 – Diagram of Experimental Semi-Active System

3.5 Signal Processing Methods

To implement methods of digital signal processing several assumptions are made. The system is assumed to be causal and stationary. The system is linear and the dynamic behavior can be explained by a second-order differential equation. The uncorrelated content is assumed to exist on the measured responses of the system.

The floor frequency is below 10 Hz and the fastest rate possible by the MR is 100 Hz; therefore, aliasing is not a concern because the annoying floor frequency is well below the Nyquist frequency. The SigLab dynamic signal analyzer was used to capture and monitor all system measurements and anti-aliasing enabled. Floor accelerance, the phase between the force input and floor response, and coherence of the input to output were given the most attention. The auto-spectrum had to be used for walking since the excitation was not captured. The time spectrum was used to observe the measured force and response of the floor and PTMD. The resolution of each signal for every test was adjusted to a point of imminent signal overload to obtain the maximum resolution.

The frequency response estimator, H_1, was used; the uncorrelated content is assumed to be located on the output. To establish the best estimation of H_1, several averages were taken from an ensemble of time blocks. Typically, five averages were used. A boxcar windowing function was applied to every block of time. With this estimator, the measured response is always greater than the true system response.

3.6 Experimental Control Policy

Semi-active control policy is dictated by phase and not amplitude of the response signals. The measured responses from the accelerometers were used as control feedback. These signals can be converted into floor displacement and relative velocity via observation of the relationship between harmonic signals acceleration, velocity, and displacement.

The control policy requires the floor displacement and relative velocity between the floor and PTMD. In terms of phase, the floor displacement is equal to the negative of the floor acceleration. The relative velocity was obtained by shifting the phase of the measured relative accelerance between the PTMD and floor by 90 degrees. An integration filter, Equation 3.3, was developed and implemented into the Simulink routine

given in Appendix R by (Koo, 2003). The resulting time history is shown in Figure 3.19. The control policy is evident via the superimposed current signal sent from dSPACE to the MR damper.

$$\frac{0.25s}{0.25s^2 + 0.7s + 1} \tag{3.3}$$

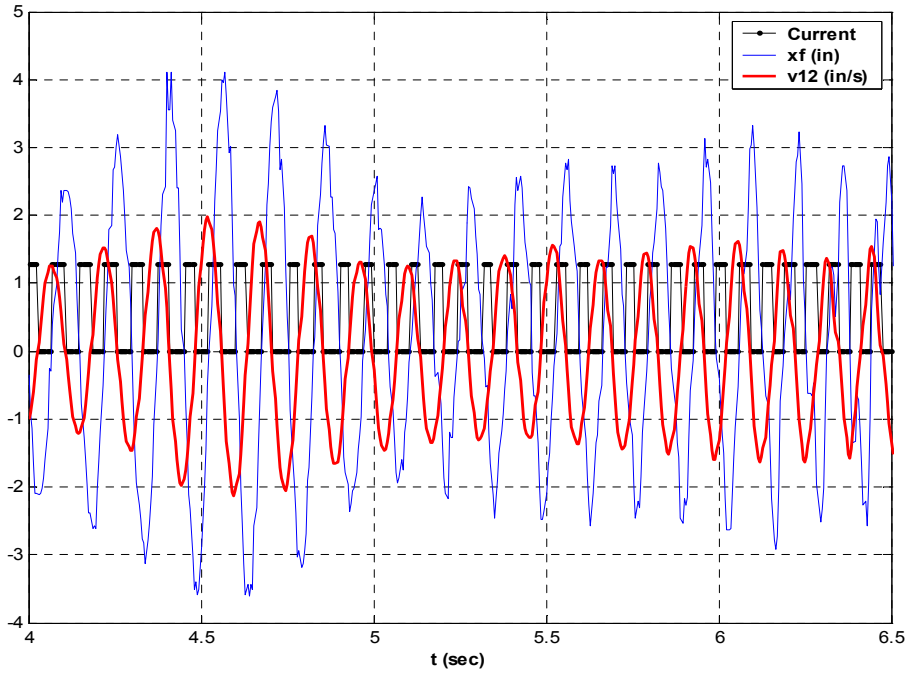

Figure 3.19 – Semi-Active Time History

Figure 3.19 is the actual representation of the control policy. For every positive product of relative velocity and floor displacement the current is applied to the damper to establish the MR damper "on" state. The switch of the damper is seen at every zero crossing. For every negative product, the current it turned off; this action switches the damper to its "off" state.

3.6.1 Floor Dynamic Properties

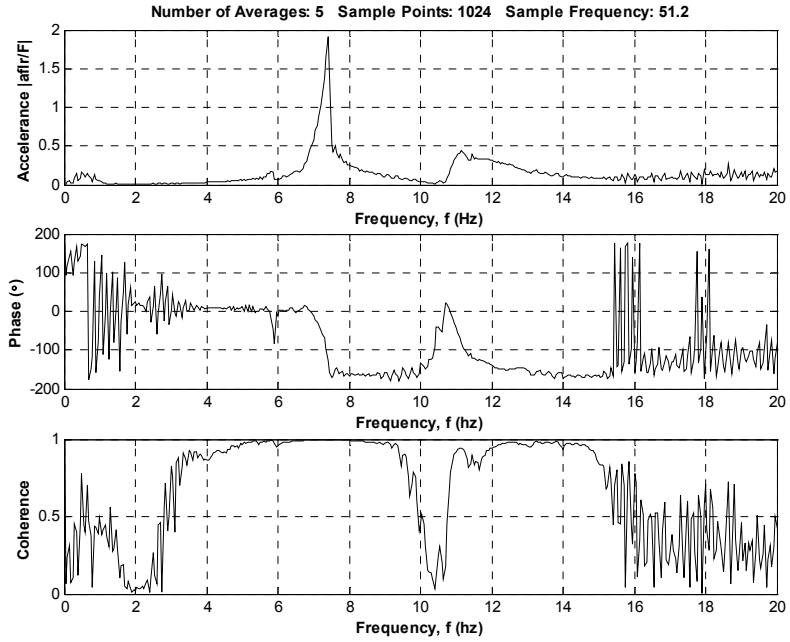

Figure 3.20 – Experimental Floor Frequency Response

Figure 3.20 gives the response of the bare floor. Three modes can be identified. The first mode, at approximately 5.8 Hz is the floor longitudinal lateral mode that occurs from the floor rocking at the supports. See Figure 3.21. The second mode, at approximately 7.4 Hz, is the first bending mode of the floor. See Figure 3.22. The third mode, at approximately 11.8 Hz, is the torsional mode of the floor. See Figure 3.23.

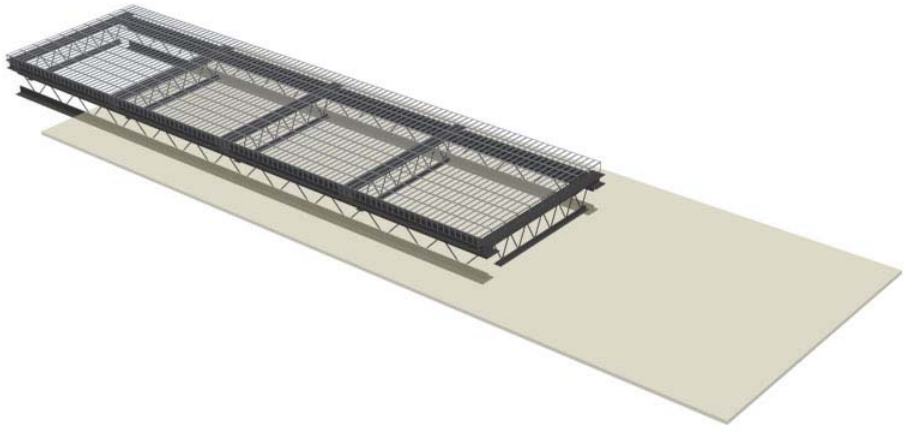

Figure 3.21 – First Mode (Lateral Mode)

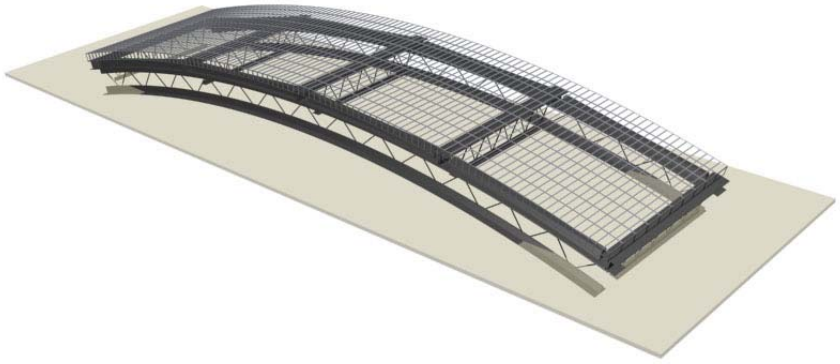

Figure 3.22 – Second Mode (First Bending Mode)

Figure 3.23– Third Mode (Torsional Mode)

The effective mass of the floor was established from the results of a modal analysis of the floor. The modal analysis was focused on the first bending mode of the floor using the electromagnetic shaker placed at the center of the floor, node 28 in Figure 3.24. An accelerometer was placed successively at all of the 55 points shown. A chirp signal excited the floor; and the response of each point was captured. The final result is given in Figure 3.25.

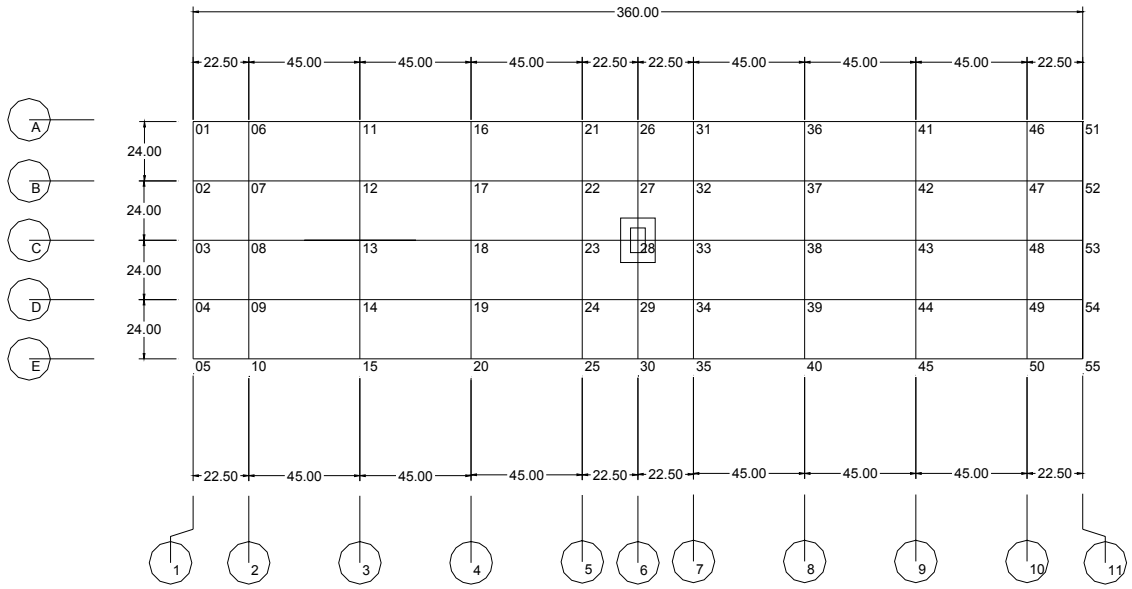

Figure 3.24 – Experimental Floor Modal Points (Dimensions in in.)

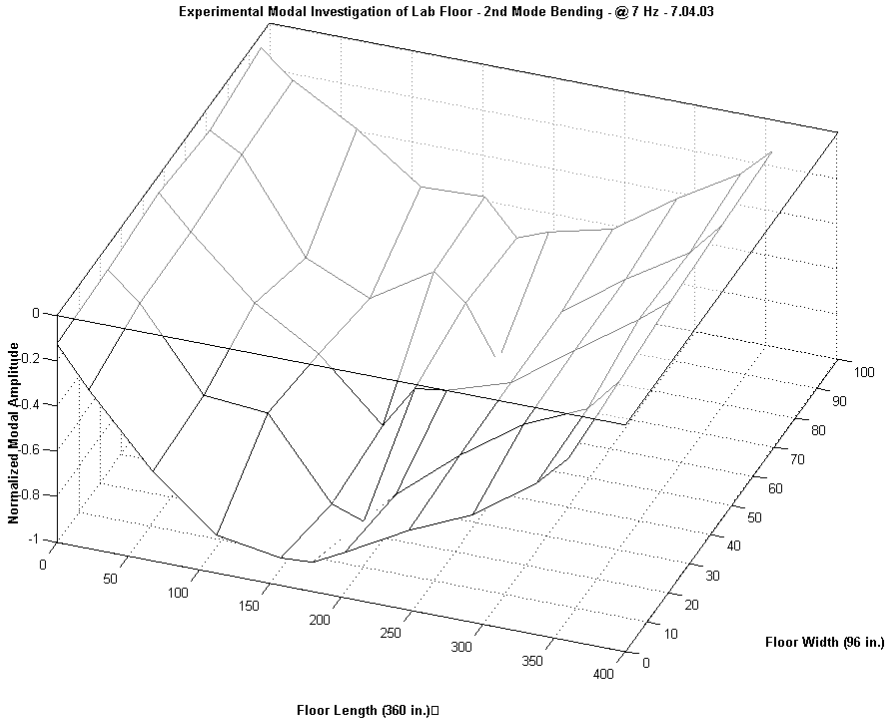

Figure 3.25 – Experimental Floor Response Bending Mode Shape

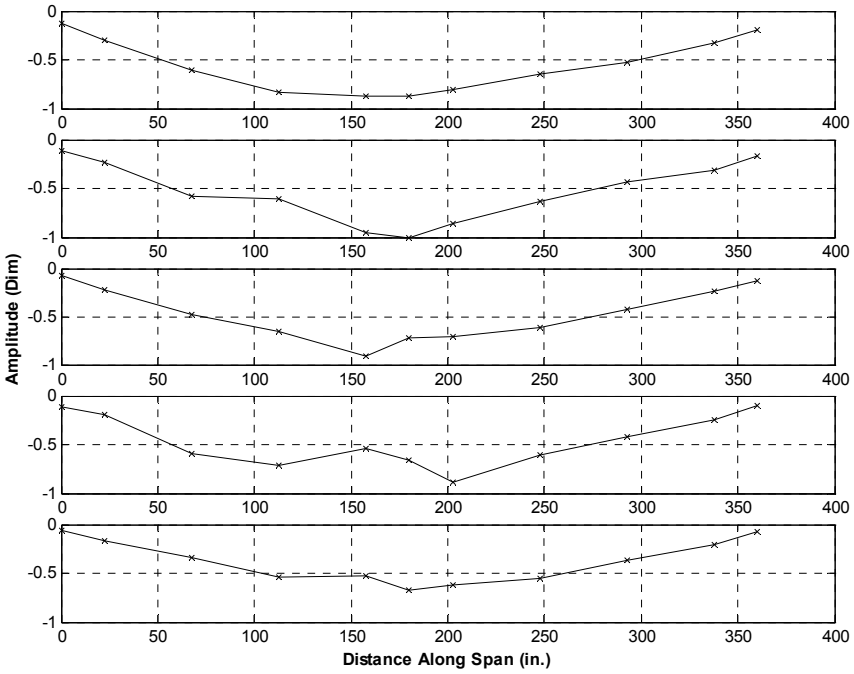

Figure 3.26 - Sectional Profiling of Mode Shape Given in Figure 3.25

Figure 3.26 shows the deflected shape of the system at each of the 5 longitudinal sections. During excitation of the bending mode of the floor, there were lateral components associated with the rotation at the girder supports which contribute to the vertical motion of the floor. The inadequate anchoring of the floor is evident in the deflection vertically at the supports. This is an appreciable amount of deflection.

$$\phi(x) = Z(1) \quad Z(2) \quad ... \quad Z(i) \tag{3.4}$$

Figure 3.27 is the resulting average mode shape of the floor. The mode shape, Equation 3.4, was achieved by averaging across the width of the floor the deflections, Z, for the entire span. This was done to get an overall estimation of the floor since the floor length is significantly large compared to the width. This will be used to determine the effective mass of the floor.

The total floor weight, approximately 14,400 lbs, was distributed uniformly along the span of the floor, approximately 480 pounds per foot. Using the tributary width for each point, a lumped mass was assigned. The shape is normalized with respect to the maximum mid-span deflection. The mass matrix was developed with Equation 3.5 and the effective mass, Equation 3.6. The effective mass is approximately 0.0129 k s^2 / in.

The analytical approximation of half the floor mass, using the mode shape of from a simply supported beam, gives an effective mass of 0.0188 k s^2 / in. The discrepancy comes from a non-uniform mass distribution and the end restraint provided, Figure 3.3.

$$\boldsymbol{M} = \begin{matrix} m(1) & 0 & 0 & 0 \\ 0 & m(2) & 0 & 0 \\ 0 & 0 & \mathrm{O} & \mathrm{M} \\ 0 & 0 & \Lambda & m(i) \end{matrix} \tag{3.5}$$

The index "i" refers to each of the lumped masses along the length of the span. The effective mass is given by Equation 3.6.

$$\boldsymbol{M}_{eff} = \phi^T * \boldsymbol{M} * \phi \tag{3.6}$$

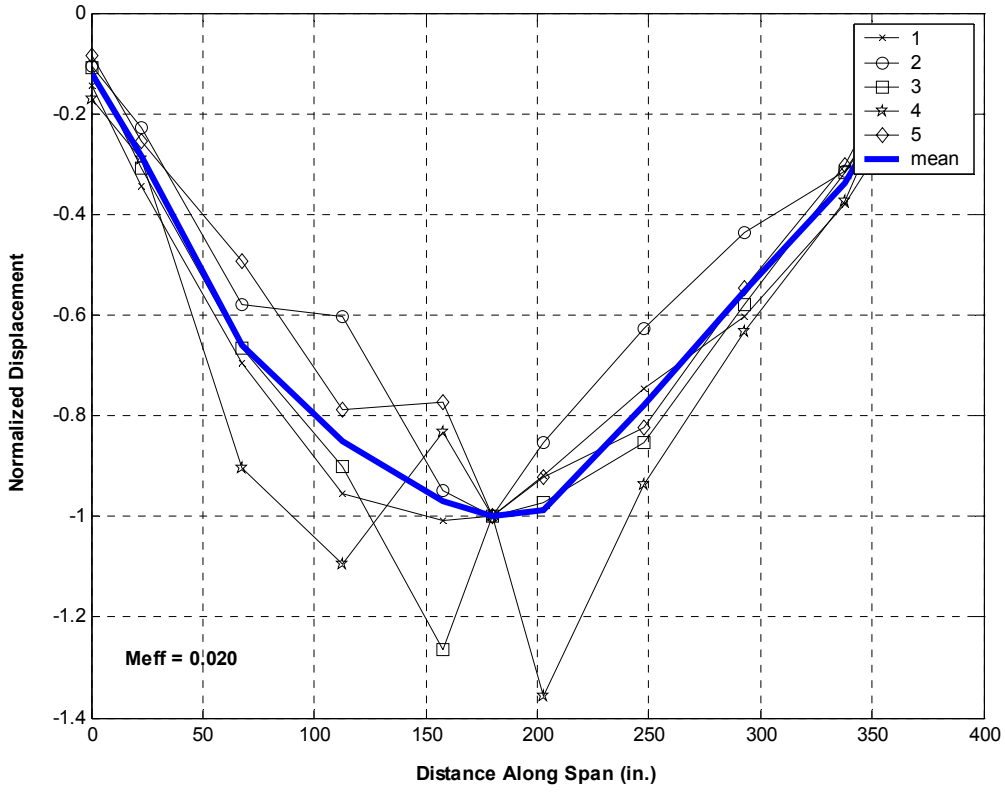

Figure 3.27 – Average Mode Shape Overlaid on the Composted Longitudinal Sections Figure 3.9

Damping of the floor was determined from ME scope from Vibrant Technology Inc. The accelerance responses for each node were assigned to the corresponding points on the floor model in ME scope. ME scope used a global polynomial fit on an isolated extraction within the frequency response spectrum. A linear regression is used to compute the polynomial coefficients and obtain a measure of damping. A damping value of 0.8% was obtained for the first bending mode of the floor. Table 3.1 summarizes the approximate floor dynamic parameters.

Table 3.1 – Summary of Floor Parameters

Floor Parameters		
$W_{Flr,tot}$	14.339	kips
$m_{1,efff}$	.020	$k\ s^2$ / in.
k_1	27.5	k / in.
c_1	0.015	k in./ s
ω_1	46.5	rad / s
f_{n1}	7.4	Hz
ξ_1	0.008	dim

3.6.2 PTMD Dynamic Properties

Several experimental tests were conducted to gain an understanding of the provided PTMD system. An impact hammer was used to establish the natural modes of the system. Setting up PTMD on load cells gave the total weight and center of mass. A deflection test was used to obtain the spring stiffness.

The PTMD's weight consists of 16, 43.85 lb, plates for a total of 700 lbs. See Table 3.2. The total weight of the PTMD from a weight take-off is 810 lbs, Appendix G. To determine the overall mass experimentally, four tests where conducted using load cells. The data is given in Appendix H. With a load cell under the tip of the PTMD, and the pin support supported on stack of plates, a measured weight of approximately 405 lbs was obtained. This value does not include the weight of the pin assembly because it is

resting at the support; therefore, the total measured weight is approximately 810 lbs. This agrees with the take-off in Appendix G value and the discrepancy arises from the resolution of the load cell and the tabulated values provided in the manual because of manufacturing tolerances.

Table 3.2 – Mass of PTMD Plates

	Plate Weights (lbs)			
	Stack 1(S1)	**Stack 2 (S2)**	**Stack 3 (S3)**	**Stack 4 (S4)**
Plate 1 (P1)	43.82	44.12	43.94	44.16
Plate 2 (P2)	43.92	43.8	43.9	43.76
Plate 3 (P3)	43.74	43.6	43.78	43.92
Plate 4 (P4)	43.66	43.7	43.96	43.76
Totals	175.14	175.22	175.58	175.6
Total Weight	701.5	lbs		
Average Plate Weight	43.8	lbs		

The spring stiffness was obtained from a static deflection test. The PTMD was placed on the ground and anchored. A stack of 10 lb plates were placed along the spring line in increments of 10 lbs. Each plate was measured to obtain its true weight and recorded. The deflection was measured with a dial gauge with resolution of 0.001 in. See Figure 3.28. The collected data is presented in Appendix I and plotted in Figure 3.29. The resulting stiffness is approximately 3264 lbs/in. Numerically, a value of 3250 lbs/in. is used.

Figure 3.28 – Dial-Gauge Location

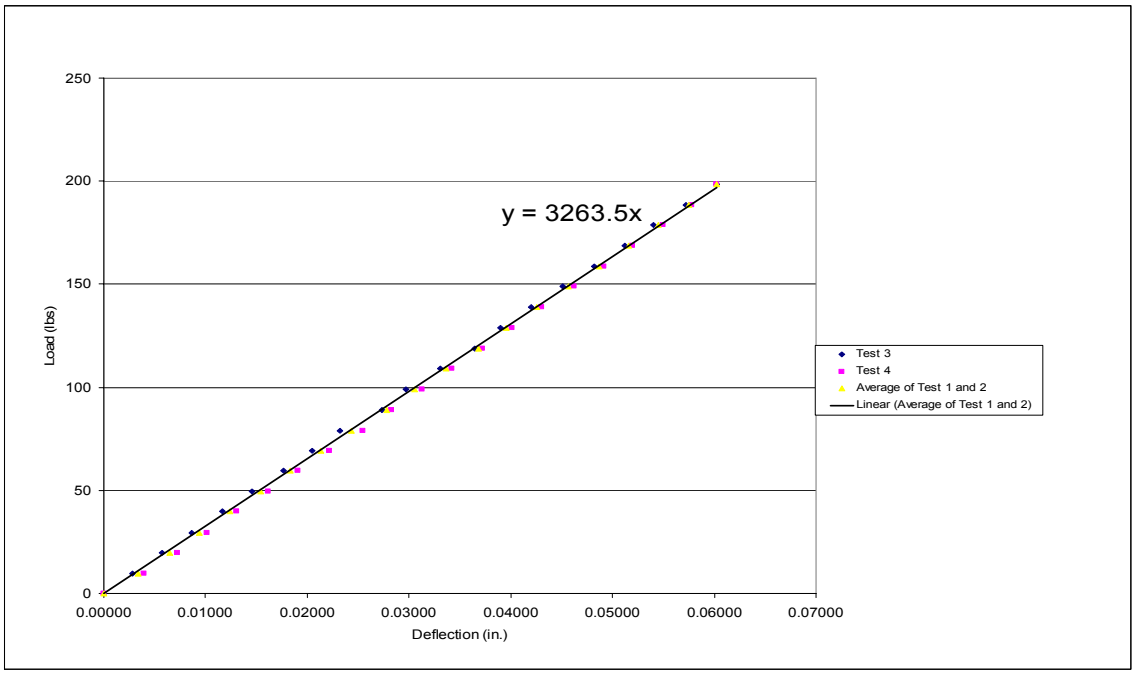

Figure 3.29 – Experimental Spring Stiffness

The modal characteristics of the PTMD were determined in the frequency domain to establish the dynamic behavior the PTMD. The PCB impulse force hammer, Figure 3.9, is used to excite the PTMD by striking it at the tip. The accelerometer is also located at the tip of the PTMD, see Figure 3.30. The first mode is rigid arm rotation about the pin support, and the first mode occurs at approximately 6.95 Hz. The second mode is the lateral mode at approximately 8.64 Hz. The third mode is the torsion mode of the PTMD and occurs at approximately 46.85 Hz. The first mode is the mode that is tuned to quell the floor vibration.

Figure 3.30 – PTMD Modal Testing: Bending Mode (Left) and Torsion Mode

Figure 3.30 (cont.) – PTMD Modal Testing: Lateral Mode

3.7 Experimental Optimization

An experimental tuning of the PTMD was conducted for both passive and semi-active systems. The floor accelerance response was monitored to establish the tuned response of the system. A chirp excitation was applied to the floor via the shaker on the force plate. A frequency sweep from 4 -15 Hz in 20 seconds was performed with five averages.

Figure 3.31 is the bare floor response. Figure 3.32 shows the Floor Response with passive control using both the MR (MR used in passive mode, i.e., $c_{on} = c_{off} = c$) and Airpot Dampers. Figure 3.33 is the floor response with semi-active control. Figure 3.34 is a composite plot for a direct comparison in peak reduction.

For peak reduction of the acceleration of the system, the passive air damper, passive MR, and semi-active MR damper produce the same amount of reduction, Figure 3.34. The low coherence is a result of the floor excited at the center of the floor and therefore, a node line for the torsion mode. The difference is very small, approximately 2.7%. Therefore, no benefit is gained at the optimal state by implementing a semi-active displacement based control policy, with an MR damper in the PTMD to minimize peak. The MR damper frequency bandwidth is limited to the resonant frequency of the floor and does not mitigate adjacent modes, such as the one at 5.8 Hz.

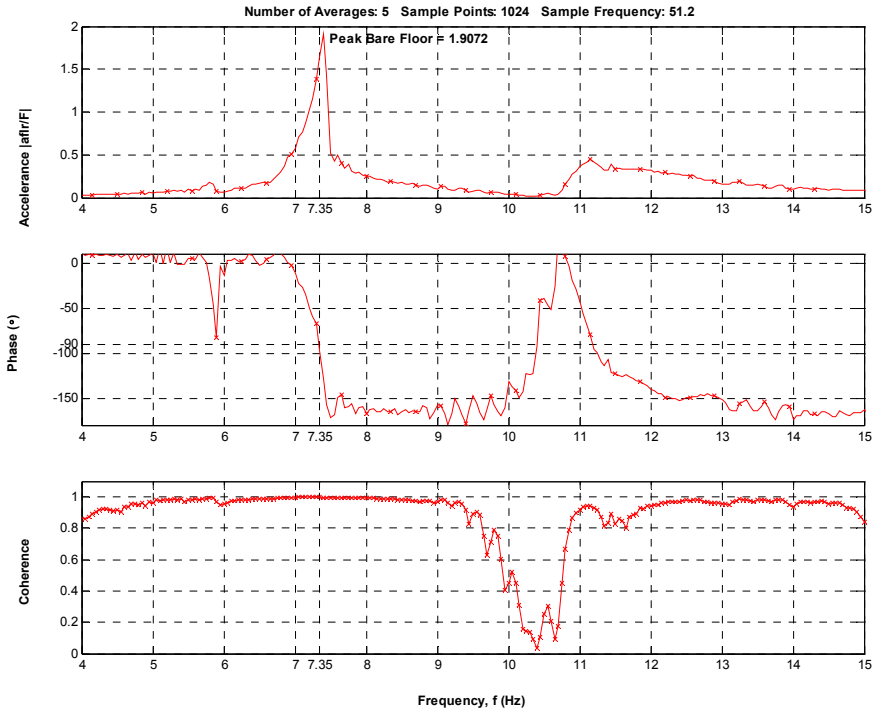

Figure 3.31 – Floor Response to Chirp (4-15 Hz) Excitation.

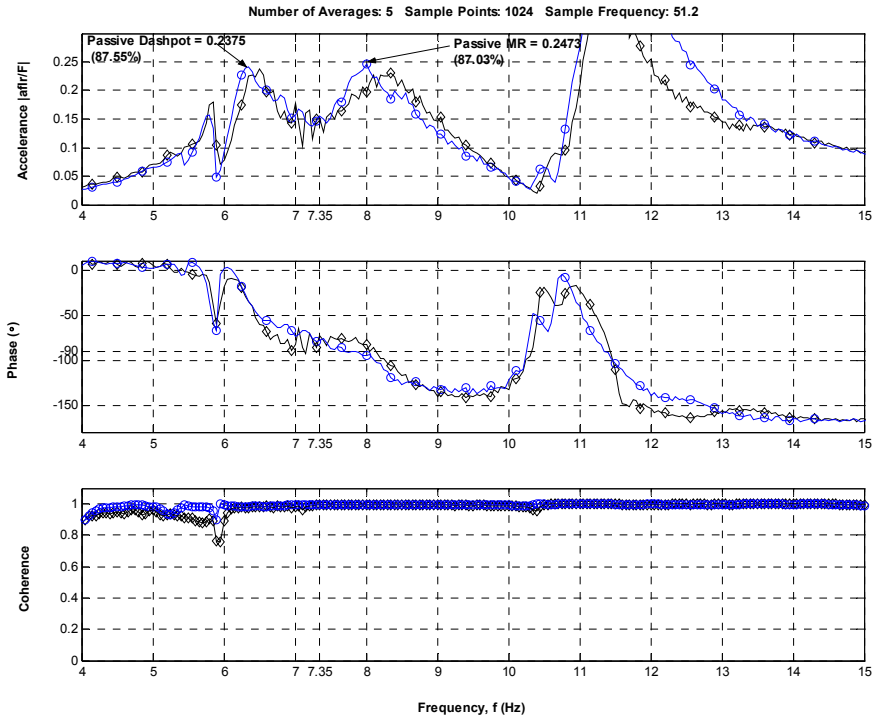

Figure 3.32 – Overlay of Tuned System Floor Responses: Passive and Passive MR

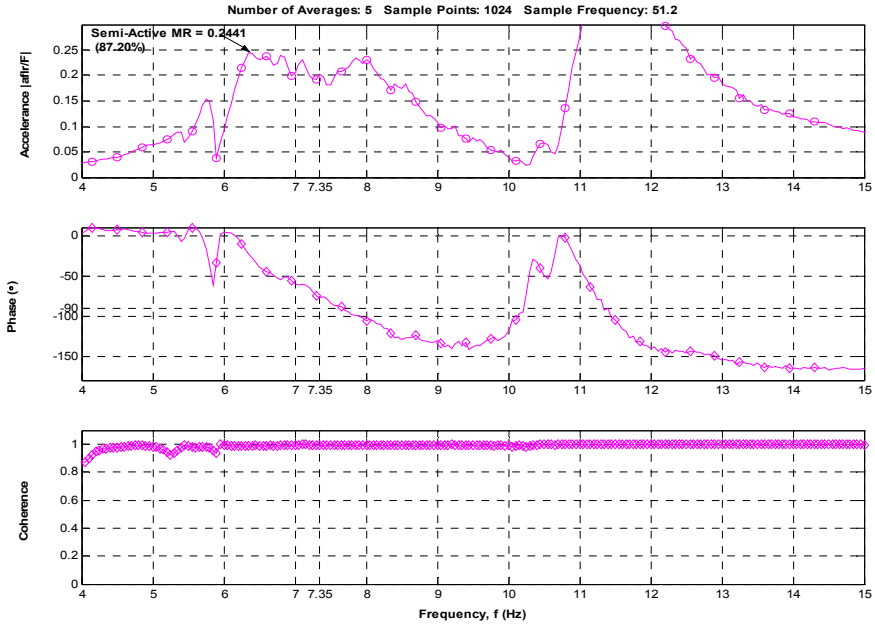

Figure 3.33 –Tuned System Floor Response: Semi-active

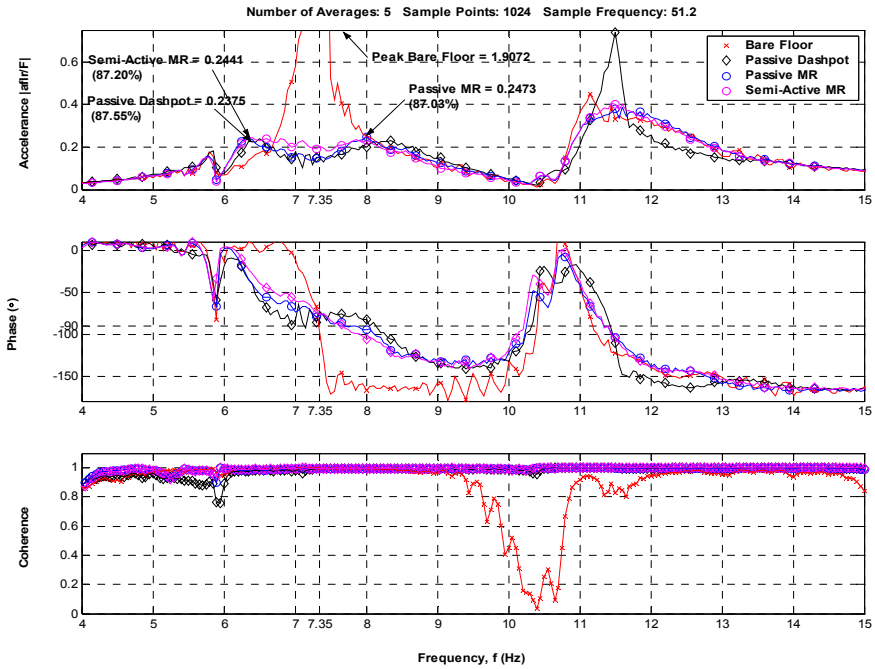

Figure 3.34 – Overlay of Tuned System Floor Responses: Passive, Passive MR, and Semi-active

3.8 Experimental System Off-Tuning

3.8.1 Mass Off-Tuning Due to Presence of People

A comparison of the ability of the passive and semi-active control schemes to accommodate the introduction of humans on the floor was experimentally tested. Sixteen people were placed on the floor as shown in Figure 3.35 and 3.36 along modal lines B and D. Their distribution was such to minimize the enhancement of the torsion mode; therefore, their weights were distributed symmetrically about the longitudinal axis of the floor. Their weights are given in Table 3.3 and a complete documentation of people for experimental testing for bare floor, passive PTMD, and semi-active PTMD is given in Appendix P.

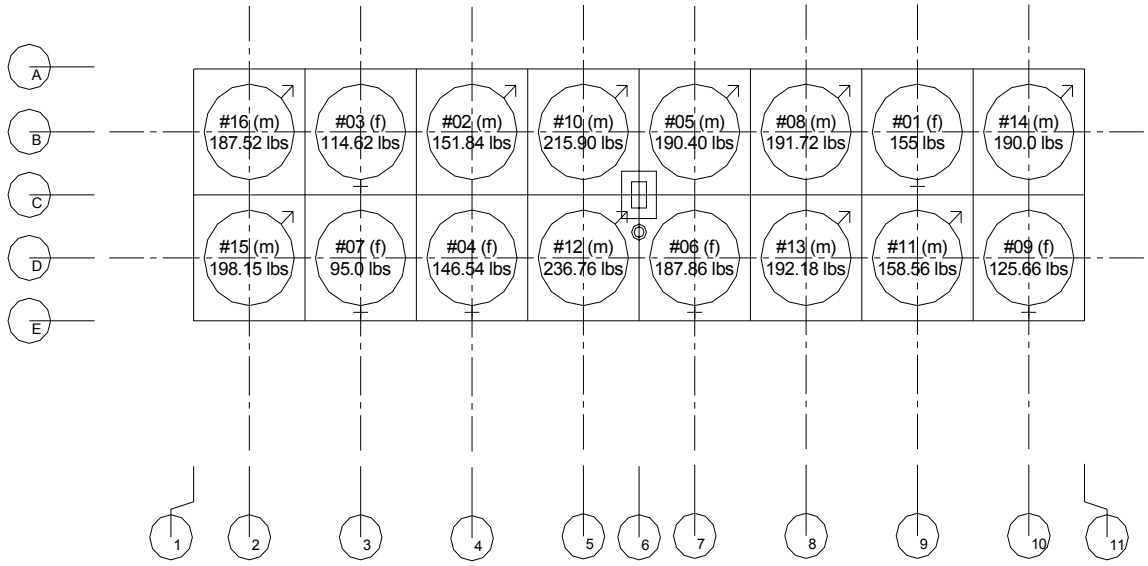

Figure 3.35 – Typical Human Locations for 16, 12, 10, and 8 People

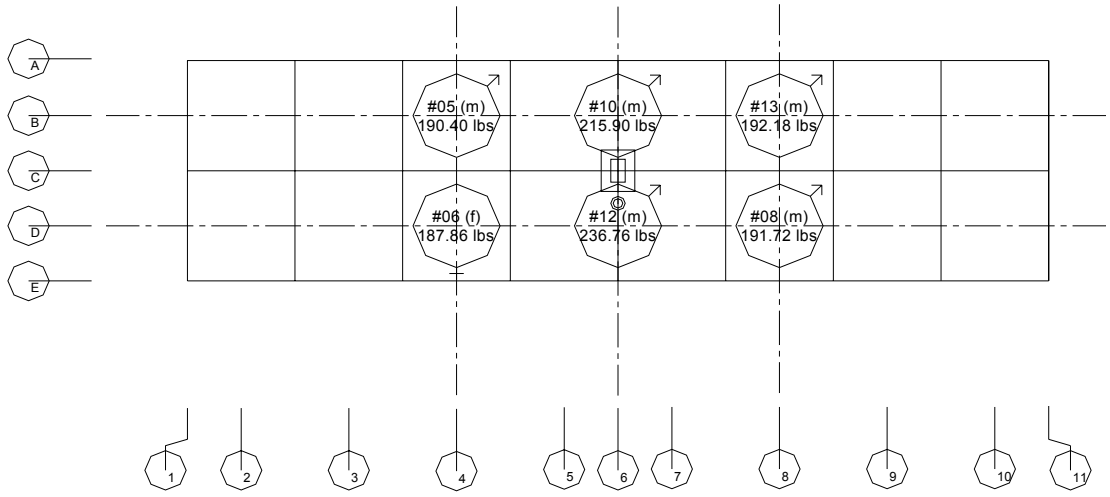

Figure 3.36 – Typical Human Locations for 2 and 6 People

The humans were tested in three positions – standing, seated, and with their legs bent approximately 30 degrees at the knee. The various positions are shown in Figure 3.37. These tests were performed with the passive PTMD and the semi-active PTMD on the floor at different times. The floor was excited with a chirp swept from 4 to 15 Hz and the floor response measured. Six sets of tests (2, 4, 6, 8, 12, 16 people) were performed for each control system and the three positions (sitting, standing, bent knees) were taken for each test set. Sixteen people were chosen for this floor to approximate the upper bound on distributed mass on typical commercial floors, 12 psf. Therefore, 16 people, approximately each weighing 180 lbs, were used.

Table 3.3 – Live Human Weight Added to Floor per Test for Passive (top) and Semi-Active (bottom)

		No. of People					
		2	4	6	8	12	16
Modal Line	1	0	0	0	0	0	0
	2	0	0	0	0	0	385.67
	3	0	0	0	0	209.62	209.62
	4	0	0	378.26	298.38	298.38	298.38
	5	0	378.26	0	452.66	452.66	452.66
	6	382.58	0	452.66	0	0	0
	7	0	383.9	0	378.26	378.26	378.26
	8	0	0	383.9	383.9	383.9	383.9
	9	0	0	0	0	313.56	313.56
	10	0	0	0	0	0	315.66
	11	0	0	0	0	0	0
	Total (lbs)	382.58	762.16	1214.82	1513.2	2036.38	2737.71

		No. of People					
		2	4	6	8	12	16
Modal Line	1	0	0	0	0	0	0
	2	0	0	0	0	0	256
	3	0	0	0	0	267.68	267.68
	4	0	0	339.9	294.7	294.7	294.7
	5	0	340.5	0	339.9	339.9	339.9
	6	409.7	0	409.7	0	0	0
	7	0	410	0	409.7	409.7	409.7
	8	0	0	310.18	310.18	310.18	310.18
	9	0	0	0	0	278.26	278.26
	10	0	0	0	0	0	219.6
	11	0	0	0	0	0	0
	Total (lbs)	409.7	750.5	1059.78	1354.48	1900.42	2376.02

Figure 3.37 – Humans on Experimental Footbridge Standing Straight Leg (Left), Standing with Legs Bent (Right)

Figure 3.37 (cont.) – Humans on Experimental Footbridge Sitting

The experimental floor peak accelerance versus the number of people is given in Figures 3.38 through 3.40. These figures show that the semi-active PTMD does not perform as well as the passive system when humans are on the floor. One reason is suggested by Figures 3.38 through 3.40 which show the variation in phase at the natural frequency of the floor, between the floor response and the applied force, with the number of people added to the floor. The passive is system is closer to 90 degrees at the floor frequency than for semi-active.

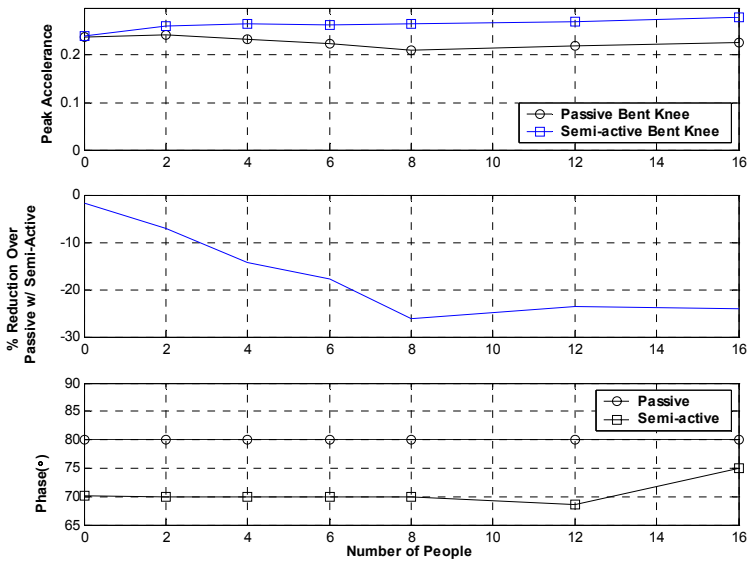

Figure 3.38 – Overlay of Human Tests for Passive and Semi-active Control – Bent Knees – Peak Amplitude (top) and Phase (bottom) versus the Number of Humans

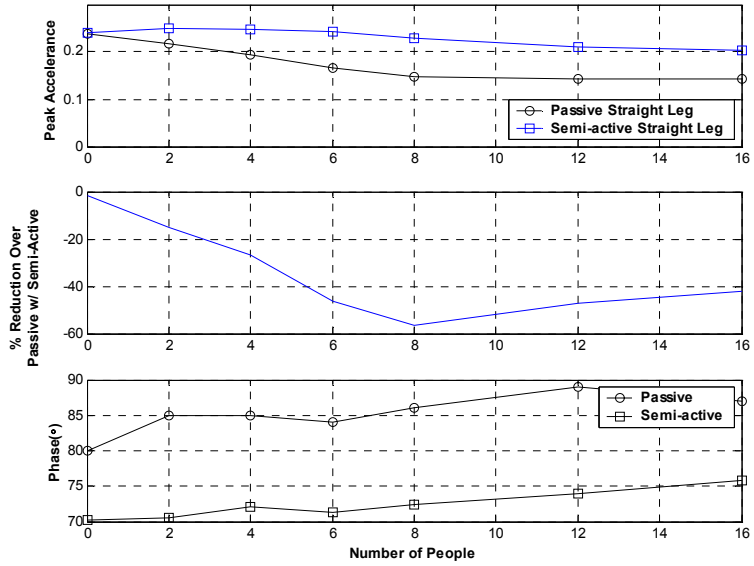

Figure 3.39 – Overlay of Human Tests for Passive and Semi-active Control – Standing with Legs Straight – Peak Amplitude(top) and Phase (bottom) versus the Number of Humans

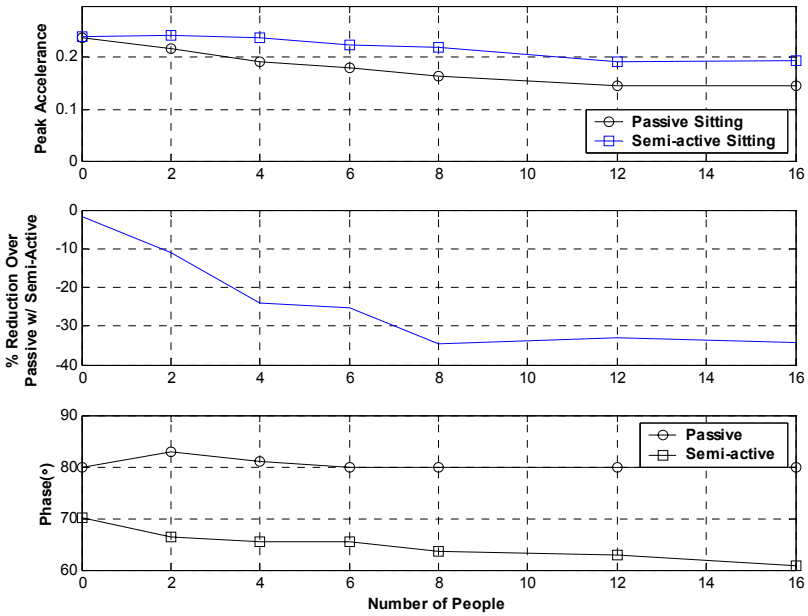

Figure 3.40 – Overlay of Human Tests for Passive and Semi-active Control – Sitting – Peak Amplitude (top) and Phase (bottom) versus the Number of Humans

To gain further insight, the bare floor response was observed with the presence of people and their equivalent dead weight (see Appendix P for this set of humans). This is shown in Figure 3.41. By inspection, the expected trend of increasing the floor mass is seen. The peak response has reduced and the location of this peak, shifts downward in the frequency spectrum. The peak response as the number of humans is increased on the floor does not show this trend. The peak response shifts upward (i.e., the resonance frequency increases), reduces in magnitude, and broadens in band. This suggests humans act as an additional dynamic system on the floor, not just added mass to the floor.

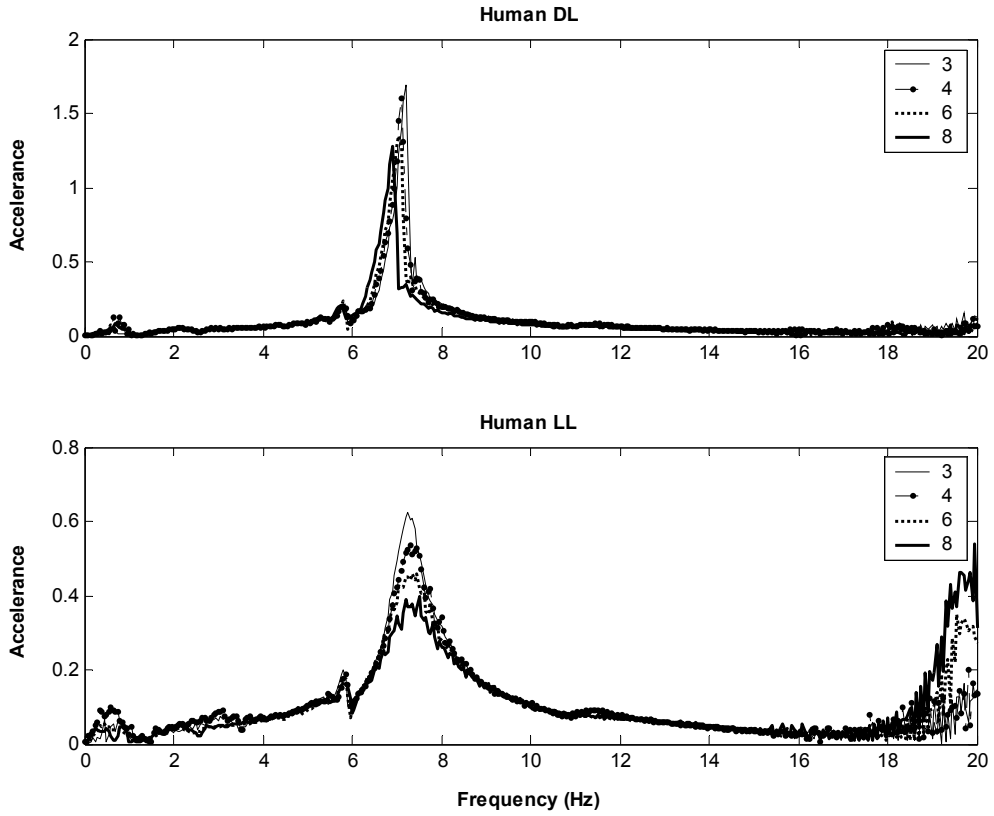

Figure 3.41 – Floor Response with Increasing Equivalent Human Dead Weight on Floor (top) and Increasing the Number of Humans Standing on the Floor (bottom)

An analytical attempt is made as a first approximation of the system to gain a possible insight into the human structural interaction with the system. First, the bare floor with human equivalent dead weights were investigated with the mass of humans obtained experimentally, Figure 3.42. Its analytical counterpart is given in Figure 3.43. Both of these demonstrate the variation in peak amplitude with the number of humans

included in the system. As can be noticed from Figure 3.42 and Figure 3.43, the analytical and experimental results have similar trends.

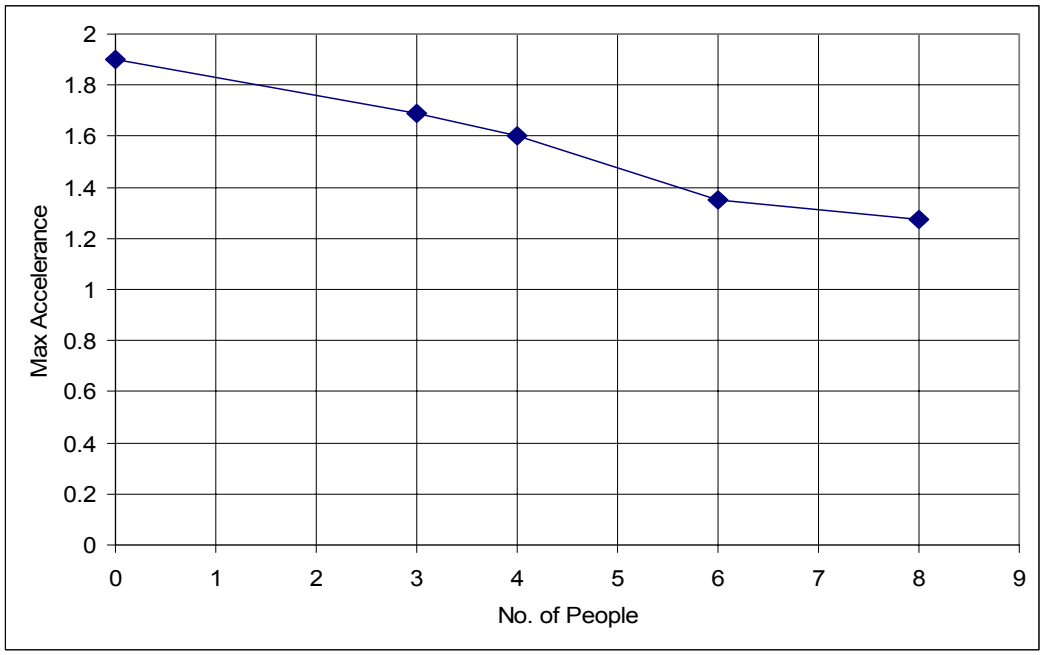

Figure 3.42 – Experimental Response of Bare Floor Response with Equivalent Human Dead Weight

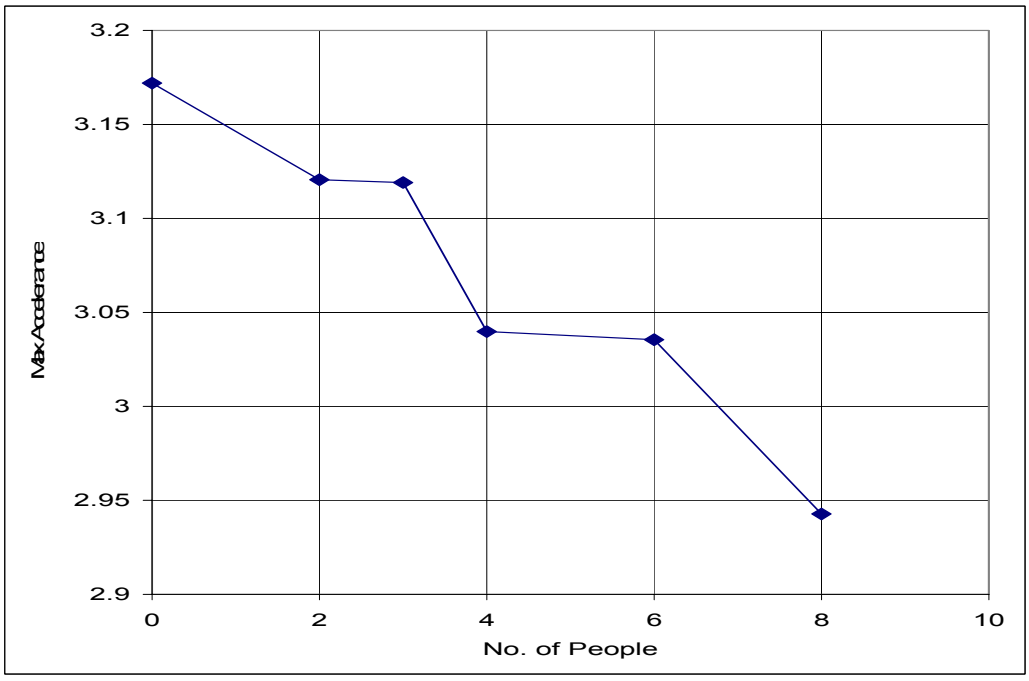

Figure 3.43 – Analytical Response of Bare Floor Response with Equivalent Human Dead Weight

Figures 3.44 and 3.45 show the peak accelerance of the floor experimentally and analytically respectively for the addition of humans to the uncontrolled floor.

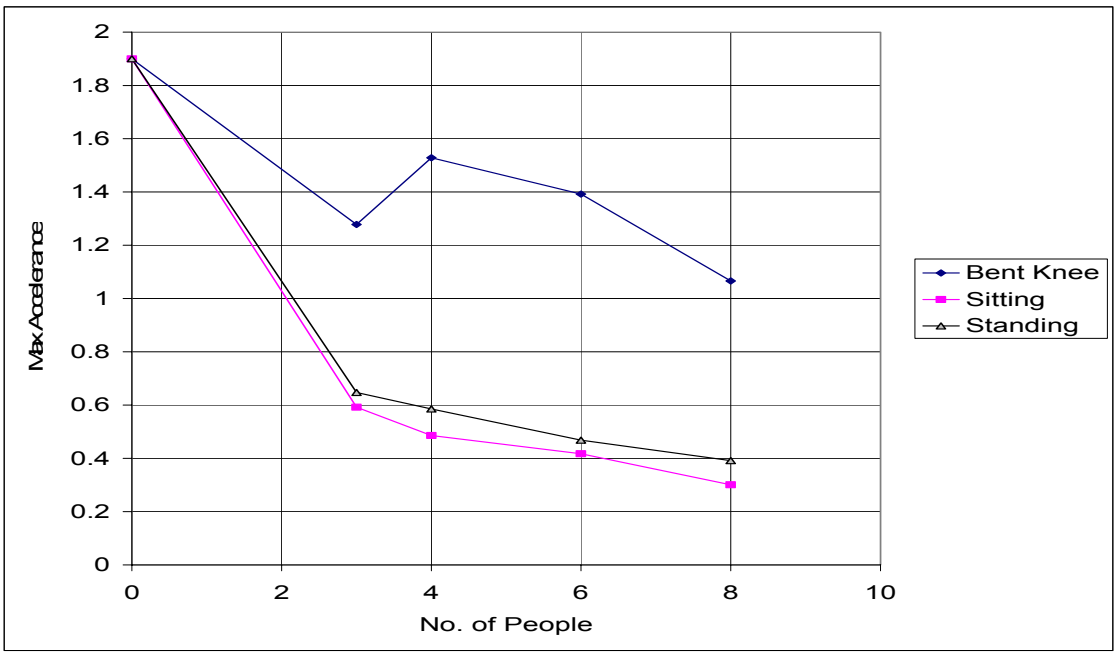

Figure 3.44 – Experimental Response of the Bare Floor with Humans Standing, Sitting, and with Knees Bent

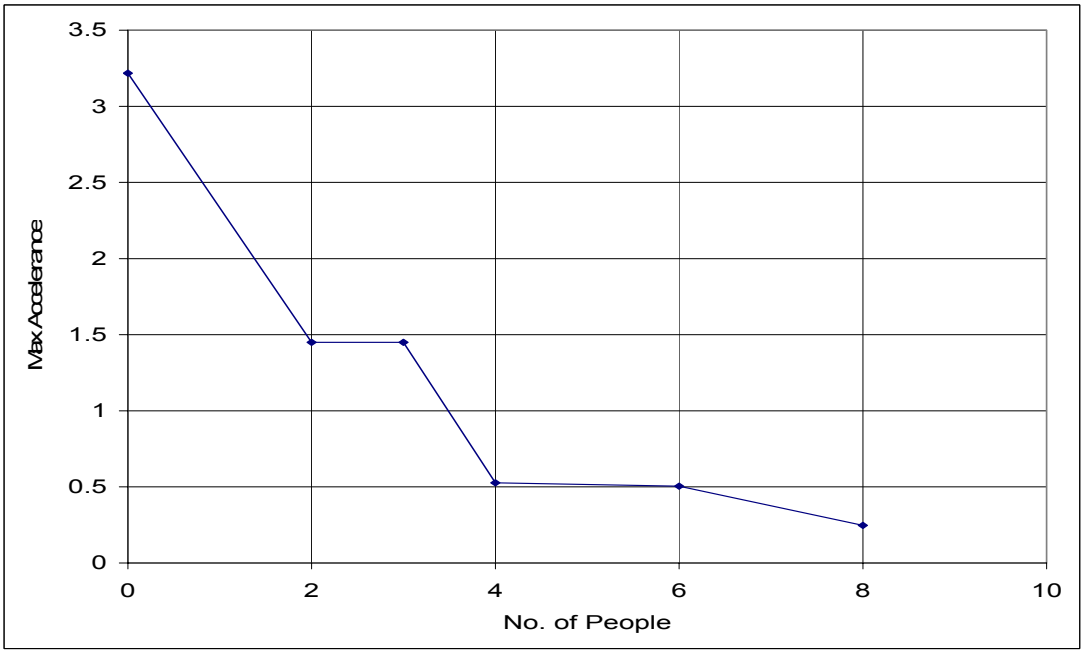

Figure 3.45 – Analytical Response of the Bare Floor with Humans

By inspection of the experimental response, it was deemed appropriate to model the human as another degree of freedom to the floor, Figure 3.46

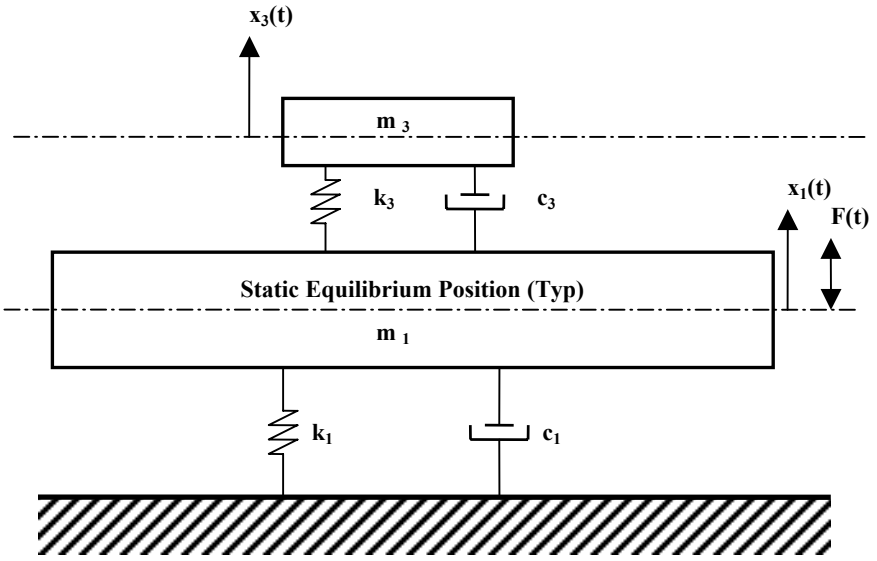

Figure 3.46 – Two-Degree-of-Freedom Model of Floor and Human

The natural frequency of the humans was set at 5.5 Hz and a damping ratio of 45% based on values found in literature. These parameters were adjusted but the overall results between them were very similar and appear independent of these variations with frequency from 5.5 to 5.9 and damping form 35% to 45%. A general value of mass, 90% of the total human mass present was used and the overall response was still the same.

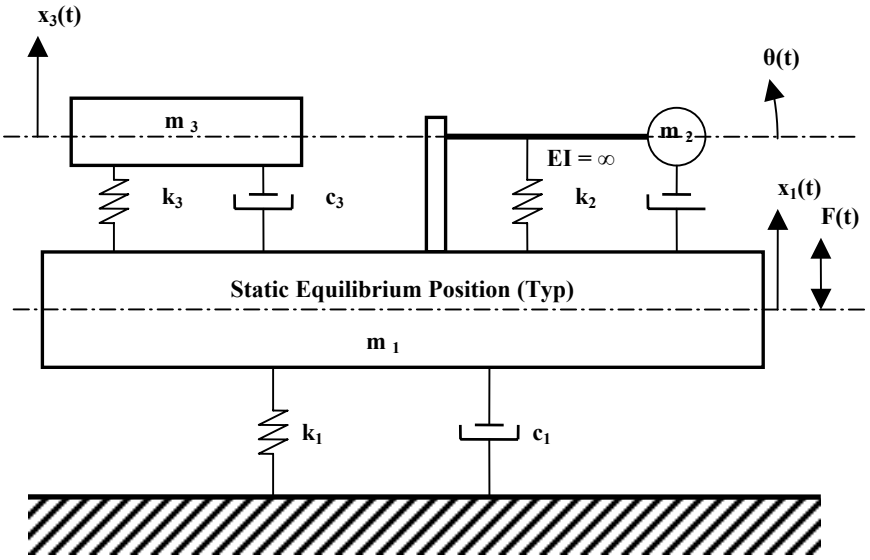

Figure 3.47 – Three-Degree-of-Freedom Model of Floor, PTMD, and Human

A three degree of freedom model consisting of the floor, PTMD, and human model was developed. Figure 3.47 shows the dynamic model used, m_3 represents the total effective mass of human occupants. The following shows the dynamic equations of motion for the three-degree-of-freedom system:

$$\begin{bmatrix} m_1+m_2 & l_m m_2 & 0 \\ l_m m_2 & l_m^2 m_2 & 0 \\ 0 & 0 & m_3 \end{bmatrix} \begin{Bmatrix} \ddot{x}_1 \\ \ddot{\theta} \\ \ddot{x}_3 \end{Bmatrix} + \begin{bmatrix} c_1+c_3 & 0 & -c_3 \\ 0 & l_d^2 c_2 & 0 \\ -c_3 & 0 & c_3 \end{bmatrix} \begin{Bmatrix} \dot{x}_1 \\ \dot{\theta} \\ \dot{x}_3 \end{Bmatrix} + \begin{bmatrix} k_1+k_3 & 0 & -k_3 \\ 0 & l_s^2 k_2 & 0 \\ -k_3 & 0 & k_3 \end{bmatrix} \begin{Bmatrix} x_1 \\ \theta \\ x_3 \end{Bmatrix} = \begin{Bmatrix} F(t) \\ 0 \\ 0 \end{Bmatrix} \tag{3.7}$$

With the above dynamic system parameters, the floor response was found analytically to obtain a trend similar to that demonstrated experimentally with humans introduced into the system. The equations of motion were solved using the Runge-Kutta algorithm with a 100 Hz sampling rate for the PTMD with MR damper. The floor response is given in Figure 3.48. The respective masses for each case study were used in the corresponding analytical model. The overall response is very similar to what was observed experimentally.

Introspective analysis into the depicted response is not performed, the overall goal was to obtain a fundamental understanding that humans are the cause for the trend seen experimentally with humans on the floor for each type of control system.

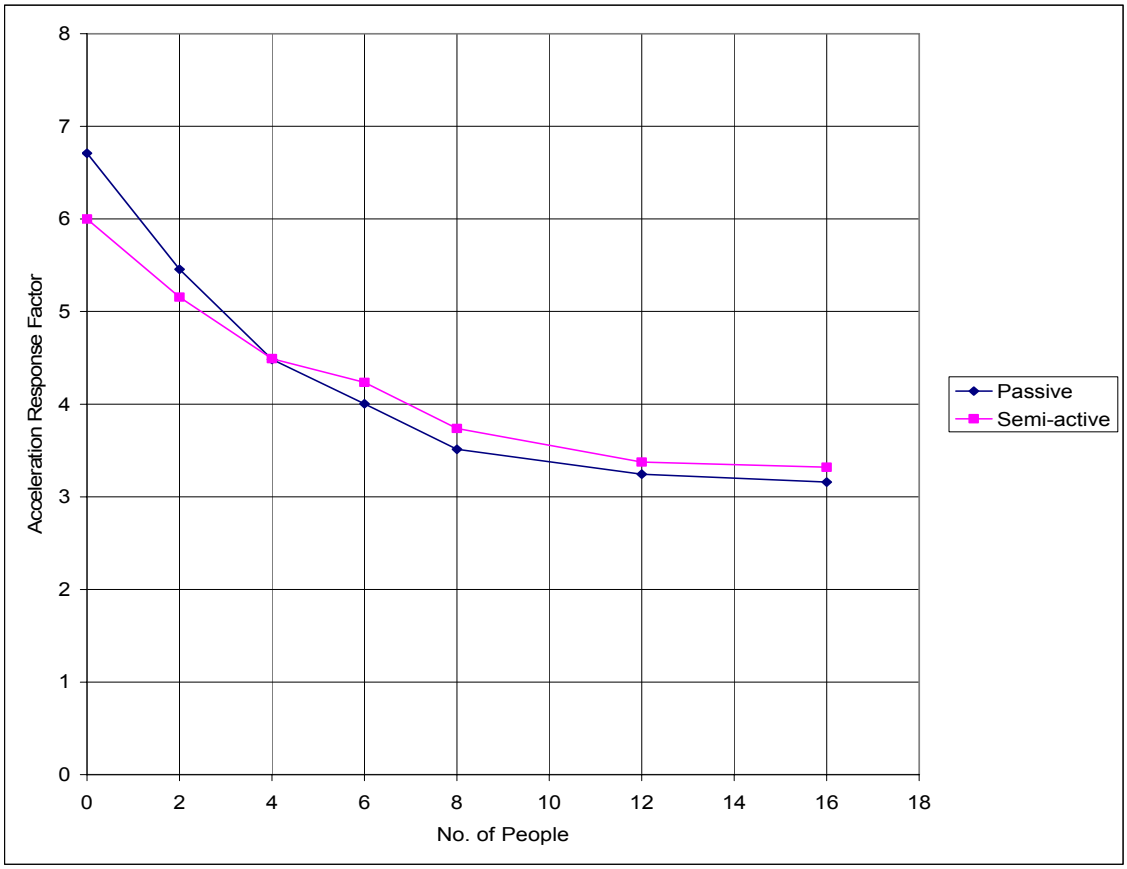

Figure 3.48 – Analytical Comparison of Semi-active and Passive Control of the Bare Floor with Humans on the Floor

The scope of this thesis is limited to the reduction in acceleration with the application of a magneto-rheological damper in a tuned-mass damper. Therefore, it can be stated that the semi-active system does not lend itself to the addition of humans to the floor in these various positions when a human's structural interaction is predominant. As a result a more comprehensive study is required to understand the exact interaction of the system when humans are introduced.

The trend exhibited in for the analytical and experimental studies are similar. However, for fewer the four people, there is a discrepancy between the analytical and experimental results. This may be due to changes in human dynamic parameters with different number of participants.

3.8.2 Mass Off-Tuning due to the Addition of Dead Mass to Floor

Figure 3.49 demonstrates the trend of peak accelerance with changes in the dead load on the floor. Figure 3.50 shows the analytical result with the same variation in floor mass. Table 3.4 gives the equivalent human cinder block weight per test used for the passive and semi-active tests to the corresponding number of individuals present on the floor, Figure 3.51. The experiment mode shape of the floor developed previously was used to establish the effective mass of the floor system with the additional mass. The percent change in floor mass was determined from this value and plotted with the corresponding change in peak floor accelerance.

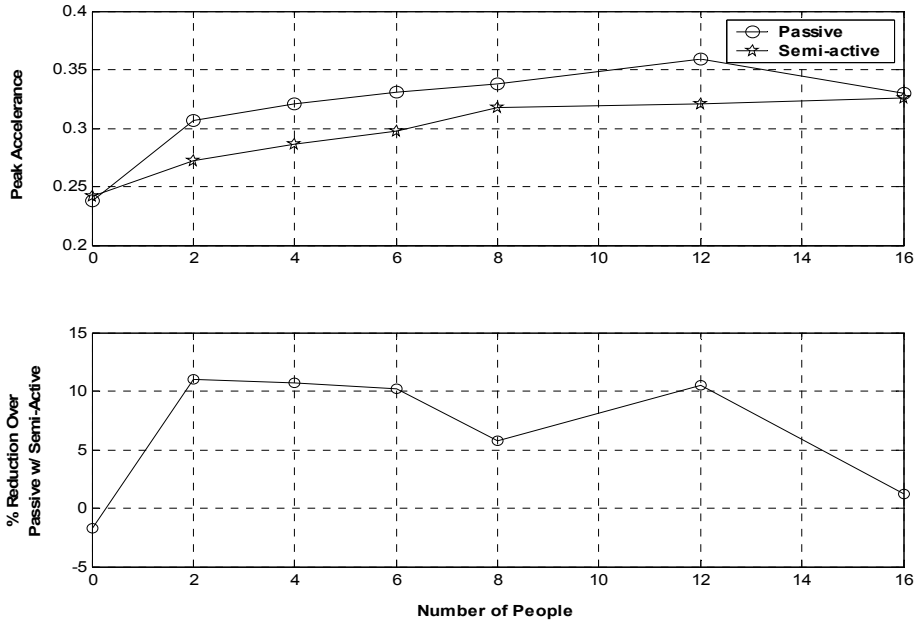

Figure 3.49 – Off-Tuning Response of Passive and Semi-Active System to Increase in Floor Mass from the Tuned System

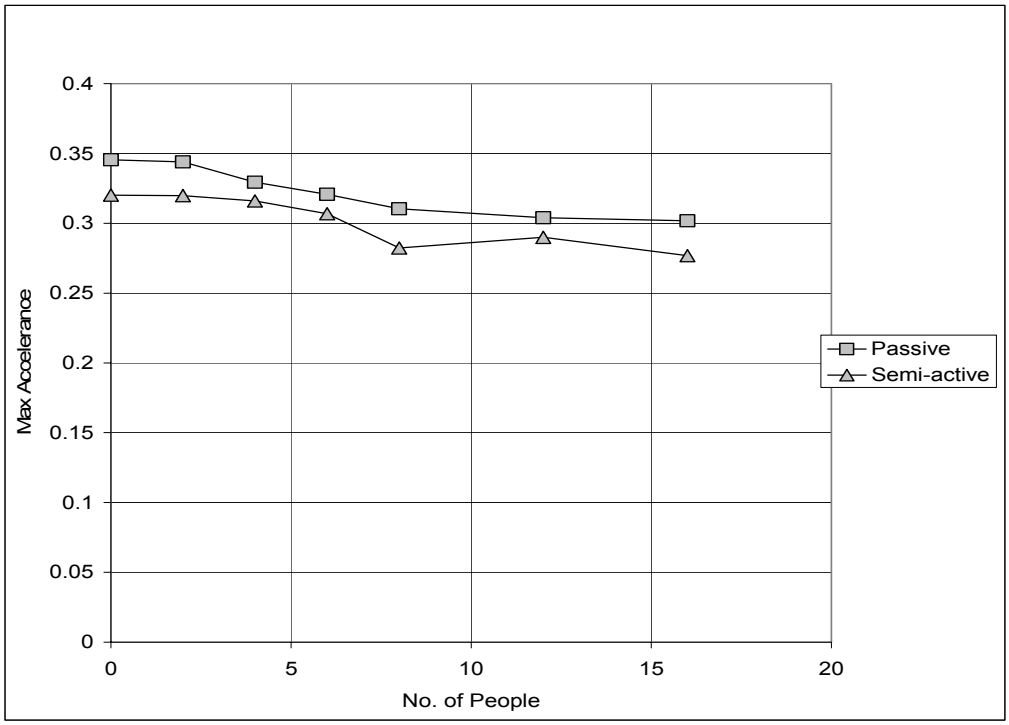

Figure 3.50 – Analytical Comparison of Semi-active and Passive Control of the Floor with Equivalent Humans Dead Weight on the Floor

		No. of People					
		2	**4**	**6**	**8**	**12**	**16**
Modal Line	**1**	0	0	0	0	0	0
	2	0	0	0	0	0	400
	3	0	0	0	0	210	210
	4	0	0	380	295	295	295
	5	0	380	0	450	450	450
	6	380	0	450	0	0	0
	7	0	380	0	380	380	380
	8	0	0	380	380	380	380
	9	0	0	0	0	315	315
	10	0	0	0	0	0	315
	11	0	0	0	0	0	0
	Total (lbs)	**380**	**760**	**1210**	**1505**	**2030**	**2745**

		No. of People					
		2	**4**	**6**	**8**	**12**	**16**
Modal Line	**1**	0	0	0	0	0	0
	2	0	0	0	0	0	255
	3	0	0	0	0	265	265
	4	0	0	340	295	295	295
	5	0	340	0	340	340	340
	6	410	0	410	0	0	0
	7	0	410	0	410	410	410
	8	0	0	315	315	315	315
	9	0	0	0	0	280	280
	10	0	0	0	0	0	220
	11	0	0	0	0	0	0
	Total (lbs)	**410**	**750**	**1065**	**1360**	**1905**	**2380**

Table 3.4 – Equivalent Human Weight Added to Floor per Test for Passive (top) and Semi-Active (bottom)

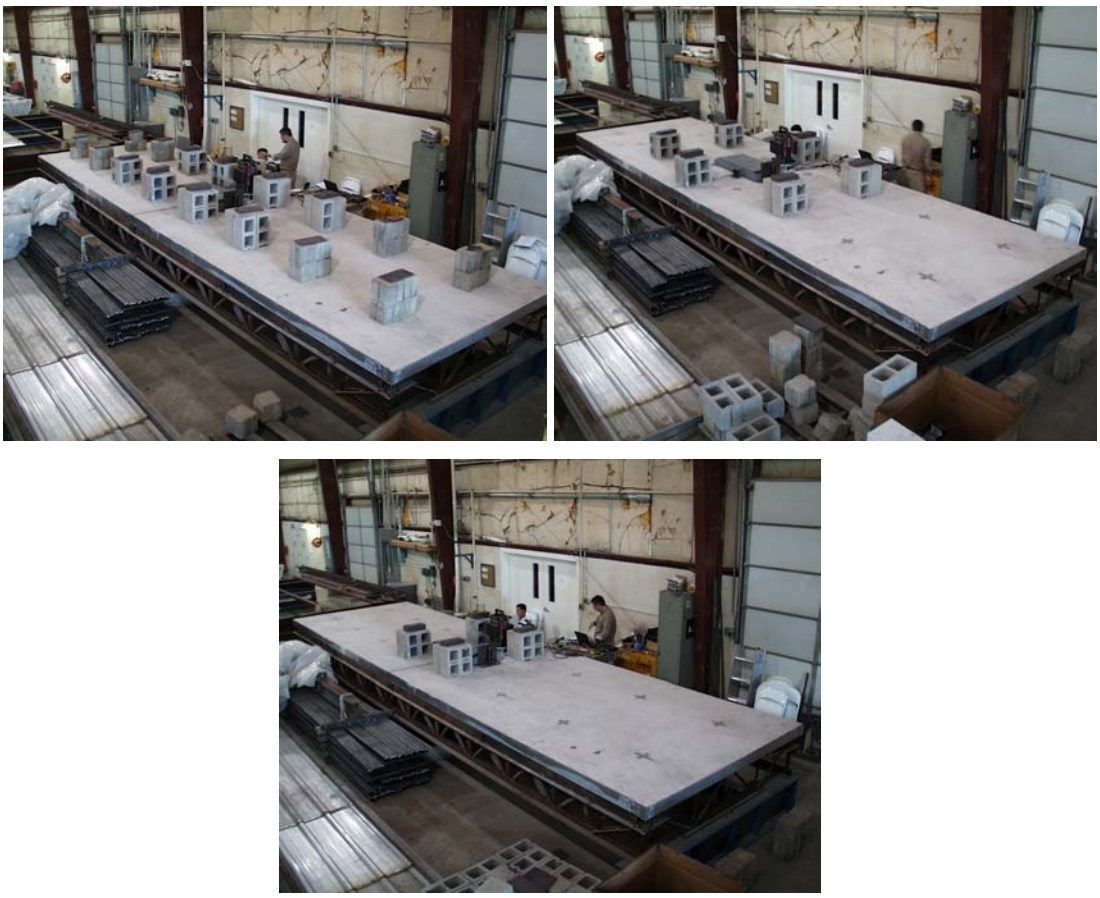

Figure 3.51 – Dead Human Weight Added to Floor for Passive and Semi-Active: 16 (top left), 6 (top right), 4 (bottom)

3.8.3 Frequency Off-Tuning due to the Variation of Spring Location of the Semi-Active PTMD

Variation in frequency ratio of the system was performed experimentally by varying the location of the spring, thus the stiffness of the PTMD. The spring location was varied from the optimum position to the locations corresponding to 29.5 in., 30.5 in., 31.5 in. and 32.5 in.

This study is effectively investigating the ability of each type of system to accommodate changes in the frequency ratio of the system. The interaction of the PTMD with the floor depends on this ratio to bring the damping to the floor modal frequency that is causing problematic acceleration.

Two different sets of tests were conducted and the results are shown in Figure 3.52. Problems occurred with the MR damper – inconsistency between tests, low reliability in the MR damper performance, and experimental adjustments in equipment parameters. Figure 3.52 is the ratio of the response for each system from their optimum point, and to note the response seen in the second set of tests had a very low correlation to those from first set shown in Figure 3.52.

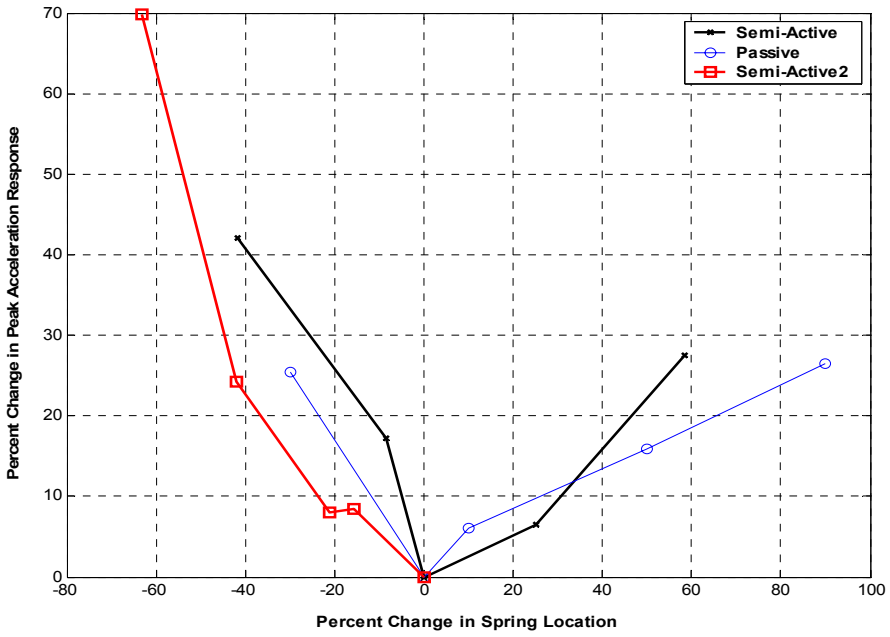

Figure 3.52 – Off-Tuning Response of Passive and Semi-Active System to Changes in PTMD Stiffness, i.e. Changes in Frequency Ratio

3.8.4 Floor Response Off-Tuning to Changes in Semi-Active Damping

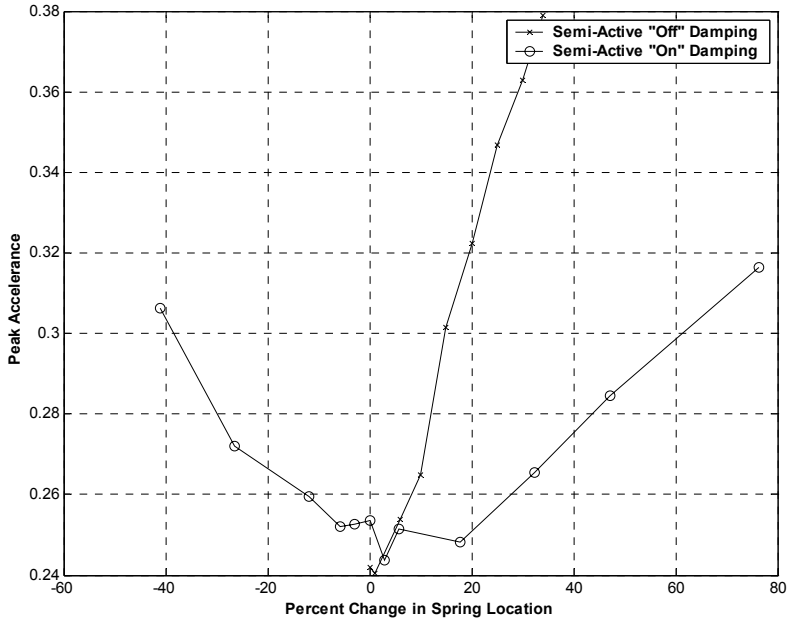

Figure 3.53 – Off-Tuning Response of Semi-Active System to Changes in MR Damping

Variation in MR on- and off-damping is given in figure 3.53. The respective peak floor accelerance is plotted for each change. These deviate from the trend shown analytically, because the presence of stiffness within damper is prevalent for small floor motion. It can be ignored for large motion (Koo et al. 2003). The analytical model assumes pure damping is provided for both the on and off state of the MR damper.

3.9 Floor Response to Human Excitation

3.9.1 Heel Drop

Figure 3.54 and 3.55 show the systems accelerance and time response respectively to a heel drop of a 210 lb person on the force plate with the electromagnetic shaker removed. The heel drop was performed on the "tuned" system and 5 averages were taken of the response. Theoretically, the result should be same; therefore, the accelerance response should be the same for any excitation as long as the excitation provides enough energy to excite the mode adequately. This is verified by the passive response that shows the optimal curve. The semi-active demonstrates an off-tuning of the system to the applied excitation. Overall, there is no benefit in the system response to a

heel drop beyond an optimally tuned passive system with MR for the experimental system being tested. Two tests, "a" and "b", are given for the floor and semi-active to show consistency of measurement.

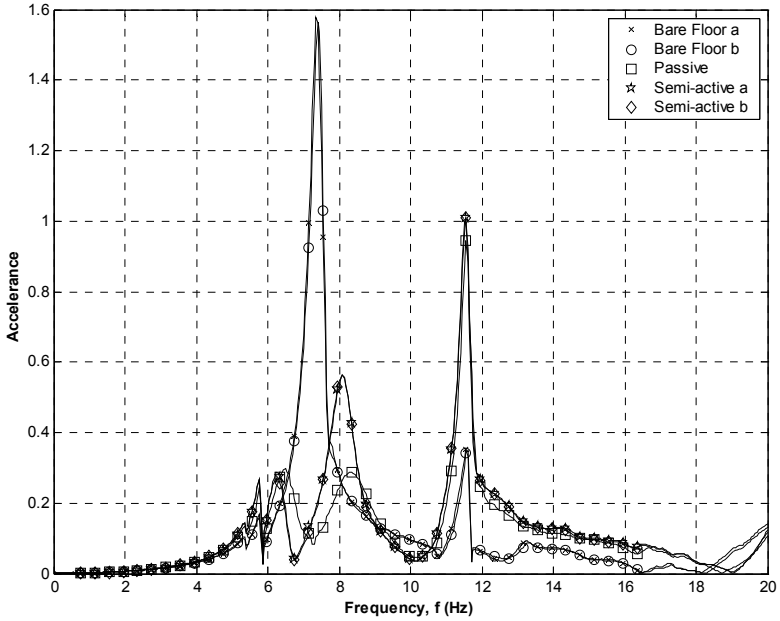

Figure 3.54 –Frequency Response of Bare Floor, Passive, and Semi-Active System to an Imparted Heel Drop on the Force Plate

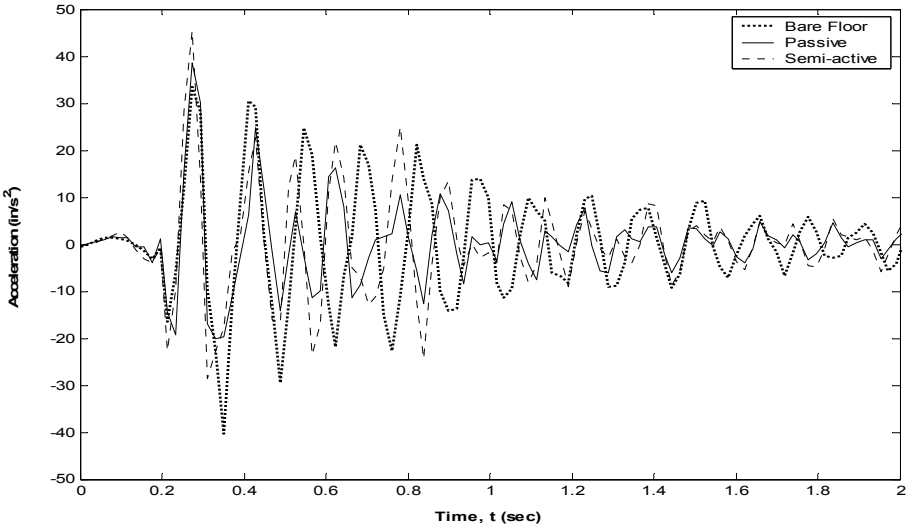

Figure 3.55 –Time Response of Bare Floor, Passive, and Semi-Active System to an Imparted Heel Drop on the Force Plate

3.9.2 Walking

The time response of the bare floor, passive control, and semi-active control system to walking at 150 bpm by a 220 lbs person is given in Figures 3.56 through 3.58 respectively. The root-mean square of acceleration is given in Table 3.5. By inspection the figures and tabulated values, the passive system provides a much larger reduction in overall response of the floor subjected to human walking. Two tests, "a" and "b", are given for the floor and semi-active to show consistency of measurement.

Intuitively, the reduction in semi-active should be nearly equal to the passive reduction in floor acceleration. The discrepancy returns to the issue of the semi-active control used with the MR damper trying to mitigate the response by achieving a 90 degrees phase shift between the PTMD and floor. The dampers response resolution is inadequate for this type of system and unable to moderate the response fast enough. Another source of error is the system response is so small and has an effect on the damper performance. It has not been tailored to quell small motion; therefore, this is a physical design issue for this damper.

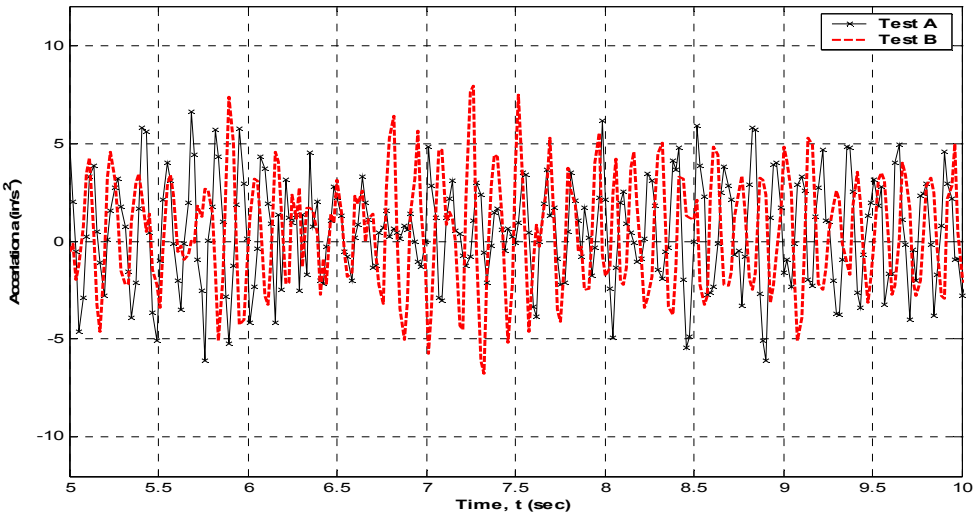

Figure 3.56 –Time Response of Bare Floor to Walking @ 150 bpm

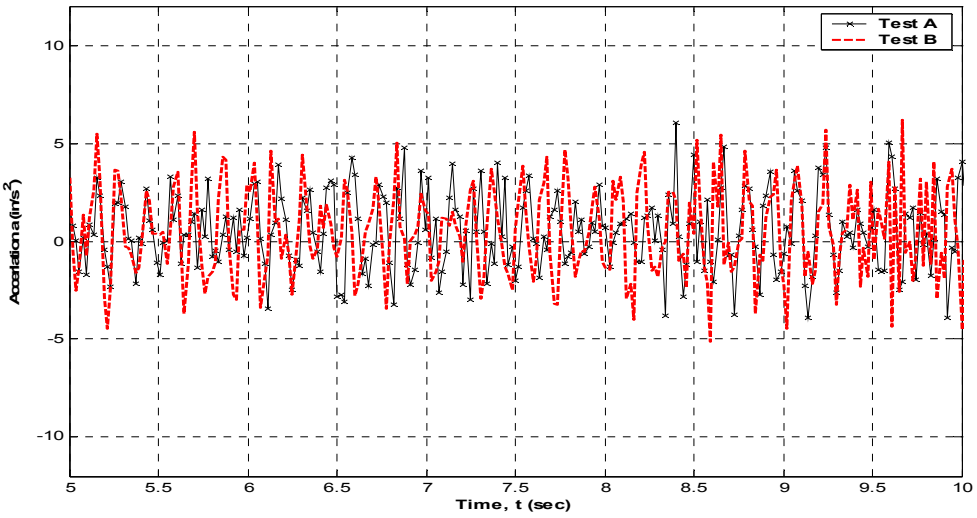

Figure 3.57 –Time Response of Floor with Passive Control to Walking @ 150 bpm

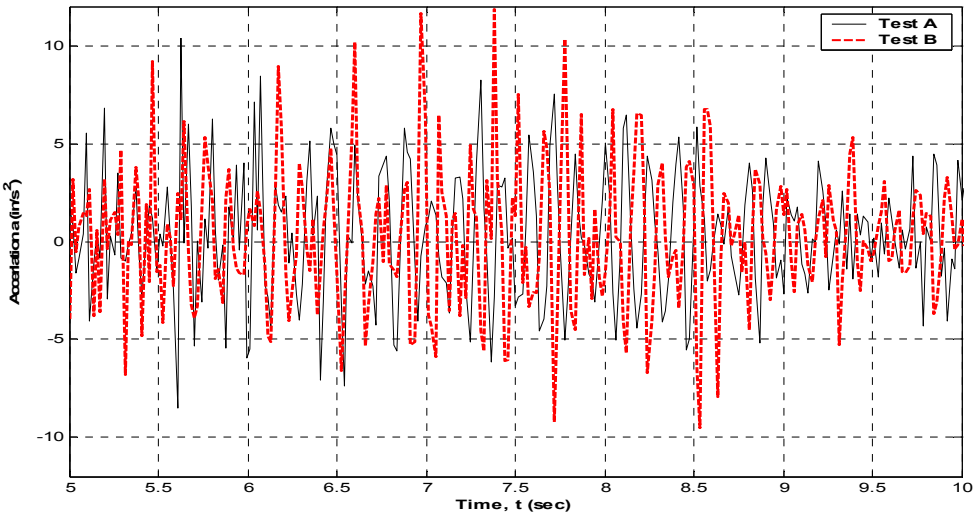

Figure 3.58 –Time Response of Floor with Semi-active Control to Walking @ 150 bpm

Table 3.5 –Root-Mean-Squared of Floor Acceleration Response due to Walking

	Test a (in/s^2)	Test b (in/s^2)	Average (in/s^2)	% Reduction from Bare Floor Acceleration
Bare Floor	3.9249	3.611	3.76795	N/A
Passive	1.9889	2.4799	2.2344	40.70%
Semi-active	3.2857	3.4373	3.3615	10.79%

CHAPTER 4

CONCLUSIONS AND RECOMMENDATIONS

4.1 Summary and Conclusions

The introduction of a magneto-rheological damper into a pendulum tuned mass damper to reduce annoying floor vibrations was studied. Displacement based ground-hook control (Koo et al. 2003) was used. The response of the floor with a semi-active PTMD was compared to an equivalent passive PTMD analytically and experimentally.

Analytical evaluation of the system performance was investigated. Using Rayleigh's Quotient (Chopra, 1995) an equivalent single-degree of freedom system was established. The equation of motion of the overall configuration was developed. This equation was integrated into an optimization routine to obtain the optimum design parameters of the PTMD based on the largest reduction in peak floor acceleration. The optimized semi-active system reduction was only 10% greater than an equivalent optimized passive system. A parametric study established the ability of each system to accommodate system changes in all the parameters of system. The semi-active system showed the greatest ability to accommodate such changes beyond passive; this was due to the implemented control policy used by the MR damper.

Experimental investigation of the system gave insight into actual performance and system characteristics. Experimental modal analysis of each component system, floor and PTMD, allowed for the extraction of mode shape, natural frequency, and damping. Experimental tuning of both passive and semi-active system was performed. The floor response reduction using tuned semi-active PTMD was not greater than an equivalent optimized passive system. Addition of dead load to the floor revealed the semi-active control kept the system more tuned than its equivalent passive counterpart. Changing the spring stiffness showed the semi-active PTMD was able to accommodate the change, as it is shown analytically. An experimental study was conducted with the introduction of humans on the floor. The semi-active PTMD appeared to hinder the response reduction with the addition of humans, compared to system with a passive tuned-mass damper.

4.2 Errors

Analytical discrepancies arise from the assumed purity of the system. The analytical modeling assumed the floor to be simply supported, perfectly continuous distribution of mass, and linear. The actual floor is none of the above. The large floor end restraint leads to discrepancy between the analytical and experimental results.
The MR damper has its own assumptions. The MR damper is assumed piece-wise linear, only supplies damping, zero off-state damping, and switches from on to off-state between each point in time instantaneously. Experimentally, the piece-wise linearity and small switch time between states are valid assumptions and justified by observation of the time history of the response. The damper did not purely provide damping; there was an associated stiffness.

The MR damper used was not suited for small vibration. Semi-active tests measurements showed inconsistencies within the system as compared to the reliability of the passive system which was re-established after a few months to the initial tuned parameters and the system was tuned. Therefore, test repeatability with MR is very low for this particular floor and PTMD system with its respective experimental equipment.

4.3 Recommendations

For further insight into a plausible semi-active system to control floor vibrations, the following recommendations are suggested for further study. Develop an alternate control scheme to accommodate the floor system acceleration. A different configuration of PTMD more tailored to MR that responds more readily to small motion. Development and study of an MR damper that is tailored to small motion is suggested. To gain insight into the structural interaction of humans with a structural system, a more detailed study should be performed with and without PTMD on typical commercial size floors. A finite element model that incorporates the semi-active control policy on a multi-degree of freedom system would lend itself to more advanced study of the system dynamics rather than an equivalent approximation.

LIST OF REFERENCES

Allen, D. L. and Pernica, G. (1984). "A Simple Absorber For Walking Vibrations." *Canadian Journal of Civil Engineering*., 11(17513), 112-117.

Bachmann, H., et al. (1995). *"Vibration Problems in Structures: Practical Guidelines."* Birkhauser Verlag. Basel; Boston; Berlin.

Bell, D. H. (1994). "A Tuned Mass Damper to Control Occupant Induced Floor Vibration." *Proceedings of the Eighteenth Annual Meeting of the Vibration Institute.,* (June) , 184-185.

Chopra, A. K. (1995). Dynamics of Structures: Theory and Applications to Earthquake Engineering, Prentice-Hall, Inc. Englewood Cliffs, New Jersey.

Calson, J. D. and Weiss, K. D. (1994). "A Growing Attraction To Magnetic Fluids." *Machine Design.,* (August), 61-64.

Chrzan, M. J. and Carlson, J. D. (2001). "MR Fluid Sponge Devices And Their Use In Vibration Control Of Washing Machines." *Proceedings of SPIE – The International Society for Optical Engineering,*. 4331, 370-378.

Collette, S. (2002) "Tuned Mass Dampers for a Suspended Structure of Footbridges and Meeting Boxes" *Proceedings of the Conference Footbridge 2002, Design and Dynamic Behavior of Footbridges*. November 20-22.

Den Hartog, J. P. (1947). "Mechanical Vibrations." Dover Publications Inc. New York.

ESI Engineering Inc. (1970)

Hanagan, L. M. and Murray, T. M. (1995). "Active Control of Floor Vibration: Implementation Case Studies." *Proceedings of the American Control Conference*., 3(95CH35736), 1911-1915.

Hatanaka, A. and Kwon, Y. (2002). "Retrofit of Footbridge for Pedestrian Induced Vibration Using Compact Tuned Mass Damper" *Proceedings of the Conference Footbridge 2002, Design and Dynamic Behavior of Footbridges*. November 20-22.

Hibbeler, R. C. (2001). *Engineering Mechanics: Dynamics.*, Macmillian, Inc. New York.

Inman, D. J. (1994) *Engineering Vibration.*, Prentice-Hall, Inc. Englewood Cliffs, New Jersey.

Koo, J., Ahmadian, M., Setareh, M., and Murray, T. M. (2003). *"Experimental Dynamic Analysis of Magneto-Rheological Tuned Vibration Absorbers."* Proceedings of DETC: ASME Design Engineering Technical Conference.

Lenzen, K. H. (1966). "Vibration Of Steel Joist – Concrete Slab Floors." *Engrg. J.,* AISC *3*(3), 133-136.

Murray, T. M., Allen, D. E., and Ungar, E. E. (1997). *AISC Steel Design Guide Series 11: Floor Vibrations Due to Human Activity.* AISC., Chicago, IL.

Occhiuzzi, A., Spizzuoco, M., and Serino, G. (2002). "Semi-Active MR Dampers in TMD's for Vibration Control of Footbridges, Part1: Numerical Modeling and Control Algorithm" *Proceedings of the Conference Footbridge 2002, Design and Dynamic Behavior of Footbridges*. November 20-22.

Ohta, M., Masaki, N., Sakamoto, T., and Fujita, S. (1996). "Development of Semi-Active Damper Using Electrorheological Fluid for Reduction of Floor Vibration." *Seismic, Shock and Vibration American Society of Mechanical Engineers.*, Pressure Vessels Piping Division (Publication) PVP. ASME, New York, NY, USA. 341, 99-104.

Ormondroyd, J. and Den Hartog, J. P. (1928). "The Theory Of The Dynamic Vibration Absorber." *Trans. American Society of Mech. Engineers.,* APM-50-7, 9-22.

Recktenwald, G. (2000). *Numerical Methods with Matlab: Implementation and Application*., Prentice-Hall Inc. Englewood Cliffs, New Jersey.

Seiler, C., Fischer, O., and Huber, P. (2002). "Semi-Active MR Dampers in TMD's for Vibration Control of Footbridges, Part2: Numerical Analysis and Practical Realization" *Proceedings of the Conference Footbridge 2002, Design and Dynamic Behavior of Footbridges*. November 20-22.

Setareh, M. and Hanson, R. D. (1992). "Tuned Mass Dampers for Balcony Vibration Control." *Journal of Structural Engineering – ASCE*., 118(3), 723-740.

Shope, R. L. and Murray, T. M. (1995). "Using Tuned Mass Dampers to Eliminate Annoying Floor Vibrations." *Restructuring: America and Beyond Structures Congress – Proceedings*., ASCE, New York, NY, USA. 1, 339-348.

Thornton, C. H., Cuoco, D. A., and Velivasakis, E. E. (1990). "Taming Structural Vibrations." *Civil Engineering* (New York)., 60 (11), 57-59.

Webster, A. C. and Vaicaitis, R. (1992). "Application of Tuned Mass Dampers to Control Vibrations of Composite Floor Systems." AISC Engineering Journal., 3rd Qtr. 116-124.

Warmoth, F. J. Jr. (2002) “Floor Vibrations: Girder Effective Moment of Inertia and Cost Study.” M.S. Thesis, Virginia Polytechnic Institute and State University, Blacksburg, Virginia.

APPENDIX A: COMMON VOCBULARY AND TERMINOLOGY

The following is a list of the terminology used throughout this thesis and common to vibrations and modal analysis.

Static Deflection – the equilibrium position of a system resulting from applied static loads and self-weight**.**

Vibration – a subset of dynamics, the description of a body's motion about its static equilibrium position.

System – an integrated arrangement of components.

Frequency (f) – the number of oscillatory cycles per second that a system experiences.

Period (T) – the time required for the system to oscillate one full cycle of vibration and repeat itself.

Steady-State– an excitation or response of a system acting periodically.

Box - Car Window – a mathematical function with constant amplitude of one, defined for a specific time range and multiplied by the measured response.

Mode Shape – an intrinsic characteristic of the system, the relative, displaced oscillatory configuration assumed by a freely vibrating system at a particular modal frequency.

Normal Mode – the modal configuration of a system oscillating at a phase of zero or 180 degrees. Node lines are stationary.

Complex Mode – the modal configuration is complex and can have any phase relationship. Node lines are not stationary.

Node – a point-location on a mode shape of zero displacement.

Node line – a line of zero displacement on a surface mode shape.

Anti-node – a point-location on a mode shape of maximum displacement.

Damping – mathematical measure of energy dissipated. See viscous, structural, and frictional/coulomb damping.

Critical Damping – the mathematical upper bound of damping that oscillatory decay will cease and the decay will become aperiodic.

Damping ratio – the ratio of the system damping – viscous, structural, coulomb – over the critical damping value for the system.

Viscous Damping – a mathematical value to describe the amount of the energy dissipated through the resistance of motion contributed by a fluid.

Structural Damping – a mathematical value to describe the amount of energy dissipated through the interaction of system components.

Frictional/Coulomb Damping **–** a mathematical value to describe the energy dissipated at the interface of two surfaces moving relative to one another.

Modal Mass – the effective inertial mass in a system that contributes to the vibration of a system excited at a particular natural frequency.

Periodic Function – function that repeats itself at every interval of the period.

Natural modes – the natural frequencies and modes shapes that are characteristic to a system.

Stiffness – an element or system characteristic that describes the amount of force to displace the element or system a unit amount.

Frequency Response Function - the complex ratio of the output and input frequency spectrums.

Heel Drop – the heel impact of a 190 pound person raised on the balls of their feet 2 in.

Chirp – a harmonic function with constant amplitude and an excitation frequency that changes as a function of time.

Harmonic Function – the individual or combination of the trigonomic functions sin(wt) and cos(wt) as an applied force or response.

Resonance – the state of a system excited by a force at the system's natural frequency and obtaining an "unbounded oscillation in the undamped case and a response with a maximum amplitude in the damped case" (Inman, 298).

Phase Angle – shift of the first peak of a harmonic function, measured, from the origin.

Step-Frequency – the rate of footfalls of a human; the number of steps taken per second.

Walking – the excitation of a system via footfalls from a person at a particular step-frequency.

Transducer – an instrument, such as an accelerometer, to measure the response of a system.

Analog to digital (A/D) conversion – the process of converting a measured analog signal to a digital signal that is utilized by a computer.

Causal System – a system that will not vibrate until an excitation is introduced**.**

Harmonic – an integer multiple of the frequency of an applied repetitive force.

Frequency Response Estimator – a model assumed for a system that places on the error in the measured to be on the input or output measurement**.**

Frequency Response Spectrum – a trace of a system's amplitudes over a range of frequencies.

Linearity – a relationship stating one parameter is directly proportional to another.

Modal Analysis – the analytical or experimental process to establish the modal frequencies, mode shapes and modal damping of system.

Transient – the time-variant response of parameter.

Natural Frequency – the frequencies of the systems that significant amplitudes of motion.

Fundamental Frequency – the lowest natural frequency of a system. The frequency of the floor that is prone to be the most problematic.

Excitation – an applied forcing function –heel drop, walking, bouncing, etc. - to vibrate a system.

Acceleration – the displacement of a system per the square of time. It is typically expressed as percentage of gravity in structural vibrations induced by human activities.

Velocity – the displacement of a system per unit time.

Displacement – the measure of distance that a point moves from its static equilibrium position.

Periodic – a characteristic of a function that repeats itself at each interval of time equal to the period.

Aperiodic – a characteristic description of a function in the time domain that is arbitrary.

APPENDIX B: FLOOR WEIGHT TAKE OFF (Matcad 2002)

System Mass:

Compenent Weight Method:

$Span := 30$ ft $g := 386$ in / s^2

$Grdr\_spacing := 8$ ft

Joist Girder (2L 3x3x1/4 (9.80 plf) T&B) $w_{joist\_grdr} := 2 \cdot 9.80$

$w_{joist\_grdr} = 19.6$ plf

Transverse Joist (1.4 plf) $w_{joist} := 1.4 \cdot \frac{Grdr\_spacing}{2} \cdot 3 \cdot \frac{1}{Span}$

$w_{joist} = 0.56$ plf

Concrete Deck (51 psf) $w_{deck\_conc} := 51 \cdot \frac{Grdr\_spacing}{2}$

$w_{deck\_conc} = 204$ plf

HSS 5x3x5/16 (14.83 plf) $w_{HSS} := 14.83$ plf

$w_{tot} := w_{joist\_grdr} + w_{joist} + w_{deck\_conc} + w_{HSS}$

$w_{tot} = 238.99$ $w_{tot} := 240$ plf

convert to kips per inch

$\frac{w_{tot}}{1000 \cdot 12} = 0.02$ kips / in -- per joist girder

total system weight: $W := 2 \cdot \frac{w_{tot}}{1000 \cdot 12} \cdot Span \cdot 12$ $W = 14.4$ kips

system mass: $M := \frac{W}{g}$ $M = 0.0373$ kips s^2 / in

APPLYING THE CONSERVATION OF MASS AND USING J. WARMOTH'S (jw) VALUES FOR FREQUENCY AND MOMENT OF INERTIA, BACK CALCULATE THE DISTRIBUTED WEIGHT T(FIND THE MASS (THESE VALUES SHOULD AGREE).

$fn_{jw} := 8.56$ Hz $I_{jw} := 927.2$ in ^ 4

$$fn_{jw} = \frac{\pi}{2} \cdot \sqrt{\frac{g \cdot E \cdot I_{jw} \cdot 2}{w_{jw} \cdot (Span \cdot 12)^4}}$$

APPENDIX C: PTMD Model Mathcad Calculations

$L := 49.37$ $k := 3250$ $l_s := 30.25$ $E := 29 \cdot 10^6$ $I := 8.64$

RAYLEIGH RITZ: CHOPRA: implementation of a an approximate, normalized, shape function.

$\psi(x) := \frac{-x}{L}$ $\psi(0) = 0$ $\psi\left(\frac{l_s}{2}\right) = -0.306$ $\psi(l_s) = -0.613$ $\psi(L) = -1$

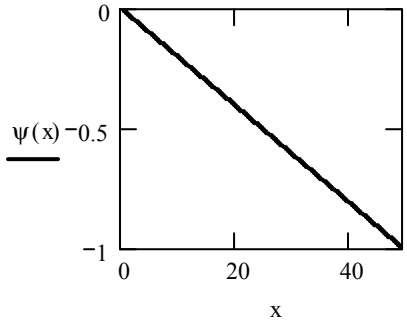

$w_a := 0.81$ lb / in.

$l_p := 38$ $l_o := 5.13$ $m_1 := \frac{2 \cdot w_a}{386}$ $m_2 := \frac{700}{386 \cdot l_p}$

$M_1 := \frac{w_a \cdot 17.37}{386}$ $M_2 := \frac{w_a \cdot 2 \cdot 6}{386}$ $M_3 := \frac{w_a \cdot 17.37}{386}$ $l_{sa} := 31.313$

$$f_n := \frac{1}{2 \cdot \pi} \cdot \sqrt{\frac{\int_0^L E \cdot I \cdot \left(\frac{d^2}{dx^2} \psi(x)\right)^2 dx + k \cdot \psi(l_s)^2}{\int_0^L m_1 \cdot \psi(x)^2 dx + \int_{l_o}^{l_p + l_o} m_2 \cdot \psi(x)^2 dx + \left(M_1 \cdot \psi(l_o)^2 + M_2 \cdot \psi(l_{sa})^2 + M_3 \cdot \psi(L)^2\right)}}$$

$f_n = 6.956$ $f_n^{-1} = 0.14376$

$T_{SAP} := .1442$ SAP second mode $f_{SAP} := T_{SAP}^{-1}$ $f_{SAP} = 6.935$

$\frac{f_{SAP}}{f_n} \cdot 100 = 99.698$ percent

APPENDIX D: Passive Optimization of PTMD Acceleration (Closed Form)

```
Clc;  clear all;  close all
%Optimization
%Initial Guess
      x0=[.9773 .1378]';

%Lower (lb) and Upper (ub) Bounds
      lb=[0 0]';
      ub=[2 2]';
%Turn off Large-Scale Algorithms
options = optimset('LargeScale','off','display','iter','DiffMinChange',1e-
3,'DiffMaxChange',1);

%Optimization Routine
[x,fval]=fmincon(@mypend,x0,[],[],[],[],lb,ub,[],options)
%
%Plot the Optimized Solution
Zeta1=0.01037;
u=.0494;
g=0:.005:2;
 f=x(1); Zeta2=x(2);

%Turn on if plot for no TMD
%f=0
 %Zeta2=0
%u=0
fn1=7.35
N=(f^2-g.^2).^2+(2*Zeta2*g*f).^2;
D=((1-g.^2).*(f^2-g.^2)-f*g.^2.*(f*u+4*Zeta1*Zeta2)).^2+4*g.^2.*(Zeta1*(f.^2-
g.^2)+Zeta2*f.*(1-g.^2-g.^2*u)).^2;
```

```
%RECEPTANCE
%HT=sqrt(N./D);
%ACCELERANCE
HT=g.^2.*sqrt(N./D);
%
plot(fn1.*g,HT)
grid

% title(['\bfHartog - Optimized Curve'date]);
xlabel('\bfFrequency, f (hz)');

ylabel('\bfa1.*m1/F')
% ylabel('\bfReceptance')
% gtext(['\bff = ' num2str(x(1))])
% gtext(['\bfu = ' num2str(u)])
% gtext(['\bfZeta1 = ' num2str(Zeta1)])
% gtext(['\bfZeta2 = ' num2str(x(2))])

[x,y]=max(HT);
text(fn1.*g(y),x,['\bfPeak Response = ',
num2str(max(HT)),'\rightarrow\bullet'],'HorizontalAlignment','right')
```

```
function HTF=mypend(x)

Zeta1=0.01037;
u=.0494;
g=0:.005:2;
f=x(1);
Zeta2=x(2);

N=(f^2-g.^2).^2+(2*Zeta2*g*f).^2;
```

```
D=((1-g.^2).*(f^2-g.^2)-f*g.^2.*(f*u+4*Zeta1*Zeta2)).^2+4*g.^2.*(Zeta1*(f.^2-
g.^2)+Zeta2*f.*(1-g.^2-g.^2*u)).^2;

HT=g.^2.*sqrt(N./D); %Accelerance
%HT=sqrt(N./D);      %Receptance

HTF=max(HT);
```

APPENDIX E: Semi-active Optimization of PTMD Acceleration (Runge-Kutta)

```
clc;  clear all;  close all
%Optimization
'started'
fix(clock)

%Initial Guess
      x0=[1.0 .7 .08]';

%Lower (lb) and Upper (ub) Bounds
      lb=[0  0.1  0.01]';
      ub=[1.5  .7 .09]';


%Turn off Large-Scale Algorithms
options = optimset('LargeScale','off','display','iter','DiffMinChange',1e-
4,'DiffMaxChange',1);

%Optimization Routine
[x,fval]=fmincon(@MRPENDRK4,x0,[],[],[],[],lb,ub,[],options)

'complete'
fix(clock)
```

```
function HTF=MRPENDRK4(x)

%SYSTEM INPUTPARAMETERS
Zeta1=0.0104;
mu=0.0494;

var=x
f=x(1);
Zeta2_on=x(2);
Zeta2_off=x(3);

%Floor Properties
m1=.012946;
fn1=7.35;
k1=(2*pi*fn1).^2*m1;
wn1=2*pi*fn1;
c1=Zeta1*2*m1*wn1;

%TMD Properties
fn2=fn1*f;
wn2=2*pi*fn2;
```

```
m2=m1*mu;
lm=49.37;

k2=3.25; %kip / in.
ls=2*fn2*pi*lm*1/(sqrt(k2/m2));

lc=51.31;

c_on=2*Zeta2_on*wn2*m2*lm^2/lc^2;
c_off=2*m2*wn2*Zeta2_off*lm^2/lc^2;


T=30;
wo=2*pi/T;
N=3000;
dt=T/N;
F=1;

% g=[.8379/fn1];
% iteration=1;
xst=F/k1;
g=0.75:0.01:1.25;

for iteration=1:size(g,2);
prcnt=0.20;
%SYSTEM MATRICES
K=[k1 0;0 k2*ls^2];
M=[m1+m2 m2*lm; m2*lm m2*lm^2];

%
=====================================================================
==================================
%                                RK45 - FORCE ACTION
%
=====================================================================
==================================

h=dt;
tn=T;
y0=[0;0;0;0];

B=[F; 0]; w=g(iteration)*wn1;
ff=inv(M)*B;

t = (0:h:tn)';                %  Column vector of elements with spacing h
```

```
n = length(t);                  %  Number of elements in the t vector
y = y0*ones(n,1)';              %  Preallocate y for speed
h2 = h/2;  h3 = h/3;  h6 = h/6;  %  Avoid repeated evaluation of constants

for j=2:n

    if y(1,j-1)*(y(3,j-1)-lm.*y(4,j-1))>=0;
       C=[c1 0; 0 c_on*lc^2];
       A1=[zeros(2) eye(2); -inv(M)*K -inv(M)*C];

    else
       C=[c1 0; 0 c_off*lc^2];
       A1=[zeros(2) eye(2); -inv(M)*K -inv(M)*C];

    end

   kk1 = A1*y(:,j-1)+[0;0;ff]*sin(w*t(j-1));

   kk2 = A1*(y(:,j-1)+h2*kk1)+[0;0;ff]*sin(w*(t(j-1)+h2));

   kk3 = A1*(y(:,j-1)+h2*kk2)+[0;0;ff]*sin(w*(t(j-1)+h2));

   kk4 = A1*(y(:,j-1)+h*kk3)+[0;0;ff]*sin(w*(t(j-1)+h));

   y(:,j) = y(:,j-1) + h6*(kk1+kk4) + h3*(kk2+kk3);

end

%obtaining acceleration in frequency domain and then covert back to time domain

% fftv1=fft(y(3,:));
% ffta11=fftv1(2:N/2).*(j*wo.*[1:N/2-1]);
% ffta12=fliplr(conj(ffta11));
% ffta1=[0 ffta11 fftv1(N/2+1).*(N/2*j*wo) ffta12];
% ffta1m=ffta1;
% av1=real(1/N.*ifft(ffta1m));
% differentiation of velocity in time to obatin acceleration
av(1)=0;
for i=1:N-1;
av1(i+1)=(y(3,i+1)-y(3,i))./dt;    %(REF:http://mathworld.pdox.net/math/d/d.htm)
av2(i+1)=(y(4,i+1)-y(4,i))./dt;
end
% fftv1=fft(y(4,:));
% ffta11=fftv1(2:N/2).*(j*wo.*[1:N/2-1]);
% ffta12=fliplr(conj(ffta11));
% ffta1=[0 ffta11 fftv1(N/2+1).*(N/2*j*wo) ffta12];
```

```
% ffta1m=ffta1;
% av2=real(1/N.*ifft(ffta1m));

% ymax1(iteration)=max(y(1,round(size(y,2)-prcnt*size(y,2)):size(y,2)));
% ymax2(iteration)=max(y(2,round(size(y,2)-prcnt*size(y,2)):size(y,2)));
%
% vmax1(iteration)=max(y(3,round(size(y,2)-prcnt*size(y,2)):size(y,2)));
% vmax2(iteration)=max(y(4,round(size(y,2)-prcnt*size(y,2)):size(y,2)));
%
amax1(iteration)=max(av1(1,round(size(av1,2)-prcnt*size(av1,2)):size(av1,2)-10));
% amax2(iteration)=max(av2(1,round(size(av2,2)-prcnt*size(av2,2)):size(av2,2)-10));

end  %<----IF DOING TIME ANALYSIS, TURN THIS "END STATEMENT" OFF
```

APPENDIX F: Finite Element Modeling Data

; File C:\Documents and Settings\jritchey\Desktop\FinalSapModel8_03\PendTMD\ClosdPend.$2k saved 8/10/03 10:28:09 in Kip-in

SYSTEM
  DOF=UX,UZ,RY LENGTH=IN FORCE=Kip PAGE=SECTIONS

JOINT
  1 X=49.37 Y=0 Z=48
  2 X=25.655 Y=0 Z=24
  4 X=39.81 Y=0 Z=48
  7 X=35.03 Y=0 Z=48
  8 X=44.59 Y=0 Z=48
  9 X=30.374 Y=0 Z=48
  10 X=30.374 Y=0 Z=24
  16 X=51.31 Y=0 Z=0
  17 X=51.31 Y=0 Z=24
  18 X=51.31 Y=0 Z=48
  19 X=0 Y=0 Z=0
  20 X=0 Y=0 Z=24
  21 X=0 Y=0 Z=48
  22 X=25.655 Y=0 Z=0

RESTRAINT
  ADD=2 DOF=U1,U2,R1,R2,R3
  ADD=16 DOF=U1,U2,U3,R1,R2,R3
  ADD=17 DOF=U1,U2,R1,R2,R3
  ADD=19 DOF=U1,U2,U3,R1,R2,R3
  ADD=20 DOF=U1,U2,R1,R2,R3
  ADD=21 DOF=U1,U2,R1,R3

```
  ADD=22  DOF=U1,U2,U3,R1,R2,R3

PATTERN
  NAME=DEFAULT

MASS
  ADD=1  U3=.0006395
  ADD=17  U3=.006473
  ADD=20  U3=.006473

MATERIAL
  NAME=STEEL  IDES=S  M=7.324E-07  W=.000283
    T=0  E=29000  U=.3  A=.0000065  FY=36
  NAME=CONC  IDES=C  M=2.246377E-07  W=.0000868
    T=0  E=3600  U=.2  A=.0000055
  NAME=OTHER  IDES=N  M=2.246377E-07  W=.0000868
    T=0  E=3600  U=.2  A=.0000055
  NAME=S1  IDES=S
    T=0  E=3.3132  U=0  A=0  FY=36
  NAME=S2  IDES=S
    T=0  E=.78  U=0  A=0  FY=36
  NAME=R  IDES=S
    T=0  E=1E+09  U=0  A=0  FY=36

FRAME SECTION
  NAME=S1 MAT=S1 SH=R T=10,10 A=100 J=1408.333 I=833.3333,833.3333 AS=0,0
  NAME=S2 MAT=S2 SH=R T=10,10 A=100 J=1408.333 I=833.3333,833.3333 AS=0,0
  NAME=R MAT=R SH=R T=1,1 A=1 J=.1408333 I=8.333334E-02,8.333334E-02
AS=0,0

NLPROP
```

```
 NAME=D1    TYPE=Damper
  DOF=U1  KE=0  CE=0  K=2480  C=.012436  CEXP=1
 NAME=D2    TYPE=Damper
  DOF=U1  KE=0  CE=0  K=14074  C=.007037  CEXP=1

FRAME
 1  J=20,2  SEC=R  NSEG=4  ANG=0
 2  J=2,10  SEC=R  NSEG=4  ANG=0
 3  J=10,17  SEC=R  NSEG=4  ANG=0
 6  J=1,18  SEC=R  NSEG=4  ANG=0
 9  J=16,17  SEC=S1  NSEG=2  ANG=0  IREL=R3  JREL=R3
 11  J=19,20  SEC=S1  NSEG=2  ANG=0  IREL=R3  JREL=R3
 12  J=20,21  SEC=R  NSEG=2  ANG=0  IREL=R3
 14  J=21,9  SEC=R  NSEG=4  ANG=0  IREL=R3
 18  J=9,7  SEC=R  NSEG=4  ANG=0
 19  J=9,10  SEC=S2  NSEG=2  ANG=0  IREL=R3  JREL=R3
 20  J=7,4  SEC=R  NSEG=4  ANG=0
 21  J=4,8  SEC=R  NSEG=4  ANG=0
 22  J=8,1  SEC=R  NSEG=4  ANG=0

NLLINK
 1  J=22,2  NLP=D1  ANG=0
 2  J=17,18  NLP=D2  ANG=0

LOAD
 NAME=LOAD1  CSYS=0
  TYPE=FORCE
   ADD=2  UZ=-1

MODE
 TYPE=EIGEN  N=2  TOL=.00001
```

```
FUNCTION
  NAME=PNT8 DT=0 NPL=1 PRINT=Y FILE=0pnt8.txt
  NAME=PNT9 DT=0 NPL=1 PRINT=Y FILE=0pnt9.txt
  NAME=1PT0 DT=0 NPL=1 PRINT=Y FILE=1pnt0.txt
  NAME=1PT1 DT=0 NPL=1 PRINT=Y FILE=1pnt1.txt
  NAME=1PT2 DT=0 NPL=1 PRINT=Y FILE=1pnt2.txt
  NAME=1PT05 DT=0 NPL=1 PRINT=Y FILE=1pnt05.txt
  NAME=0PT97 DT=0 NPL=1 PRINT=Y FILE=0pnt97.txt
  NAME=PT95 DT=0 NPL=1 PRINT=Y FILE=0pnt95.txt

HISTORY
  NAME=PT9 TYPE=NON NSTEP=4000 DT=.005 DAMP=0 DTMAX=0 ENVE=Y
    LOAD=LOAD1 FUNC=PNT9 SF=1 AT=0
  NAME=PT8 TYPE=NON NSTEP=4000 DT=.005 DAMP=0 DTMAX=0
    LOAD=LOAD1 FUNC=PNT8 SF=1 AT=0
  NAME=PT97 TYPE=NON NSTEP=4000 DT=.005 DAMP=0 DTMAX=0
    LOAD=LOAD1 FUNC=0PT97 SF=1 AT=0
  NAME=1PT0 TYPE=NON NSTEP=4000 DT=.005 DAMP=0 DTMAX=0
    LOAD=LOAD1 FUNC=1PT0 SF=1 AT=0
  NAME=1PT05 TYPE=NON NSTEP=4000 DT=.005 DAMP=0 DTMAX=0
    LOAD=LOAD1 FUNC=1PT05 SF=1 AT=0
  NAME=1PT1 TYPE=NON NSTEP=4000 DT=.005 DAMP=0 DTMAX=0
    LOAD=LOAD1 FUNC=1PT1 SF=1 AT=0
  NAME=1PT2 TYPE=NON NSTEP=4000 DT=.005 DAMP=0 DTMAX=0
    LOAD=LOAD1 FUNC=1PT2 SF=1 AT=0
  NAME=PT95 TYPE=NON NSTEP=4000 DT=.005 DAMP=0 DTMAX=0
    LOAD=LOAD1 FUNC=PT95 SF=1 AT=0

OUTPUT
; No Output Requested
```

```
END

; The following data is used for graphics, design and pushover analysis.
; If changes are made to the analysis data above, then the following data
; should be checked for consistency.
SAP2000 V7.44 SUPPLEMENTAL DATA
  GRID GLOBAL  X "1"  0
  GRID GLOBAL  X "2"  25.655
  GRID GLOBAL  X "3"  30.374
  GRID GLOBAL  X "4"  49.37
  GRID GLOBAL  X "5"  51.31
  GRID GLOBAL  Y "6"  0
  GRID GLOBAL  Z "7"  0
  GRID GLOBAL  Z "8"  24
  GRID GLOBAL  Z "9"  48
  GRID GLOBAL  Z "10"  72
  MATERIAL STEEL FY 36
  MATERIAL S1 FY 36
  MATERIAL S2 FY 36
  MATERIAL R FY 36
  MATERIAL CONC FYREBAR 60 FYSHEAR 40 FC 4 FCSHEAR 4
  FRAMESECTION S1 AS2 83.33334 MFAS2 0 AS3 83.33334 MFAS3 0
  FRAMESECTION S2 AS2 83.33334 MFAS2 0 AS3 83.33334 MFAS3 0
  FRAMESECTION R AS2 .8333333 MFAS2 0 AS3 .8333333 MFAS3 0
  STATICLOAD LOAD1 TYPE DEAD
END SUPPLEMENTAL DATA
```

APPENDIX G: PTMD Mass and Center of Gravity

Misc:

Angle Base			
Side Angles			
Length (in)	44.24	in	using centerline of angles
Weight per in	0.81000	lb/in	
No of Angles	2		
Total Weight	71.6688	lbs	
End Angle (@ pin)			
Length (in)	17.37	in	
Weight per in	0.81	lb/in	
No of Angles	1		
Total Weight	14.0697	lbs	
End Angle (@ tip)			
Length (in)	17.37	in	
Weight per in	0.81	lb/in	
No of Angles	1		
Total Weight	14.0697	lbs	
Total Angle Base	99.8082		

Total Angle Base			
Perimeter (in.)	123.22	in	
Weight per in	0.81	lb/in	
No of Angles	1		
Total Weight	99.8082	lbs	o.k

Spring Angles		
Length (in)	5.75	in
Weight per in	0.81	lb/in
No of Angles	2	
Total Weight	9.315	lbs

All Dim Measured w.r.t. Pin Support

	w	y	wy
Stack 1	175.14	39	6830.46
Stack 2	175.22	28.75	5037.575
Stack 3	175.58	19.25	3379.915
Stack 4	175.6	9.75	1712.1
Side Angles	71.6688	26.685	1912.482
Angle @ tip	14.0697	48.24	678.7223
Angle @ pin	14.0697	5.13	72.17756
Spring Angles	9.315	28.688	267.2287
□w	810.6632	□wy	19890.66

□wy/□w = 24.54 in. measured from support

APPENDIX H: PTMD Experimental Mass

Test 1

Support TMD at Four Corners w/ Load Cells

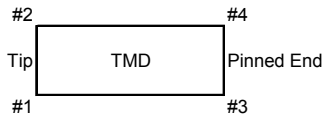

Test	#1	#2	#3	#4
1a	0.21	0.249	0.223	0.213
2a	0.215	0.251	0.221	0.201
3a	0.219	0.262	0.219	0.195
Average	**0.215**	**0.254**	**0.221**	**0.203**

lations show the tip reaction to be less than the pin reaction.

Test 2

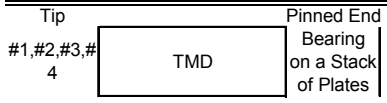

Test	1	2	3	Average
#1	0.42	0.422	0.422	0.421
#2	0.464	0.453	0.456	0.458
#3	0.398	0.393	0.393	0.395
#4	0.34	0.337	0.337	0.338
				0.403

Test 3

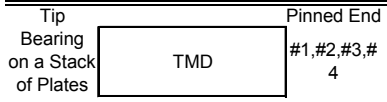

Test	1	2	3	Average
#1	0.408	0.406	0.411	0.408
#2	0.398	0.398	0.392	0.396
#3	0.457	0.454	0.459	0.457
#4	0.437	0.437	0.437	0.437
				0.425

Test 3

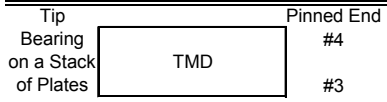

Test	1	2	3	Average
#3	0.194	0.197	0.194	0.195
#4	0.226	0.226	0.226	0.226
				0.421 O.K.

Errors	
	Resolution of the 10 kip load cell to measure loads at these low magnitudes
	Establishment of the location of the load on the PTMD pin side so the plate does not rotate when positioned onto the load cell
	Variance in height of the load cell arms
	Levelness of the TMD
	Symmetry of Loading in the PTMD

APPENDIX I: PTMD Spring Stiffness

Spring Location	30.25	in.
Gauge Location	32	in.

	Load (lbs)							
Plate No.	**Plate Weight**	**Load Applied**	**Load per Spring**	**? North @ Gauge (in.)**	**? North @ Spring (in.)**	**? South @ Gauge (in.)**	**? South @ Spring (in.)**	**? Average @ Total (in.)**
0	0	0	0	0	0.00000	0.00000	0.00000	0.00000
1	9.8	9.8	4.9	0.0031	0.00293	0.00290	0.00274	0.00284
2	9.88	19.68	9.84	0.0062	0.00586	0.00590	0.00558	0.00572
3	9.88	29.56	14.78	0.0092	0.00870	0.00900	0.00851	0.00860
4	10.14	39.7	19.85	0.0125	0.01182	0.01220	0.01153	0.01167
5	9.76	49.46	24.73	0.0158	0.01494	0.01510	0.01427	0.01461
6	9.98	59.44	29.72	0.0189	0.01787	0.01840	0.01739	0.01763
7	9.8	69.24	34.62	0.0218	0.02061	0.02150	0.02032	0.02047
8	9.76	79	39.5	0.0244	0.02307	0.02470	0.02335	0.02321
9	10	89	44.5	0.0293	0.02770	0.02852	0.02696	0.02733
10	9.92	98.92	49.46	0.0316	0.02987	0.03130	0.02959	0.02973
11	10.04	108.96	54.48	0.035	0.03309	0.03490	0.03299	0.03304
12	9.9	118.86	59.43	0.0392	0.03706	0.03790	0.03583	0.03644
13	10.06	128.92	64.46	0.0414	0.03914	0.04100	0.03876	0.03895
14	9.84	138.76	69.38	0.0445	0.04207	0.04440	0.04197	0.04202
15	10.22	148.98	74.49	0.0478	0.04519	0.04760	0.04500	0.04509
16	9.8	158.78	79.39	0.051	0.04821	0.05090	0.04812	0.04816
17	9.98	168.76	84.38	0.0541	0.05114	0.05420	0.05124	0.05119
20	9.88	178.64	89.32	0.0571	0.05398	0.05730	0.05417	0.05407
19	9.86	188.5	94.25	0.0604	0.05710	0.06070	0.05738	0.05724
18	9.98	198.48	99.24	0.0636	0.06012	0.06390	0.06041	0.06026

	Load (lbs)							
Plate No.	**Plate Weight**	**Load Applied**	**Load per Spring**	**? North @ Gauge (in.)**	**? North @ Spring (in.)**	**? South @ Gauge (in.)**	**? South @ Spring (in.)**	**? Average @ Total (in.)**
0	0	0	0	0	0.00000	0.00000	0.00000	0.00000
1	9.8	9.8	4.9	0.0042	0.00397	0.00410	0.00388	0.00392
2	9.88	19.68	9.84	0.0079	0.00747	0.00740	0.00700	0.00723
3	9.88	29.56	14.78	0.0107	0.01011	0.01070	0.01011	0.01011
4	10.14	39.7	19.85	0.014	0.01323	0.01370	0.01295	0.01309
5	9.76	49.46	24.73	0.0171	0.01616	0.01710	0.01616	0.01616
6	9.98	59.44	29.72	0.0202	0.01910	0.02020	0.01910	0.01910
7	9.8	69.24	34.62	0.0234	0.02212	0.02350	0.02221	0.02217
8	9.76	79	39.5	0.0269	0.02543	0.02690	0.02543	0.02543
9	10	89	44.5	0.0299	0.02826	0.03000	0.02836	0.02831
10	9.92	98.92	49.46	0.0331	0.03129	0.03310	0.03129	0.03129
11	10.04	108.96	54.48	0.0362	0.03422	0.03620	0.03422	0.03422
12	9.9	118.86	59.43	0.0395	0.03734	0.03920	0.03706	0.03720
13	10.06	128.92	64.46	0.0426	0.04027	0.04230	0.03999	0.04013
14	9.84	138.76	69.38	0.0456	0.04311	0.04550	0.04301	0.04306
15	10.22	148.98	74.49	0.0489	0.04623	0.04900	0.04632	0.04627
16	9.8	158.78	79.39	0.0519	0.04906	0.05200	0.04916	0.04911
17	9.98	168.76	84.38	0.055	0.05199	0.05500	0.05199	0.05199
20	9.88	178.64	89.32	0.058	0.05483	0.05820	0.05502	0.05492
19	9.86	188.5	94.25	0.0609	0.05757	0.06130	0.05795	0.05776
18	9.98	198.48	99.24	0.0636	0.06012	0.06390	0.06041	0.06026

Average		
? North @ Spring (in.)	**? South @ Spring (in.)**	**? Total (in.)**
0.00000	0.00000	0.00000
0.00345	0.00331	0.00338
0.00666	0.00629	0.00648
0.00941	0.00931	0.00936
0.01253	0.01224	0.01238
0.01555	0.01522	0.01538
0.01848	0.01824	0.01836
0.02136	0.02127	0.02132
0.02425	0.02439	0.02432
0.02798	0.02766	0.02782
0.03058	0.03044	0.03051

APPENDIX J: Experimental Modal Analysis of Floor

```
clear all; close all; clc;
test=[

'Mode01_trf';'Mode02_trf';'Mode03_trf';'Mode04_trf';'Mode05_trf';'Mode06_trf';'Mode0
7_trf';'Mode08_trf';'Mode09_trf';'Mode10_trf';

'Mode11_trf';'Mode12_trf';'Mode13_trf';'Mode14_trf';'Mode15_trf';'Mode16_trf';'Mode1
7_trf';'Mode18_trf';'Mode19_trf';'Mode20_trf';

'Mode21_trf';'Mode22_trf';'Mode23_trf';'Mode24_trf';'Mode25_trf';'Mode26_trf';'Mode2
7_trf';'Mode28_trf';'Mode29_trf';'Mode30_trf';

'Mode31_trf';'Mode32_trf';'Mode33_trf';'Mode34_trf';'Mode35_trf';'Mode36_trf';'Mode3
7_trf';'Mode38_trf';'Mode39_trf';'Mode40_trf';

'Mode41_trf';'Mode42_trf';'Mode43_trf';'Mode44_trf';'Mode45_trf';'Mode46_trf';'Mode4
7_trf';'Mode48_trf';'Mode49_trf';'Mode50_trf';
   'Mode51_trf';'Mode52_trf';'Mode53_trf';'Mode54_trf';'Mode55_trf'];


for i=1:55;

%=================================================================
=========
%=================================================================
=========
%=================================================================
=========

a_data=wk1read(test(i,:));
f=a_data(:,1)';
Factor=386/(0.41845*1000);
mag21=Factor.*10.^(a_data(:,2)./20)';
phase21=a_data(:,3)';


% figure(i)
%    subplot(2,1,1)
%       plot(f,mag21); grid;
%
start1=110;
stop1=120;
[x1,y1]=max(mag21(start1:stop1));
% line([f(y1+start1-1) f(y1+start1-1)],[0 x1],'LineStyle',':','LineWidth',3,'Color','r')
```

```
MagMode(i,1)=x1;    %mag of mode 1

start2=130;
stop2=160;
[x2,y2]=max(mag21(start2:stop2));
% line([f(y2+start2-1) f(y2+start2-1)],[0 x2],'LineStyle',':','LineWidth',3,'Color','k')

MagMode(i,2)=x2;    %mag of mode 2

start3=237;
stop3=245;
[x3,y3]=max(mag21(start3:stop3));
% line([f(y3+start3-1) f(y3+start3-1)],[0 x3],'LineStyle',':','LineWidth',3,'Color','b')

MagMode(i,3)=x3;    %mag of mode 3


% subplot(2,1,2)
% plot(f,phase21); grid;

%     line([f(y1+start1-1) f(y1+start1-1)],[min(phase21)
max(phase21)],'LineStyle',':','LineWidth',3,'Color','r')
PhaseMode(i,1)=phase21(y1+start1-1); %phase of mode 1 in degrees
%     line([f(y2+start2-1) f(y2+start2-1)],[min(phase21)
max(phase21)],'LineStyle',':','LineWidth',3,'Color','k')
PhaseMode(i,2)=phase21(y2+start2-1); %phase of mode 2 in degrees
%     line([f(y3+start3-1) f(y3+start3-1)],[min(phase21) max(phase
21)],'LineStyle',':','LineWidth',3,'Color','b')
PhaseMode(i,3)=phase21(y3+start3-1); %phase of mode 3 in degrees


ModeAmp(i,1)=MagMode(i,1).*sin(pi/180.*PhaseMode(i,1));
ModeAmp(i,2)=MagMode(i,2).*sin(pi/180.*PhaseMode(i,2));
ModeAmp(i,3)=MagMode(i,3).*sin(pi/180.*PhaseMode(i,3));

end

number_of_rows=5;
number_of_cols=11;

n=0;
for j=1:number_of_cols;
      Z1(:,j)=ModeAmp(n+1:n+number_of_rows,1);
      Z2(:,j)=ModeAmp(n+1:n+number_of_rows,2);
      Z3(:,j)=ModeAmp(n+1:n+number_of_rows,3);
      n=n+number_of_rows;
```

```
end
%Floor Coordinates
Y=[0 24 48 72 96];
X=[0 22.5 67.5 112.5 157.5 180 202.5 247.5 292.5 337.5 360];
%Plane Coordinates
X0=[0 400]
Y0=[0 100]
Z0=[0 0; 0 0]

% figure(11)
 a=max(abs(Z1));b=max(a);
% surf(X,Y,Z1/b);
% hold on
% surf(X0,Y0,Z0,'FaceAlpha',0.5);
%

figure(2)
a=max(abs(Z2));b=max(a);
surf(X,Y,Z2/b);
hold on
surf(X0,Y0,Z0,'FaceAlpha',0.5);

%plot section individually
figure(22)
subplot(5,1,1)
plot(X,1/b.*Z2(1,:),'kx-');grid; title(['\bfSectional Mode Shape - 7 hz    'date]);

subplot(5,1,2)
plot(X,1/b.*Z2(2,:),'kx-');grid

subplot(5,1,3)
plot(X,1/b.*Z2(3,:),'kx-');grid;ylabel('\bfAmplitude (Dim)');

subplot(5,1,4)
plot(X,1/b.*Z2(4,:),'kx-');grid

subplot(5,1,5)
plot(X,1/b.*Z2(5,:),'kx-'); grid;
xlabel('\bfDistance Along Span (in.)');


%Effective Mass for each modal section of second mode
lengths=[11.25 33.75 45 45 33.75 22.5 33.75 45 45 33.75 11.25]; %trib lengths
w=2*240/(12*1000); %distributed weight per unit length
mpnt=w.*lengths/386; %mass per location in kips s^2 / in.
```

```
Meff1=[1/min(Z2(1,:)).*Z2(1,:)]*diag(mpnt)*[1/min(Z2(1,:)).*Z2(1,:)]';
Meff2=[1/min(Z2(2,:)).*Z2(2,:)]*diag(mpnt)*[1/min(Z2(2,:)).*Z2(2,:)]'
Meff3=[1/min(Z2(3,:)).*Z2(3,:)]*diag(mpnt)*[1/min(Z2(3,:)).*Z2(3,:)]'
Meff4=[1/min(Z2(4,:)).*Z2(4,:)]*diag(mpnt)*[1/min(Z2(4,:)).*Z2(4,:)]'
Meff5=[1/min(Z2(5,:)).*Z2(5,:)]*diag(mpnt)*[1/min(Z2(5,:)).*Z2(5,:)]'
Meff=[Meff1 Meff2 Meff3 Meff4 Meff5]
meanMeff=mean(Meff)


%Find the Mean Deflected Shape
shape=[mean(Z2(:,1)) mean(Z2(:,2)) mean(Z2(:,3)) mean(Z2(:,4)) mean(Z2(:,5)) ...
      mean(Z2(:,6)) mean(Z2(:,7)) mean(Z2(:,8)) mean(Z2(:,9))mean(Z2(:,10))  ...
      mean(Z2(:,11))]
figure(23)
plot(X,shape./min(shape)); grid; xlabel('\bfDistance Along Span (in.)');
ylabel('\bfAmplitude (Dim)'); title(['\bfMean Mode Shape 'date]);
meanMeff2=shape*diag(mpnt)*shape'; text(25,.9, ['\bfMeff = 'num2str(meanMeff2)])
%3RD MODE
% figure(3)
% a=max(abs(Z3));b=max(a);
% surf(X,Y,Z3/b);
% hold on
% surf(X0,Y0,Z0,'FaceAlpha',0.5);
%
% figure(4);
% surf(X0,Y0,Z0,'FaceAlpha',0.5);
%following did not work, but kept the arrays for effort and time
%try another type of plot below with one 3d matrix
% Xs=[[zeros(11,1)]; X(2).*ones(11,1); X(3).*ones(11,1); X(4).*ones(11,1);
X(5).*ones(11,1)];
% Ys=[X'; X'; X'; X'; X'];
% Zs=1/b.*[Z2(1,:)';Z2(2,:)';Z2(3,:)';Z2(4,:)';Z2(5,:)']
% data=[Xs Ys Zs]
```

APPENDIX K: Force Plate Sensitivity

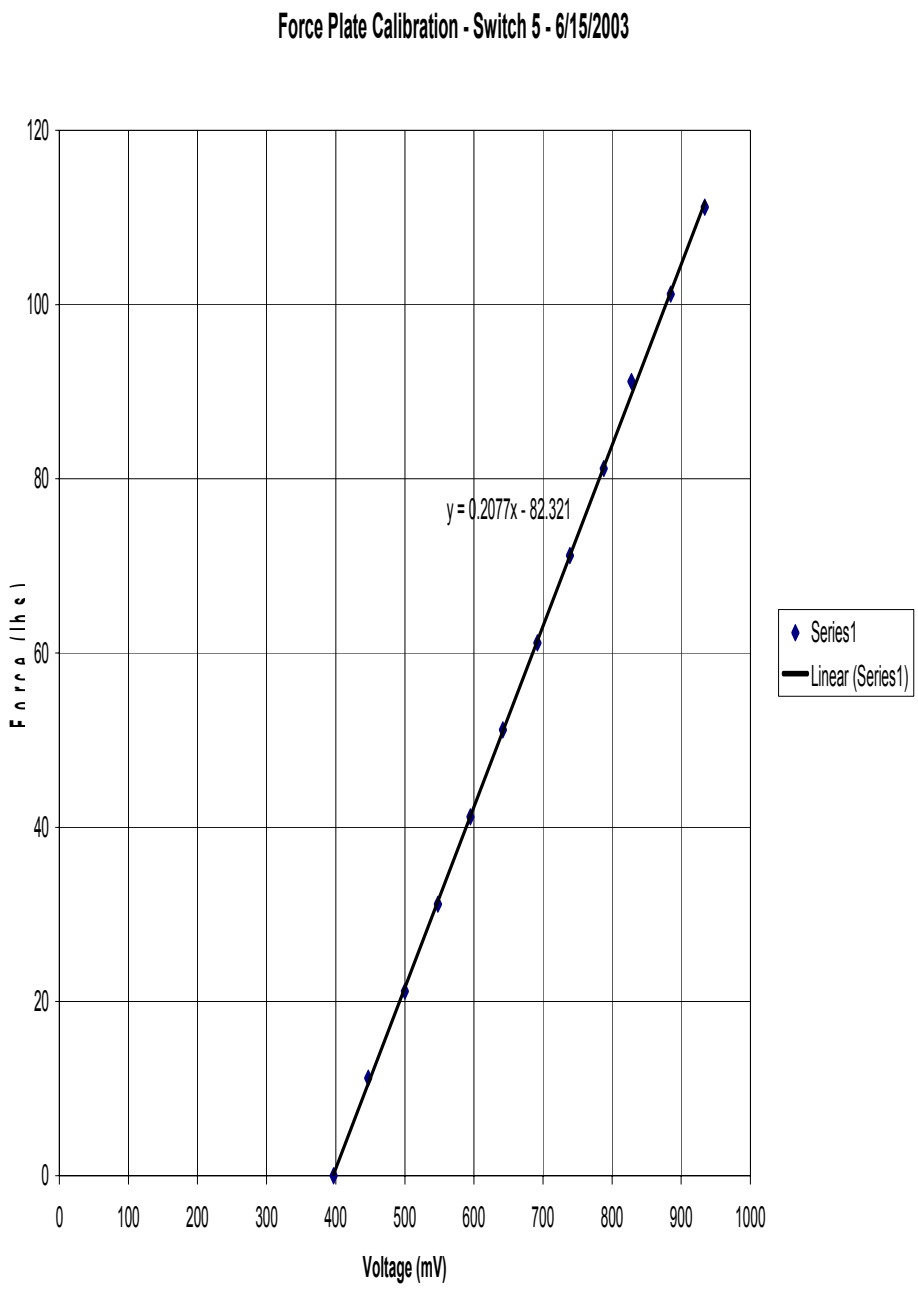

Figure K.1 – Force Plate Calibration – Force versus Voltage

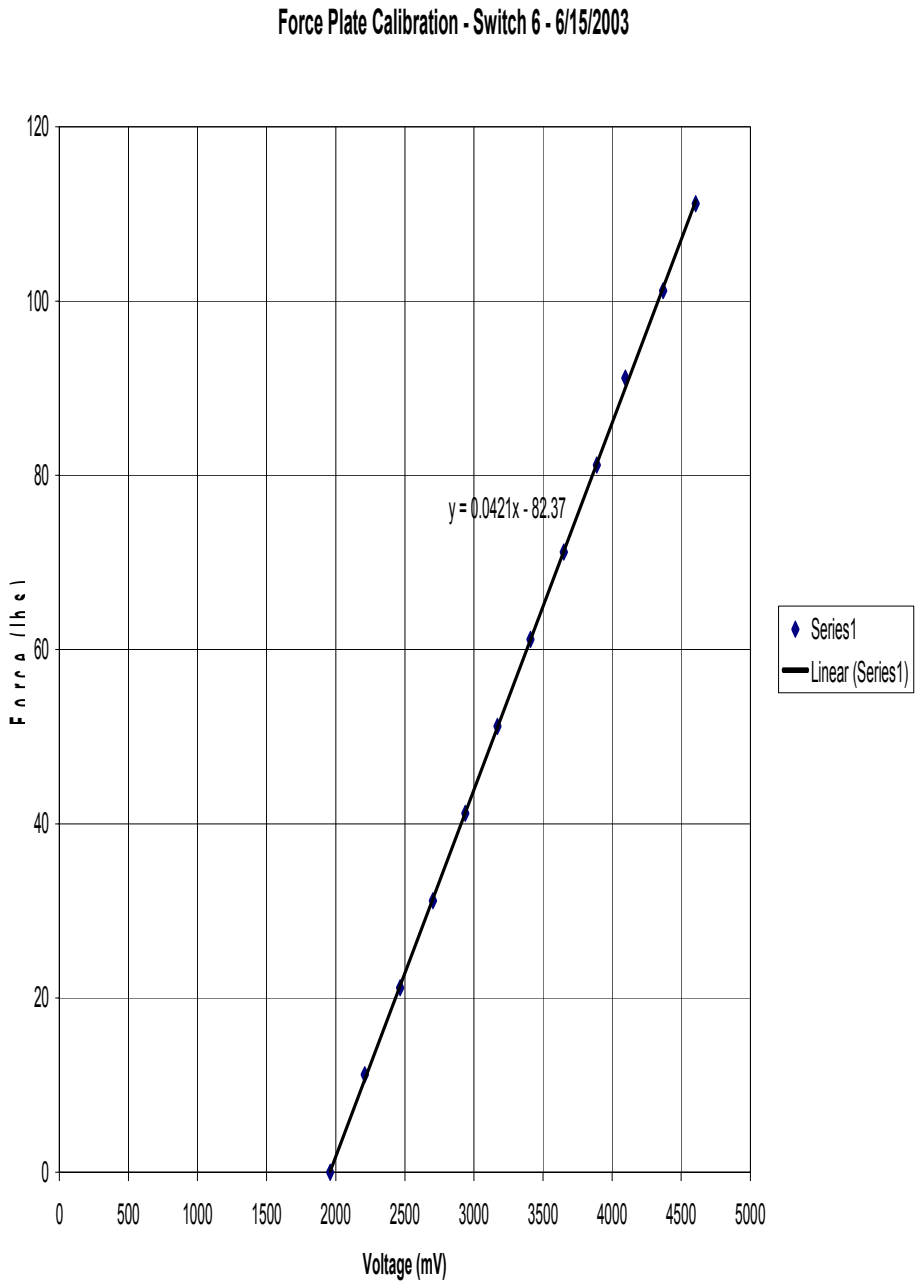

Figure K.2 – Force Plate Calibration – Force versus Voltage

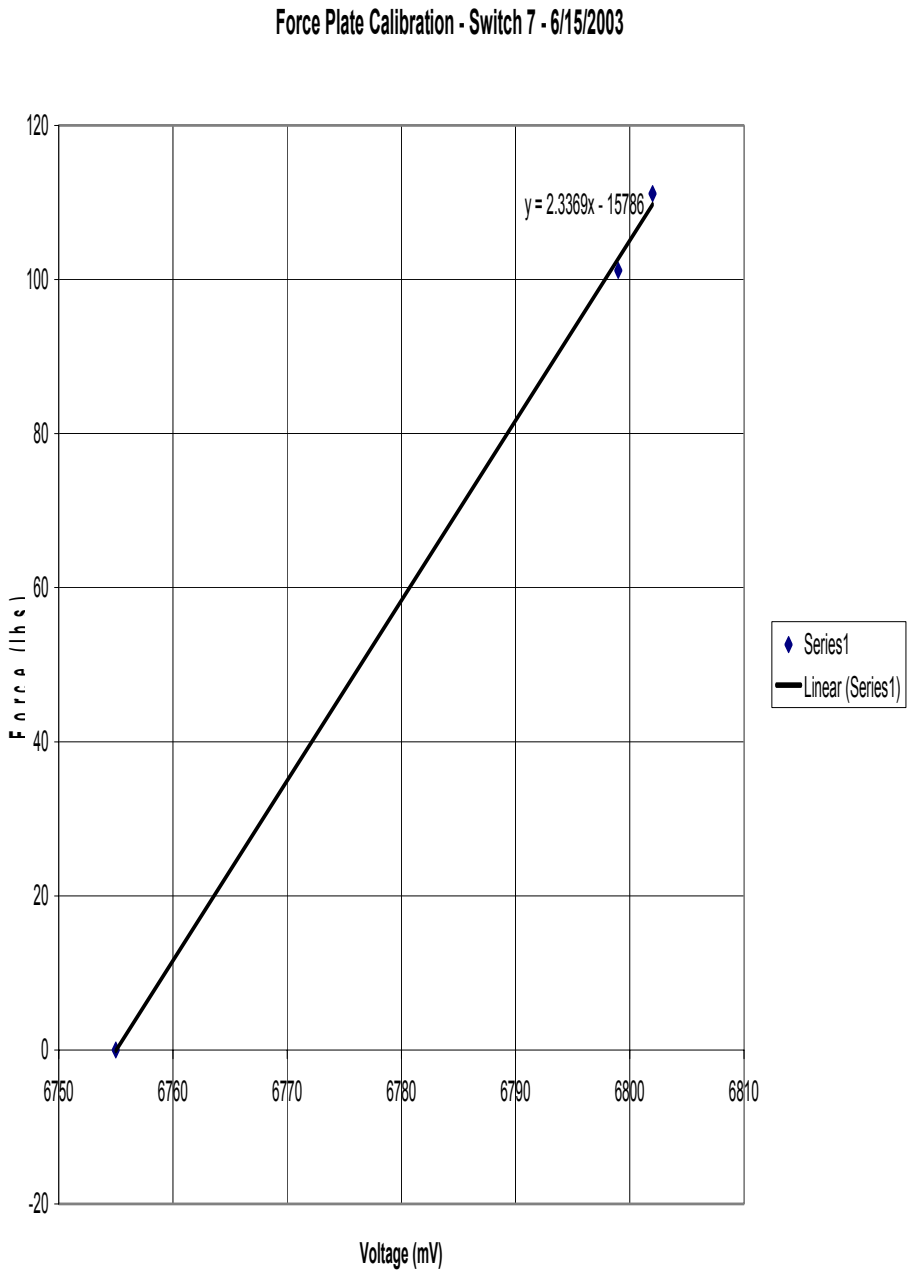

Figure K.3 – Force Plate Calibration – Force versus Voltage

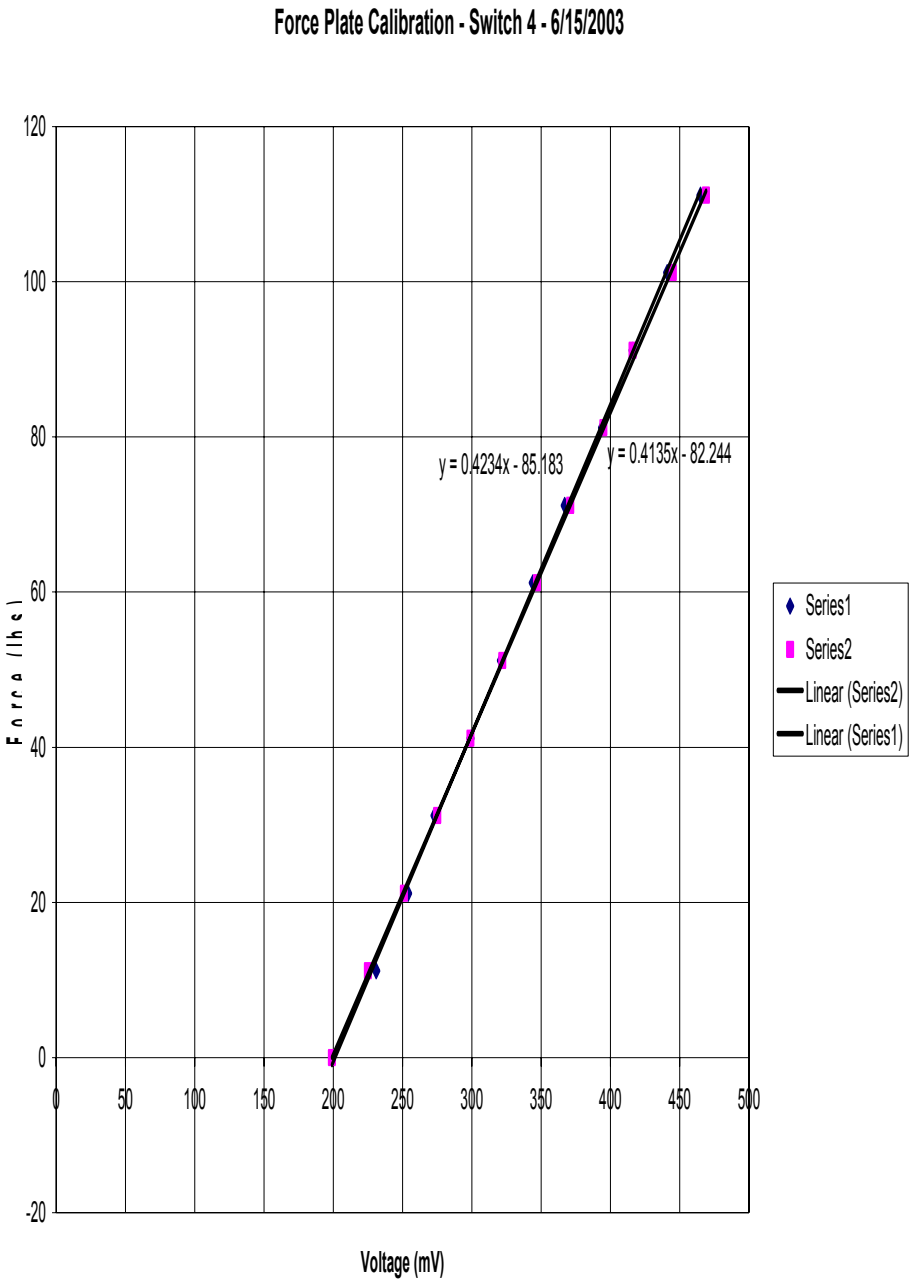

Figure K.4 – Force Plate Calibration – Force versus Voltage

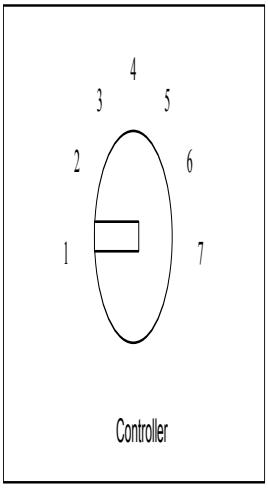

Plate Weight (lbs)
11.18

			Switch*			Gain Switch*					
		Load	1	2	3	4	4	5	6	7	
Weight of Added Plates (lbs)	Sensitivity					0.4234	0.4135	0.2077	0.0421	2.3369	lb/mV
	Sensitivity					0.41845		0.2077	0.0421	2.3369	lb/mV
	GAIN					9.94		4.93	1.00	55.51	
0		0	0	0	0	199	199	397	1960	6755	
0		11.18	5	23	46	231	225	447	2211		
10		21.18	6	26	51	254	251	500	2466		
20		31.18	6	28	54	273	275	548	2704		
30		41.18	6	30	59	299	299	595	2938		
40		51.18	7	32	64	321	322	642	3170		
50		61.18	7	35	69	344	347	692	3409		
60		71.18	8	37	73	367	371	739	3651		
70		81.18	8	39	78	394	395	788	3890		
80		91.18	9	42	83	416	416	828	4096		
90		101.18	9	44	88	441	445	885	4370	6799	
100		111.18	10	47	93	465	469	934	4605	6802	

*all measurements are in millivolts (mV)

Switch locations 1,2, and 3 are the respective load cell values.

Switch 4,5,6 and 7 contain a respective gain and the value reported is the sum from the switch 1,2, and 3 multiplied by the switch gain factor.

Figure K.5 – Force Plate Calibration: Gain and Summer Sensitivity and Signal Amplification

APPENDIX L: Frequency Test Data – Bare Floor

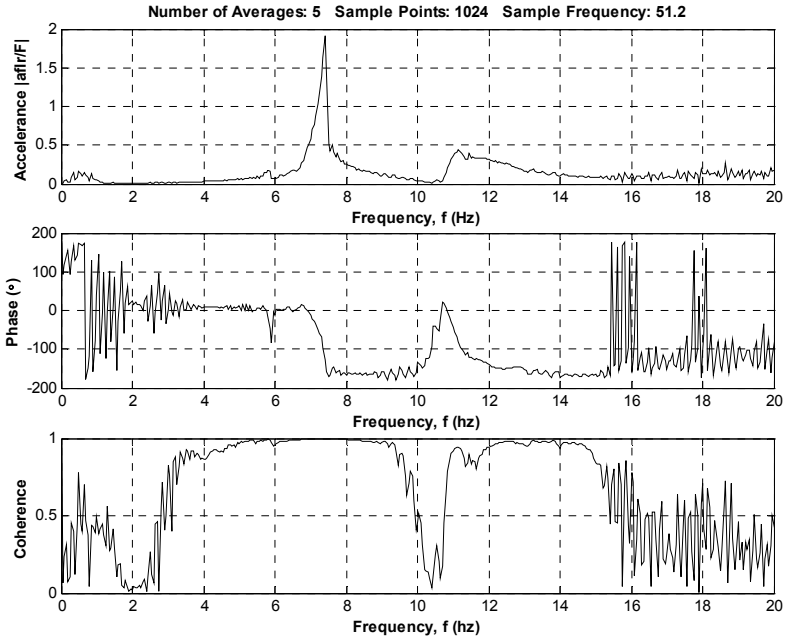

Figure L.1 – Bare Floor Accelerance Response, Phase, and Coherence - Chirp (4-15 Hz)

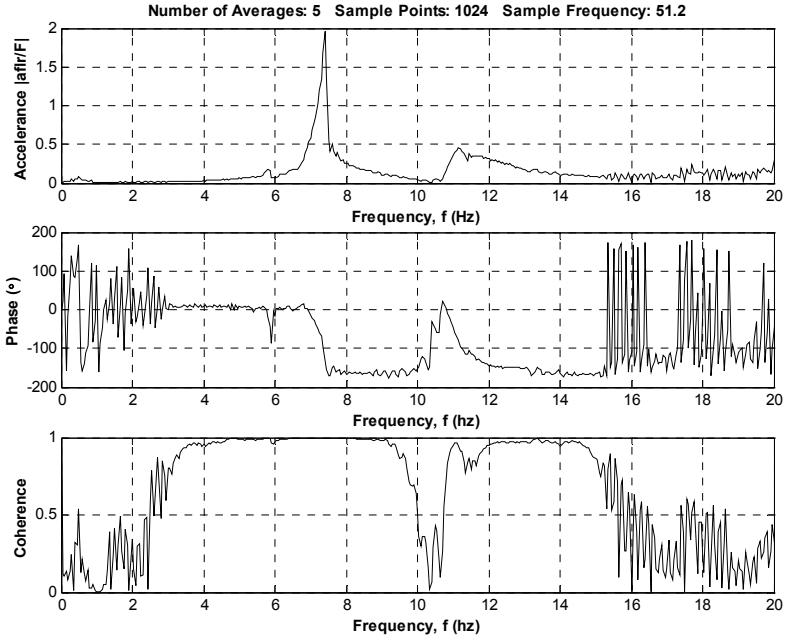

Figure L.2 – Bare Floor Accelerance Response, Phase, and Coherence - Chirp (4-15 Hz)

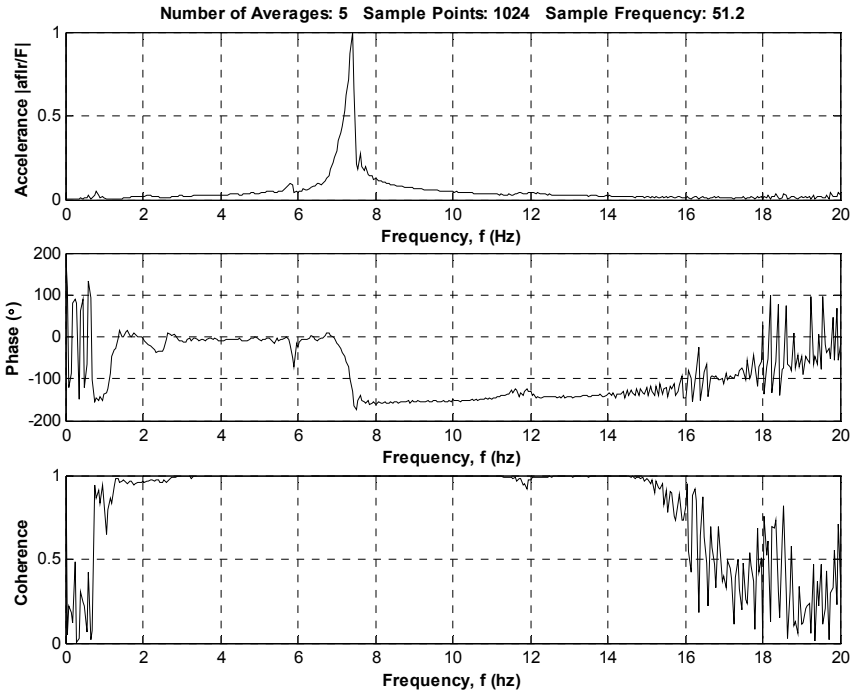

Figure L.3 – Bare Floor Accelerance Response, Phase, and Coherence - Chirp (4-15 Hz)

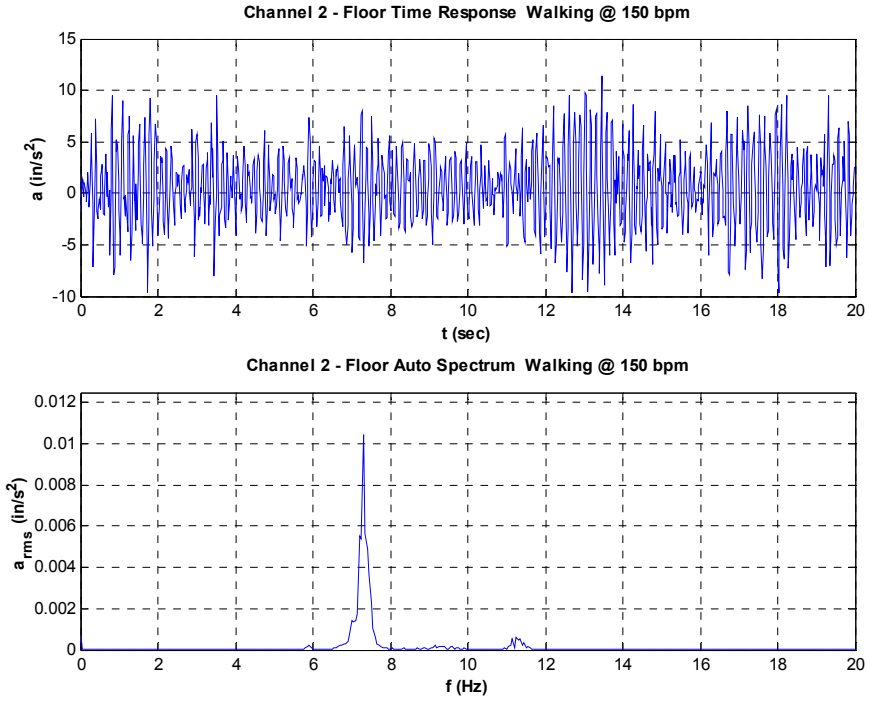

Figure L.4 – Bare Floor Time and Auto-spectrum Response to Walking at 150 bpm

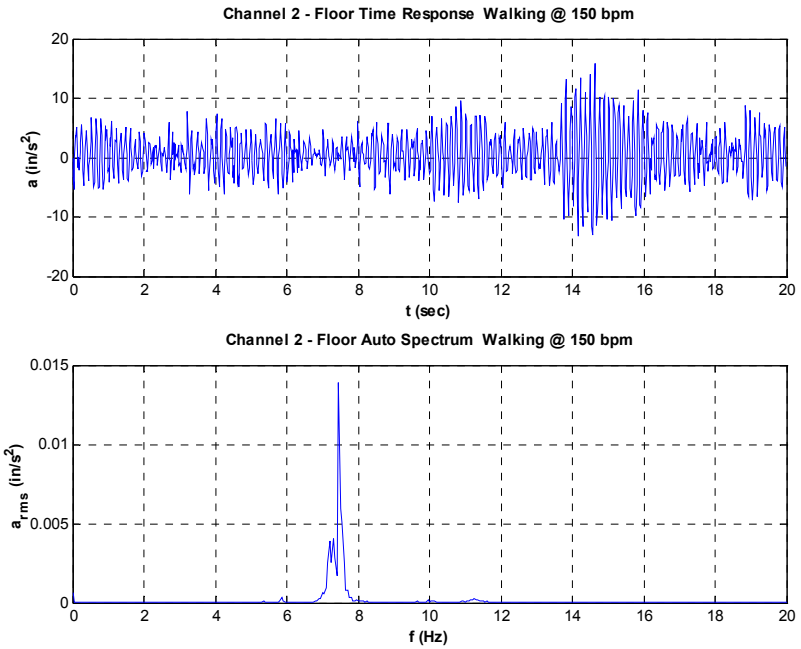

Figure L.5 – Bare Floor Time and Auto-spectrum Response to Walking at 150 bpm

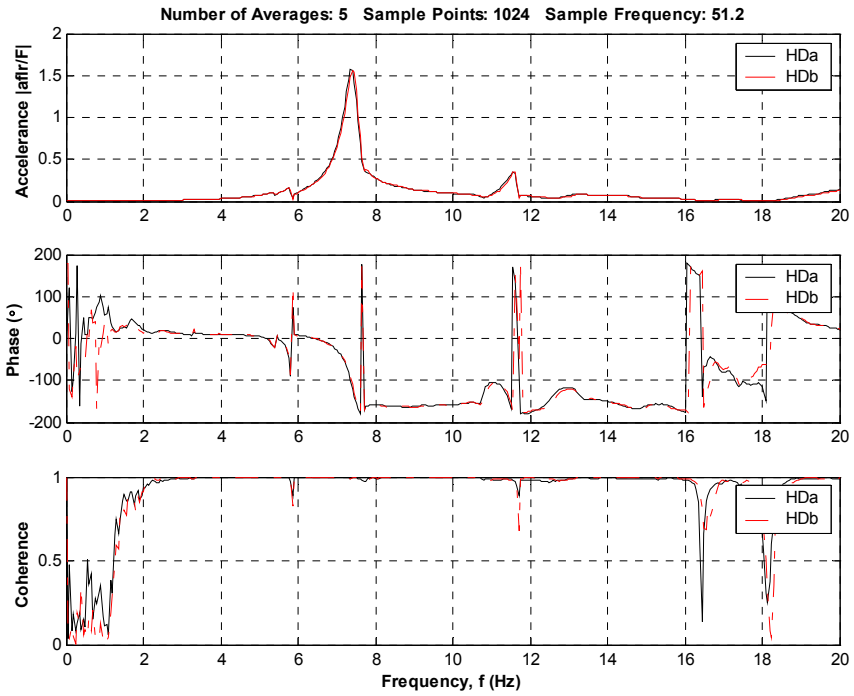

Figure L.6 – Bare Floor Accelerance Response, Phase, and Coherence – Heel Drop at Center of Floor

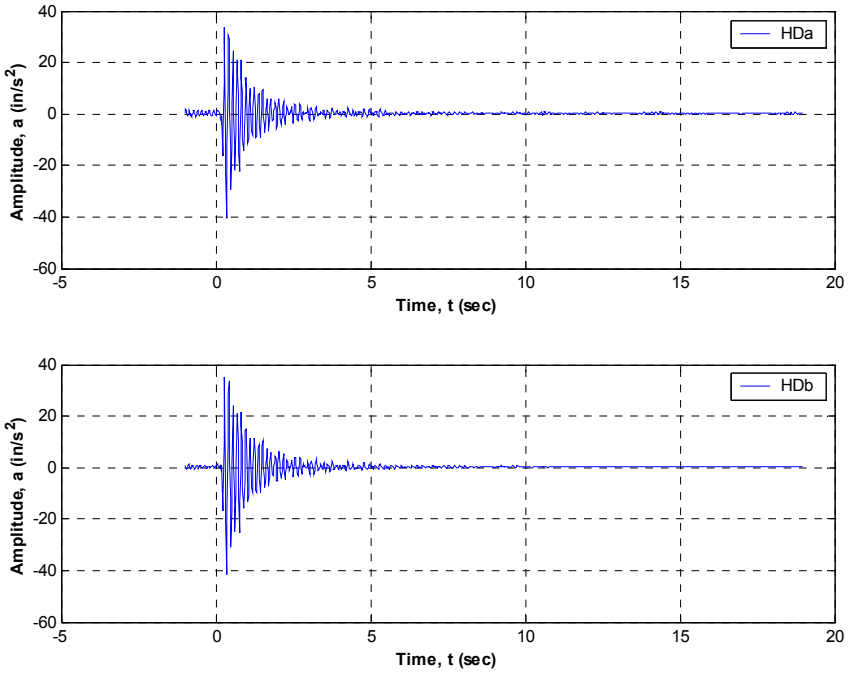

Figure L.7 – Bare Floor Heel Drop at Center of Floor Time Spectrum

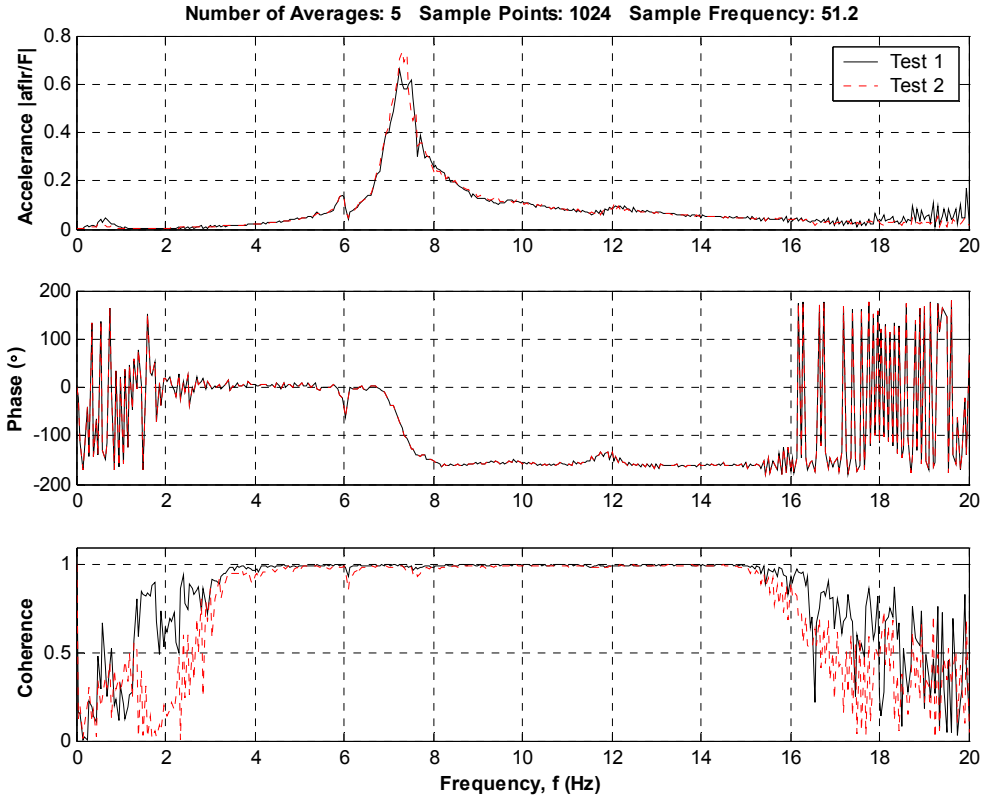

Figure L.8 – Floor Response of 16 People Standing on Bare Floor with Knees Bent

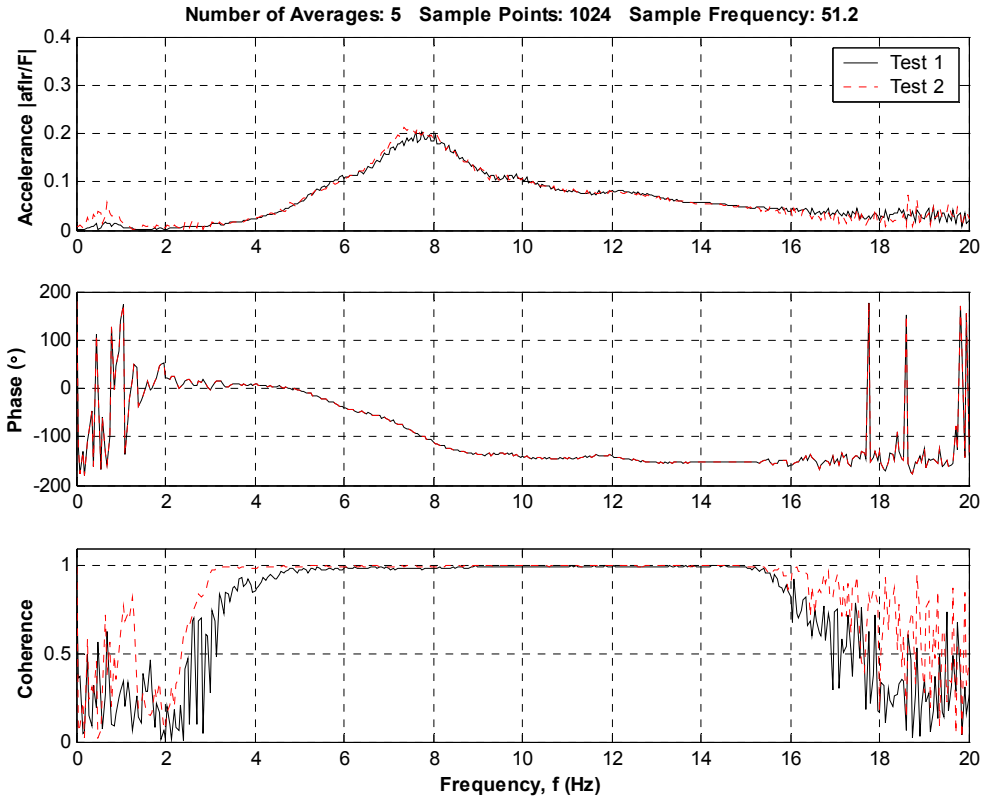

Figure L.9 – Floor Response of 16 People Sitting on Bare Floor

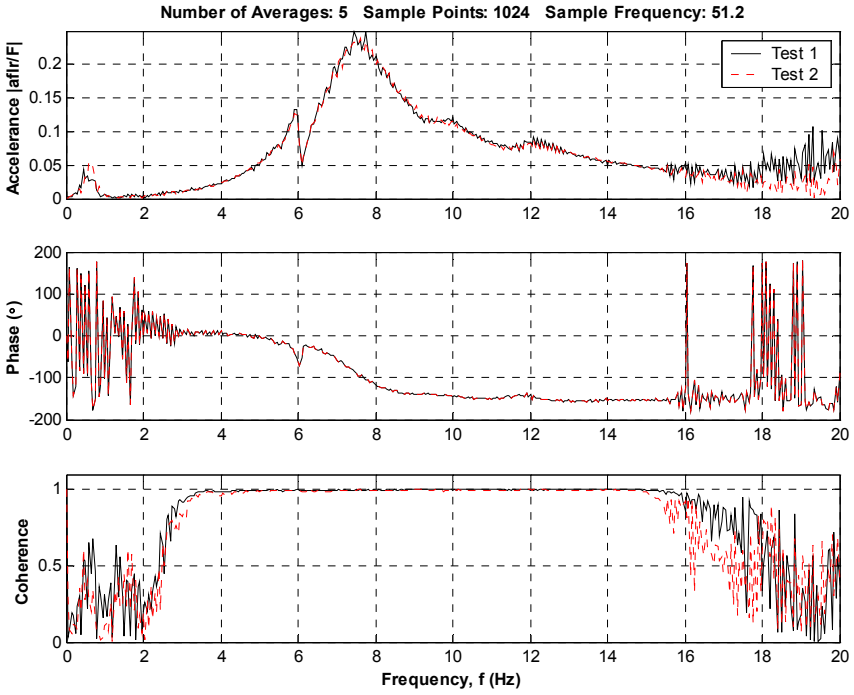

Figure L.10 – Floor Response of 16 People Standing on Bare Floor with Legs Straight

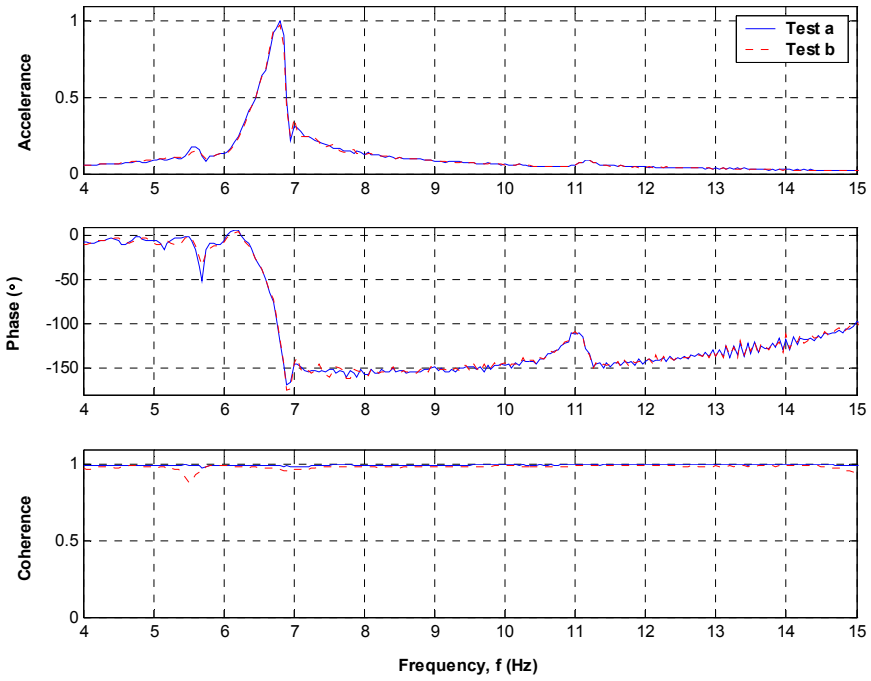

Figure L.11 – Bare Floor 16 People Dead Equivalent Weight

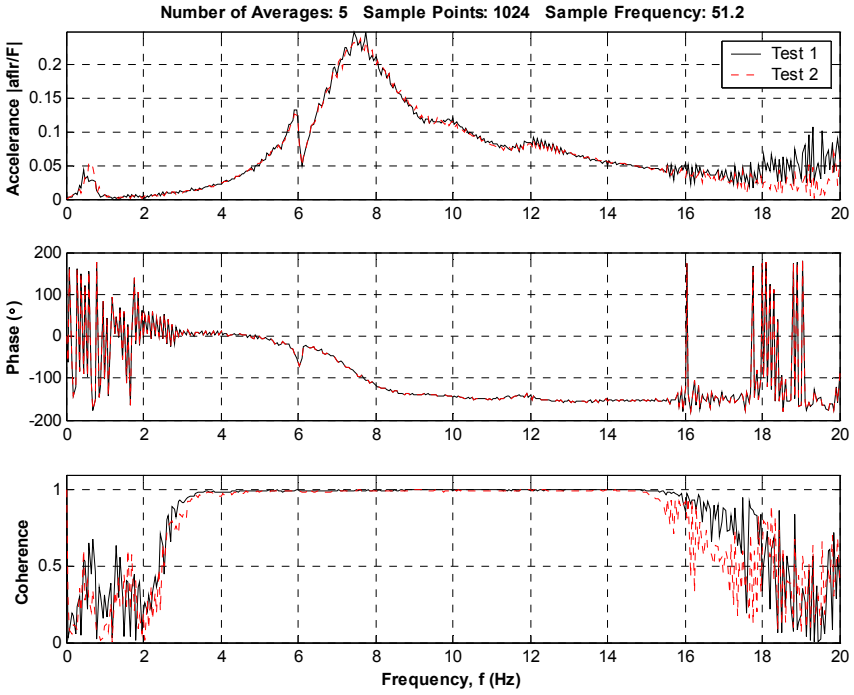

Figure L.12 – Bare Floor Response with 16 People Standing

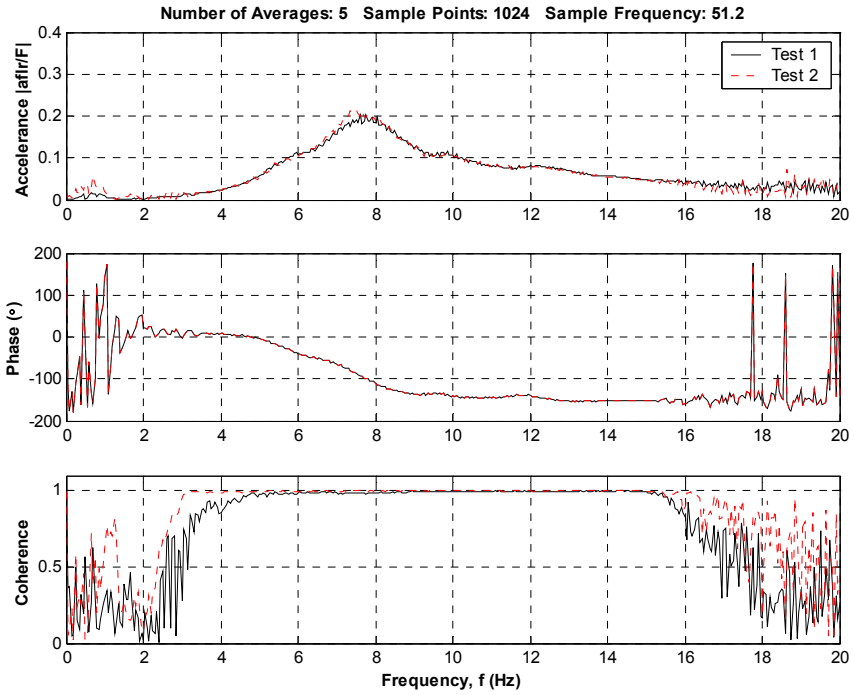

Figure L.13 – Bare Floor Response with 16 People Sitting

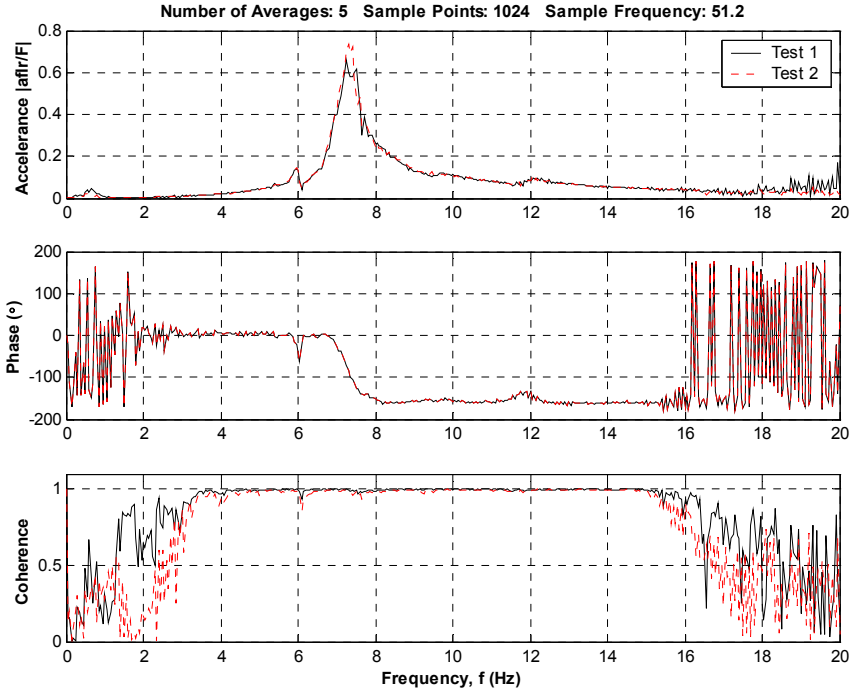

Figure L.14 – Bare Floor Response with 16 People Bent Knees

		No. of People
		16
Modal Line	1	0
	2	265.02
	3	327.32
	4	321.16
	5	423.67
	6	0
	7	382.04
	8	364.84
	9	298.66
	10	210.78
	11	0
	Total (lbs)	2593.49

Table L.1 – Weight of 16 People on Bare Floor

APPENDIX M: Frequency Test Data – PTMD

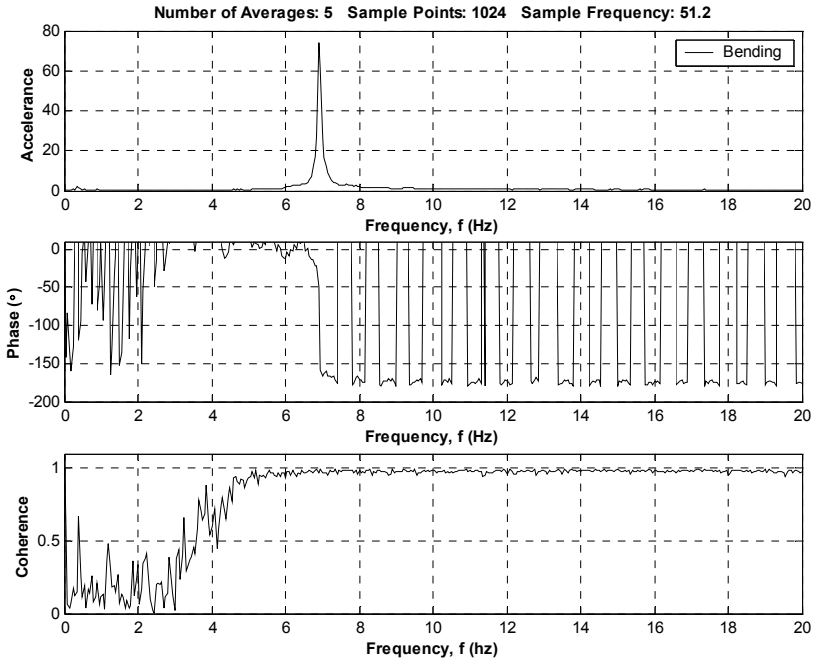

Figure M.1 – Frequency Response of PTMD Using Impact Hammer to Excite the First Mode – Bending

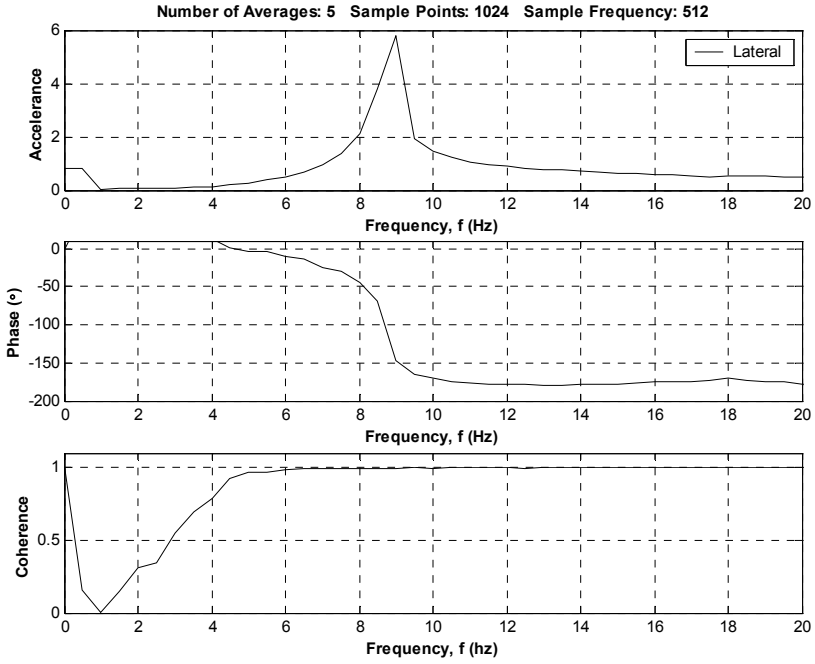

Figure M.2 – Frequency Response of PTMD Using Impact Hammer to Excite the Second Mode – Lateral

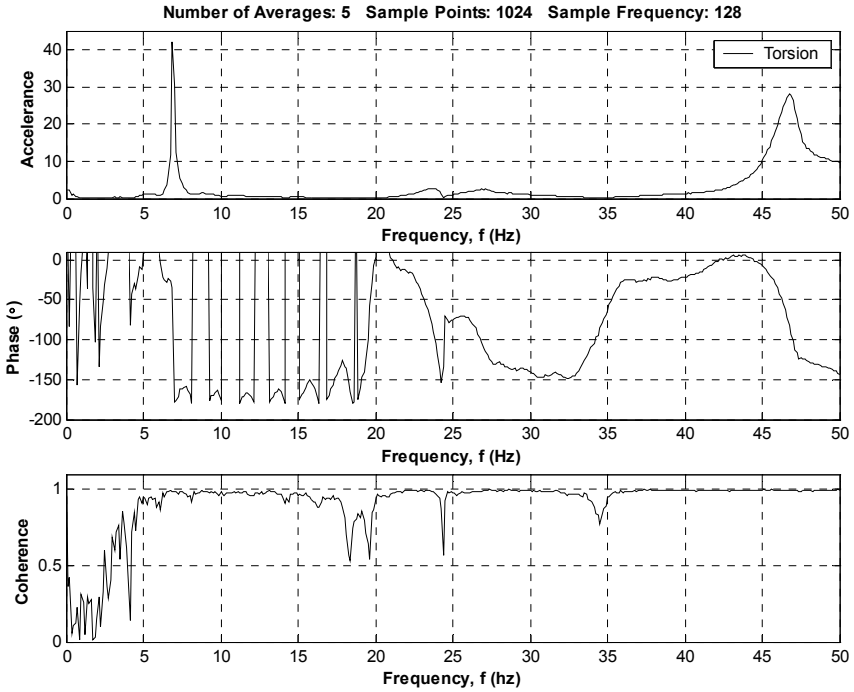

Figure M.3 – Frequency Response of PTMD Using Impact Hammer to Excite the Third Mode - Torsion

APPENDIX N: Frequency Test Data – Passive PTMD on Floor

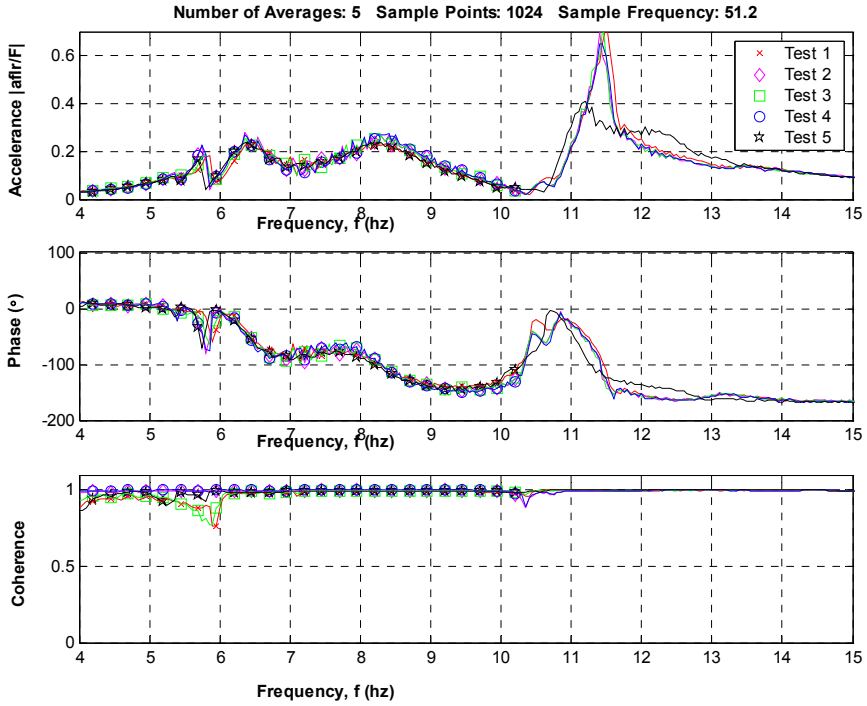

Figure N.1 – Floor Response with Tuned Passive PTMD

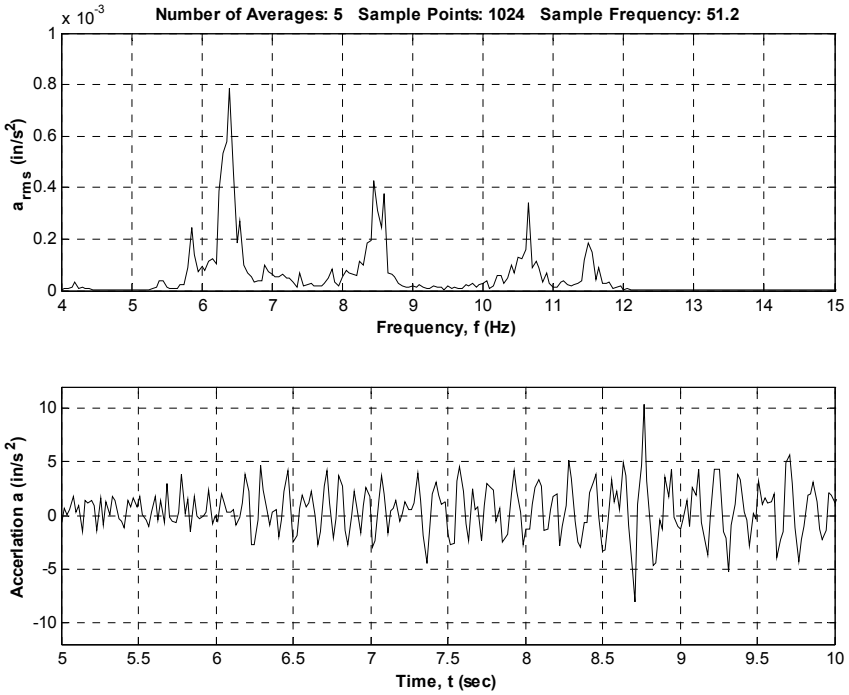

Figure N.2 – Floor Response with Tuned Passive PTMD to Walking at 132 bpm

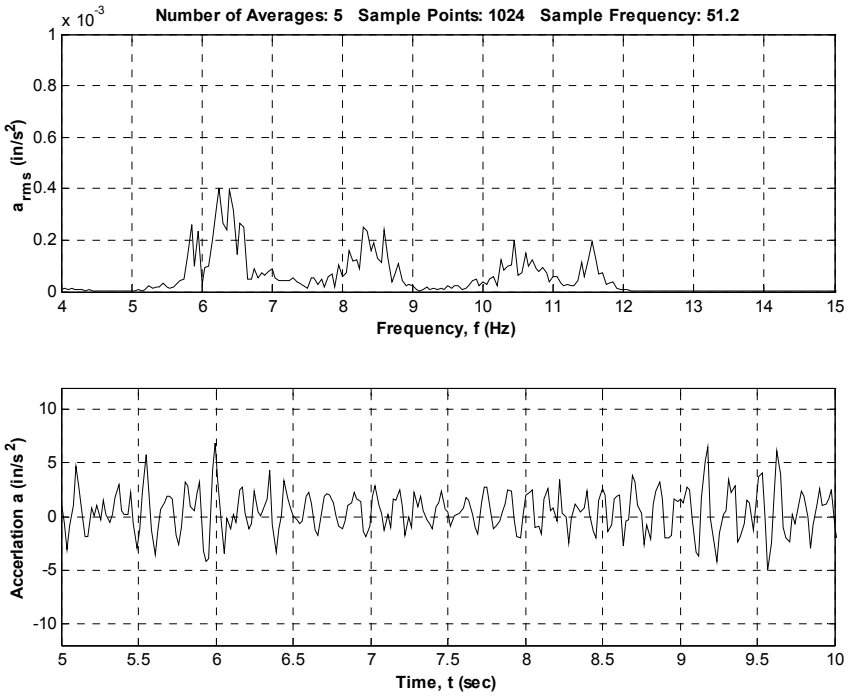

Figure N.3 – Floor Response with Tuned Passive PTMD to Walking at 132 bpm

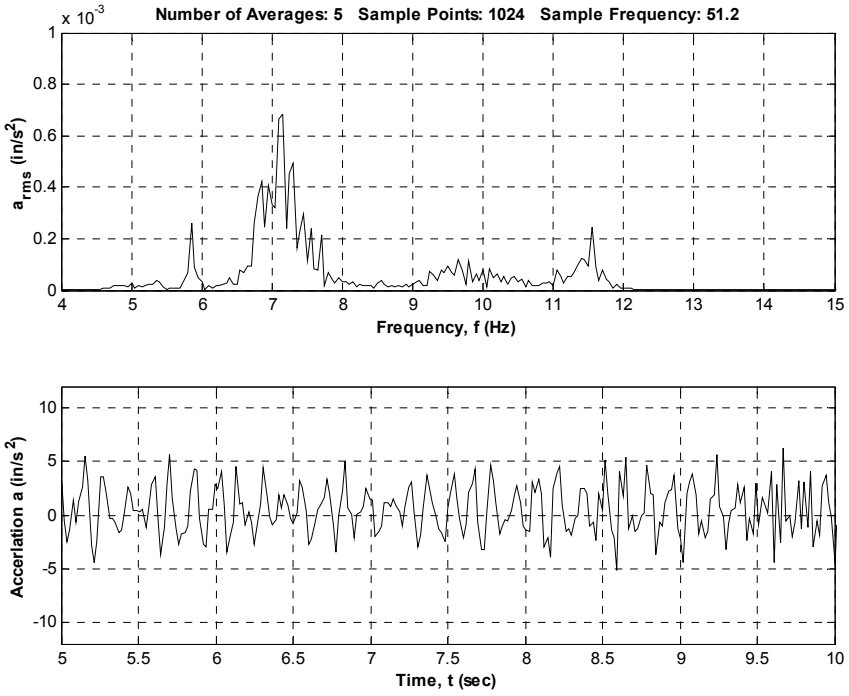

Figure N.4 – Floor Response with Tuned Passive PTMD to Walking at 150 bpm

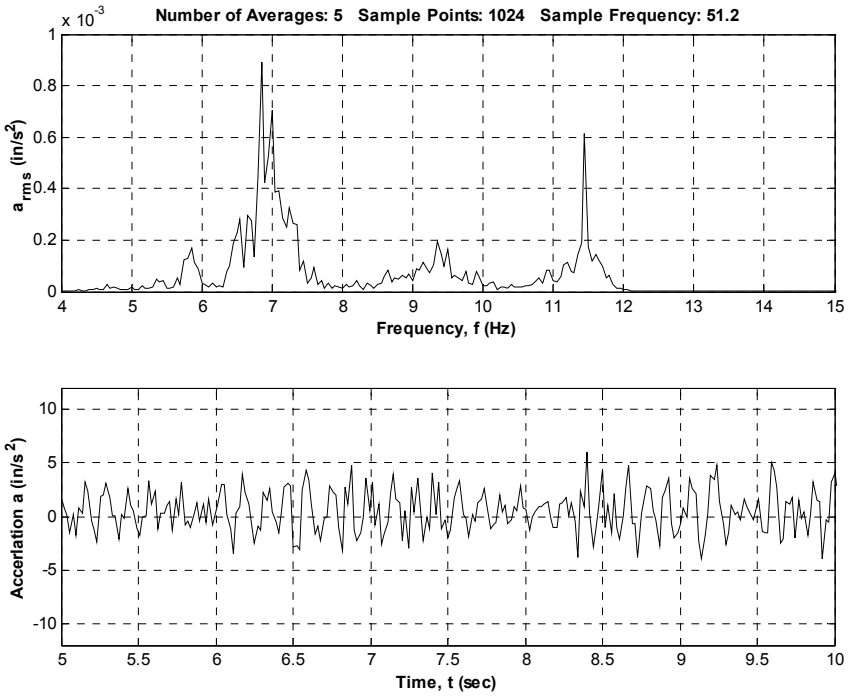

Figure N.5 – Floor Response with Tuned Passive PTMD to Walking at 150 bpm

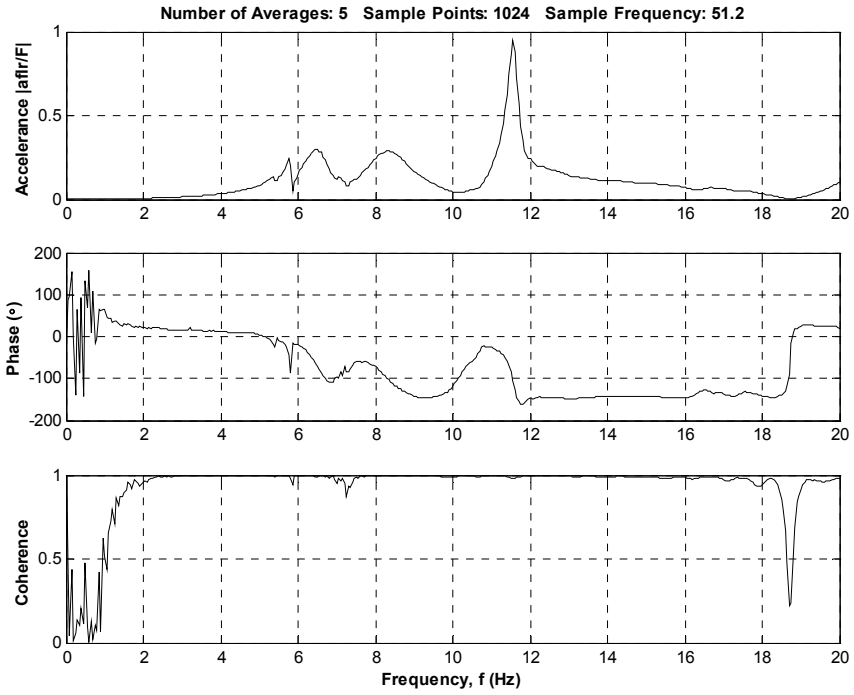

Figure N.6 – Floor Response with Tuned Passive PTMD to a Heel Drop at Center of Floor

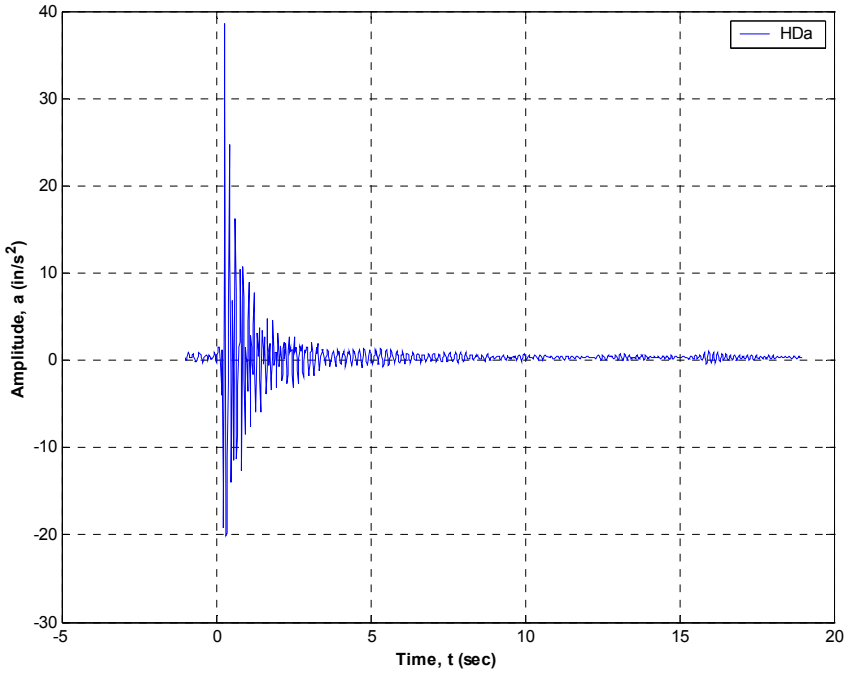

Figure N.7 – Floor Response with Tuned Passive PTMD to a Heel Drop at Center of Floor

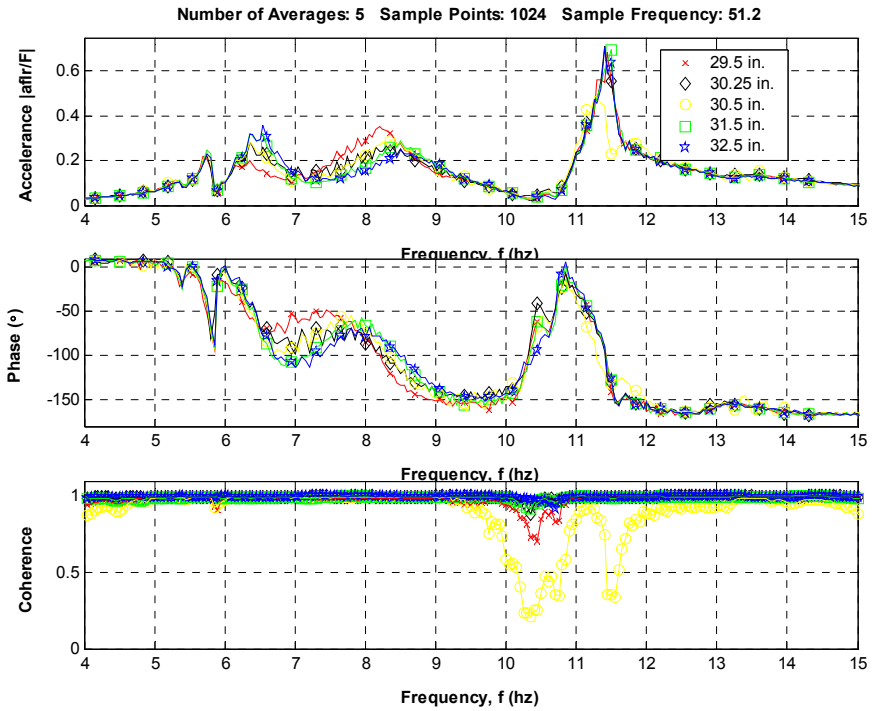

Figure N.8 – Variation in Floor Response to Change in Passive PTMD Spring Location

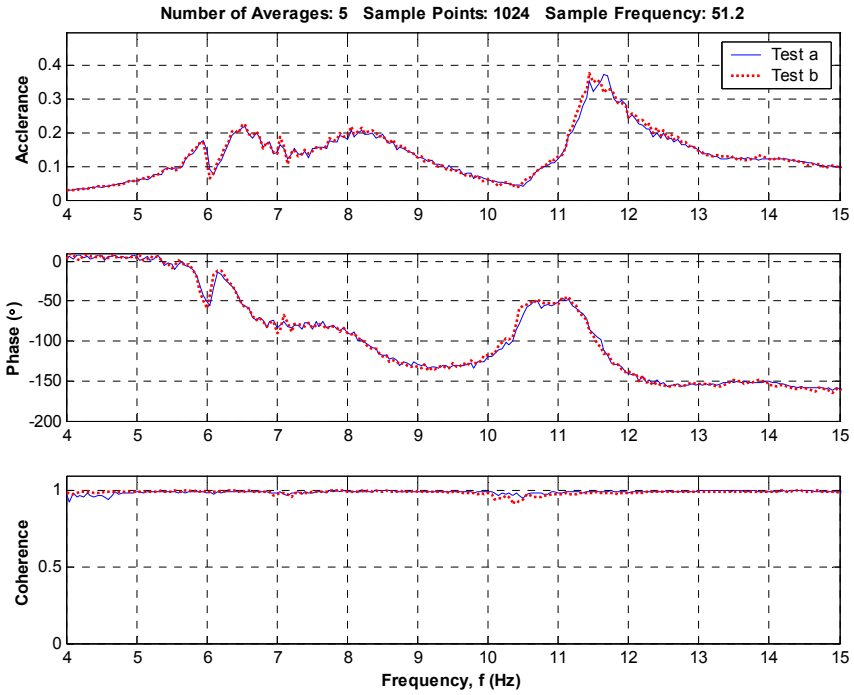

Figure N.9 – Floor Response with Passive PTMD – 16 People Standing with Knees Bent

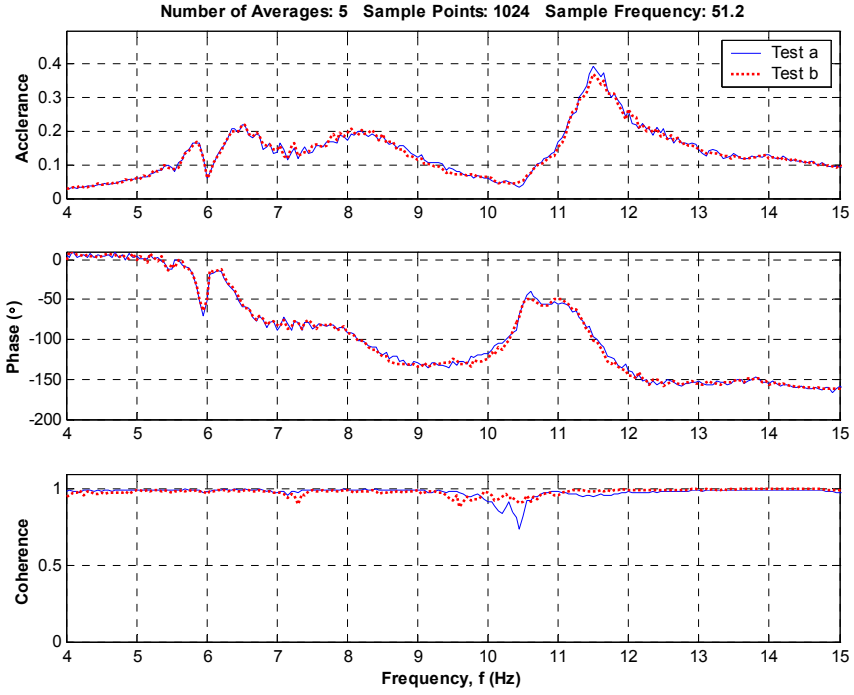

Figure N.10 – Floor Response with Passive PTMD – 12 People Standing with Knees Bent

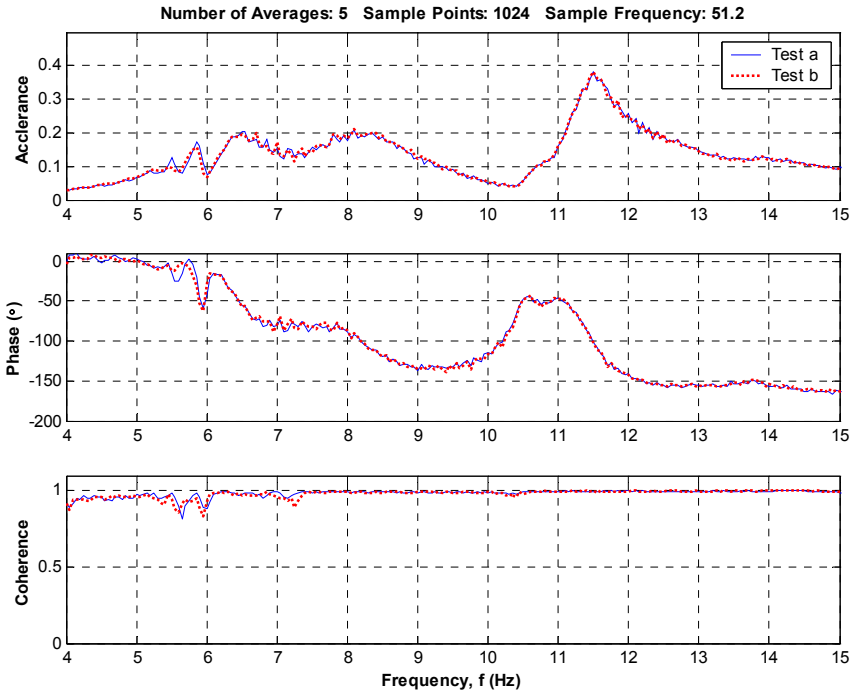

Figure N.11 – Floor Response with Passive PTMD – 8 People Standing with Knees Bent

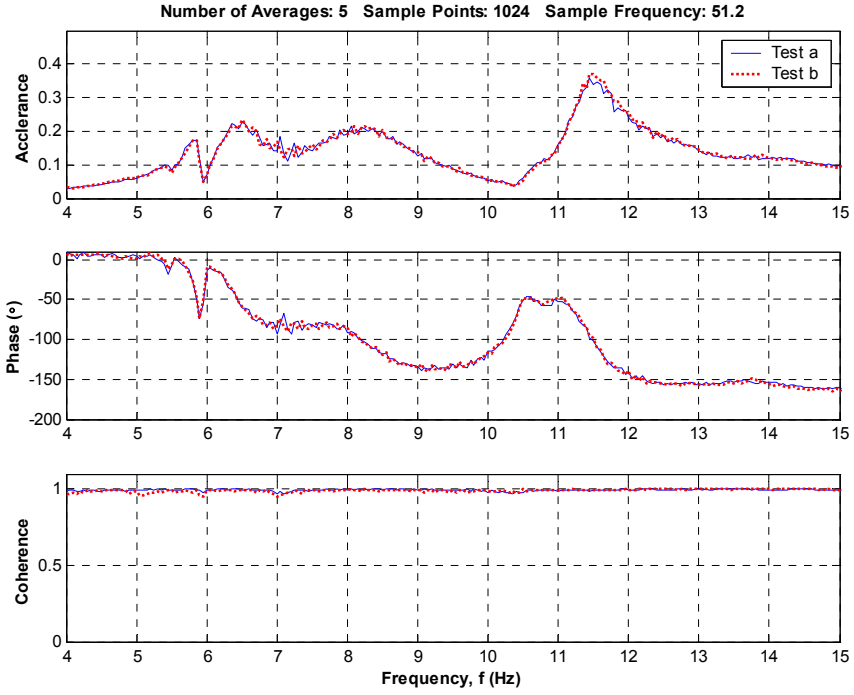

Figure N.12 – Floor Response with Passive PTMD – 6 People Standing with Knees Bent

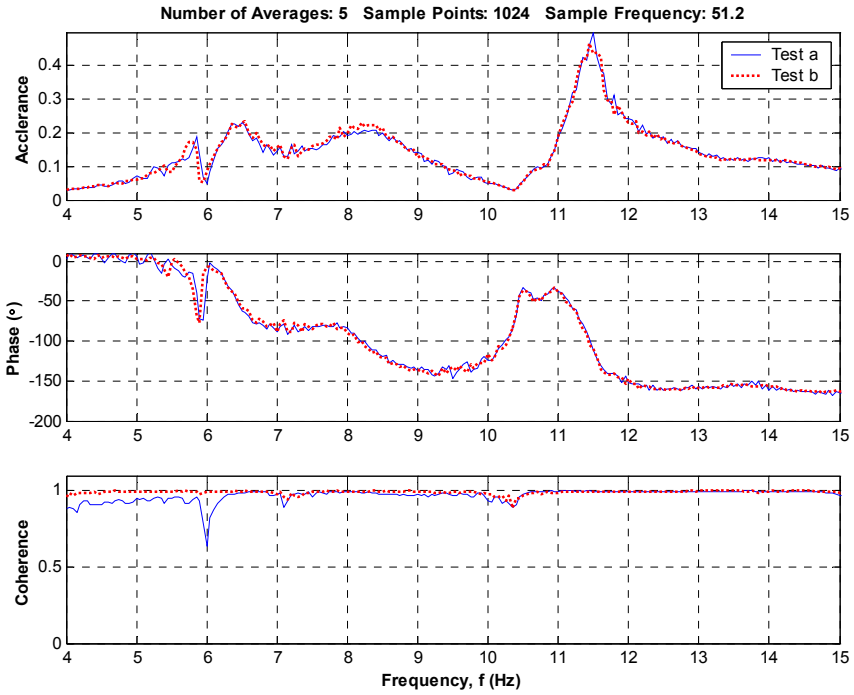

Figure N.13 – Floor Response with Passive PTMD – 4 People Standing with Knees Bent

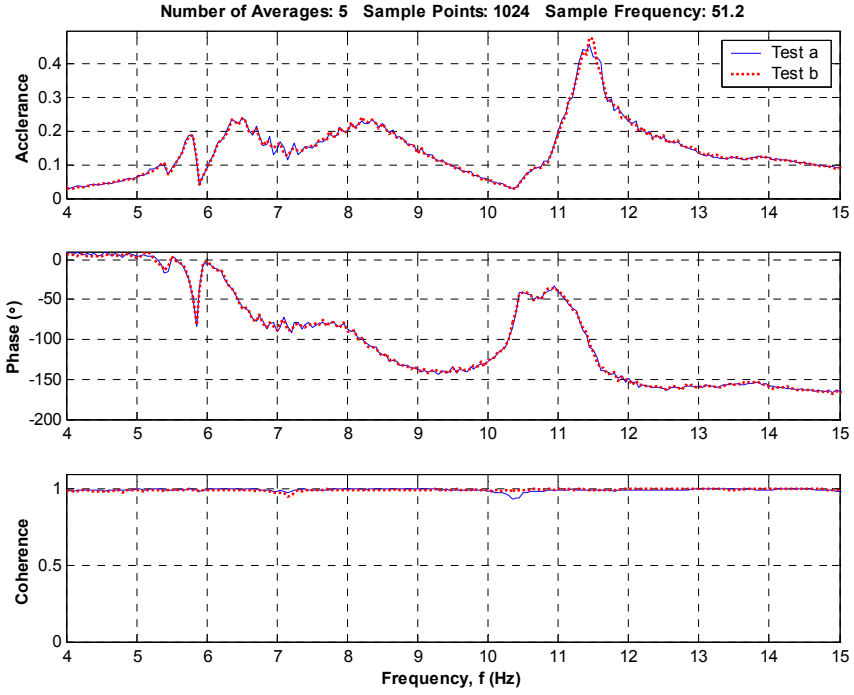

Figure N.14 – Floor Response with Passive PTMD – 2 People Standing with Knees Bent

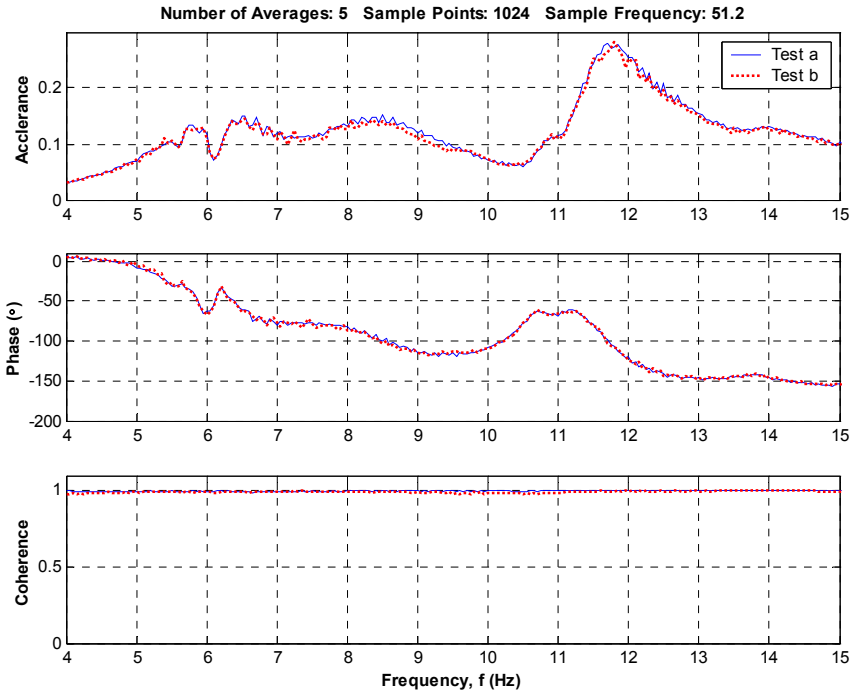

Figure N.15 – Floor Response with Passive PTMD – 16 People Sitting

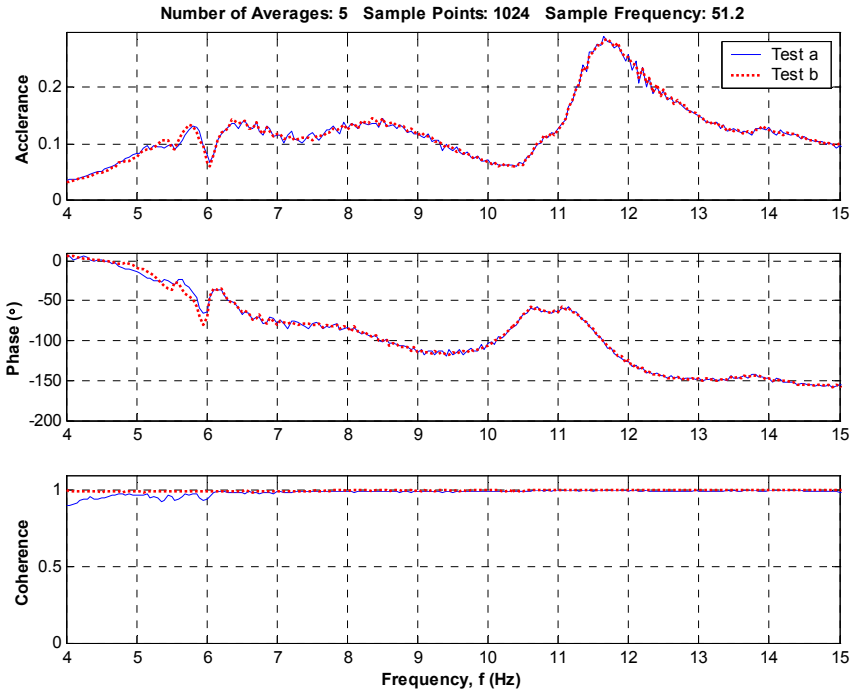

Figure N.16 – Floor Response with Passive PTMD – 12 People Sitting

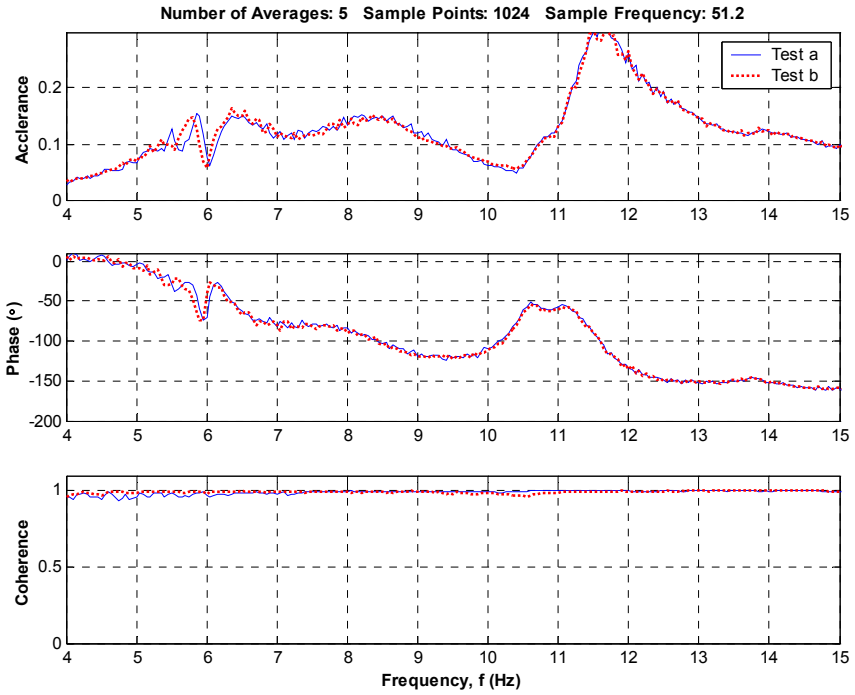

Figure N.17 – Floor Response with Passive PTMD – 8 People Sitting

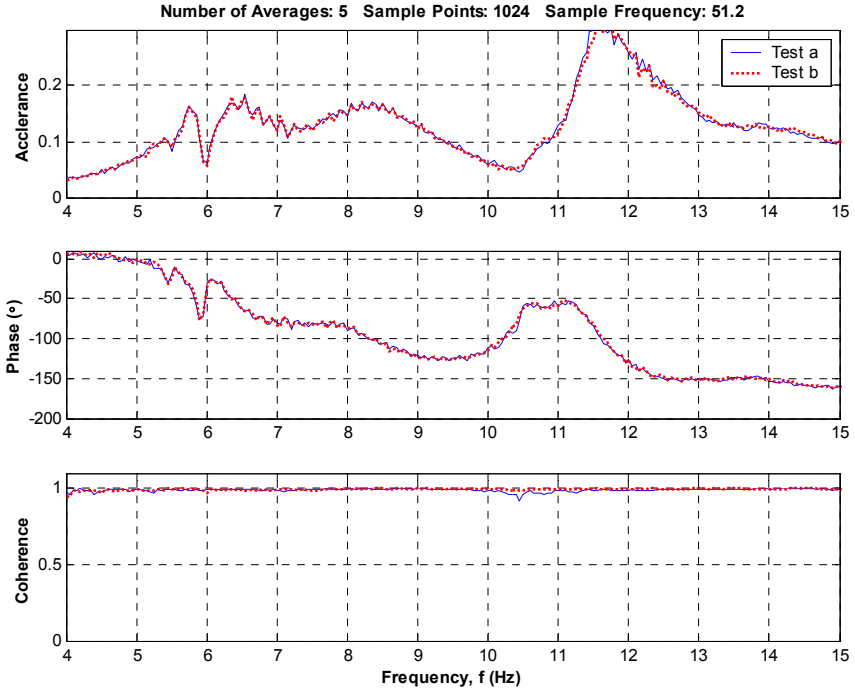

Figure N.18 – Floor Response with Passive PTMD – 6 People Sitting

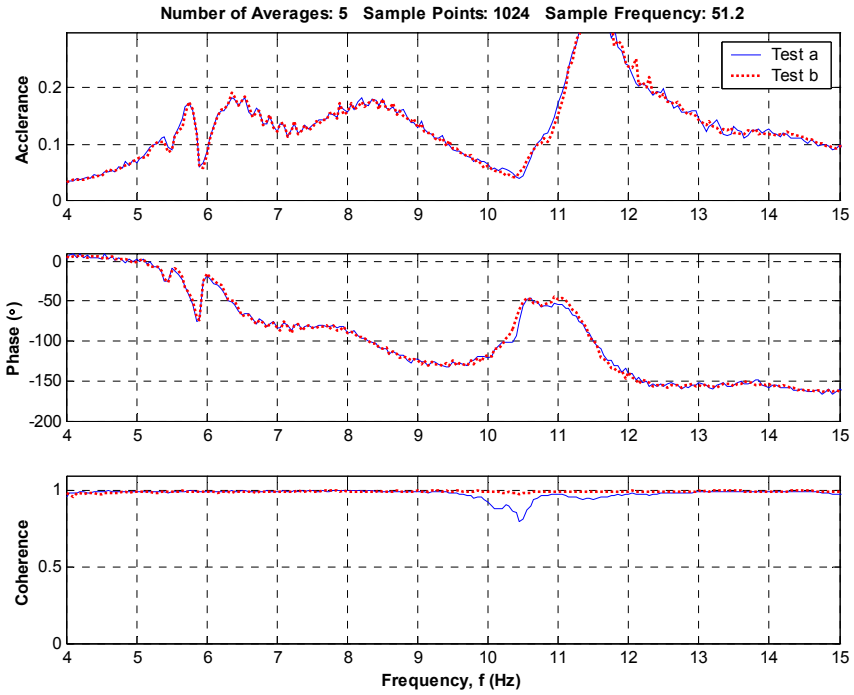

Figure N.19 – Floor Response with Passive PTMD – 4 People Sitting

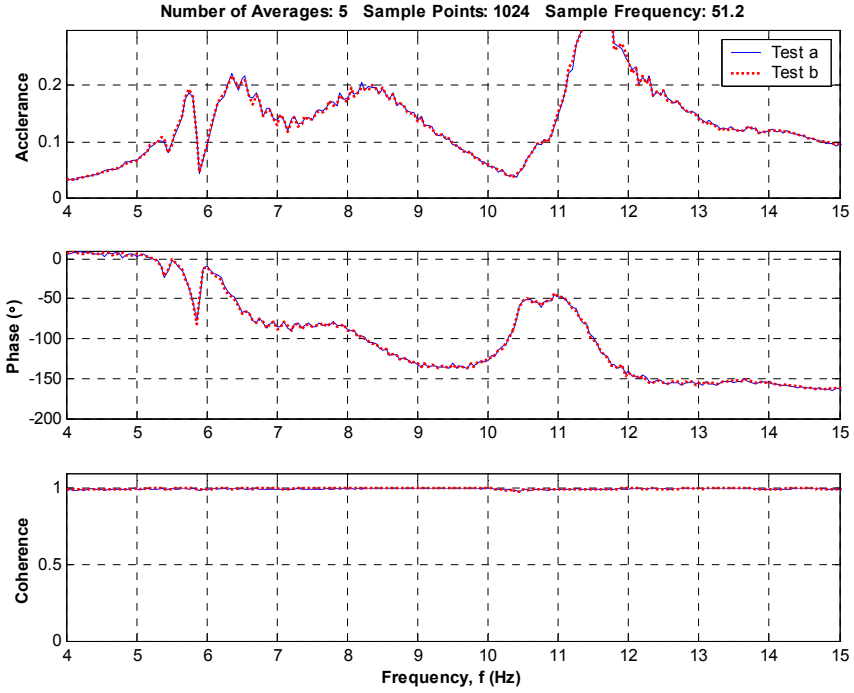

Figure N.20 – Floor Response with Passive PTMD – 2 People Sitting

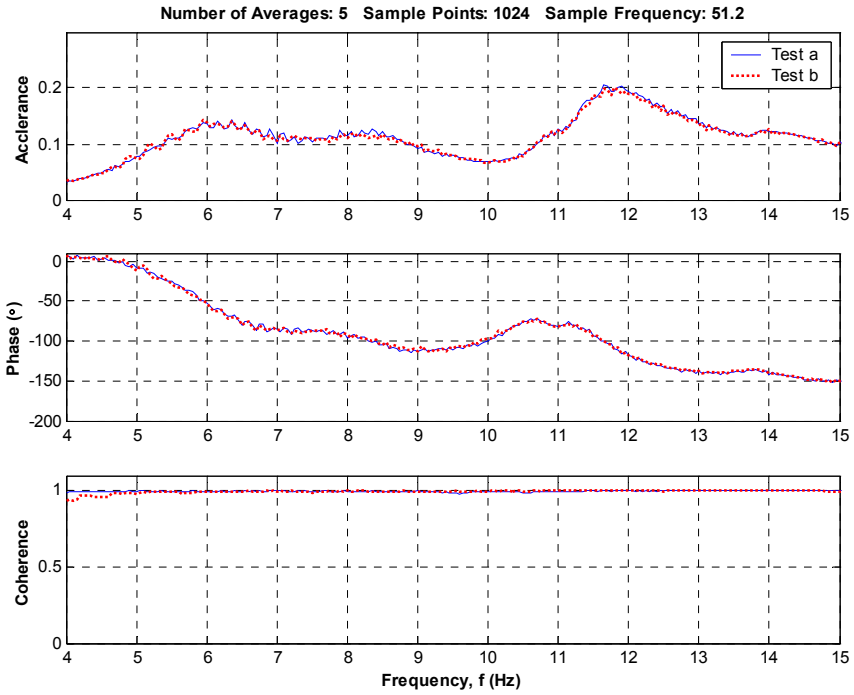

Figure N.21 – Floor Response with Passive PTMD – 16 People Standing with Straight Legs

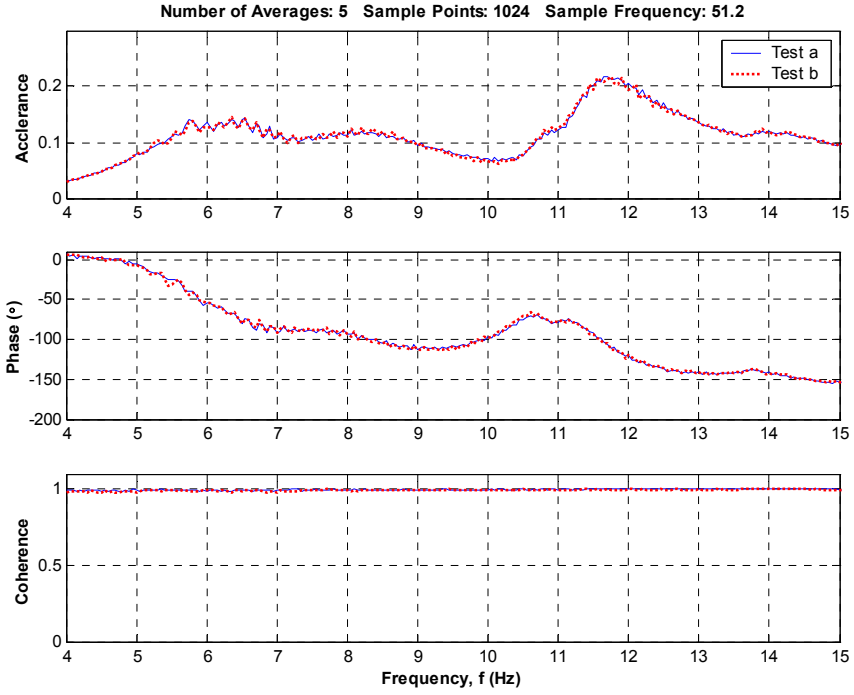

Figure N.22 – Floor Response with Passive PTMD – 12 People Standing with Straight Legs

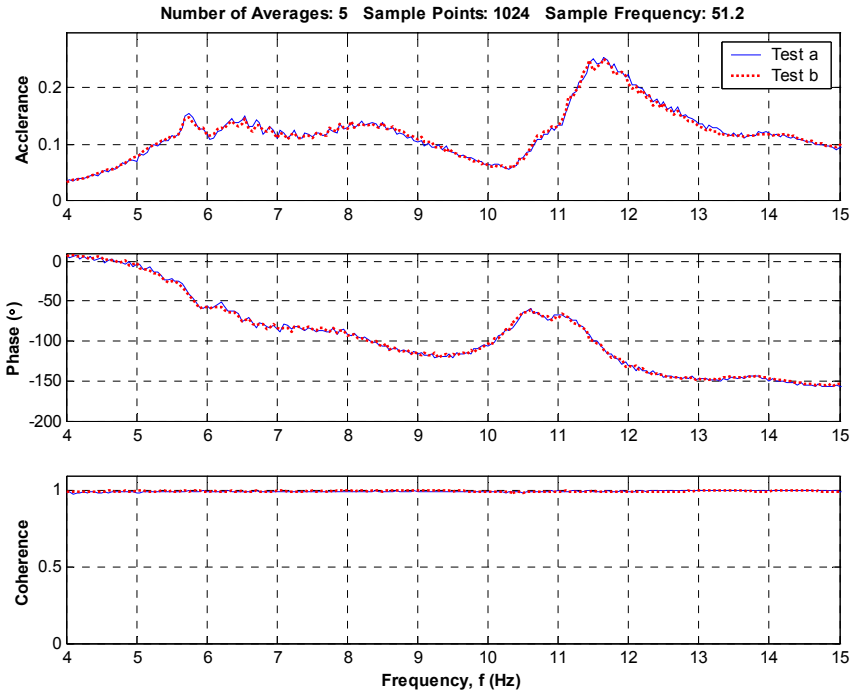

Figure N.23 – Floor Response with Passive PTMD – 8 People Standing with Straight Legs

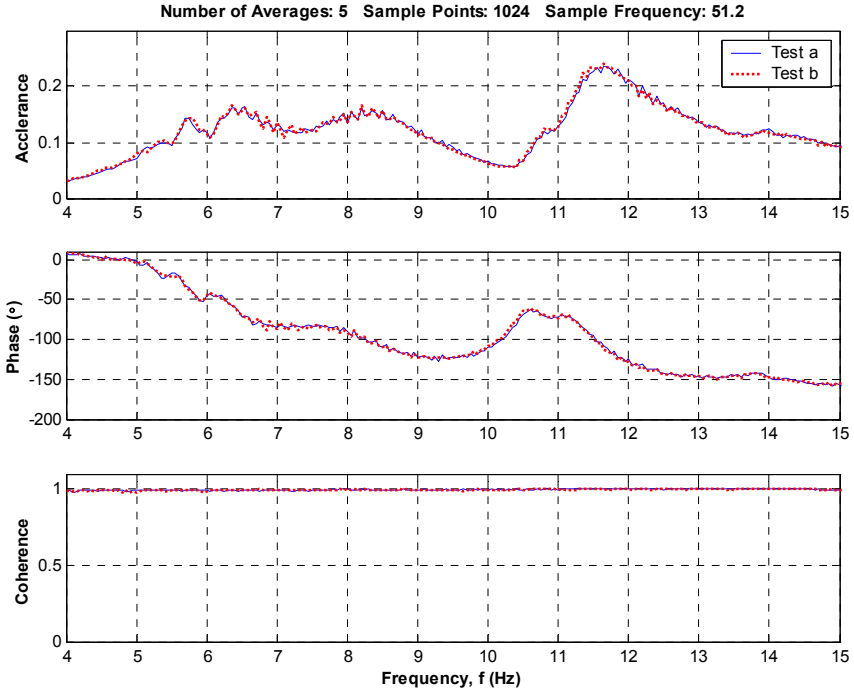

Figure N.24 – Floor Response with Passive PTMD – 6 People Standing with Straight Legs

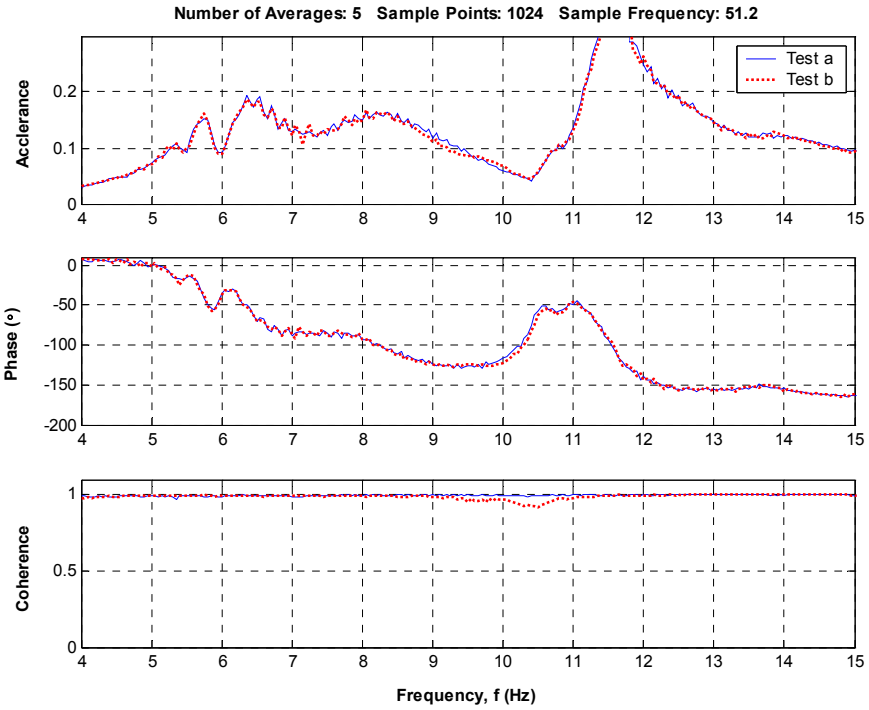

Figure N.25 – Floor Response with Passive PTMD – 4 People Standing with Straight Legs

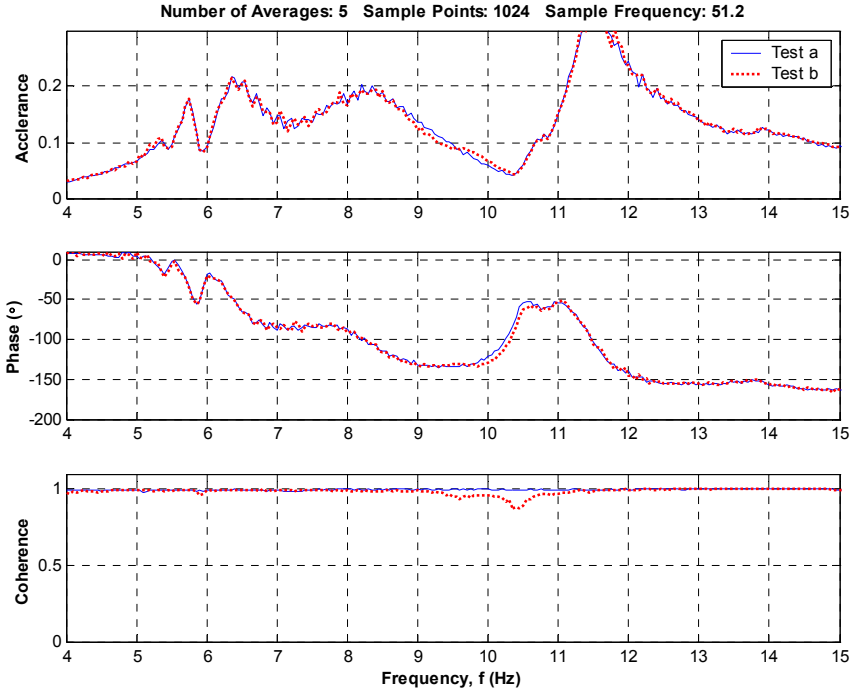

Figure N.26 – Floor Response with Passive PTMD – 2 People Standing with Straight Legs

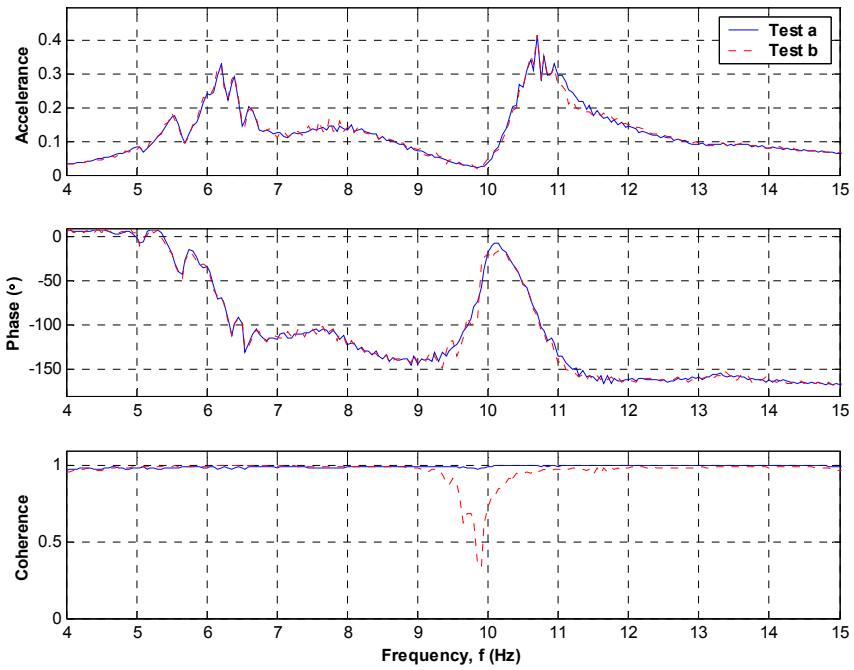

Figure N.27 – Floor Response with Passive PTMD – Equivalent Dead Mass of 16 People

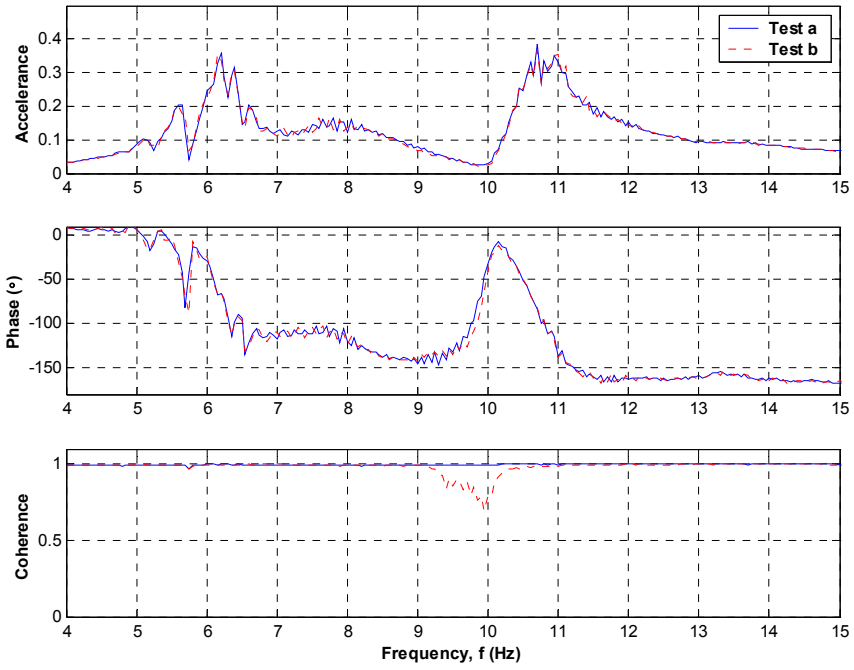

Figure N.28 – Floor Response with Passive PTMD – Equivalent Dead Mass of 12 People

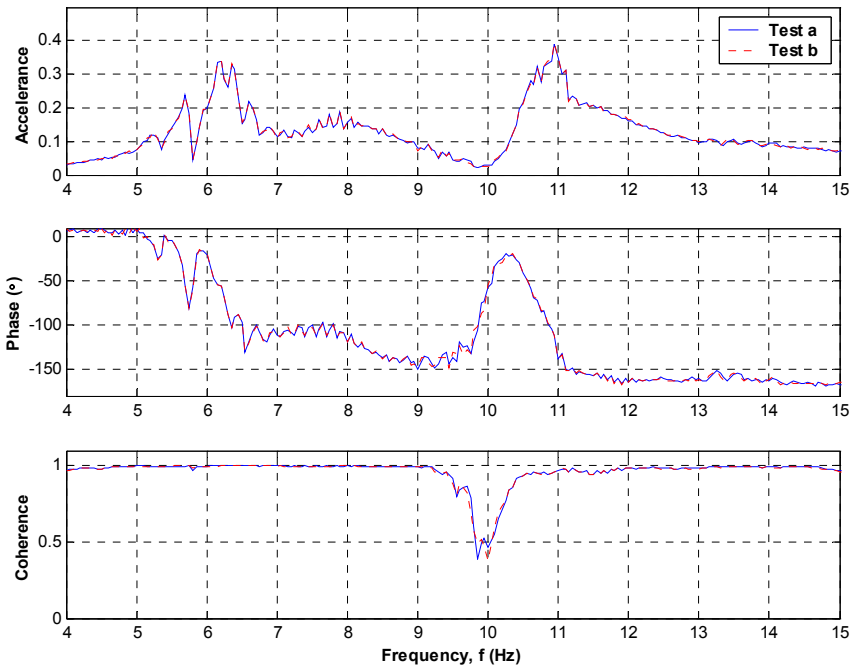

Figure N.29 – Floor Response with Passive PTMD – Equivalent Dead Mass of 8 People

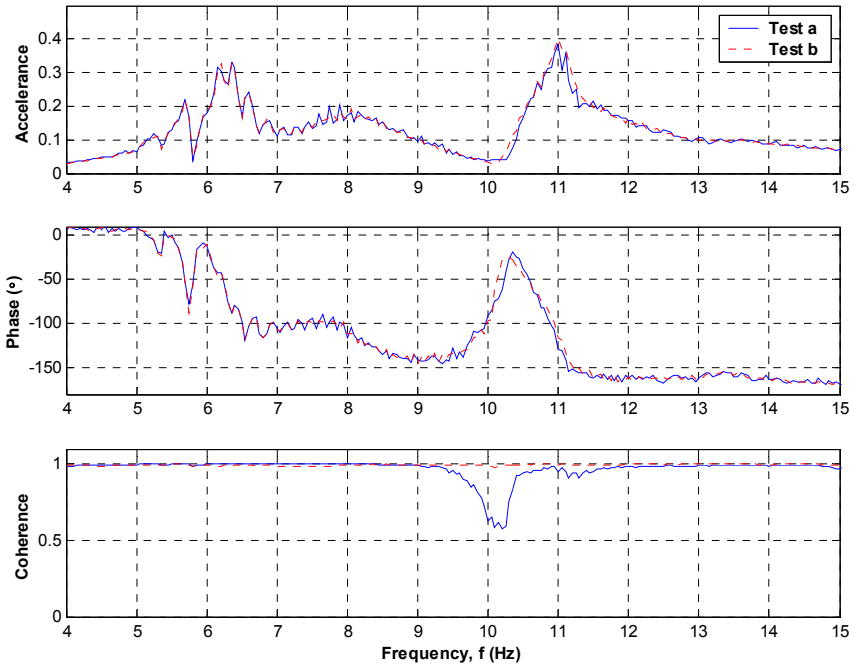

Figure N.30 – Floor Response with Passive PTMD – Equivalent Dead Mass of 6 People

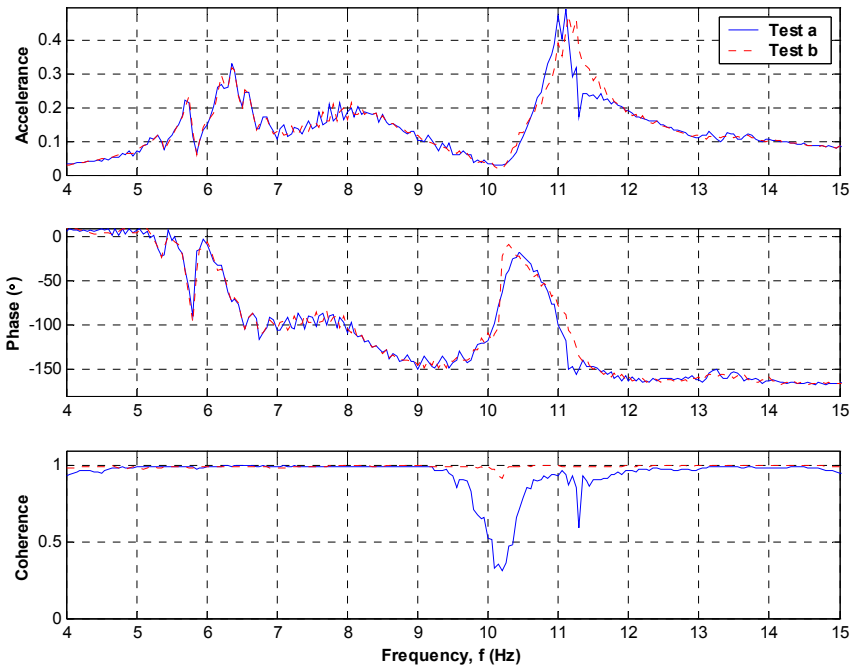

Figure N.31 – Floor Response with Passive PTMD – Equivalent Dead Mass of 4 People

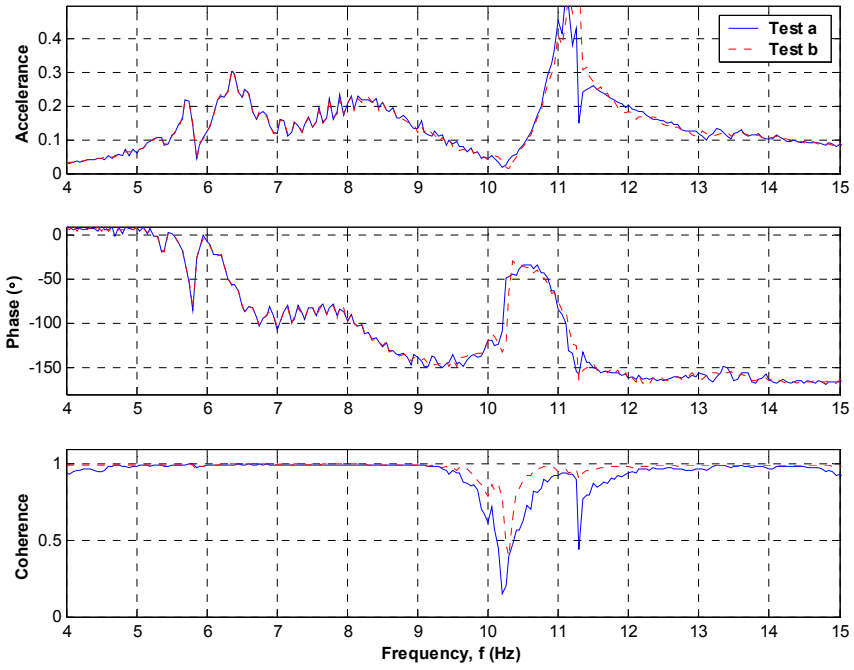

Figure N.32 – Floor Response with Passive PTMD – Equivalent Dead Mass of 2 People

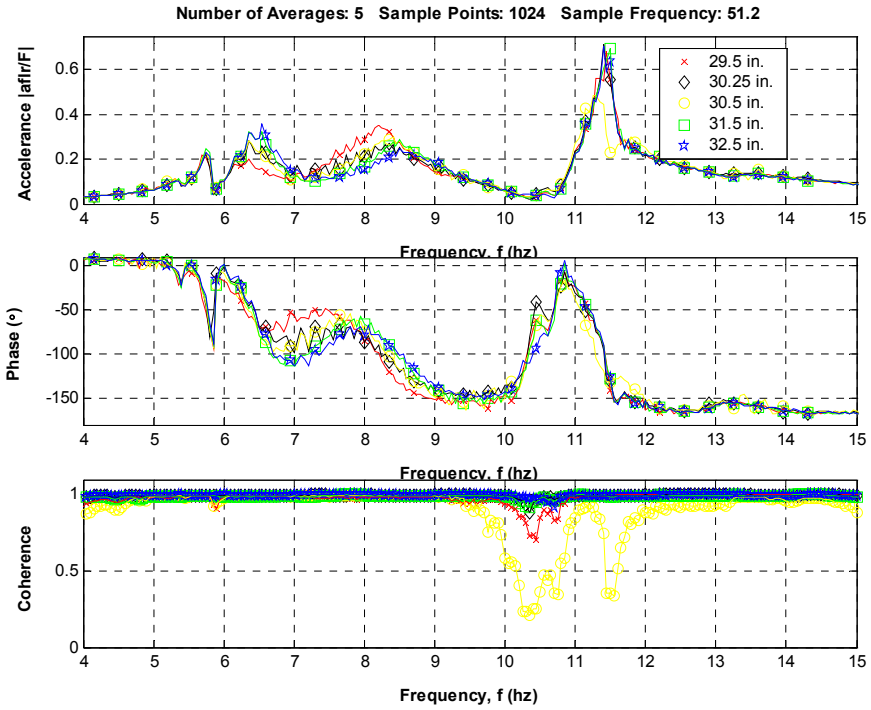

Figure N.33 – Floor Response with Passive PTMD – Variation of Spring Location

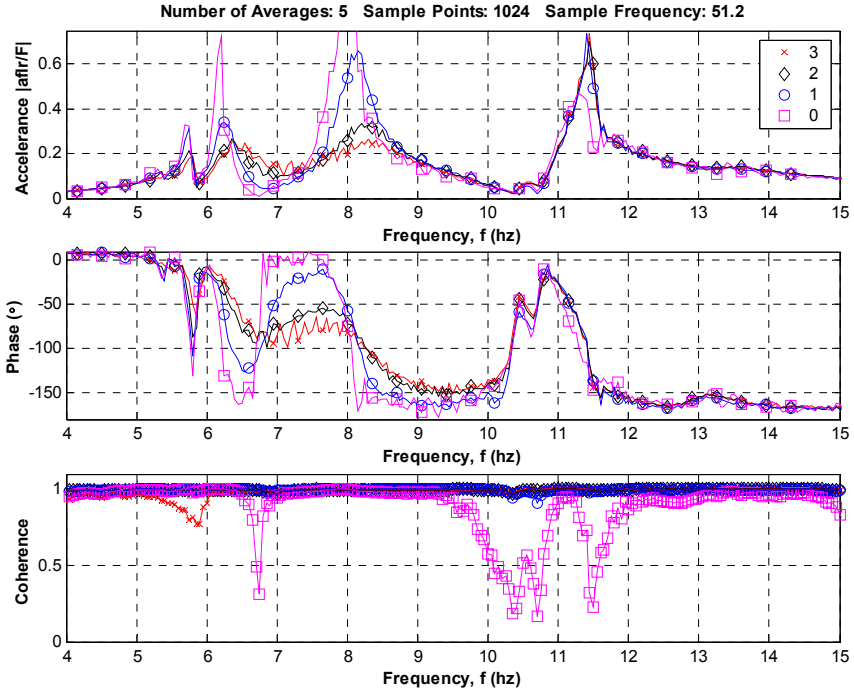

Figure N.34 – Floor Response with Passive PTMD – Variation in Number Dampers

APPENDIX O Frequency Test Data – Semi-Active PTMD on Floor

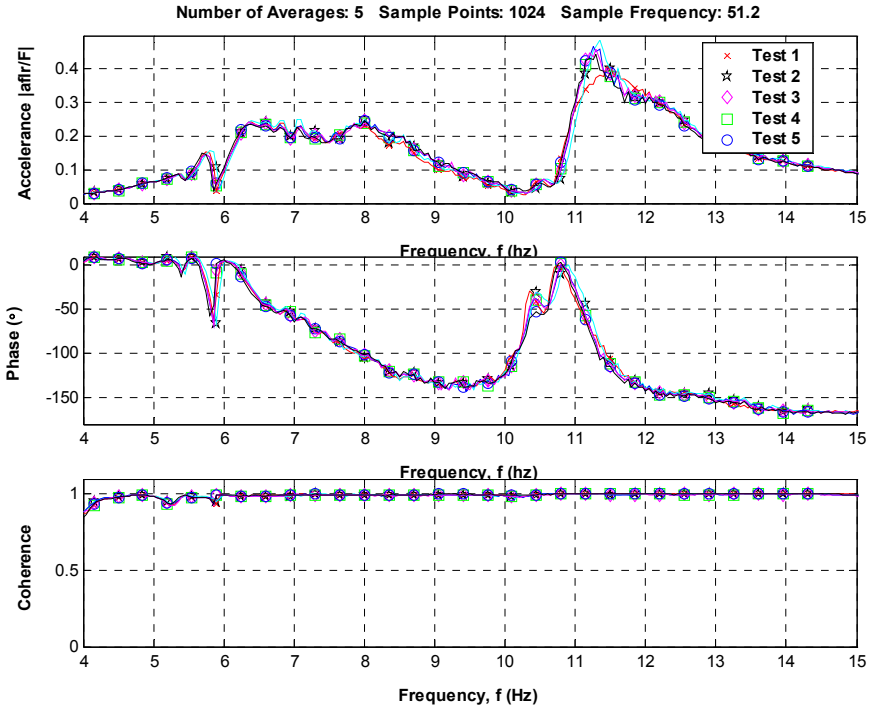

Figure O.1 – Floor Response with Tuned Semi-active PTMD

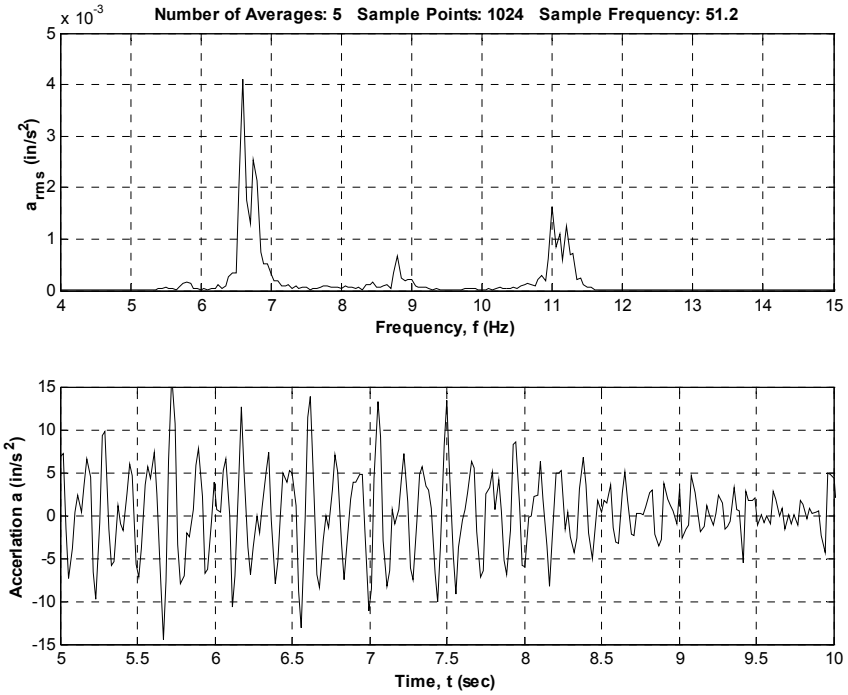

Figure O.2 – Floor Response with Tuned Semi-active PTMD to Walking at 132 bpm

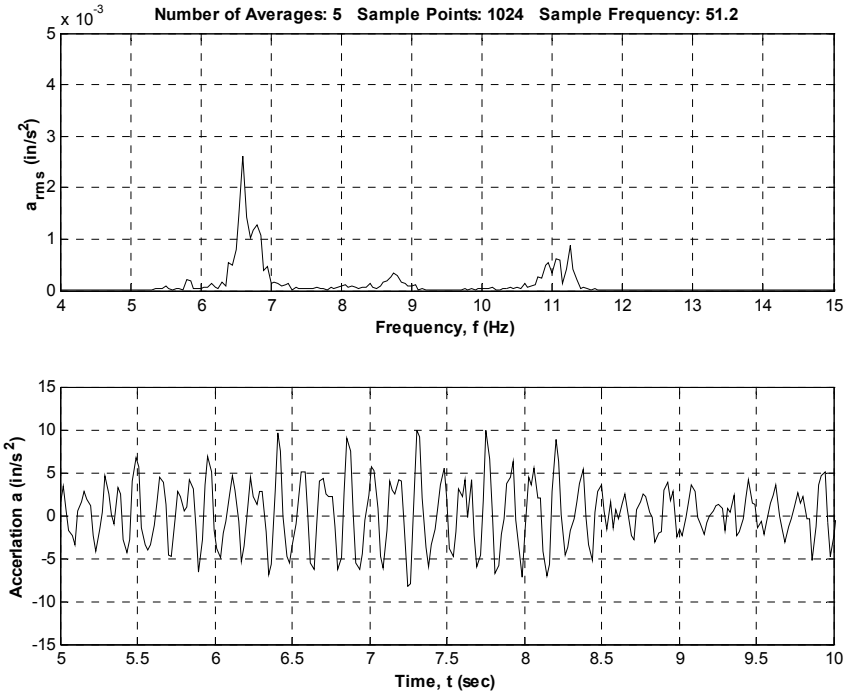

Figure O.3 – Floor Response with Tuned Semi-active PTMD to Walking at 132 bpm

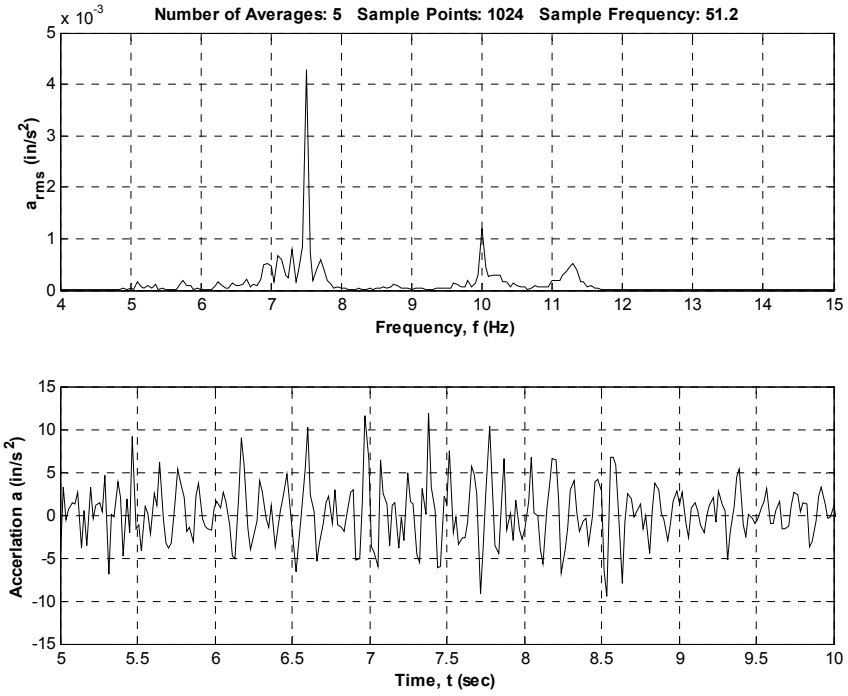

Figure O.4 – Floor Response with Tuned Semi-active PTMD to Walking at 150 bpm

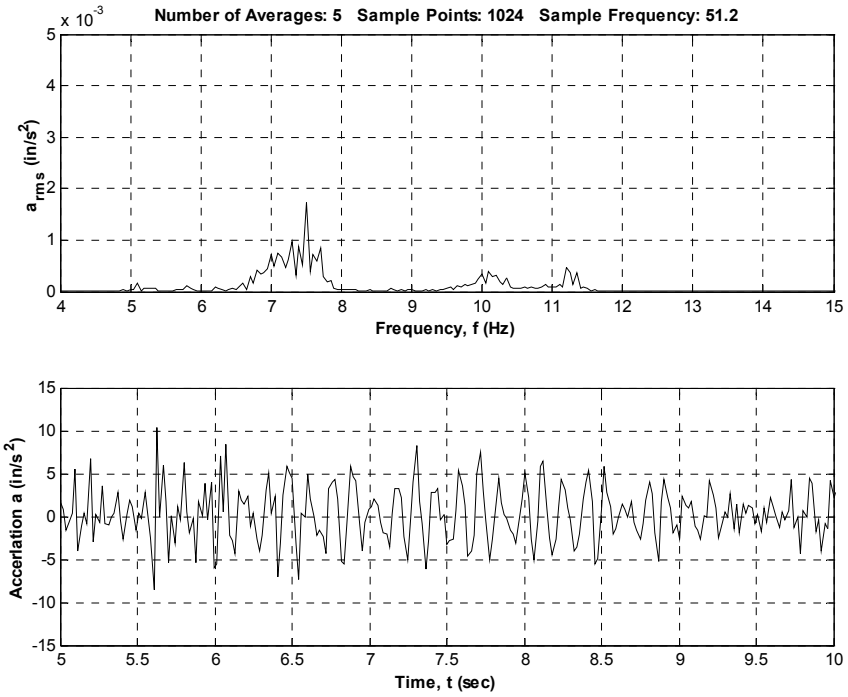

Figure O.5 – Floor Response with Tuned Semi-active PTMD to Walking at 150 bpm

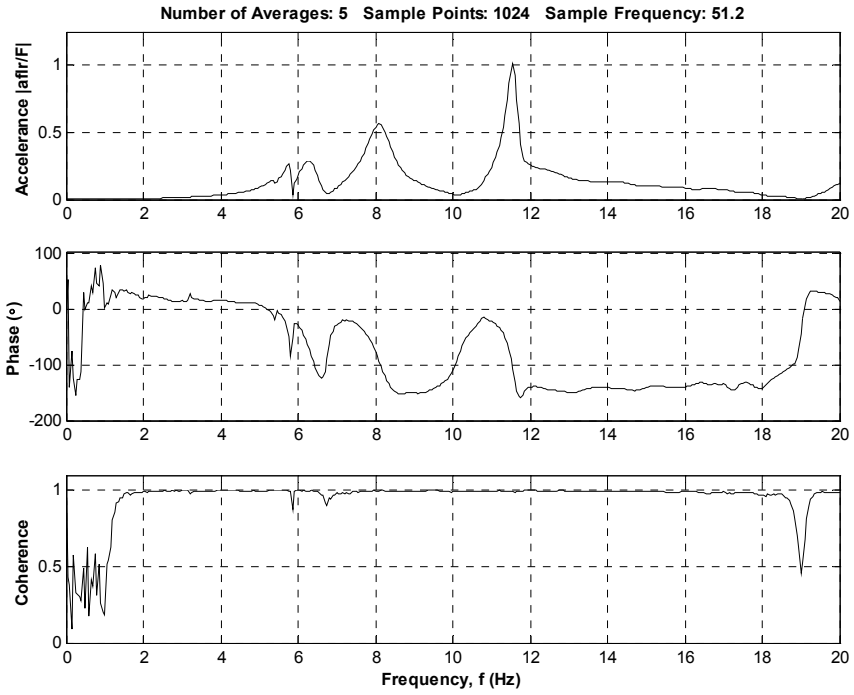

Figure O.6 – Floor Response with Tuned Semi-active PTMD to a Heel Drop at Center of Floor

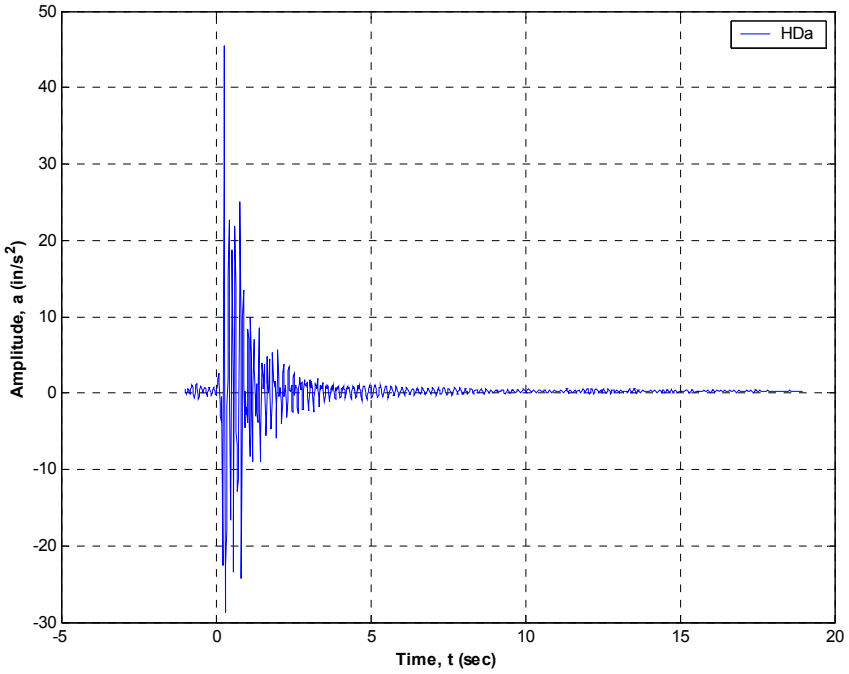

Figure O.7 – Floor Response with Tuned Passive PTMD to a Heel Drop at Center of Floor

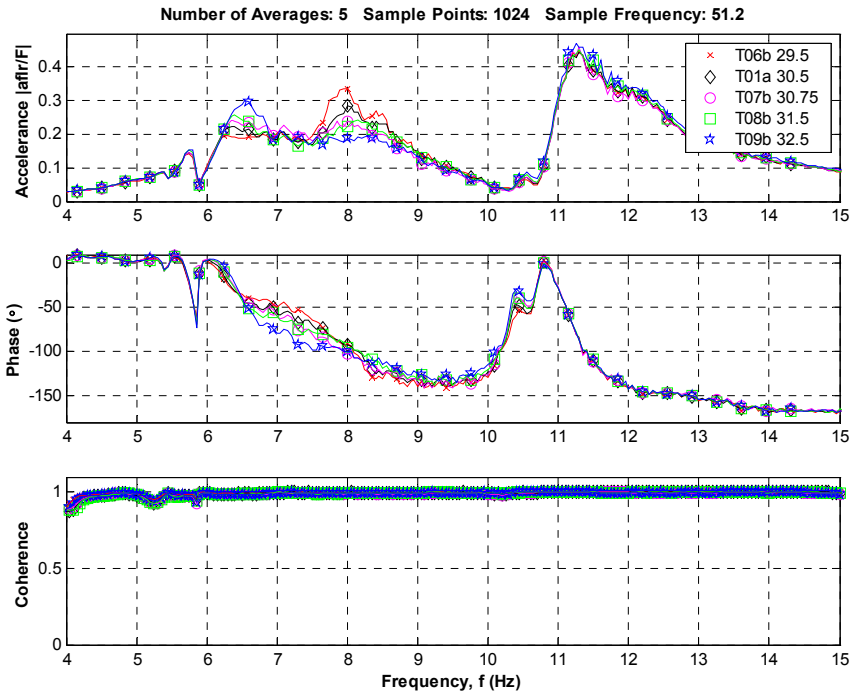

Figure O.8 – Variation in Floor Response to Change in Semi-active PTMD Spring Location

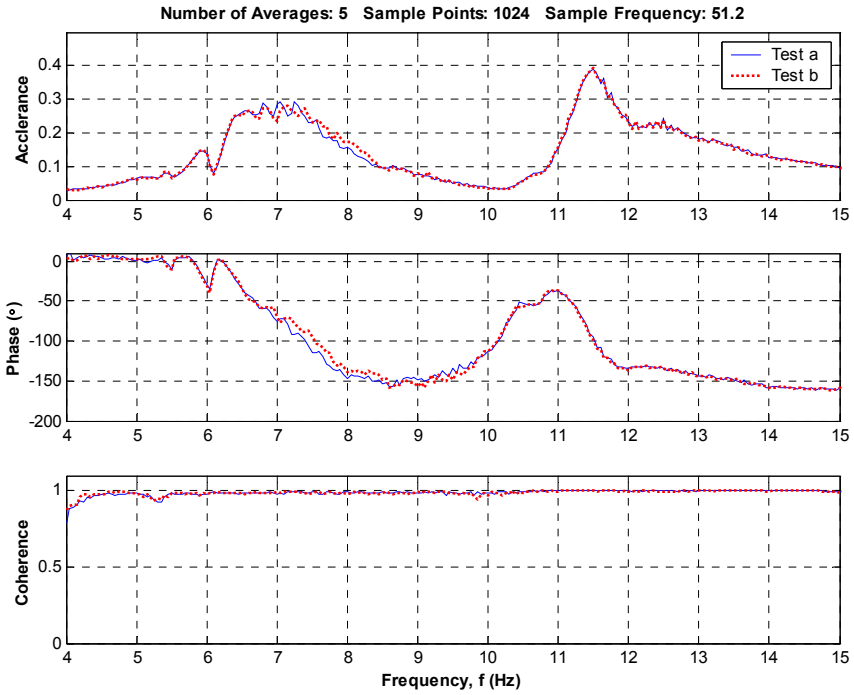

Figure O.9– Floor Response with Semi-active PTMD – 16 People Standing with Knees Bent

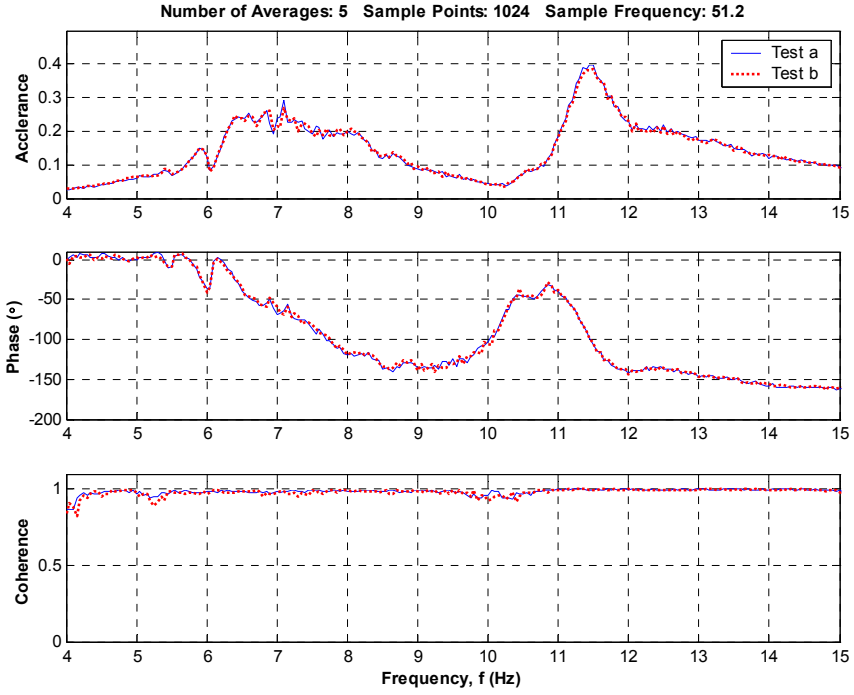

Figure O.10 – Floor Response with Semi-active PTMD – 12 People Standing with Knees Bent

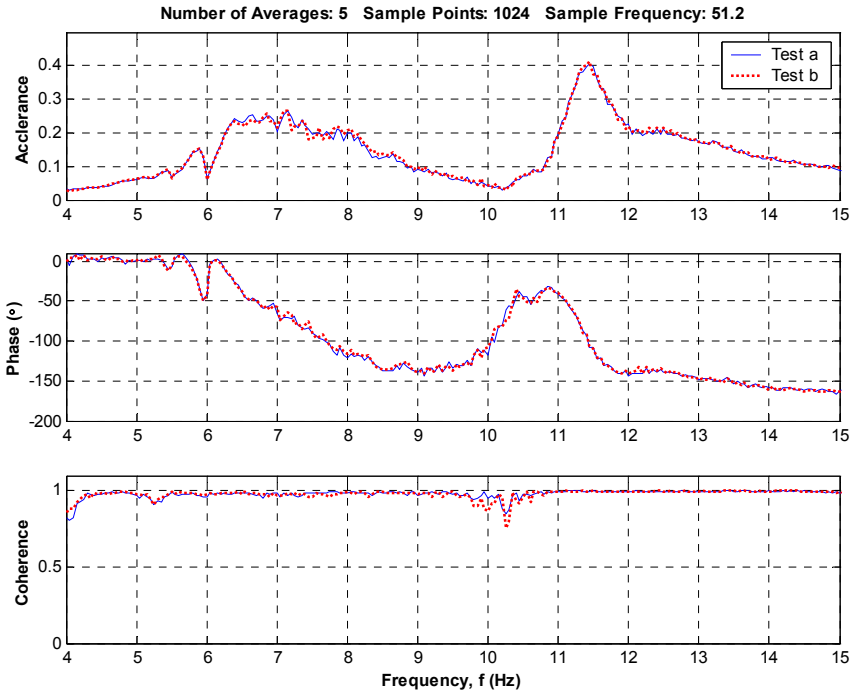

Figure O.11 – Floor Response with Semi-active PTMD - 8 People Standing with Knees Bent

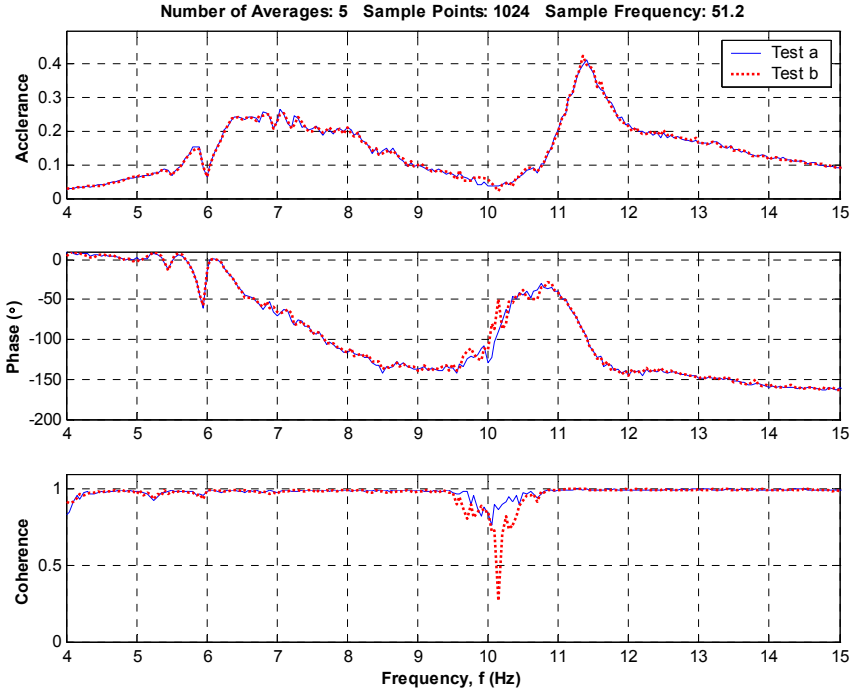

Figure O.12 – Floor Response with Semi-active PTMD – 6 People Standing with Knees Bent

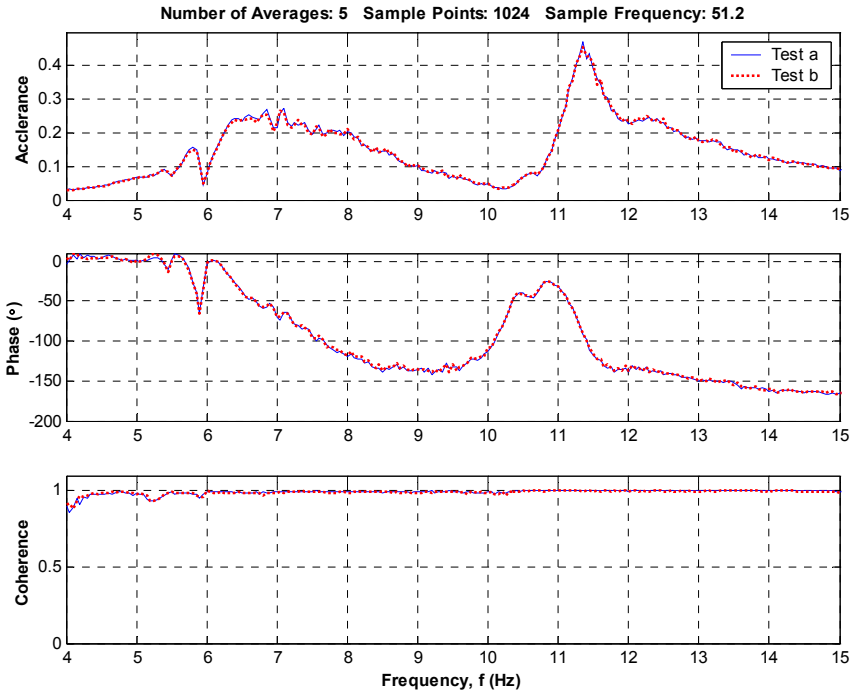

Figure O.13 – Floor Response with Semi-active PTMD – 4 People Standing with Knees Bent

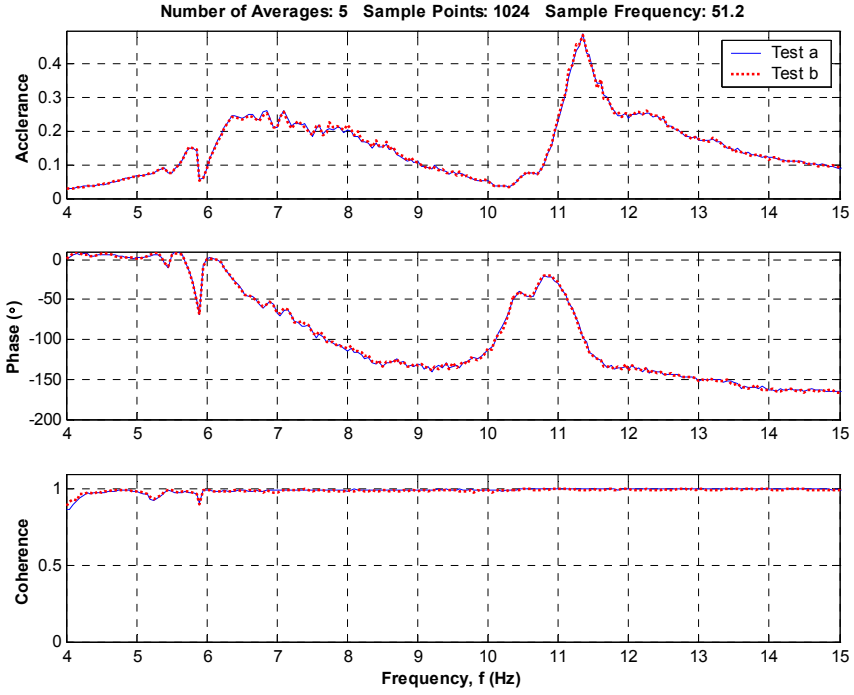

Figure O.14 – Floor Response with Semi-active PTMD – 2 People Standing with Knees Bent

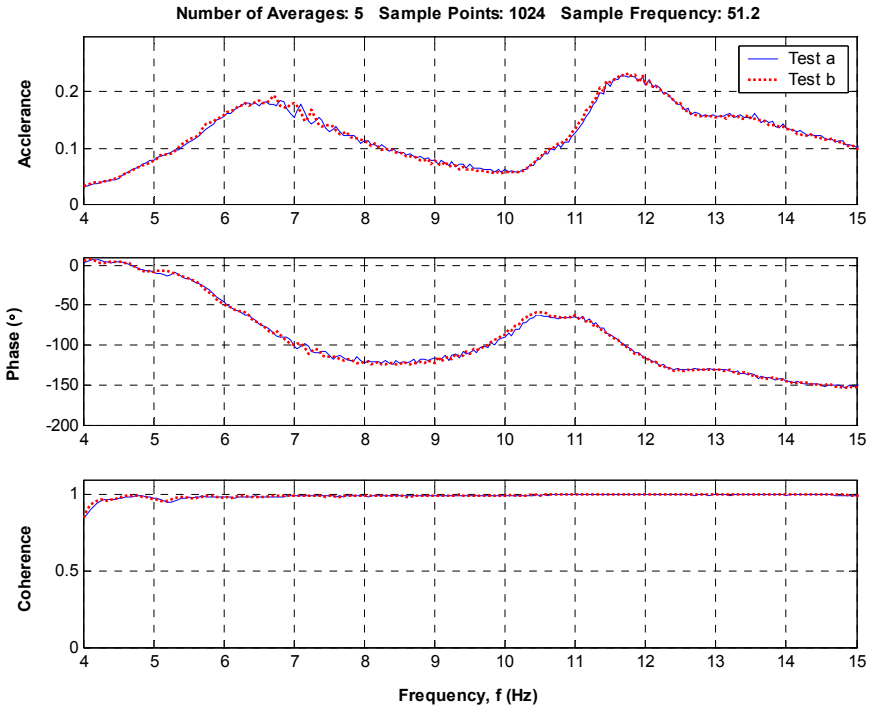

Figure O.15 – Floor Response with Semi-active PTMD – 16 People Sitting

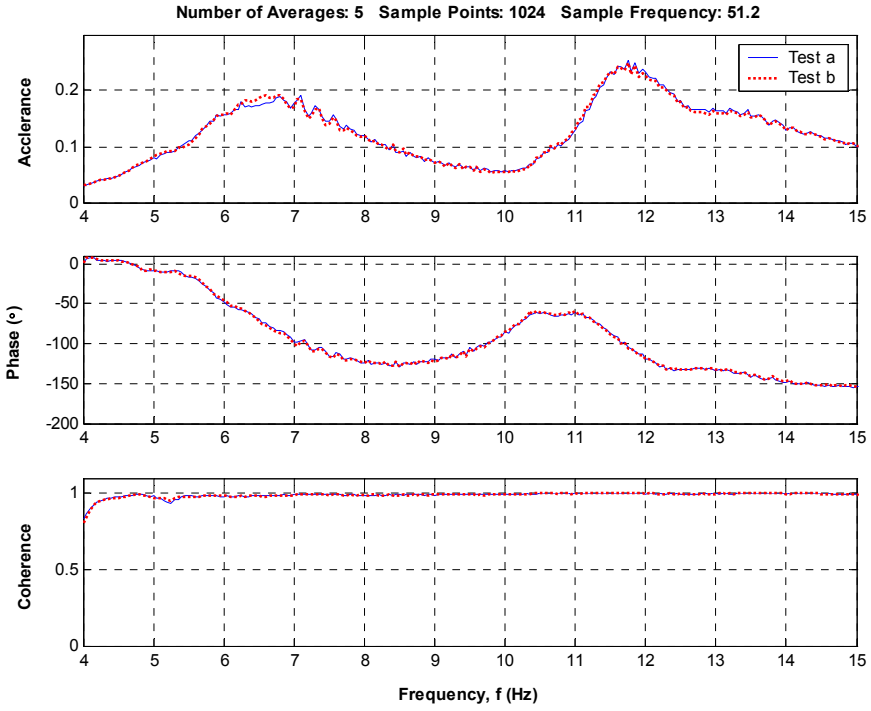

Figure O.16 – Floor Response with Semi-active PTMD – 12 Sitting

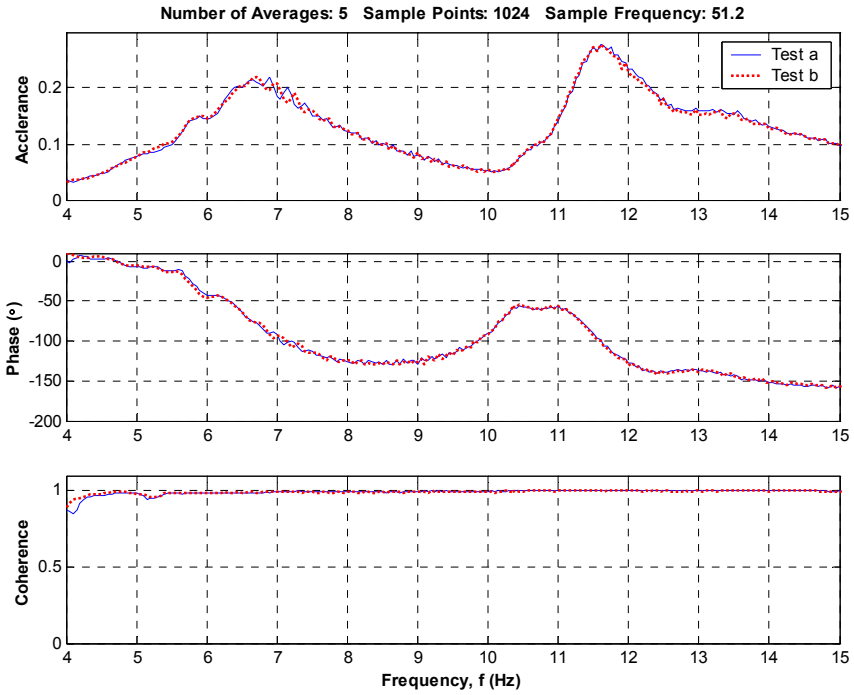

Figure O.17 – Floor Response with Semi-active PTMD – 8 Sitting

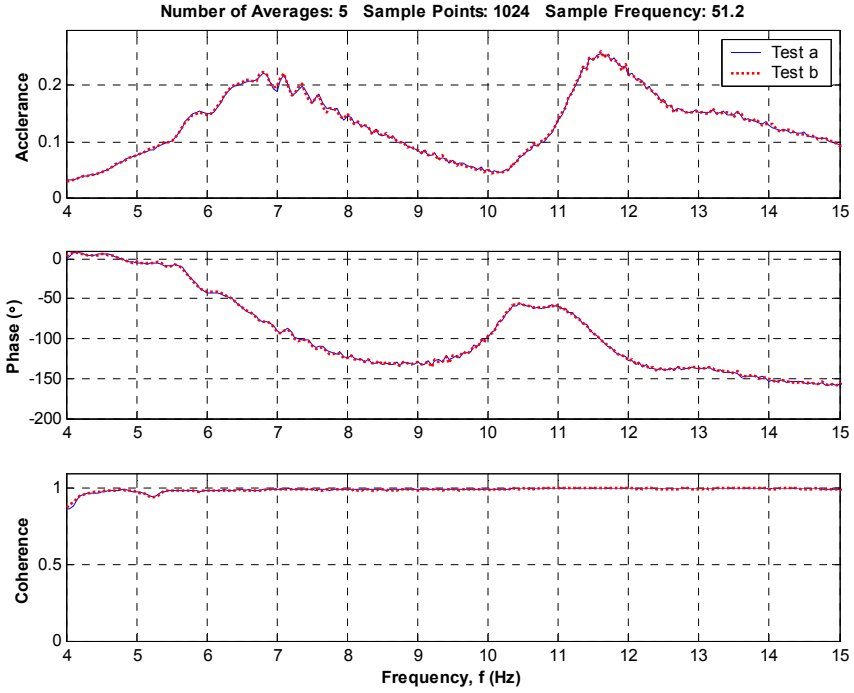

Figure O.18 – Floor Response with Semi-active PTMD – 6 Sitting

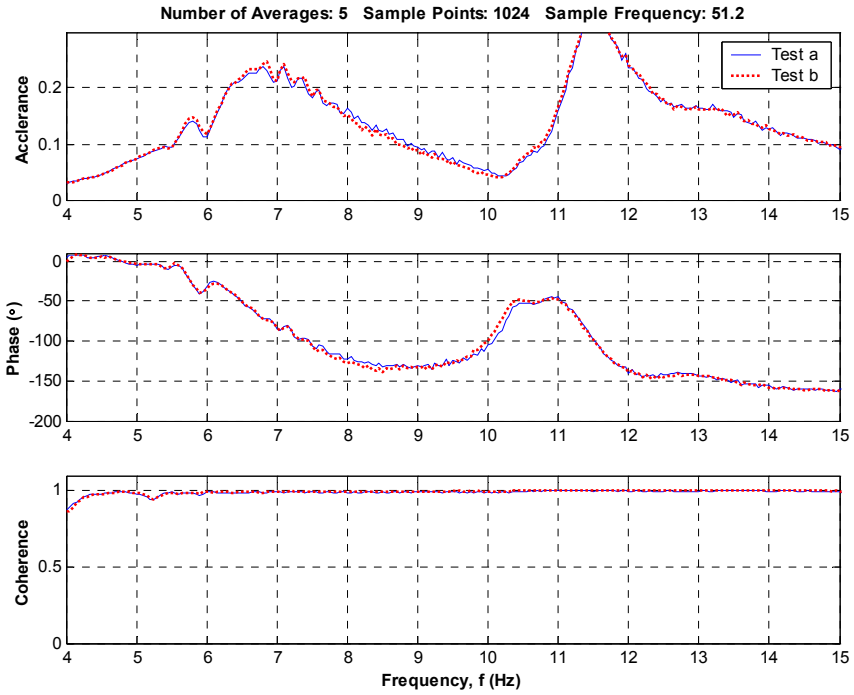

Figure O.19 – Floor Response with Semi-active PTMD – 4 Sitting

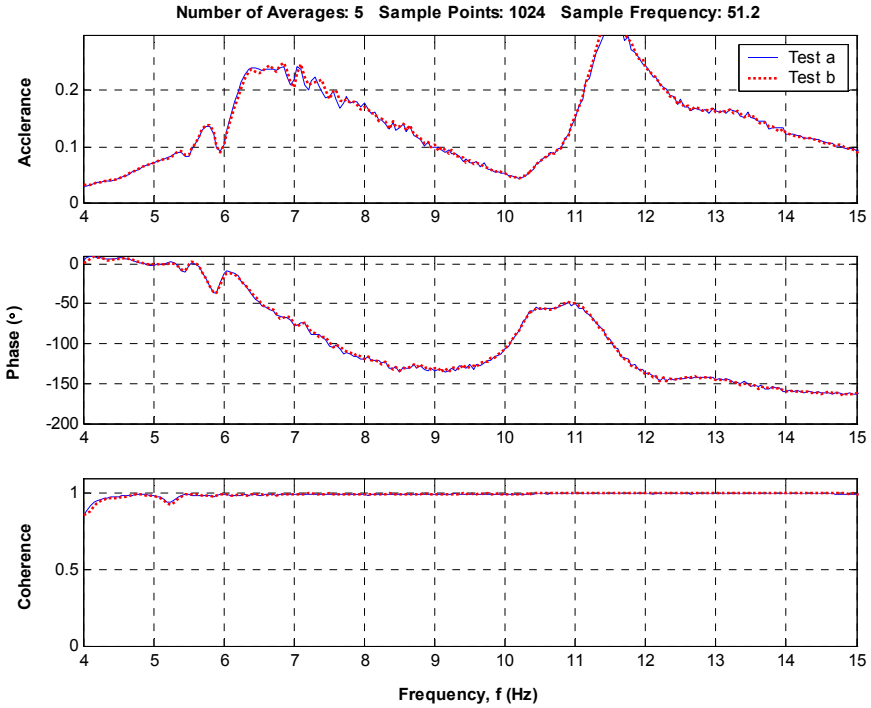

Figure O.20 – Floor Response with Semi-active PTMD – 2 Sitting

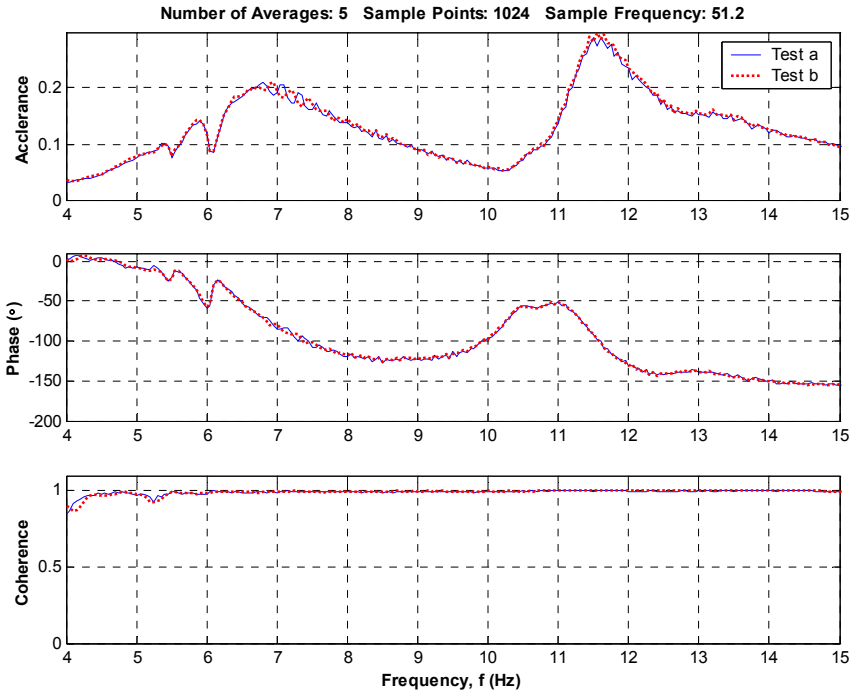

Figure O.21 – Floor Response with Semi-active PTMD – 16 People Standing with Straight Legs

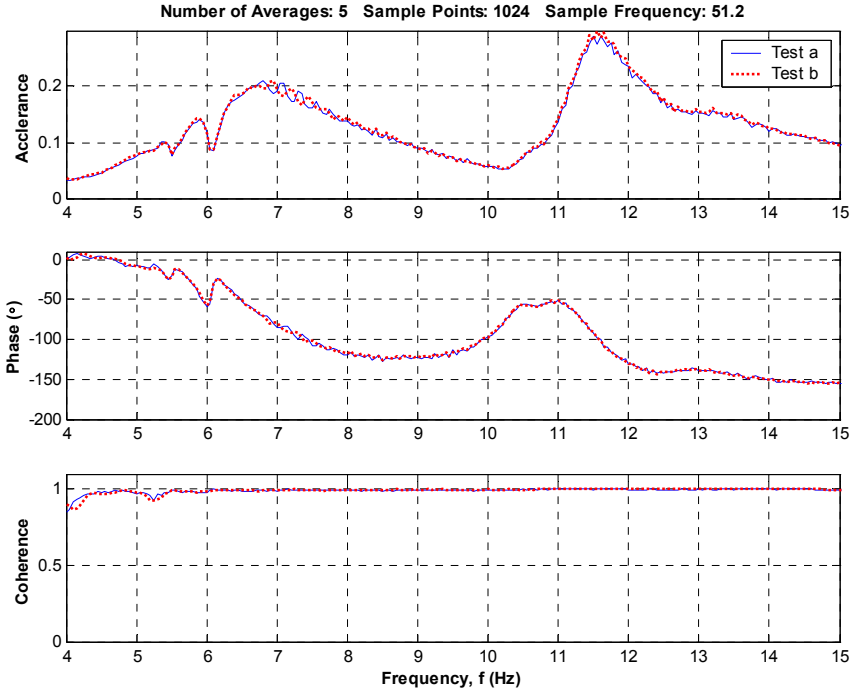

Figure O.22 – Floor Response with Semi-active PTMD – 12 People Standing with Straight Legs

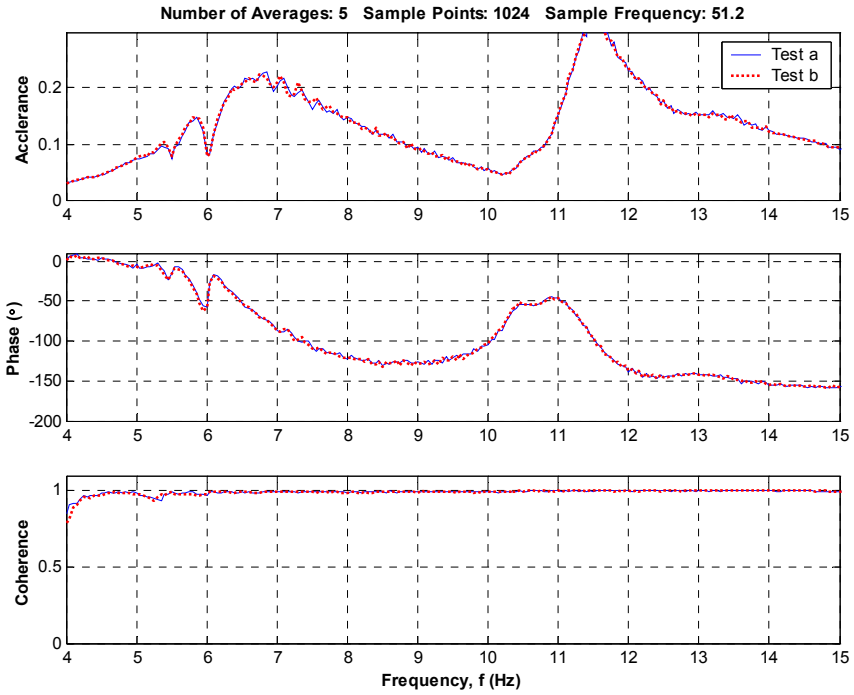

Figure O.23 – Floor Response with Semi-active PTMD – 8 People Standing with Straight Legs

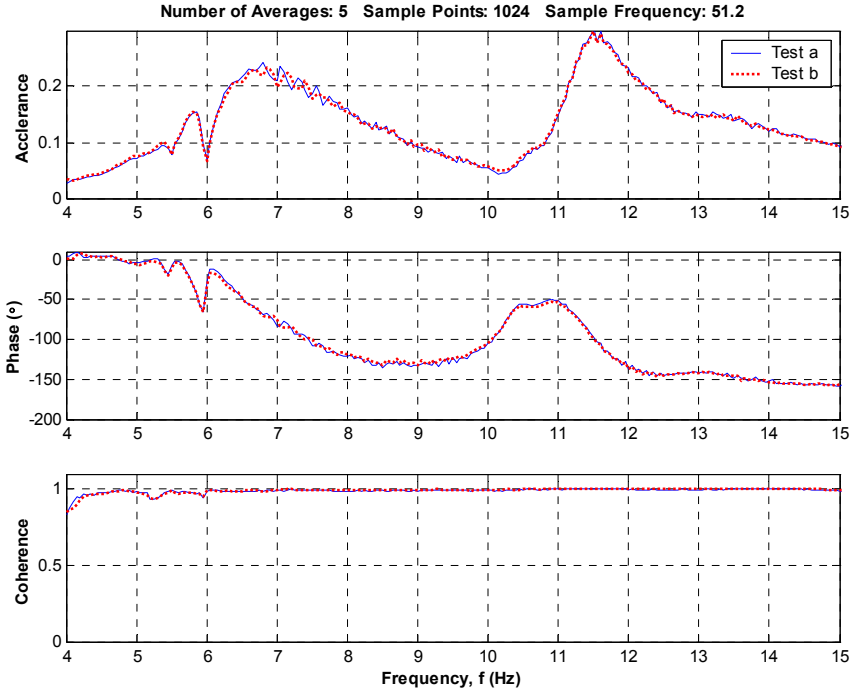

Figure O.24 – Floor Response with Semi-active PTMD – 6 People Standing with Straight Legs

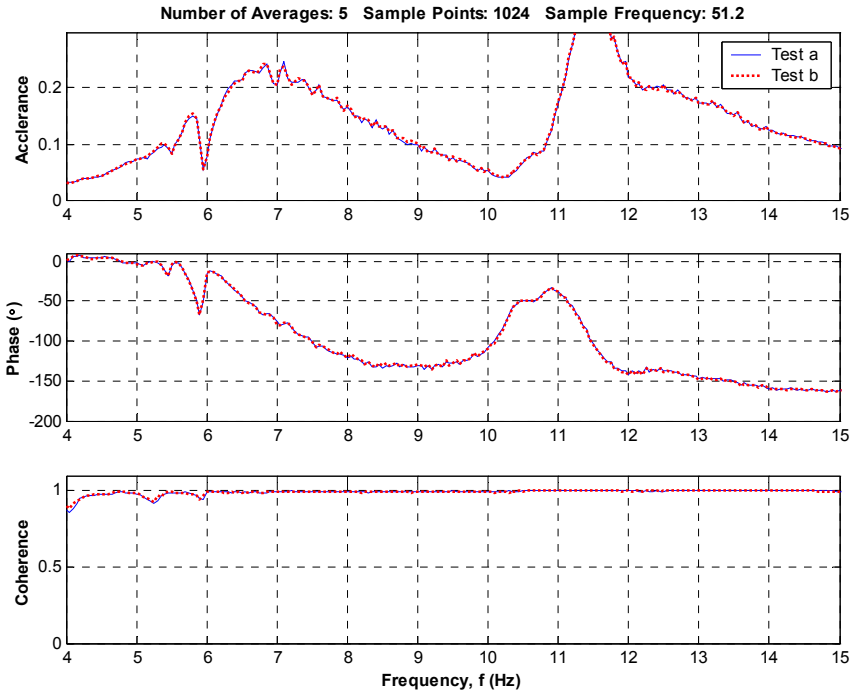

Figure O.25 – Floor Response with Semi-active PTMD – 4 People Standing with Straight Legs

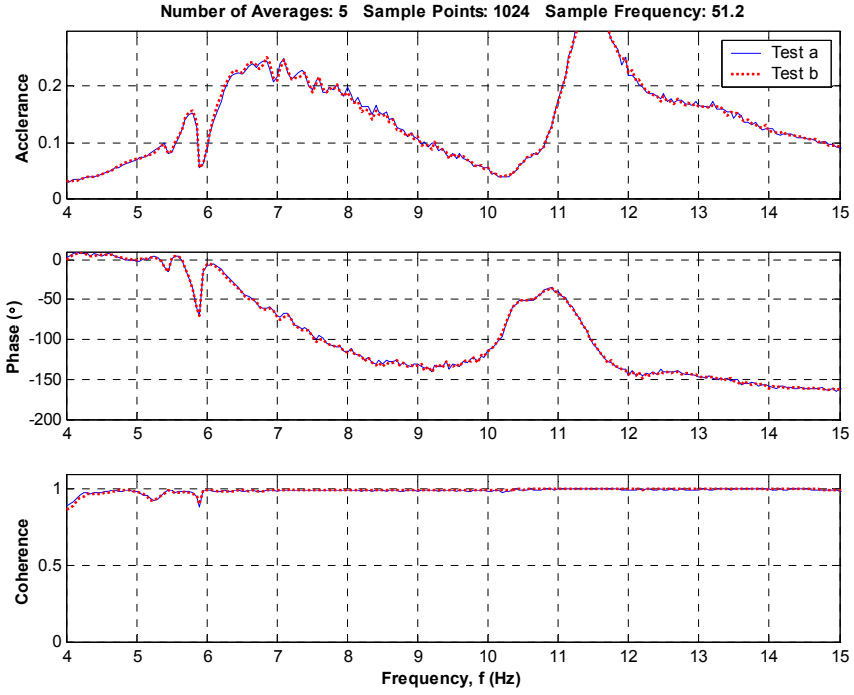

Figure O.26 – Floor Response with Semi-active PTMD – 2 People Standing with Straight Legs

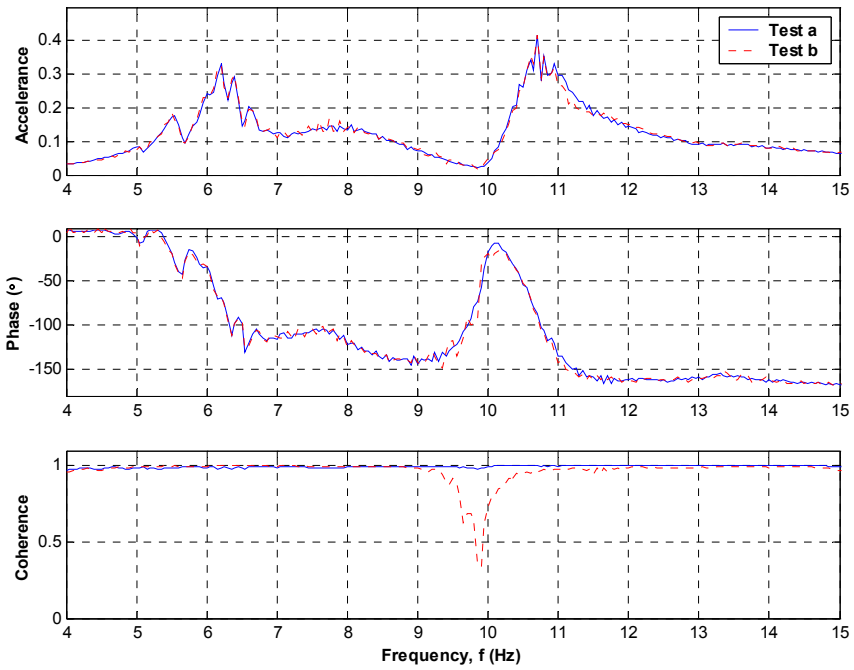

Figure O.27 – Floor Response with Semi-active PTMD – Equivalent Dead Mass of 16 People

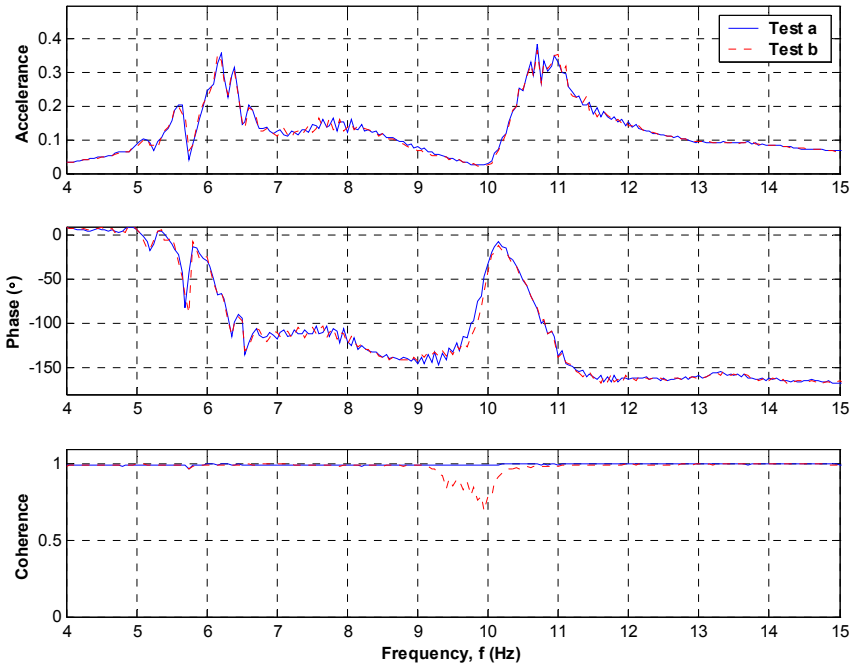

Figure O.28 – Floor Response with Semi-active PTMD – Equivalent Dead Mass of 12 People

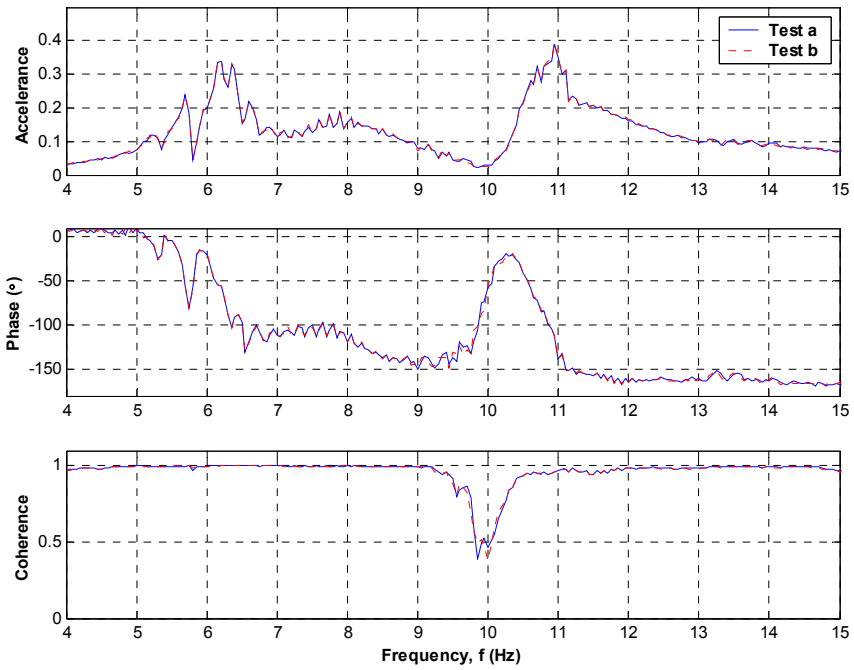

Figure O.29 – Floor Response with Semi-active PTMD – Equivalent Dead Mass of 8 People

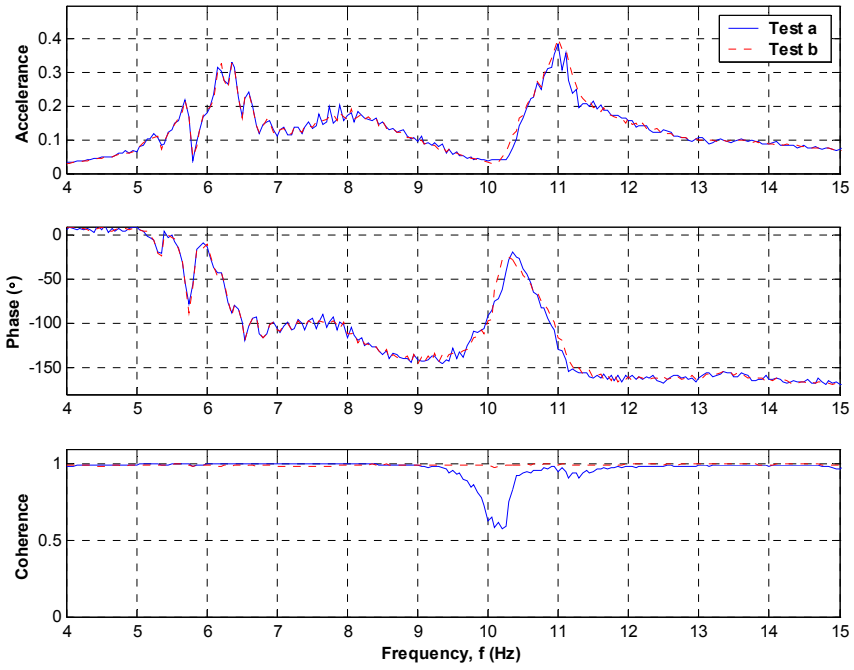

Figure O.30 – Floor Response with Semi-active PTMD – Equivalent Dead Mass of 6 People

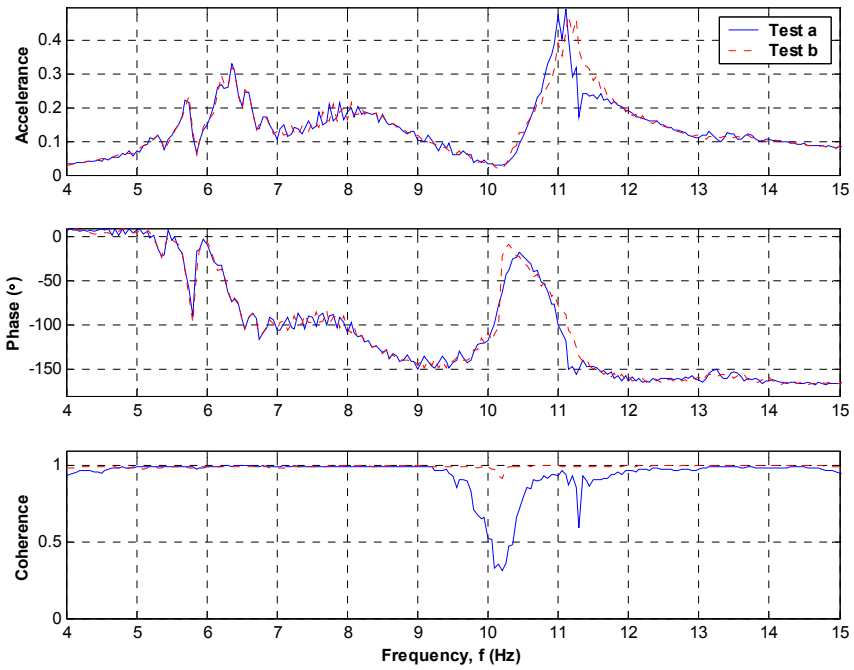

Figure O.31 – Floor Response with Semi-active PTMD – Equivalent Dead Mass of 4 People

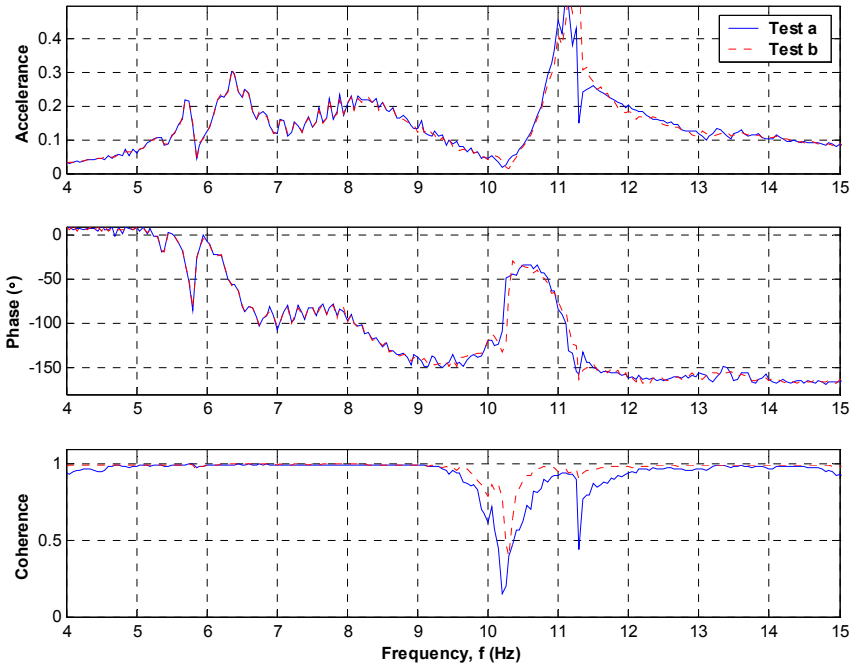

Figure O.32 – Floor Response with Semi-active PTMD – Equivalent Dead Mass of 2 People

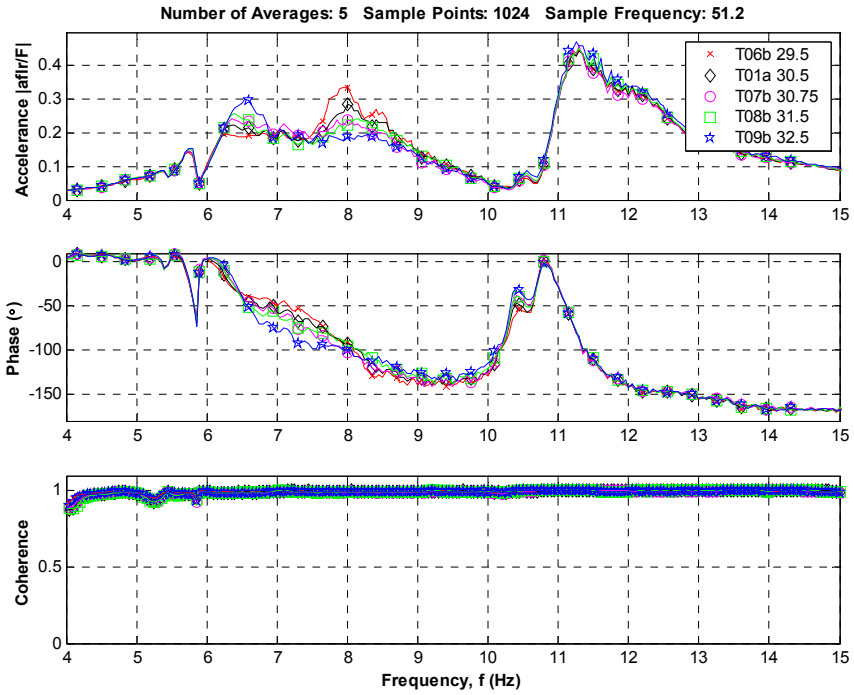

Figure O.33 – Floor Response with Semi-active PTMD – Variation in Stiffness – Test A

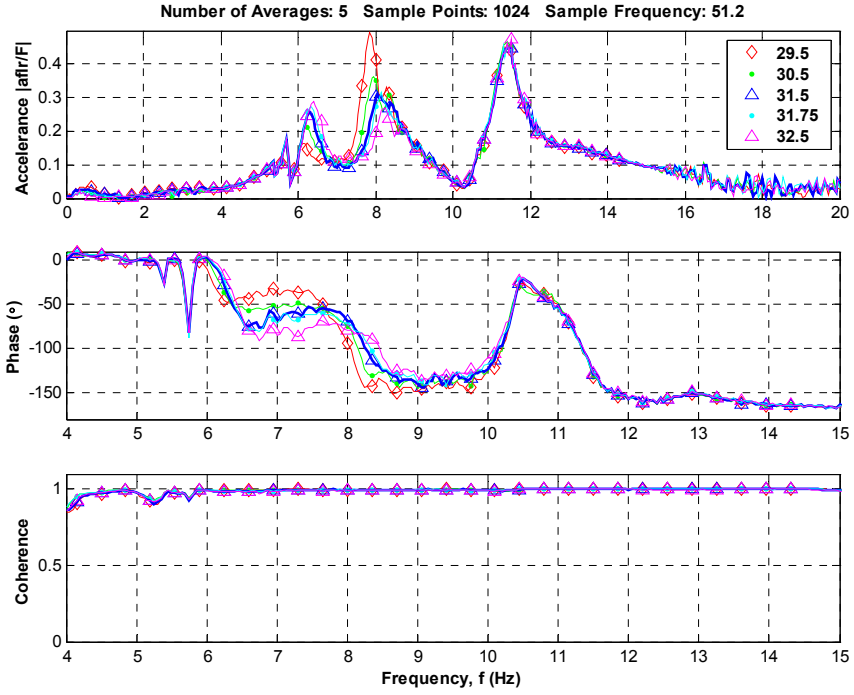

Figure O.34 – Floor Response with Semi-active PTMD – Variation in Stiffness – Test B

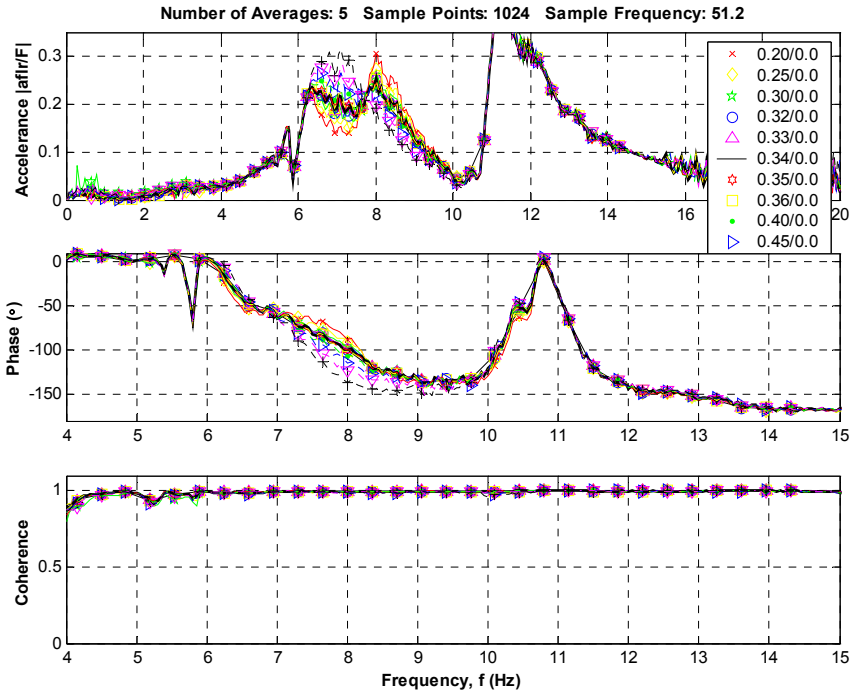

Figure O.35 – Floor Response with Semi-active PTMD – Variation in On Damping

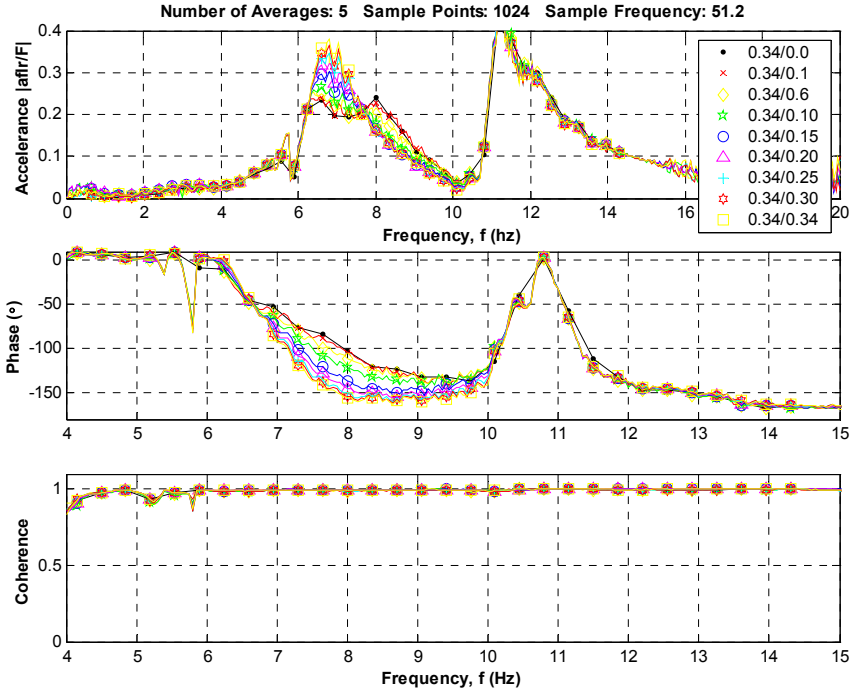

Figure O.36 – Floor Response with Semi-active PTMD – Variation in Off Damping

APPENDIX P: Human Locations

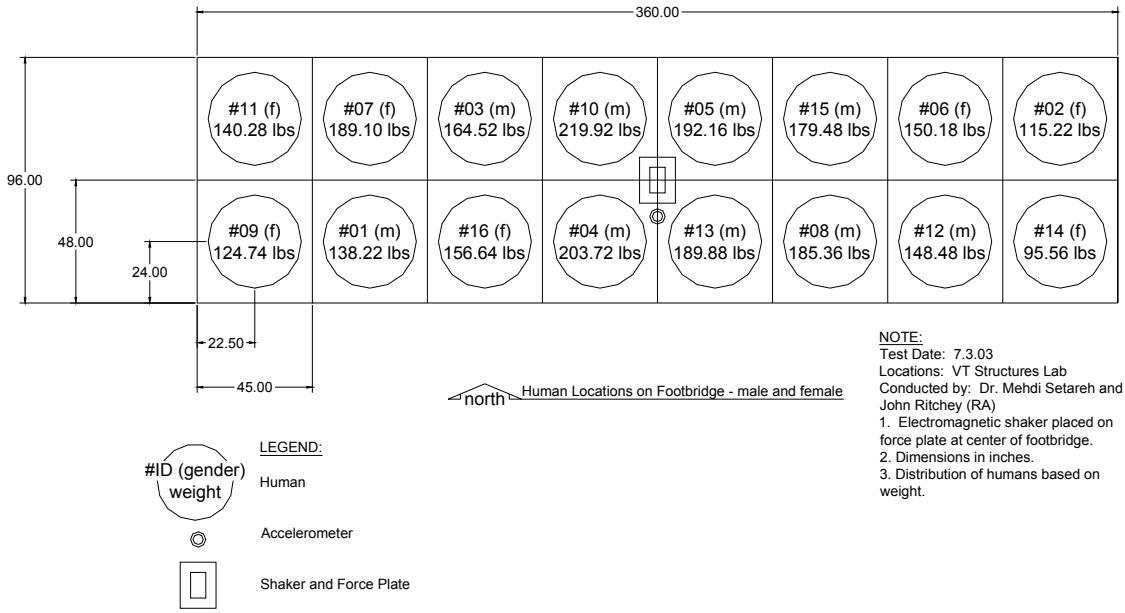

Figure P.1 – Floor Plan of Human Locations with Bare Floor – 16 People

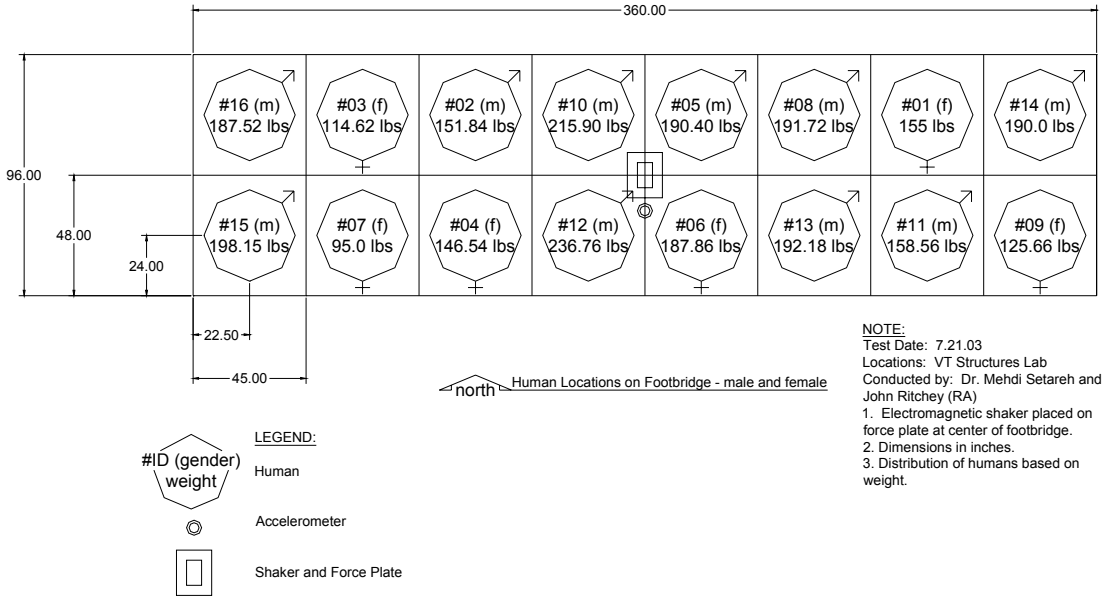

Figure P.2 – Floor Plan of Human Locations with Passive PTMD – 16 People

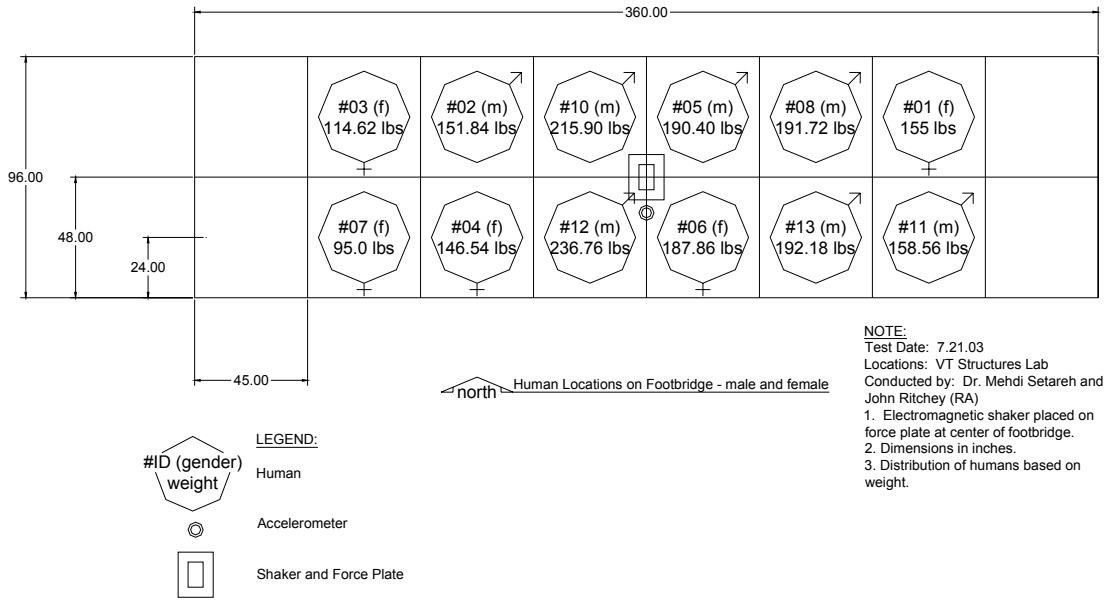

Figure P.3 – Floor Plan of Human Locations with Passive PTMD – 12 People

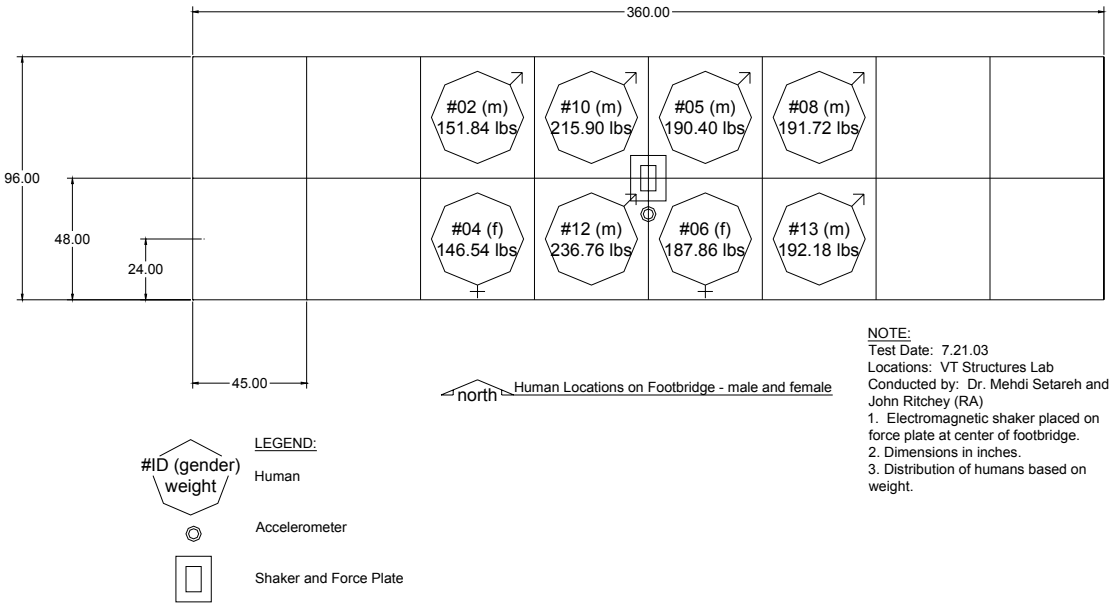

Figure P.4 – Floor Plan of Human Locations with Passive PTMD – 8 People

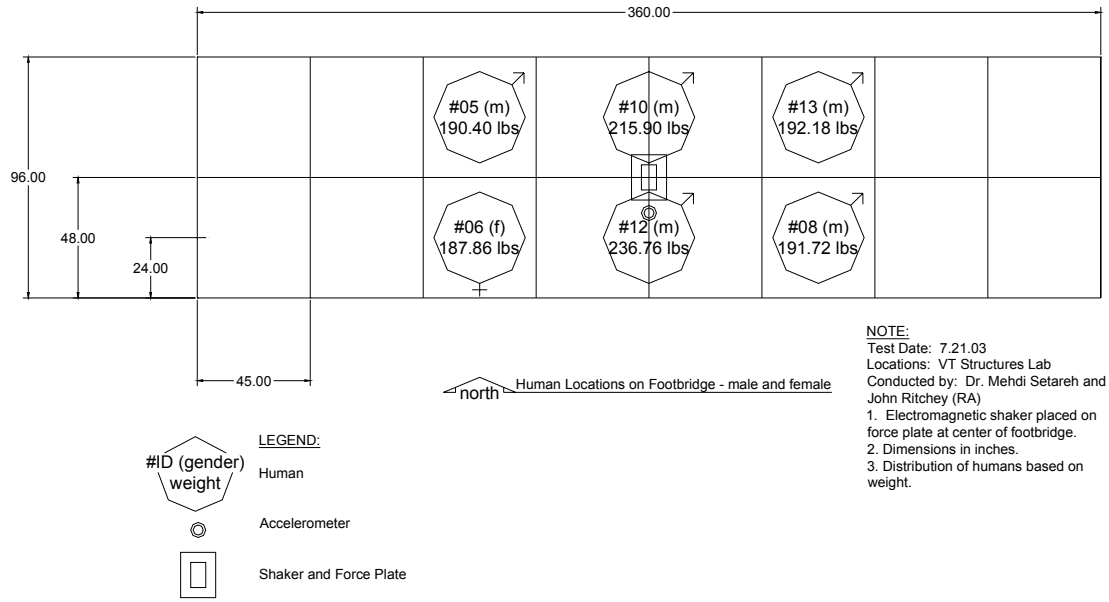

Figure P.5 – Floor Plan of Human Locations with Passive PTMD – 6 People

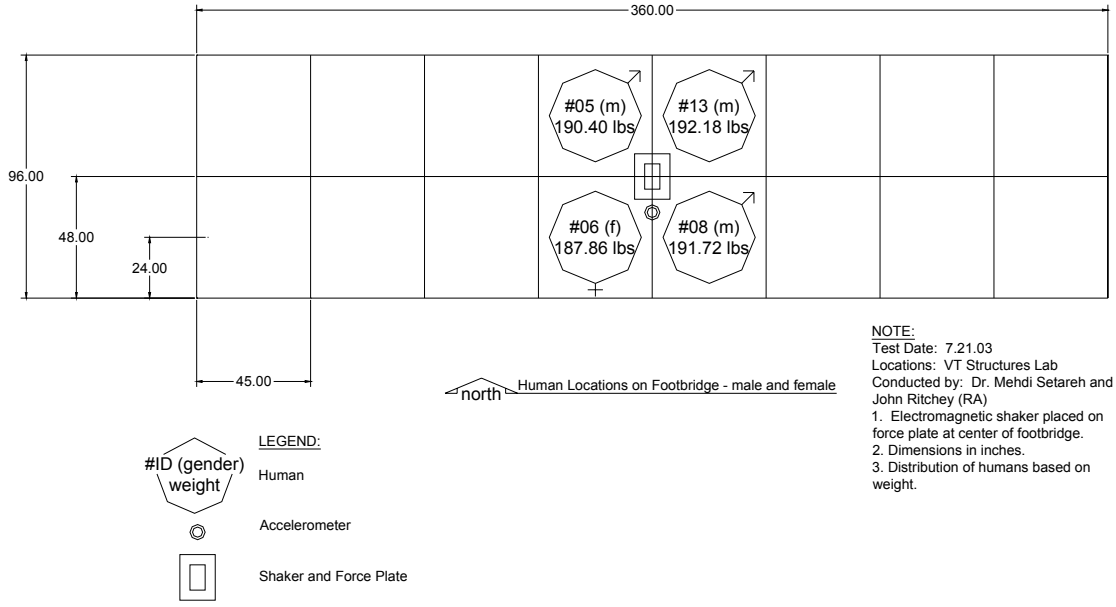

Figure P.6 – Floor Plan of Human Locations with Passive PTMD – 4 People

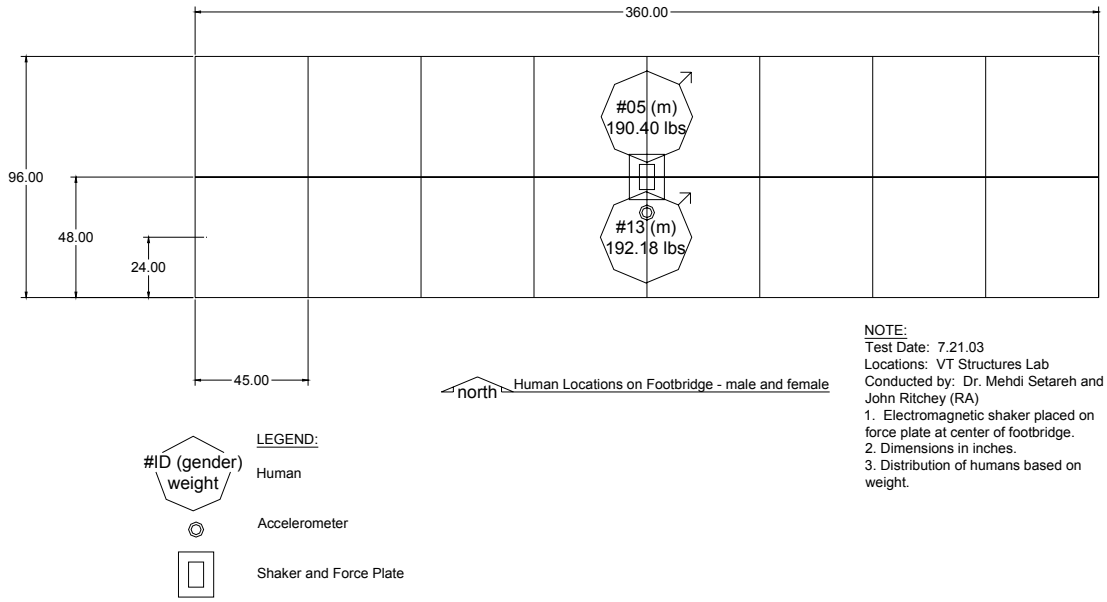

Figure P.7 – Floor Plan of Human Locations with Passive PTMD – 2 People

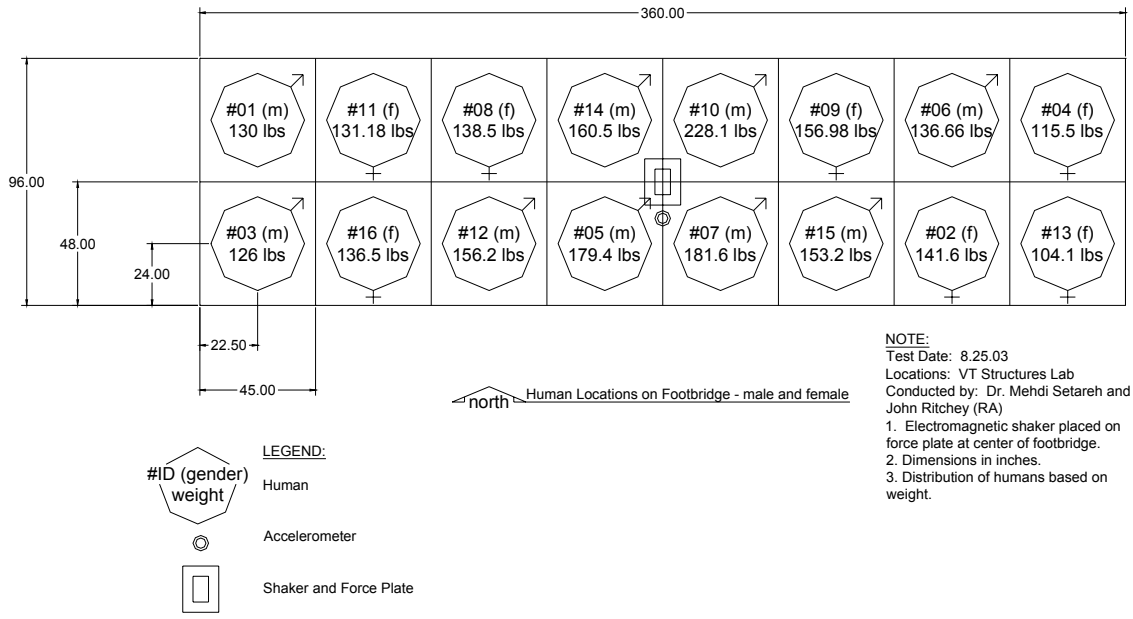

Figure P.8 – Floor Plan of Human Locations with Semi-Active PTMD – 16 People

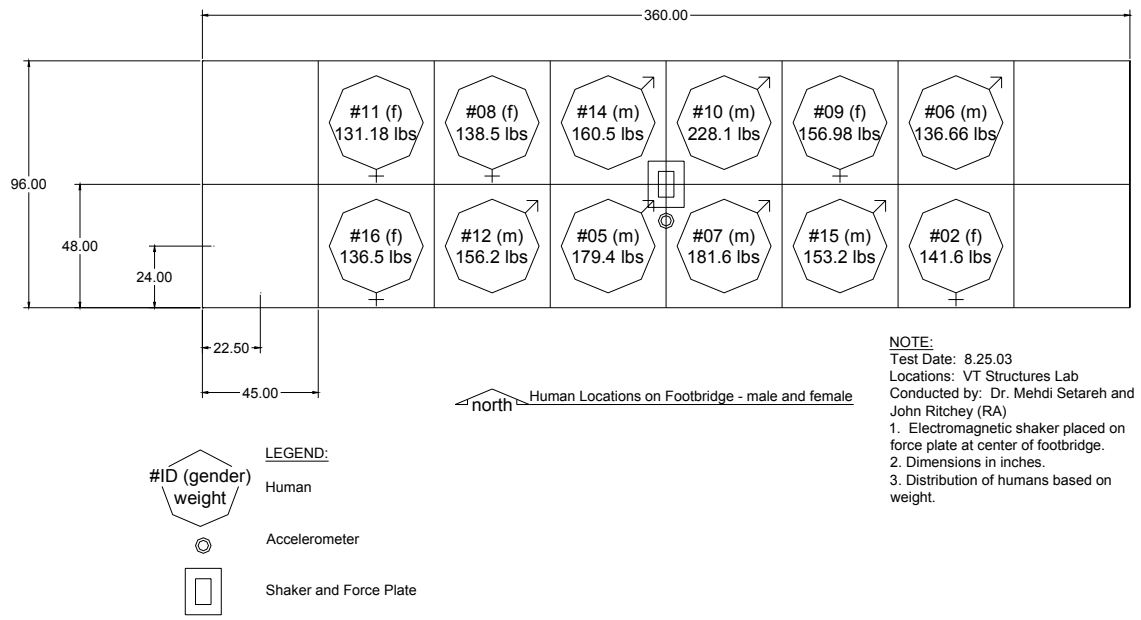

Figure P.9 – Floor Plan of Human Locations with Semi-Active PTMD – 12 People

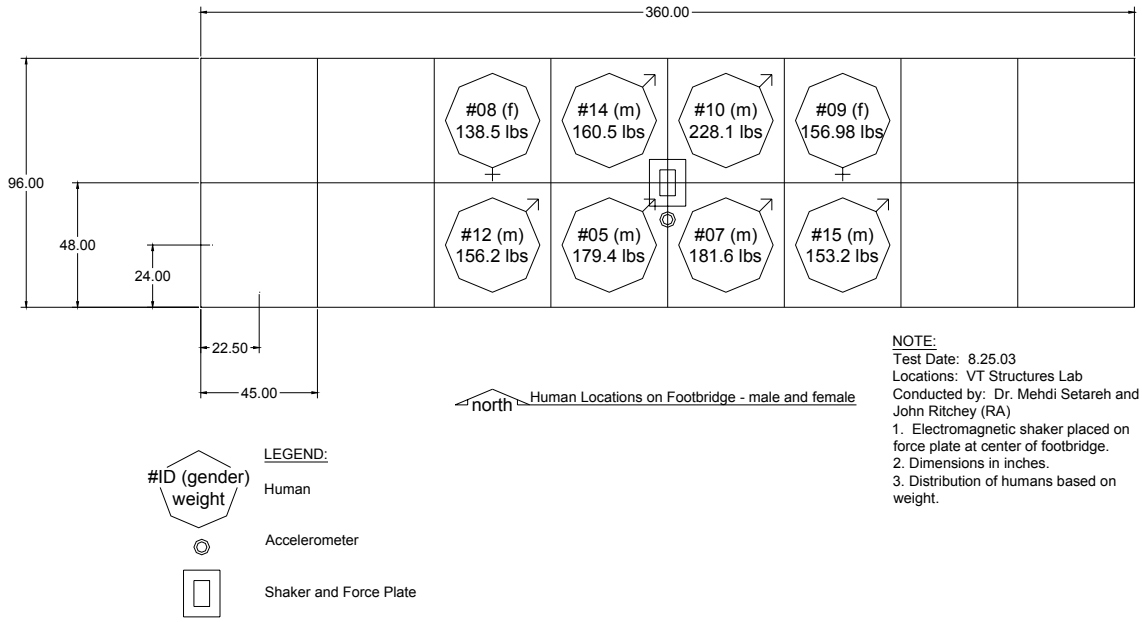

Figure P.10 – Floor Plan of Human Locations with Semi-Active PTMD –8 People

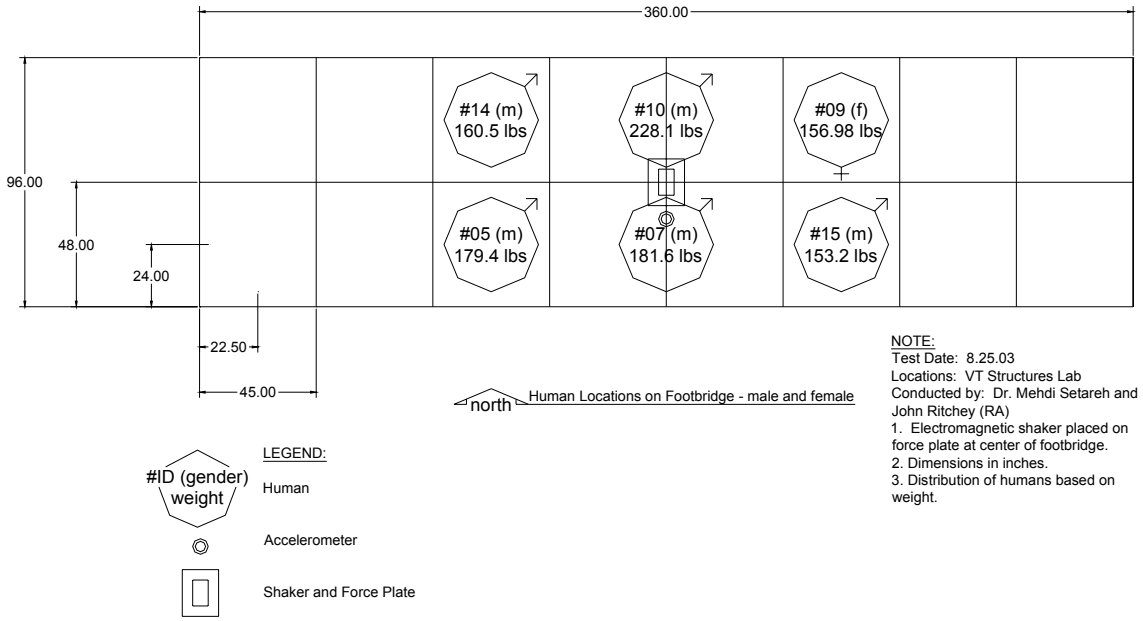

Figure P.11 – Floor Plan of Human Locations with Semi-Active PTMD – 6 People

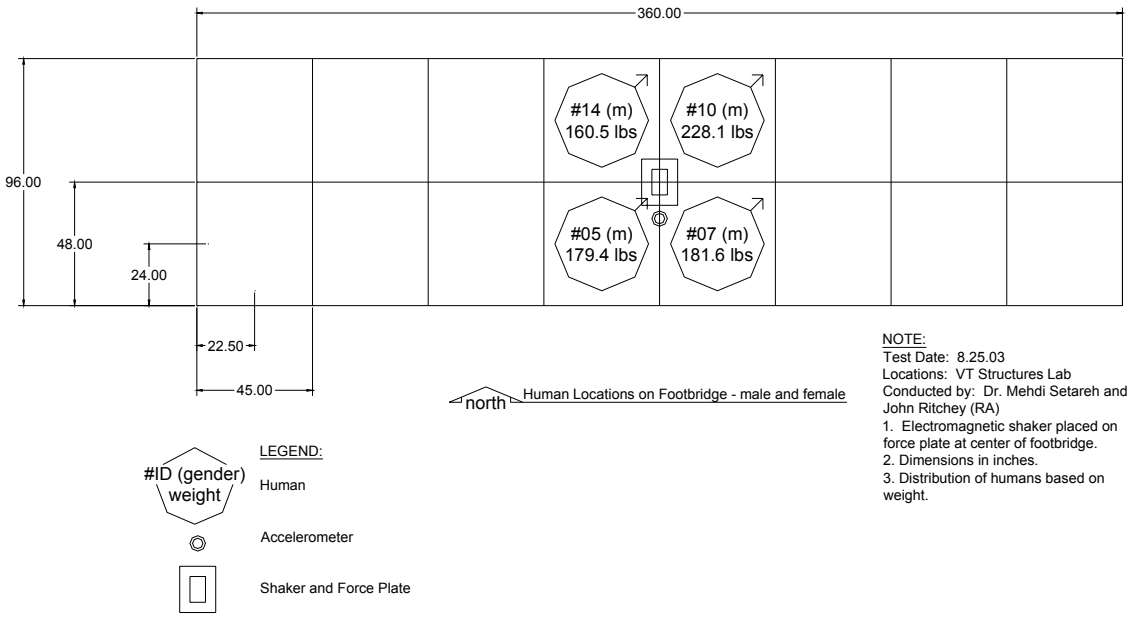

Figure P.12 – Floor Plan of Human Locations with Semi-Active PTMD – 4 People

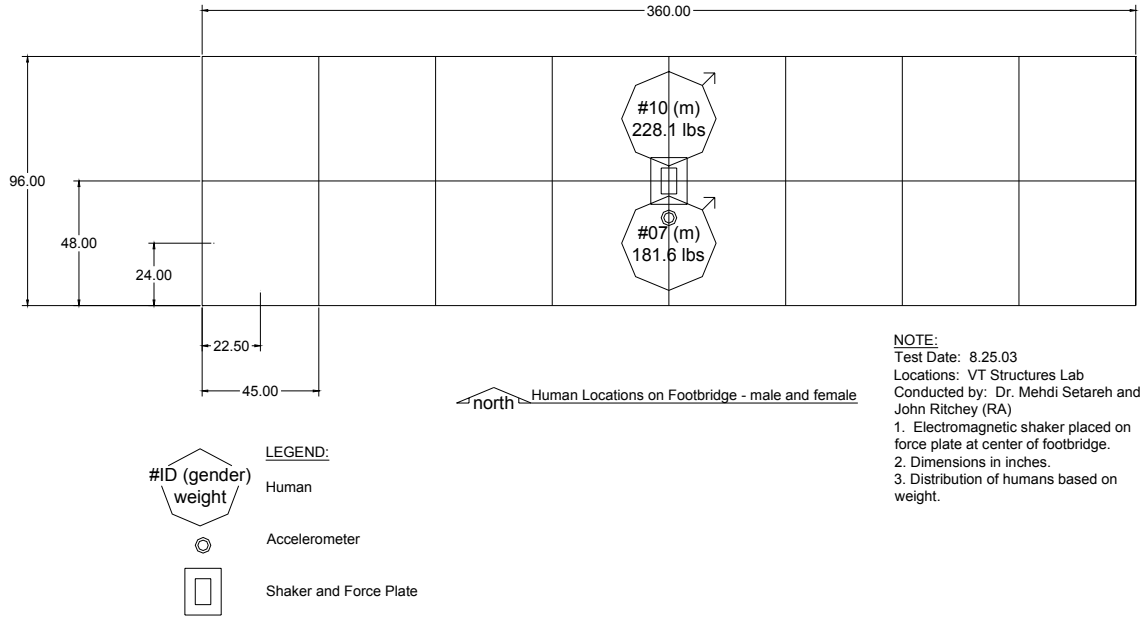

Figure P.13 – Floor Plan of Human Locations with Semi-Active PTMD – 2 People

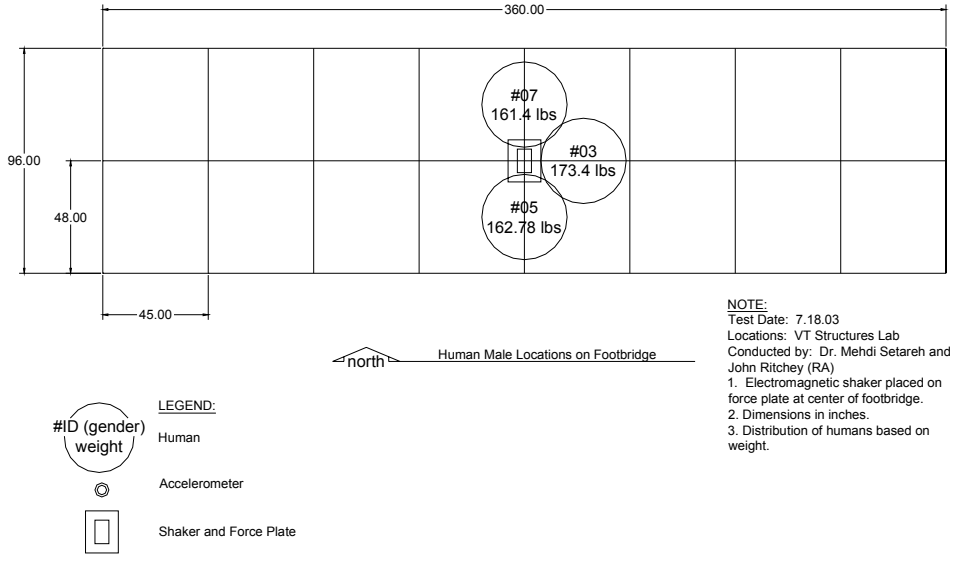

Figure P.14 – Floor Plan of Human Locations on Bare Floor – 3 People

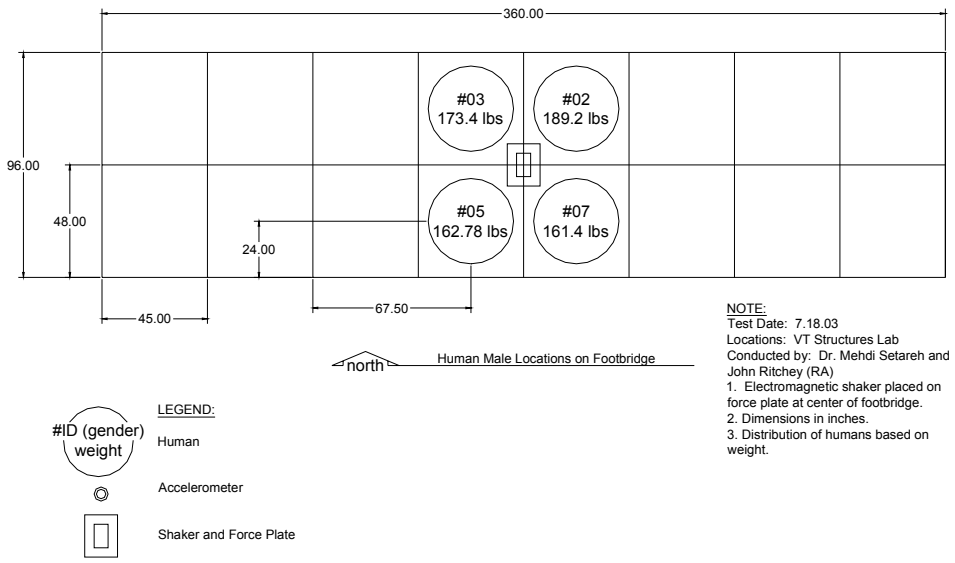

Figure P.15 – Floor Plan of Human Locations on Bare Floor – 4 People

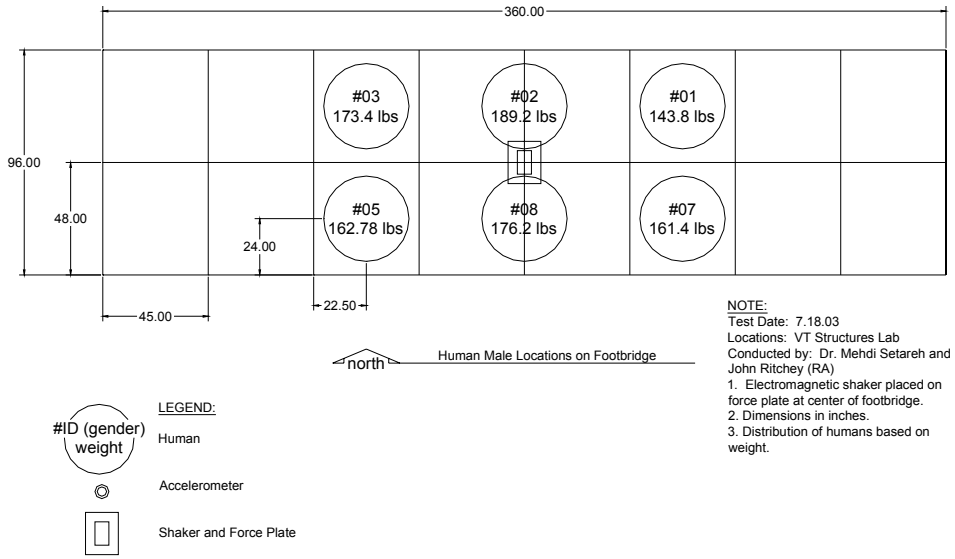

Figure P.16 – Floor Plan of Human Locations on Bare Floor – 6 People

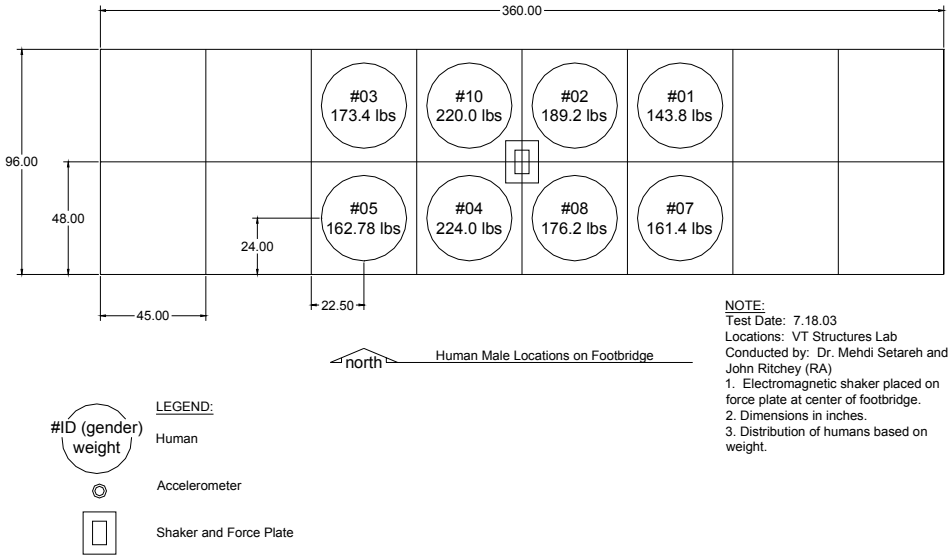

Figure P.17 – Floor Plan of Human Locations on Bare Floor – 8 People

APPENDIX Q: Simulink Block Diagram (Koo, 2003)

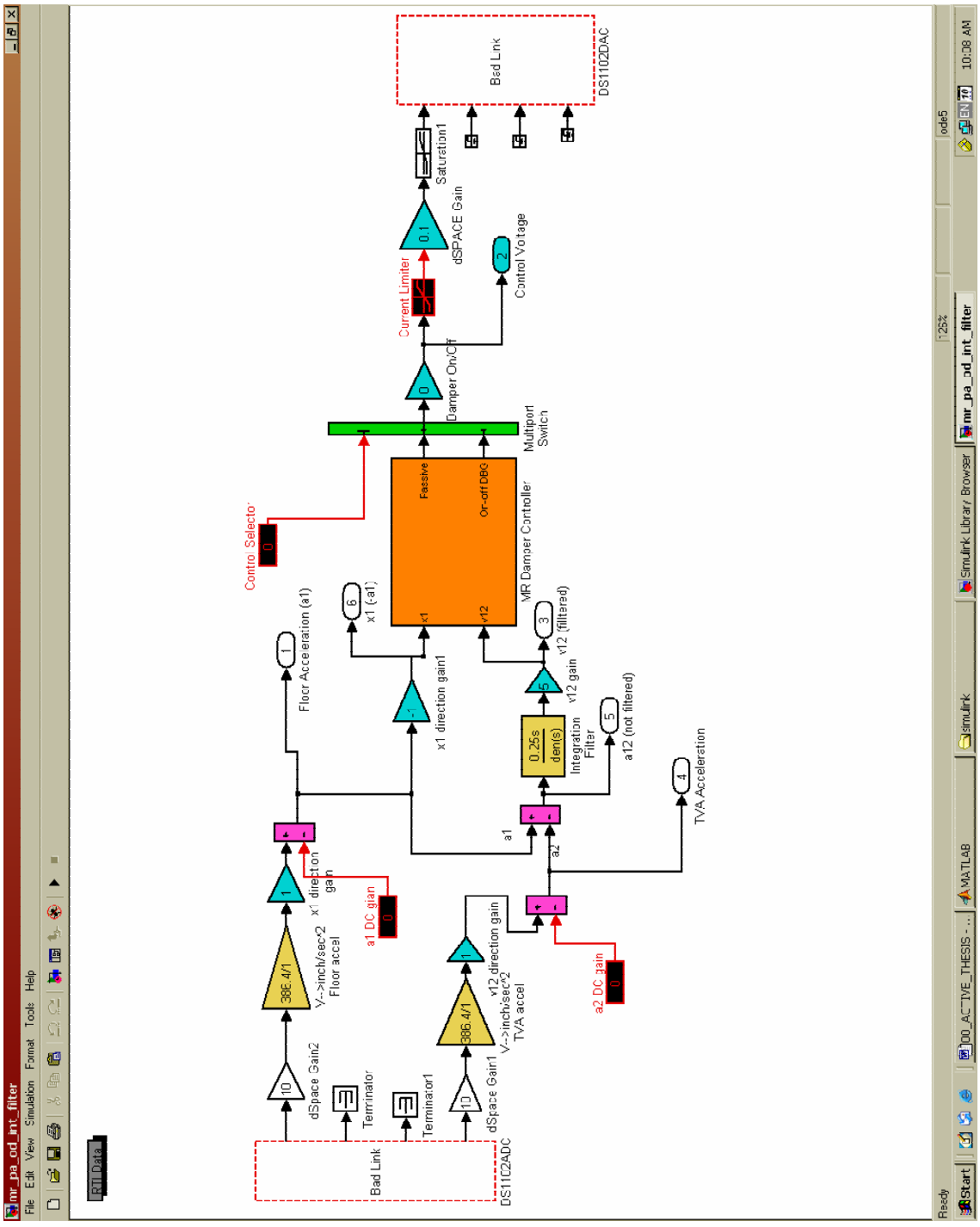

Figure Q.1 – Simulink Block Diagram

APPENDIX R: Integration in the Frequency Domain Routine

```
clear all; close all; clc;

g=386;
ZAD=50;  %ZAD = NUMBER OF ZEROS TO BE PUT INTO PLACE OF LOW FREQ
NO.S IN FREQ DOMAIN.
test=['test11'; 'test12'; 'test13'; 'test14'; 'test15';'test16'];
% i=1
for i=1:6;

a_data=wk1read(test(i,:));
t=a_data(:,1)';  %time
a1=g.*a_data(:,2)'; %channel 1
a2=g.*a_data(:,3)'; %channel 2

%TMD properties
m=720/386;   %lb s^2 / in.
wn=2*pi*7; %rad / s
k=wn^2*m;    %lb / in.
c=11.8/100*2*wn*m; %lb s / in.
N=size(t,2);
tf=t(N);
wo=2*pi/tf;



a1=a1-mean(a1);     a2=a2-mean(a2);

ffta1=fft(a1);      ffta2=fft(a2);

%VELOCITY CHANNEL 1
```

```
fftv11=ffta1(2:N/2)./(j*wo.*[1:N/2-1]);
fftv12=fliplr(conj(fftv11));
fftv1=[0 fftv11 ffta1(N/2+1)./(N/2*j*wo) fftv12];
fftv1m=fftv1;
fftv1m(1:ZAD)=zeros(1,ZAD);
fftv1m(N-ZAD+1:N)=zeros(1,ZAD);  %FFTVLM = MODIFIED VELOCITY TO GET
RID OF THE LOW FREQ CONTENT
v1=ifft(fftv1m);

%VELOCITY CHANNEL 2
fftv21=ffta2(2:N/2)./(j*wo.*[1:N/2-1]);
fftv22=fliplr(conj(fftv21));
fftv2=[0 fftv21 ffta2(N/2+1)./(N/2*j*wo) fftv22];

fftv2m=fftv2;
fftv2m(1:ZAD)=zeros(1,ZAD);
fftv2m(N-ZAD+1:N)=zeros(1,ZAD);
v2=ifft(fftv2m);

%DISPLACEMENT CHANNEL 1
fftx11=fftv1(2:N/2)./(j*wo.*[1:N/2-1]);
fftx12=fliplr(conj(fftx11));
fftx1=[0 fftx11 fftv1(N/2+1)./(N/2*j*wo) fftx12];
fftx1m=fftx1;
fftx1m(1:ZAD)=zeros(1,ZAD);
fftx1m(N-ZAD+1:N)=zeros(1,ZAD);  %FFTVLM = MODIFIED VELOCITY TO GET
RID OF THE LOW FREQ CONTENT
x1=ifft(fftx1m);

%DISPLACEMENT CHANNEL 2
fftx21=fftv2(2:N/2)./(j*wo.*[1:N/2-1]);
```

```
fftx22=fliplr(conj(fftx21));
fftx2=[0 fftx21 fftv2(N/2+1)./(N/2*j*wo) fftx22];

fftx2m=fftx2;
fftx2m(1:ZAD)=zeros(1,ZAD);
fftx2m(N-ZAD+1:N)=zeros(1,ZAD);
x2=ifft(fftx2m);

%DF=DAMPING FORCE
DF(i,:)=-1*(m.*a2+k.*(real(x2)-real(x1)));
%
% %new damping force - damping extension action
% hi=1*12; ho=52; %distance in inches
% D3=(hi+ho)/ho;
% %
% hi=2*12; ho=52; %distance in inches
% D4=(hi+ho)/ho;

rv(i,:)=v2-v1;
% rv3(i,:)=D3.*v2-v1;
% rv4(i,:)=D4.*v2-v1;

% rx(i,:)=x2-x1;
xchan1(i,:)=x1;
xchan2(i,:)=x2;
% rx3(i,:)=D3.*x2-x1;
% rx4(i,:)=D4.*x2-x1;
%
% DF3(i,:)=-1*(m.*D3.*a2+k.*(D3.*real(x2)-real(x1)));
% DF4(i,:)=-1*(m.*D4.*a2+k.*(D4.*real(x2)-real(x1)));
end
```

```
titles=['Test 11 - Heel Drop'; 'Test 12 - Heel Drop'; 'Test 13 - Heel Drop'; 'Test 14 - Heel
Drop'; 'Test 15 - Walking  '; 'Test 16 - Walking  '; ];
%
%  for i=1:6;
%    figure(i)
%
%    subplot(2,1,1)  %realtive velocity
%
%     experiment=['  TMD ON - ' titles(i,:) ' Center of Floor - 3/17/03       ']
%    plot(t,real(rv(i,:)),'k-')
%    title(['\bfRelative Velocity = v2-v1   'experiment date]);
%    xlabel('\bfTime (sec)');
%    ylabel('\bfv21 (in/s)'); grid
%
%    rvpnt=rv(i,:);
%
%   [V,L]=max(abs(real(rv(i,:))));
%    text(t(L), real(rvpnt(L)),...
%    [ '\bullet\bf\leftarrow\fontname{times} v21_p_e_a_k = '  num2str(real(rvpnt(L)))],...
%    'FontSize',10)
%    subplot(2,1,2) %damping force
%
%    experiment=['  TMD ON - ' titles(i,:) ' Center of Floor - 3/17/03       ']
%    plot(t,DF(i,:),'k-')
%    title(['\bfDamping Force = c2*v21   'experiment date]);
%    xlabel('\bfTime (sec)');
%    ylabel('\bfForce Amplitude (lbs)'); grid
%    DFpnt=DF(i,:);
%
%    [V,L]=max(abs(real(DF(i,:))));
```

```
%     text(t(L), DFpnt(L),...
%     [ '\bullet\bf\leftarrow\fontname{times} F_p_e_a_k = '  num2str(DFpnt(L))],...
%     'FontSize',10)
% end

%THIS BLOCK PLOTS THE DAMPING FORCE AND THE RELATIVE VELOCITY
IS OVERLAYED ON TO IT.
% for i=1:6;
%     figure(i)
%       experiment=['  TMD ON - ' titles(i,:) ' 3/17/03       ']
%        plot(t,DF(i,:),'k-'); hold on; plot(t,c.*real(rv(i,:)),'k:','LineWidth',2)
%        title(['\bfDamping Force = c2*v21   'experiment date]);
%        xlabel('\bfTime (sec)');
%        ylabel('\bfForce Amplitude (lbs)'); grid
%        legend('Equation of Motion','Relative Velocity');
%
% end

%THIS BLOCK PLOTS THE DAMPING FORCE AND THE Displacement of the TMD

for i=1:6;
   figure(i)
      experiment=['  TMD ON - ' titles(i,:) ' 3/17/03       ']
       plot(t,real(xchan2(i,:)),'k-'); hold on;
       title(['\bfTMD Displacement'experiment date]);
       xlabel('\bfTime (sec)');
       ylabel('\bfAmplitude (lbs)'); grid


end
```

```
% %This block plost sthe relative displacement for each test/ 3 plots for each type, relative, channel 1 and 2;
% for i=1:6;
% figure(i)
% subplot(3,1,1)
%    experiment=['  TMD ON - ' titles(i,:) ' 3/17/03       ']
%     plot(t,rx(i,:),'k-');
%     title(['\bfRelative Displacement = x21   'experiment date]);
%     xlabel('\bfTime (sec)');
%     ylabel('\bfAmplitude (in.)'); grid
%        rxpnt=rx(i,:);
%          [V,L]=max(abs(real(rx(i,:))));
% text(t(L), real(rxpnt(L)),...
% [ '\bullet\bf\leftarrow\fontname{times} x21_p_e_a_k = '  num2str(real(rxpnt(L)))],...
% 'FontSize',10)
% subplot(3,1,2)
%    experiment=['  TMD ON - ' titles(i,:) ' 3/17/03       ']
%     plot(t,xchan1(i,:),'k-');
%     title(['\bfRelative Displacement = x1   'experiment date]);
%     xlabel('\bfTime (sec)');
%     ylabel('\bfAmplitude (in.)'); grid
%        rxpnt=xchan1(i,:);
%          [V,L]=max(abs(real(xchan1(i,:))));
% text(t(L), real(rxpnt(L)),...
% [ '\bullet\bf\leftarrow\fontname{times} x1_p_e_a_k = '  num2str(real(rxpnt(L)))],...
% 'FontSize',10)
%
% subplot(3,1,3)
%    experiment=['  TMD ON - ' titles(i,:) ' 3/17/03       ']
%     plot(t,xchan2(i,:),'k-');
%     title(['\bfRelative Displacement = x2   'experiment date]);
```

```
%     xlabel('\bfTime (sec)');
%     ylabel('\bfAmplitude (in.)'); grid
%       rxpnt=xchan2(i,:);
%         [V,L]=max(abs(real(xchan2(i,:))));
% text(t(L), real(rxpnt(L)),...
% [ '\bullet\bf\leftarrow\fontname{times} x2_p_e_a_k = '  num2str(real(rxpnt(L)))],...
% 'FontSize',10)
%
% end
% figure(200) %overlay heel drop plots
%     plot(t,DF(1,:),'kx-');     hold     on;     plot(t,DF(2,:),'ks-','LineWidth',1);hold     on;
plot(t,DF(3,:),'k','LineWidth',2); hold on; plot(t,DF(4,:),'k-.','LineWidth',2);
% title(['Damping Force = c2*v21 - Heel Drop - Test Date: 3/17/03  ' date])
% ylabel('\bfF_D_a_m_p_i_n_g (lbs)')
% xlabel('\bfTime (sec)')
% legend('Test 11','Test 12','Test 13','Test 14');
% grid
% figure(201) %overlay walking plots
% plot(t,DF(5,:),'k','LineWidth',2); hold on; plot(t,DF(6,:),'k:','LineWidth',1);
% title(['\bfDamping Force = c2*v21- Walking - Test Date: 3/17/03  ' date])
% ylabel('\bfF_D_a_m_p_i_n_g (lbs)')
% xlabel('\bfTime (sec)')
% legend('Test 15','Test 16');
% grid;

% figure(2003)
% subplot(3,2,1), plot(t,a1); ylabel('a1'); title(['Channel 1 Parameters - 3/17/03   ' date]);
grid
% subplot(3,2,3), plot(t,v1); ylabel('v1'); grid
% subplot(3,2,5), plot(t,x1); ylabel('x1'); xlabel('time (sec)'); grid
%
```

```
% subplot(3,2,2), plot(t,a2); ylabel('a2'); title(['Channel 2 Parameters - 3/17/03   ' date]);
grid
% subplot(3,2,4), plot(t,v2); ylabel('v2'); grid
% subplot(3,2,6), plot(t,x2); ylabel('x2'); xlabel('time (sec)'); grid

% gtext(['a1[ t(205) = 1.9922 sec] = 'num2str(a1(205))]);
% gtext(['v1[ t(205) = 1.9922 sec] = 'num2str(real(v1(205)))]);
% gtext(['x1[ t(205) = 1.9922 sec] = 'num2str(real(x1(205)))]);
%
% gtext(['a2[ t(205) = 1.9922 sec] = 'num2str(a2(205))]);
% gtext(['v2[ t(205) = 1.9922 sec] = 'num2str(real(v2(205)))]);
% gtext(['x2[ t(205) = 1.9922 sec] = 'num2str(real(x2(205)))]);
%
% gtext(['DF[ t(205) = 1.9922 sec] = 'num2str(real(DF(205)))]);
% i=6
% figure(505) %3 plots showing the effect of moving the damping out to and additional 1
and 2 '
% %NOTE even though it say df3 and df4 it has been changed to 1 and 2 foot extension
results.
% subplot(3,1,1) %inital position
%
%    experiment=['  TMD ON - ' titles(i,:) ' - 3/24/03       '];
%    plot(t,real(rv(i,:)),'k-')
%    title(['\bfRelative Velocity = v2-v1   'experiment date]);
%    xlabel('\bfTime (sec)');
%    ylabel('\bfv21 (in/s)'); grid
%
%    rvpnt=rv(i,:);
%
%   [V,L]=max(abs(real(rv(i,:))));
%    text(t(L), real(rvpnt(L)),...
```

```
%    [ '\bullet\bf\leftarrow\fontname{times} v21_p_e_a_k = '  num2str(real(rvpnt(L)))],...
%    'FontSize',10)
%
% subplot(3,1,2) %1 foot position
%
%  experiment=['  TMD ON - ' titles(i,:) ' - 3/24/03       '];
%    plot(t,real(rv3(i,:)),'k-')
%    title(['\bfRelative Velocity @ 1 ft = v2-v1   'experiment date]);
%    xlabel('\bfTime (sec)');
%    ylabel('\bfv21 (in/s)'); grid
%
%    rvpnt3=rv3(i,:);
%
%   [V,L]=max(abs(real(rv3(i,:))));
%    text(t(L), real(rvpnt3(L)),...
%                          [     '\bullet\bf\leftarrow\fontname{times}     v21_p_e_a_k     =     '
num2str(real(rvpnt3(L)))],...
%    'FontSize',10)
%
%
% subplot(3,1,3) %4 foot position
%
%
%  experiment=['  TMD ON - ' titles(i,:) ' - 3/24/03       '];
%    plot(t,real(rv4(i,:)),'k-')
%    title(['\bfRelative Velocity = v2-v1   'experiment date]);
%    xlabel('\bfTime (sec)');
%    ylabel('\bfv21 (in/s)'); grid
%
%    rvpnt4=rv4(i,:);
%
```

```
%    [V,L]=max(abs(real(rv4(i,:))));
%     text(t(L), real(rvpnt4(L)),...
%                          [      '\bullet\bf\leftarrow\fontname{times}      v21_p_e_a_k      =      '
num2str(real(rvpnt4(L)))],...
%     'FontSize',10)
% figure(506) %3 plots showing the effect of moving the damping out to and additional 3
and 4 '
% subplot(3,1,1) %inital position
%
%
%     experiment=['  TMD ON - ' titles(i,:) '- 3/24/03       '];
%     plot(t,DF(i,:),'k-')
%     title(['\bfDamping Force = c2*v21    'experiment date]);
%     xlabel('\bfTime (sec)');
%     ylabel('\bfForce Amplitude (lbs)'); grid
%
%     DFpnt=DF(i,:);
%
%     [V,L]=max(abs(real(DF(i,:))));
%     text(t(L), DFpnt(L),...
%     [ '\bullet\bf\leftarrow\fontname{times} F_p_e_a_k = '  num2str(DFpnt(L))],...
%     'FontSize',10)
%
% subplot(3,1,2) %1 foot position
%
%     experiment=['  TMD ON - ' titles(i,:) '- 3/24/03       '];
%     plot(t,DF3(i,:),'k-')
%     title(['\bfDamping Force @ 1 ft = c2*v21    'experiment date]);
%     xlabel('\bfTime (sec)');
%     ylabel('\bfForce Amplitude (lbs)'); grid
%
```

```
%    DFpnt3=DF3(i,:);
%
%    [V,L]=max(abs(real(DF3(i,:))));
%    text(t(L), DFpnt3(L),...
%    [ '\bullet\bf\leftarrow\fontname{times} F_p_e_a_k = '  num2str(DFpnt3(L))],...
%    'FontSize',10)
%
%
%
% subplot(3,1,3) %2 foot position
%
%    experiment=['  TMD ON - ' titles(i,:) '- 3/24/03       '];
%    plot(t,DF4(i,:),'k-')
%    title(['\bfDamping Force @ 2 ft = c2*v21   'experiment date]);
%    xlabel('\bfTime (sec)');
%    ylabel('\bfForce Amplitude (lbs)'); grid
%
%    DFpnt4=DF4(i,:);
%
%    [V,L]=max(abs(real(DF4(i,:))));
%    text(t(L), DFpnt4(L),...
%    [ '\bullet\bf\leftarrow\fontname{times} F_p_e_a_k = '  num2str(DFpnt4(L))],...
%    'FontSize',10)


%
++++++++++++++++++++++++++++++++++++++++++++++++++++++++++++++++++++++++
++++++

% i=5
```

```
% figure(116) %3 plots showing the effect of moving the damping out to and additional 1
and 2 '
% %NOTE even though it say df3 and df4 it has been changed to 1 and 2 foot extension
results.
% subplot(3,1,1) %inital position
%
%    experiment=['  TMD ON - ' titles(i,:) ' - 3/24/03       '];
%    plot(t,real(rx(i,:)),'k-')
%    title(['\bfRelative Displacement = x2-x1   'experiment date]);
%    xlabel('\bfTime (sec)');
%    ylabel('\bfv21 (in/s)'); grid
%
%    rxpnt=rx(i,:);
%
%   [V,L]=max(abs(real(rx(i,:))));
%    text(t(L), real(rxpnt(L)),...
%    [ '\bullet\bf\leftarrow\fontname{times} x21_p_e_a_k = '  num2str(real(rxpnt(L)))],...
%    'FontSize',10)
%
% subplot(3,1,2) %1 foot position
%
%  experiment=['  TMD ON - ' titles(i,:) ' - 3/24/03       '];
%    plot(t,real(rx3(i,:)),'k-')
%    title(['\bfbfRelative Displacement @ 1 ft = x2-x1   'experiment date]);
%    xlabel('\bfTime (sec)');
%    ylabel('\bfv21 (in/s)'); grid
%
%    rxpnt3=rx3(i,:);
%
%   [V,L]=max(abs(real(rx3(i,:))));
%    text(t(L), real(rxpnt3(L)),...
```

```
%                       [     '\bullet\bf\leftarrow\fontname{times}     x21_p_e_a_k     =     '
num2str(real(rxpnt3(L)))],...
%    'FontSize',10)
%
%
% subplot(3,1,3) %4 foot position
%
%
%  experiment=['  TMD ON - ' titles(i,:) ' - 3/24/03       '];
%    plot(t,real(rx4(i,:)),'k-')
%    title(['\bfbfRelative Displacement @ 2 = x2-x1   'experiment date]);
%    xlabel('\bfTime (sec)');
%    ylabel('\bfv21 (in/s)'); grid
%
%    rxpnt4=rx4(i,:);
%
%   [V,L]=max(abs(real(rx4(i,:))));
%    text(t(L), real(rxpnt4(L)),...
%                       [     '\bullet\bf\leftarrow\fontname{times}     x21_p_e_a_k     =     '
num2str(real(rxpnt4(L)))],...
%    'FontSize',10)
```

APPENDIX S: Slow Sweep versus Chirp Signal at a Method to Produce FRF

```
clear all; close all; clc;
%_____SYSTEM INPUT
PARAMETERS_____
Zeta1=0.0104;
mu=0.0494;
x(1)=.9795
x(2)=.1313
x(3)=0.1313

f=x(1);
Zeta2_on=x(2);
Zeta2_off=x(2);


%Floor Properties
m1=.012946;
fn1=7.35;
k1=(2*pi*fn1).^2*m1;
wn1=2*pi*fn1;
c1=Zeta1*2*m1*wn1;
%
flr=['m1: 'num2str(m1) ' ' 'c1: 'num2str(c1) ' ' 'k1: 'num2str(k1) ' '  'Zeta1: '
num2str(Zeta1)]

%TMD Properties
fn2=fn1*f;
wn2=2*pi*fn2;

m2=m1*mu;
lm=49.37;

k2=3.25; %kip / in.
ls=2*fn2*pi*lm*1/(sqrt(k2/m2));

lc=51.31;

c_on=4*Zeta2_on*pi*fn2*m2*lm^2/lc^2;
c_off=2*m2*wn2*Zeta2_off*lm^2/lc^2;
tmd=['m2: 'num2str(m2) ' ' 'c_on: 'num2str(c_on) ' ' 'k2: 'num2str(k2) ' '  'Zeta2_on: '
num2str(Zeta2_on)]

T=30;
wo=2*pi/T;
N=3000;
```

```
dt=T/N;
F=1;

% g=[.9];
% iteration=1;
xst=F/k1;
g=0.5:0.01:1.5;

for iteration=1:size(g,2);
prcnt=0.20;
%SYSTEM MATRICES

K=[k1 0;0 k2*ls^2];
M=[m1+m2 m2*lm; m2*lm m2*lm^2];

%
=================================================================
==================================
%                              RK45 - FORCE ACTION
%
=================================================================
==================================

h=dt;
tn=T;
y0=[0;0;0;0];

B=[F; 0]; w=g(iteration)*wn1;
ff=inv(M)*B;

t = (0:h:tn)';               %  Column vector of elements with spacing h
n = length(t);               %  Number of elements in the t vector
y = y0*ones(n,1)';           %  Preallocate y for speed
h2 = h/2;  h3 = h/3;  h6 = h/6;  %  Avoid repeated evaluation of constants

for j=2:n

   if y(1,j-1)*(y(3,j-1)-lm.*y(4,j-1))>=0;
      C=[c1 0; 0 c_on*lc^2];
      A1=[zeros(2) eye(2); -inv(M)*K -inv(M)*C];

   else
      C=[c1 0; 0 c_off*lc^2];
      A1=[zeros(2) eye(2); -inv(M)*K -inv(M)*C];

   end
```

```
   kk1 = A1*y(:,j-1)+[0;0;ff]*sin(w*t(j-1));

   kk2 = A1*(y(:,j-1)+h2*kk1)+[0;0;ff]*sin(w*(t(j-1)+h2));

   kk3 = A1*(y(:,j-1)+h2*kk2)+[0;0;ff]*sin(w*(t(j-1)+h2));

   kk4 = A1*(y(:,j-1)+h*kk3)+[0;0;ff]*sin(w*(t(j-1)+h));

   y(:,j) = y(:,j-1) + h6*(kk1+kk4) + h3*(kk2+kk3);

end

% %obtaining acceleration in frequency domain and then covert back to time domain

fftv1=fft(y(3,:));
ffta11=fftv1(2:N/2).*(j*wo.*[1:N/2-1]);
ffta12=fliplr(conj(ffta11));
ffta1=[0 ffta11 fftv1(N/2+1).*(N/2*j*wo) ffta12];
ffta1m=ffta1;
av1=real(1/N.*ifft(ffta1m));

fftv1=fft(y(4,:));
ffta11=fftv1(2:N/2).*(j*wo.*[1:N/2-1]);
ffta12=fliplr(conj(ffta11));
ffta1=[0 ffta11 fftv1(N/2+1).*(N/2*j*wo) ffta12];
ffta1m=ffta1;
av2=real(1/N.*ifft(ffta1m));

ymax1(iteration)=max(y(1,round(size(y,2)-prcnt*size(y,2)):size(y,2)));
ymax2(iteration)=max(y(2,round(size(y,2)-prcnt*size(y,2)):size(y,2)));

vmax1(iteration)=max(y(3,round(size(y,2)-prcnt*size(y,2)):size(y,2)));
vmax2(iteration)=max(y(4,round(size(y,2)-prcnt*size(y,2)):size(y,2)));

amax1(iteration)=max(av1(1,round(size(av1,2)-prcnt*size(av1,2)):size(av1,2)-10));
amax2(iteration)=max(av2(1,round(size(av2,2)-prcnt*size(av2,2)):size(av2,2)-10));

end  %<----IF DOING TIME ANALYSIS, TURN THIS "END STATEMENT" OFF

gchirp=g;
a1chirp=amax1;

%%%=============================================================
====================
```

```
%%%==========================================================
====================
%%%==========================================================
====================
%%%==========================================================
====================
%%%================================Slow
Sweep=======================================
%%%==========================================================
====================
%%%==========================================================
====================
%%%==========================================================
====================
%%%==========================================================
====================
%%%==========================================================
====================
%%%==========================================================
====================
clear all; close all; clc;
%_____________________________SYSTEM INPUT
PARAMETERS_____________________________
Zeta1=0.0104;
mu=0.0494;
x(1)=.9795
x(2)=.1313
x(3)=0.1313

f=x(1);
Zeta2_on=x(2);
Zeta2_off=x(2);


%Floor Properties
m1=.012946;
fn1=7.35;
k1=(2*pi*fn1).^2*m1;
wn1=2*pi*fn1;
c1=Zeta1*2*m1*wn1;
%
flr=['m1: 'num2str(m1) ' ' 'c1: 'num2str(c1) ' ' 'k1: 'num2str(k1) ' '  'Zeta1: '
num2str(Zeta1)]

%TMD Properties
fn2=fn1*f;
```

```
wn2=2*pi*fn2;

m2=m1*mu;
lm=49.37;

k2=3.25; %kip / in.
ls=2*fn2*pi*lm*1/(sqrt(k2/m2));

lc=51.31;

c_on=4*Zeta2_on*pi*fn2*m2*lm^2/lc^2;
c_off=2*m2*wn2*Zeta2_off*lm^2/lc^2;
tmd=['m2: 'num2str(m2) ' ' 'c_on: 'num2str(c_on) ' ' 'k2: 'num2str(k2) ' '  'Zeta2_on: '
num2str(Zeta2_on)]

T=30;
wo=2*pi/T;
N=3000;
dt=T/N;
F=1;

% g=[.9];
% iteration=1;
xst=F/k1;
g=0.5:0.01:1.5;

for iteration=1:size(g,2);
prcnt=0.20;
%SYSTEM MATRICES

K=[k1 0;0 k2*ls^2];
M=[m1+m2 m2*lm; m2*lm m2*lm^2];

%
==========================================================================
==================================
%                                RK45 - FORCE ACTION
%
==========================================================================
==================================

h=dt;
tn=T;
y0=[0;0;0;0];

B=[F; 0]; w=g(iteration)*wn1;
```

```
ff=inv(M)*B;

t = (0:h:tn)';                  %  Column vector of elements with spacing h
n = length(t);                  %  Number of elements in the t vector
y = y0*ones(n,1)';              %  Preallocate y for speed
h2 = h/2;  h3 = h/3;  h6 = h/6;  %  Avoid repeated evaluation of constants

for j=2:n

   if y(1,j-1)*(y(3,j-1)-lm.*y(4,j-1))>=0;
      C=[c1 0; 0 c_on*lc^2];
      A1=[zeros(2) eye(2); -inv(M)*K -inv(M)*C];

   else
      C=[c1 0; 0 c_off*lc^2];
      A1=[zeros(2) eye(2); -inv(M)*K -inv(M)*C];

   end

  kk1 = A1*y(:,j-1)+[0;0;ff]*sin(w*t(j-1));

  kk2 = A1*(y(:,j-1)+h2*kk1)+[0;0;ff]*sin(w*(t(j-1)+h2));

  kk3 = A1*(y(:,j-1)+h2*kk2)+[0;0;ff]*sin(w*(t(j-1)+h2));

  kk4 = A1*(y(:,j-1)+h*kk3)+[0;0;ff]*sin(w*(t(j-1)+h));

  y(:,j) = y(:,j-1) + h6*(kk1+kk4) + h3*(kk2+kk3);

end

% %obtaining acceleration in frequency domain and then covert back to time domain

fftv1=fft(y(3,:));
ffta11=fftv1(2:N/2).*(j*wo.*[1:N/2-1]);
ffta12=fliplr(conj(ffta11));
ffta1=[0 ffta11 fftv1(N/2+1).*(N/2*j*wo) ffta12];
ffta1m=ffta1;
av1=real(1/N.*ifft(ffta1m));

fftv1=fft(y(4,:));
ffta11=fftv1(2:N/2).*(j*wo.*[1:N/2-1]);
ffta12=fliplr(conj(ffta11));
ffta1=[0 ffta11 fftv1(N/2+1).*(N/2*j*wo) ffta12];
ffta1m=ffta1;
av2=real(1/N.*ifft(ffta1m));
```

```
ymax1(iteration)=max(y(1,round(size(y,2)-prcnt*size(y,2)):size(y,2)));
ymax2(iteration)=max(y(2,round(size(y,2)-prcnt*size(y,2)):size(y,2)));

vmax1(iteration)=max(y(3,round(size(y,2)-prcnt*size(y,2)):size(y,2)));
vmax2(iteration)=max(y(4,round(size(y,2)-prcnt*size(y,2)):size(y,2)));

amax1(iteration)=max(av1(1,round(size(av1,2)-prcnt*size(av1,2)):size(av1,2)-10));
amax2(iteration)=max(av2(1,round(size(av2,2)-prcnt*size(av2,2)):size(av2,2)-10));
```

APPENDIX T: Generalization of Semi-active versus Passive at Optimal Tuning

Table T.1 – Optimized Parameters for Figure 2.14

Semi-active

			Mass Ratio					
			0.01	**0.02**	**0.03**	**0.04**	**0.05**	**0.06**
Damping	**0.01**	**f**	1.025	1.0323	1.0287	1.0221	1.065	1..0607
		Z1	0.7	0.6971	0.7	0.7	0.7	0.6997
		Z2	0.02	0.0223	0.0406	0.0487	0.02	0.0105
		Peak	**8.3226**	**6.6778**	**6.2**	**5.7526**	**5.2**	**4.68**
	0.02	**f**	1.0241	1.0299	1.0617	1.0217	1.065	1.0642
		Z1	0.7	0.7	0.7	0.6812	0.7	0.6991
		Z2	0.0241	0.0288	0.0207	0.0618	0.02	0.0129
		Peak	**7.3769**	**5.9699**	**5.6322**	**5.3227**	**4.7577**	**4.369**
	0.05	**f**	1.0355	1.035	1.0687	1.0468	1.0682	1.07
		Z1	0.6997	0.7	0.7	0.7	0.7	0.7
		Z2	0.0246	0.02	0.0275	0.0609	0.0208	0.02
		Peak	**5.285**	**4.7073**	**4.3534**	**4.2498**	**3.8**	**3.5841**

Passive

			Mass Ratio					
			0.01	**0.02**	**0.03**	**0.04**	**0.05**	**0.06**
Damping	**0.01**	**f**	0.9957	0.991	0.9863	0.9817	0.9772	0.9742
		Z1	0.0629	0.089	0.108	0.1237	0.1374	0.1433
		Z2	0.0629	0.089	0.108	0.1237	0.1374	0.1433
		Peak	**11.2865**	**8.4575**	**7.0787**	**6.2143**	**5.6053**	**5.1592**
	0.02	**f**	0.99638	0.992	0.9875	0.9834	0.9789	0.9741
		Z1	0.0628	0.0915	0.1107	0.125	0.1388	0.1529
		Z2	0.0628	0.0915	0.1107	0.125	0.1388	0.1529
		Peak	**9.4**	**7.3561**	**6.2919**	**5.5993**	**5.1009**	**4.7178**
	0.05	**f**	1.001	0.9972	0.9928	0.9887	0.9855	0.9794
		Z1	0.0678	0.0947	0.1164	0.1325	0.1426	0.1635
		Z2	0.0678	0.0947	0.1164	0.1325	0.1426	0.1635
		Peak	**6.2004**	**5.2577**	**4.6987**	**4.3061**	**4.0105**	**3.7696**

	0.01	0.02	0.03	0.04	0.05	0.06
0.01	26.26%	21.04%	12.41%	7.43%	7.23%	9.29%
0.02	21.52%	18.84%	10.48%	4.94%	6.73%	7.39%
0.05	14.76%	10.47%	7.35%	1.31%	5.25%	4.92%

VITA

John Kenneth Ritchey was born in Kansas City, Missouri on November 9, 1976 to Kenneth Scott and Patricia Ann Ritchey. He has one older brother, William Allen Ritchey.

John graduated from Park Hill High School in Parkville, Missouri in 1995. He began his college career at the University of Missouri, Columbia in physical therapy in 1995. In 1997, he went to the University of Kansas where he received his Bachelor of Science degree in Architectural Engineering in 2002. John continued his education at Virginia Polytechnic Institute and State University to receive his Master of Science in Civil Engineering with a focus in structural engineering.